AVERTISSEMENT

Ce document est le fruit d'un long travail approuvé par le jury de soutenance et mis à disposition de l'ensemble de la communauté universitaire élargie.

Il est soumis à la propriété intellectuelle de l'auteur. Ceci implique une obligation de citation et de référencement lors de l'utilisation de ce document.

D'autre part, toute contrefaçon, plagiat, reproduction illicite encourt une poursuite pénale.

Contact : ddoc-theses-contact@univ-lorraine.fr

LIENS

Code de la Propriété Intellectuelle. articles L 122. 4
Code de la Propriété Intellectuelle. articles L 335.2- L 335.10
http://www.cfcopies.com/V2/leg/leg_droi.php
http://www.culture.gouv.fr/culture/infos-pratiques/droits/protection.htm

FACULTE DES SCIENCES & TECHNIQUES
U.F.R. Sciences & Techniques de la Matière des Procédés
Ecole Doctorale Lorraine de Chimie et Physique Moléculaires

Thèse

Présentée pour l'obtention du titre de

Docteur de l'Université Henri Poincaré

en Chimie et Physico-chimie Moléculaires

par

Na DU

Investigation of Hydrogenated and Fluorinated Surfactant Based-Systems for the Design of Porous Silica Materials

Soutenue le 23 juillet 2010

Membres du jury :

Rapporteurs :	Conxità Solans	Research Professeur CSIC / IQAC, Barcelone
	Laurent Bonneviot	Professeur École normale supérieure de Lyon
Examinateurs :	Jean Paul Decruppe	Professeur, Université Paul Verlaine Metz
	Marc Hebrant	Professeur Nancy Université
	Jean-Luc Blin	Professeur Nancy Université
	Marie-José Stébé	Directrice de Recherches CNRS Nancy Université
Invité :	Lionel Perdreau	Ingénieur Huntsman Surface Sciences

Equipe Physico-chimie des Collïdes – UMR 7565 SRSMC CNRS – Nancy Université
Faculté des Sciences et Techniques BP 239, 54506 Vandœuvre-lès-Nancy Cedex

This work has been done within the research group of Physical Chemistry of Colloids, in the Laboratory of Structure and Reactivity of Complex Molecular Systems, UMR No. 7565 of the CNRS and the Faculty of Science and Technology UHP of Nancy.

In the first place I would like to express my deep and sincere gratitude to my two supervisors, Ms. Marie-Jose STEBE and Mr. Jean-Luc BLIN, for having me into their team. Their supervision, advice, and guidance throughout the three years allowed me to develop my research work. Without them this thesis could not be completed. I am grateful to Ms Marie-Jose STEBE for her encouragement for participation in international conferences. Her care and concern not only about my work but also about my daily life during three years in every possible way made my stay in France delightful. I am also grateful to Mr. Jean-Luc BLIN for his stimulation and encouragement during my research and redaction time. His hard work and perseverance in daily set a role model for my future work.

My gratitude goes to those who have agreed to review my work. I gratefully acknowledge Ms. Conxità SOLANS, director of Institut de Quimica Avançada de Catalunya (Barcelona), for accepting to be the reviewer of dissertation committee. Many thanks to Mr. Laurent Bonneviot, Professor of École normale supérieure de Lyon, for his interest in this work by agreeing to be reviewer. We also thank Mr. Jean Paul Decruppe, Mr. Marc Hebrant and Mr. Lionel Perdreau, for giving me the honor to participate in my thesis committee.

I am grateful for the financial support provided by China Scholarship Council.

Many thanks to the Graduate School SESAMES for giving me financial support during my participation in an international conference in Stockholm.

I wish to thank Mr. Alain Kohler for his help of Scanning Electron Microscopy experiments.

I wish to thank Mr. Boubel and Mr Canet for the help of my thesis print.

I wish to thank the Ms Gareaux, Ms Florence and Ms Larcan in the French class gave me a chance to learn the most romantic language in the word—French.

I express my deep appreciation to Mr. Alain Retournard, not only for his professional skills

but also for his human qualities, his kindness and humor.

I wish to thank Tushaar for the correction of my English writing in the thesis.

Collective and individual acknowledgments are also owed to all current and former members of the team. My special thanks go to Kévin. We have spent such a pleasant time during these years in the same office full of joy. He is always available whenever I need a hand, moreover he is a “great French teacher”. Without him; the French part of this thesis would be unintelligible to read at all due to my “poor” French. My sincere appreciations go in particular to Lyne for her friendship and support in every possible way during three years. I regard her as my family in France. I will never forget the good time we shared together…… Many thanks to Florentin for the science discussion and exhilarating time we spent together. Special thanks to Rudina, Lionel (NO.1), Nicola, May, Cindy, Dorothea, Emily, Poline, Yuhui, and Lionel (NO.2) for the kindness they have shown me every day and have managed to maintain good relations within the team. Special mention must be addressed to Denise HENRYON for the help given to me on administrative procedures.

Furthermore, I would like to thank all the friends I made in France, Chasan, Thu, Andrew, Zhu Yan, Wang Zhijie, Yan Xiang, Li Zhenghui, Zhang Jinbai, Mao Fei, Tian Zhenyu, Xu Ping, Hala, Duan Junbo, Abdou, Herve, Liu Rufen, Lv Yan, Yi Li, Peng Ting, Guo Yuanyuan, Fu Taotao…

Finally, I lack the words to express respect and gratitude I feel for my parents who, despite the distance that separates us, constantly encouraged and accompanied me throughout this work. Their support, encouragement, quiet patience and unwavering love were precious to me. I thank them very much.

Table of Contents

Abbreviations **1**

Preface **3**

Chapter I. Introduction **7**

1. Surfactants based system 11

1.1 Properties of surfactant molecules 11

1.2 Phase behavior 14

1.3 Highly concentrated emulsions 18

2. Porous materials 20

2.1 Sol-gel process 22

2.2 Material-Templated by Surfactant (MTS) 23

2.3 Hierarchical porous materials 31

3. Context of study 36

Chapter II. Experimental part **37**

1. Materials 43

1.1 Surfactants 43

1.2 Hydrogenated compounds 44

1.3 Fluorocarbons 44

2. Phase diagram determination 47

3. Preparation of porous materials 48

3.1 Source of silica 48

3.2 Preparation of the mesoporous materials 49

4. Techniques of characterization 50

4.1 Polarized light microscopy 50

4.2 Small angle X-ray scattering (SAXS) 52

4.3 Nitrogen adsorption-desorption analysis 56

4.4 Dynamic light scattering (DLS) 59

4.5 Scanning electron microscopy (SEM) 60

Chapter III. Preparation and characterization of porous silica templated by $R^{H}_{12}A(EO)_9$ based-system 65

1. $R^{H}_{12}A(EO)_9$-water system 69

1.1 Characterization of the $R^{H}_{12}A(EO)_9$-water system**Error! Bookmark not defined.**

1.2 Characterization of the liquid crystal phases..... 69

1.3 Characterization of the mesoporous materials prepared from the $R^{H}_{12}A(EO)_9$-water system 71

2. Solubilization of hydrocarbons in the $R^{H}_{12}A(EO)_9$-water system 73

2.1 Phase behavior..... 73

2.2 Structural parameters of the hexagonal and the lamellar phases..... 76

2.3 Influence of the solubilization of oils on the characteristics of materials 78

3. Discussion 88

4. Conclusion 91

Chapter IV. Preparation and characterization of porous silica templated by nonionic fluorinated systems 95

1. The $C_8F_{17}C_2H_4(OC_2H_4)_9OH$ based systems 99

1.1 Phase behavior..... 99

1.2 Porous silica prepared from $R^{F}_{8}(EO)_9$/ PFD/ water $R^{F}_{8}(EO)_9$/ PFD/ water systems. 105

2. $C_7F_{15}C_2H_4(OC_2H_4)_8OH$ based systems 113

2.1 Phase behavior..... 113

2.2 Porous materials prepared from with microemulsions and emulsions..... 118

3. Discussion 125

3.1 Macroporous silica 125

3.2 Expansion of the mesopores..... 126

3.3 Pore ordering in the presence of PFOBr 127

4. Conclusion 128

Chapter V. The effect of the alcohols addition in the $R^{F}_{8}(EO)_9$-based system on the characteristics of mesoporous silica 129

1. Solubilization of methanol and iso-propanol in the $R^F_8(EO)_9$-water system 135

1.1 Ternary diagram 135

1.2 Structural parameters of hexagonal crystal liquid phase 136

1.3 Mesoporous materials prepared from system $R^F_8(EO)_9$-water with methanol or isopropanol 138

1.4 Discussion 143

2. Solubilization of butanol in the $R^F_8(EO)_9$-water system 143

2.1 Ternary diagram 144

2.2 Structural parameters of the hexagonal crystal liquid phase 144

2.3 Mesoporous materials prepared from the system $R^F_8(EO)_9$/water in the presence of butanol 151

3. Solubilization of octanol in the $R^F_8(EO)_9$-water system 156

3.1 Ternary diagram 156

3.2 Structural parameters of hexagonal crystal liquid phase 156

3.3 Mesoporous materials prepared from system $R^F_8(EO)_9$-water with octanol 159

3.4 Discussion 162

4. Solubilization of fluorinated octanol in the $R^F_8(EO)_9$- water system 163

4.1 Ternary diagram 163

4.2 Structural parameters of hexagonal crystal liquid phase 164

4.3 Mesoporous materials prepared from the system $R^F_8(EO)_9$-water in the presence of fluorinated octanol 166

4.4 Discussion 170

5. Conclusion 170

Conclusions 175

Outlooks 177

Appendix 183

References 187

Abbreviations

OMS : self-Organized Molecular System

HLB: Hydrophilic-Lipophilic Balance

PIT : Phase Inversion Temperature

Direct (1) and reverse (2) Phases :

L_1, L_2, L_3 : micellar solutions

I_1, I_2 : micellar cubic phases

V_1, V_2 : bicontinuous cubic phases

H_1, H_2 : hexagonal phases

L_α : lamellar phase

Products :

$R^H_{12}A(EO)_9$: $C_{12}H_{25}COO(C_2H_4)_9CH_3$

$R^F_m(EO)_n$: $F(CF_2)_mC_2H_4(OC_2H_4)_nOH$

$R^H_{12}(EO)_4$: $C_{12}H_{25}(OC_2H_4)_9OH$

PFD : perfluorodecaline ($C_{10}F_{18}$) 

F44E : bis (F-butyl)-1,2-ethylene ($C_4F_9CH=CHC_4F_9$)

PFOBr: perfluorooctyl bromide ($C_8F_{17}Br$)

TMOS : tetramethoxysilane $Si(OCH_3)_4$, source of silica

Φ_B : hydrophobic volume fraction

α : number of water molecules per surfactant molecule

β : number of oil molecules per surfactant molecule

γ : number of alcohol molecules per surfactant molecule

V_S : molar volumes of the surfactant

V_A : molar volumes of the polar head of the surfactant

V_B : molar volumes of the hydrophobic part of the surfactant

V_W : molar volumes of water

V_{al} : molar volumes of alcohol

V^m : molar volume of mixed surfactant

V_o : molar volume of oil.

M_S : molar weight of surfactant

M^m : average molar molecular weight

d_S : density of surfactant

d^m : average density

R_H : hydrophobic radius in the hexagonal phase

S : cross-sectional area

d_A, d_B : hydrophilic and hydrophobic thickness in the lamellar phase

a_0 : unite cell parameter

Materials :

S_{BET} : specific surface area

Ø : pore diameter

Material families :

MCM : Mobil Crystalline Materials

HMS : hexagonal mesoporous silica

SBA : Santa Barbara

MSU : Michigan State University

KIT : Korea Advanced Institute

Techniques of characterization :

SAXS : Small Angle X-ray Scattering

DLS : Dynamic Light Scattering

BET : Brunauer-Emmet-Teller method of determination of specific surface area

BJH : Barret-Joyner-Halenda method of determination of distribution of pore size

SEM: Scanning Electronic Microscopy

Preface

“Space—the final frontier.” This preamble captures the challenge encountered not only in space travel adventures, but also in the field of porous materials, which aims to control the size, shape and uniformity of the porous space and the atoms and molecules that define it. The past decade has seen significant advances in the ability to fabricate new porous solids with ordered structures from a wide range of different materials [1].

The formation of mesostructured silica using surfactants as the structure-directing agents was firstly reported in the early 1990's independently by scientists from the Mobil Oil Corp. and by Kuroda's group. The obtained materials exhibit high surface area and pores having tunable dimensions within the range 2–10 nm and a narrow pore size distribution. Such materials have several potential applications, such as heterogeneous catalysis, separation processes and host–guest chemistry. This route of synthesis immediately attracted attention in the materials science community and it is no overstatement to say that surfactant-templated synthesis of mesoporous materials has become a new field of research positioned at the border between surface chemistry and materials chemistry. Since then, ordered mesoporous materials have been extensively studied. In addition, hierarchical porous materials have been synthesized since a surfactant templating route produces such mesoporous materials with a limitation of pore size up to 30 nm. The development of ordered porous materials with pore size beyond 50 nm (macropores) was reported for the first time using colloidal templates, for example polystyrene latex spheres in a colloidal solution and oil droplets in an oil-in-water emulsion. Later, various authors reported the synthesis of macroporous materials using polymer gels, vesicles, foams and bacteria as templates. These materials are made by using self-organizing systems, as templates for the deposition of inorganic materials. In this manner it is possible to have a porous system at two or three different scales in an ordered structure with interconnectivity between pores. Materials with hierarchical pore systems benefit applications that rely on rapid distribution of molecules to a large surface area with minimal pressure build-up, such as heterogeneous catalysis. The specific architecture of porous solids, including pore size ranges and distributions, pore orientation and pore interconnectivity, can significantly influence the diffusion and reactivity of guests.

However, before coming to applications of whom in the field of catalysis, biochemistry or the others, it is essential to control the parameters that influence their structural and textural

characteristics of these materials. To carry out this study the phase behavior of surfactant is essential as it is known that the physico-chemical properties of surfactant have a significant influence on the characteristics of porous materials. We focused our work on the use of nonionic hydrogenated and fluorinated surfactants. Many literatures are devoted to the study of hydrogenated based systems. In contrast, fluorinated surfactants have been little exploited. Thanks to their high thermal stability, these compounds are considered to be the good candidates for the synthesis of porous materials. Our approach consists the study of the surfactant phase behavior in water. We also examined the effect of the solubilization of various additives, such as alkanes, fluorocarbons and alcohols. These systems are then used to prepare porous materials. Our goal is to find the correlations between physico-chemical characteristics of surfactant and the properties of the porous materials. This leads to better understanding of the formation mechanism of these materials and identifying the parameters that will govern the properties.

In Chapter I, the first part is devoted to a brief introduction to surfactant based systems and to the solubilization of oil in these systems. Then, a second part describes the main results reported in the literature concerning of porous materials.

In the experimental section, we describe the physico-chemical properties of the studied compounds and the experimental techniques used in this work.

From the study of phase behavior of a nonionic hydrogenated surfactant in water, the influence of various parameters on the characteristics of porous materials prepared with this amphiphile we is examined in detail in Chapter III. Particularly, the effect of addition of alkanes is investigated. After the study of hydrogenated system, we generalized the rule established for the design of macroporous materials by considering fluorinated systems in chapter IV. Herein, we focused on the effect of the solubilization of various fluorocarbons on the properties of recovered materials.

At last, Chapter V is devoted to the investigation of the effect of the various alcohols addition on the characteristics of mesoporous materials prepared from a fluorinated surfactant based-system.

[1] Davis, M. E., *Nature* **2002,** *417*, 813-821.

Chapitre I. Introduction

La préparation de matériaux mésoporeux organisés silicatés à l'aide de tensioactifs, utilisés comme agent structurant, a été réalisée pour la première fois au début des années 1990 par les chercheurs de chez Mobil et le groupe de Kuroda. Les matériaux obtenus présentent une surface spécifique élevée et des pores de diamètre homogène compris entre 2 et 10 nm. Ces caractéristiques confèrent à ces matériaux un réel intérêt dans des domaines variés tels que la catalyse hétérogène, la nanofiltration et la chimie supramoléculaire. Cette voie de synthèse a immédiatement attiré l'attention de la communauté scientifique et la préparation de matériaux mésoporeux à partir de tensioactif est devenue un nouveau champ de recherche qui se situe entre la chimie des interfaces et la chimie des matériaux. Depuis, les matériaux mésoporeux organisés ont été largement étudiés. De plus, d'autres méthodes ont été développées afin de synthétiser des matériaux à porosité plus grande puisque la voie initiale conduit uniquement à des matériaux mésoporeux dont le diamètre des pores est inférieur à 30 nm. Le conception de matériaux macroporeux organisés avec des tailles de pores supérieures à 50 nm a été réalisée pour la première fois à partir d'empreintes colloïdales, comme par exemple les sphères de polystyrène latex dans une solution colloïdale ou les gouttes d'huiles dans les émulsions huile dans l'eau. Dans les années suivantes, de nombreuses études ont été consacrées à la synthèse de matériaux macroporeux en utilisant des gels de polymères, des vésicules, des mousses et des bactéries comme empreinte. Pour la plupart, ces empreintes sont des systèmes auto-organisés et de cette façon, il est possible d'obtenir des systèmes poreux avec une structure organisée à deux ou trois échelles ainsi que des pores interconnectés. Les matériaux à porosité hiérarchisée sont utilisés dans des applications qui reposent sur une répartition rapide des molécules sur une surface élevée «sans accumulation de pression», telles que les supports pour la catalyse hétérogène. L'architecture spécifique de ces édifices poreux incluant distribution et taille, orientation et interconnectivité des pores peut influencer de manière significative la diffusion et la réactivité des molécules.

Cependant, avant d'atteindre le stade des applications dans les domaines de la catalyse, de la biochimie ou autres, il est essentiel de contrôler les paramètres qui influencent les caractéristiques structurales et texturales de ces matériaux. Lors de ce travail, l'étude du comportement de phase du tensioactif est prépondérante, car il est connu que les propriétés physico-chimiques du tensioactif ont une influence significative sur les caractéristiques des matériaux poreux. Seuls des tensioactifs hydrogénés et fluorés non ioniques ont été utilisés

dans ce travail. De nombreux travaux ont déjà été consacrés aux systèmes à base de tensioactifs hydrogénés, tandis que les tensioactifs fluorés ont été peu exploités. Grâce à leur stabilité thermique élevée, ces composés sont de bons candidats pour la synthèse de matériaux poreux. Notre approche consiste à étudier le comportement de phase du tensioactif dans l'eau. La solubilisation de différents additifs, dans ces systèmes tels que les alcanes, les fluorocarbures et les alcools a également été étudiée. Ces systèmes ont ensuite été utilisés pour préparer des matériaux poreux. Le but consiste à mettre en évidence les corrélations entre les caractéristiques physico-chimiques des tensioactifs et les propriétés des matériaux poreux afin de mieux comprendre les mécanismes de formation de ces matériaux et les processus qui les gouvernent.

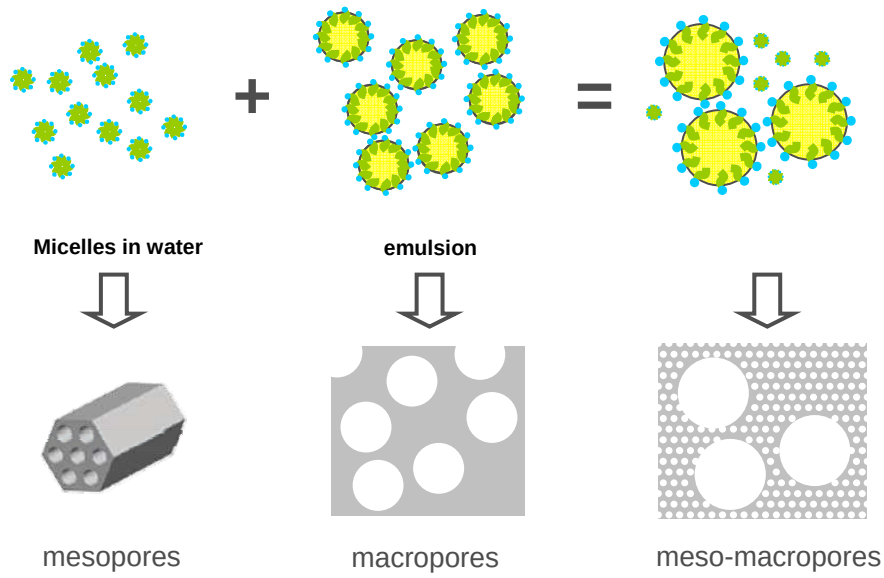
Chapter I. Introduction

1. Surfactants based system 11
1.1 Properties of surfactant molecules 11
1.2 Phase behavior 14
1.3 Highly concentrated emulsions 18
2. Porous materials 20
2.1 Sol-gel process 22
2.2 Material-Templated by Surfactant (MTS) 23
2.3 Hierarchical porous materials 31
3. Context of study 36

I. Introduction

This first chapter aims to introduce some basic notions about surfactant based systems and about porous materials and defining the subject in an introduction, the interface between chemistry of soft matter and materials science. In particular, we examine the factors that affect the behavior of phase surfactants in water and how the phase behavior is related to the characteristics of meso/macroporous materials.

At the beginning of the chapter, we start by recalling some of the basic notions on surfactants and self-Organized Molecular Systems (**OMS**) to formed in aqueous medium. We then introduce the work of the literature dealing with mesoporous and macroporous materials prepared from systems containing surfactants. We will also briefly have a look at the mechanisms involved in the formation of the hybrid mesophase briefly. At last, we will define some relation between the characteristics of mesoporous or macroporous materials and the phase behavior of the surfactant in water, eventually in the presence of oils.



1. Surfactants based system

1.1 Properties of surfactant molecules

The term surfactant is a blend of **surf**ace **act**ive **a**ge**nt** [1]. Surfactants are usually organic compounds that are amphiphilic, meaning they contain both hydrophobic groups (their "tails") and hydrophilic groups (their "heads"). Therefore, they place at the interface between water and oil. Surfactants reduce the surface tension of water by adsorbing at the liquid-gas interface. They also reduce the interfacial tension between oil and water by adsorbing at the liquid-liquid interface. Surfactants are often classified into four primary groups; anionic (carboxylate, sulfonate, sulfate), cationic (salt amine, quaternary ammonium), nonionic (ethoxylated fatty alcohols, ethoxylated alkylphenols, block copolymers) and zwitterionic (amino acids, betaines).

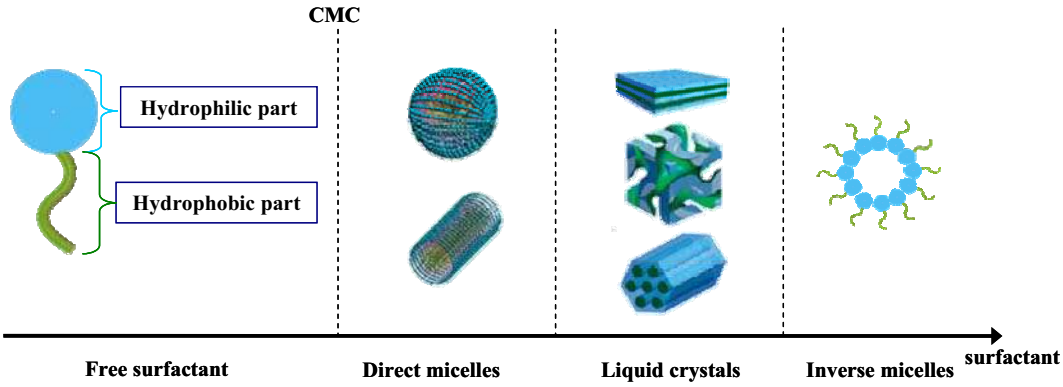


Figure I-1. *Schematic presentation of the self-organized molecular systems for a hydrophilic surfactant*

Surfactant molecules form aggregates through a self-assembly process that is driven by the hydrophobic effect when they are mixed with a solvent, which is usually in a polar medium, i.e. water. The aggregates formed by surfactant molecules are characterized by structures in which the hydrophilic head-groups shield the hydrophobic chains from contact with water. For the hydrophilic surfactant in water, micelles occur only when the concentration of the surfactant exceeds the critical micellar concentration (CMC). Above the CMC the self-assembled surfactant aggregates exist as independent entities, in equilibrium with monomeric surfactants in solution and with no long ranged orientational or positional (translational) order. These dispersions are generally referred to as micellar solution (denoted L_1), the constituent aggregates being known as micelles. At very high surfactant concentration,

inverse micelles (denoted L_2) are formed, the continuous medium formed by the alkyl chains is nonpolar, meanwhile, hydrophilic parts and water are grouped eventually in the center of the aggregate and therefore the curvature is negative. These micellar phases are characterized by their absence of long-range order, an optical isotropy and often low viscosity. Some systems who have more hydrophilic behavior also show a sponge phase (denoted L_3), usually in the dilute region. The L_3 phase is bicontinuous and multiple connected, but the structure is disordered, lacking long-range order. It is known that this kind of structure is composed of two interpenetrating continuums.

True lyotropic liquid crystalline phases are formed as the concentration of surfactant in water is increased beyond the point where the aggregates are forced to be disposed regularly in space. For surfactants that consist of a single hydrocarbon chain the concentration at which the liquid crystalline phases are formed is typically higher than 30 wt. %.

“Liquid crystals” are an intermediate state between crystalline solids and isotropic liquid. Therefore, it is more accurate to call them mesophases. They are stable from thermodynamics point of view and exhibit a long-range order. Some of them show anisotropic properties characteristic of a solid. Compared to components of solids, liquid crystals also exhibit higher mobility of molecules. Liquid crystals may form both in polar and nonpolar solvents and may consist of direct and reverse systems. The basic polymorphic varieties include the following three mesophases:

- *Hexagonal phase*

The hexagonal phase occurs over a wide range of temperatures and surfactant concentrations and can be direct H_1 or reverse H_2. It does not flow as easily as the micellar solution due to its higher viscosity. The hexagonal phase is composed of cylinders whose hydrophilic groups, in case of direct systems, are oriented towards a polar solvent (e.g., water). The cross-section of the cylinders could be round or oval-shaped. They are predominantly long cylinders resembling threads [2].

A fast method used to assess which mesophases appear is polarizing microscopy. Lyotropic liquid crystals show optical changes under polarized light. If a liquid crystal substance is placed under a microscope between crossed polarizers, rotation of polarization plane occurs. Various patterns in diverse textures can be observed in the image obtained. The texture is different for different phases. The hexagonal structures of liquid crystals display a characteristic fan texture under a polarizing microscope (**Figure I-2**).

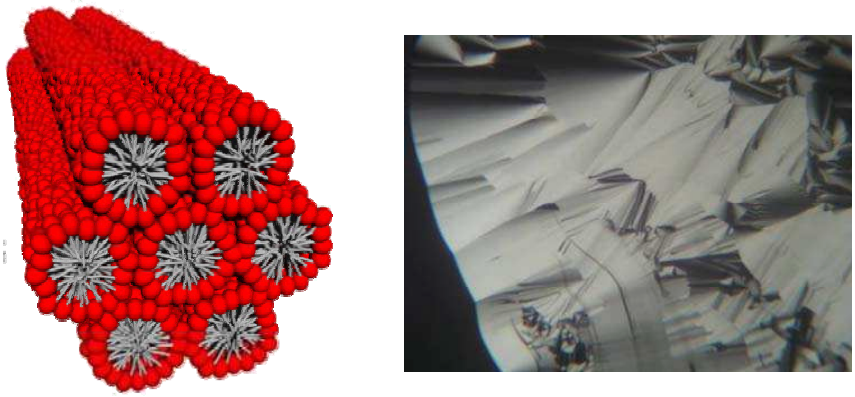


Figure I-2. *Schematic model and texture of hexagonal phase*

- *Lamellar phase*

Lamellar phases appear over a wide concentration range, usually at higher concentrations than those for hexagonal phases [3]. The characteristic feature is a decrease in viscosity compared to hexagonal phases which proves their presence. The viscosity drop is caused by the layer structure of this phase which results in easy slip planes. The lamellar phase consists of bilayers [4]. They have two planes with non-penetrating or mutually penetrating hydrocarbon chains. The sizes of the planes are theoretically limited by the size of the vessel. In fact, the planes are finite-size. The thickness of the layers can be relatively high and it may reach 10 nanometers in the case of dilute solutions [5]. Lamellar structures give “maltes cross” and “oily streaks” structures under polarizing microscope. (**Figure I-3**)

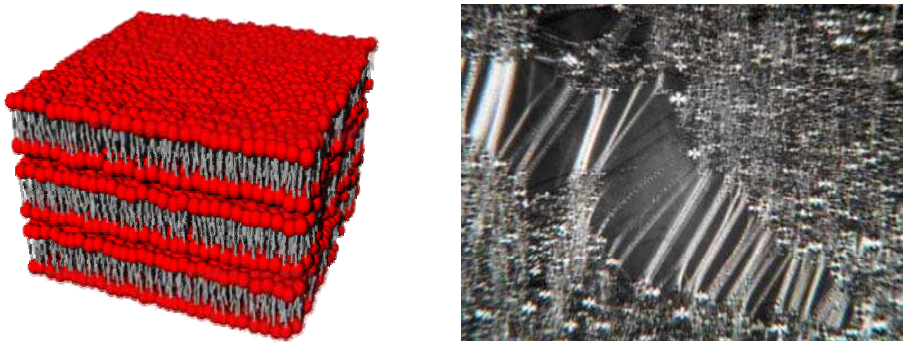


Figure I-3. *Schematic model and texture of lamellar phase.*

- *Cubic phase*

The cubic phases are divided into two distinct classes: the micellar cubic phases and the bicontinuous cubic phases. The direct micellar cubic phases (noted as I_1) correspond to an arrangement of micelles in a cubic symmetry which is body centered cubic (Im3m) or face

centered cubic. In the case of the bicontinuous one (noted as V_1) the surfactant and the solvent form independent mutually penetrating layers. The structures built of double surfactant layers have constant spacing and constant radii of curvature [6]. The most common lattices are described by space groups Ia3d and Pn3m (**Figure I-4**). The cubic phases composed of finite-size micelles appear mostly in a concentration range between the presence of micellar solutions and hexagonal structures, whereas those built of bicontinuous layers appear between concentrations determining the presence of hexagonal and lamellar phases. The reverse cubic phases (I_2, V_2) also exist. Due to its structure, the cubic phase is optically isotropic and appears black under a polarizing microscope. Therefore, small angle X-ray diffraction is the main source of information. Moreover, the cubic phase exhibits a very high viscosity as a result of the absence of slip planes.

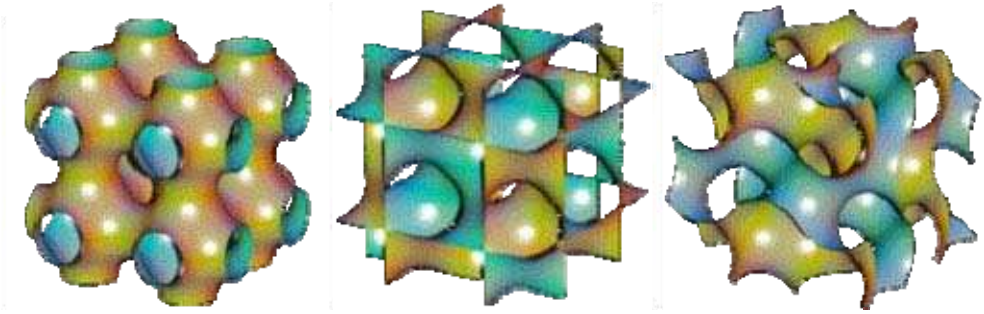


Figure I-4. *Schematic model of bicontinuous cubic phases.*

1.2 Phase behavior

In our work, we have focused on the nonionic surfactant. They are less sensible to the pH of the solution and as regard the preparation of mesoporous materials, they present some advantages. These will be developed in the section 2.2.2 (p. 26).

1.2.1 Solubilization of surfactant in water

Various self-organizing structures are formed in binary water- nonionic surfactant systems [7]. In the binary systems, the phase diagrams are usually drawn as a function of temperature, since the hydrophile-lipophile property of the surfactant is highly influenced by temperature change due to the conformational change in the hydrophilic polyoxyethylene (C_2H_4O) chain

[8]. Although only few types of surfactant aggregates appear in each phase diagram, almost all kinds of surfactant supramolecular assemblies could be formed in the water-surfactant systems if the number of motif C_2H_4O of the surfactant is successively changed at constant temperature [9]. For the surfactants having a hydrophilic characteristic, with increasing the content of surfactant, the self-organizing structures are changed from aqueous micelles to reverse micelles via hexagonal, lamellar and reverse hexagonal liquid crystals [10]. The observed phases correspond to a decrease in the curvature of the palisade layer. The ideal sequence L_1-I_1-H_1-V_1-V_2-L_α-H_2-I_2-L_2 has not been observed entirely yet in the same system.

The phase sequence can be modified by modulating the hydrophilicity of surfactant. To define the hydrophilicity of a surfactant, a parameter called **H**ydrophile-**L**ipophile **B**alance (**HLB**) was introduced [11]. The HLB number for nonionic surfactants can be calculated through the following equation:

$$HLB = 20 * \left(\frac{M_{hydrophile}}{M_{surfac\,tant}} \right)$$

Where $M_{surfactant}$ and $M_{hydrophilic}$ respectively stand for the molecular weight of the surfactant and of the hydrophilic part of the surfactant. This yields an HLB range of 1-20. Nevertheless, this method for determining HLB number is a long and laborious experimental procedure. In addition, Davies [12] developed a method for calculating the HLB number directly from chemical formulas of surfactant, using empirically determined group numbers. Griffin's HLB number is widely used, but we have to emphasize that it is used only to compare the surfactants within a given series.

The phase behavior of nonionic surfactants is affected by their HLB value. For a surfactant with a given hydrophobic chain length, in terms of hydrophilic chain length, different sequences of phases are observed. For straightforward illustration, we carry on **Figure I-5**, the two phase diagrams based on $C_{12}EO_3$ and $C_{12}EO_6$ respectively [7].

$C_{12}EO_3$ molecules (**Figure I-5** a) exhibit a hydrophobic character in the binary diagram. When introduced into the water, they only form lamellar phases and reversed micelles. On the contrary, the molecules of $C_{12}EO_6$ (**Figure I-5** b) show a hydrophilic character. They solubilize in water and form micelles that are capable of solubilizing compounds generally insoluble in water (eg. alkanes). At high surfactant concentrations, they give rise to lyotropic liquid crystals whose structure evolves with increasing concentration in a partial sequence (L_1-H_1-V_1-L_α-L_2) of the ideal sequence given above. According to the scale of Griffin, for an HLB value below 10, number of EO motifs less than 5 and hydrophobic chain consisting 10

to 12 carbon atoms, the surfactant is insoluble in water and the phase diagram

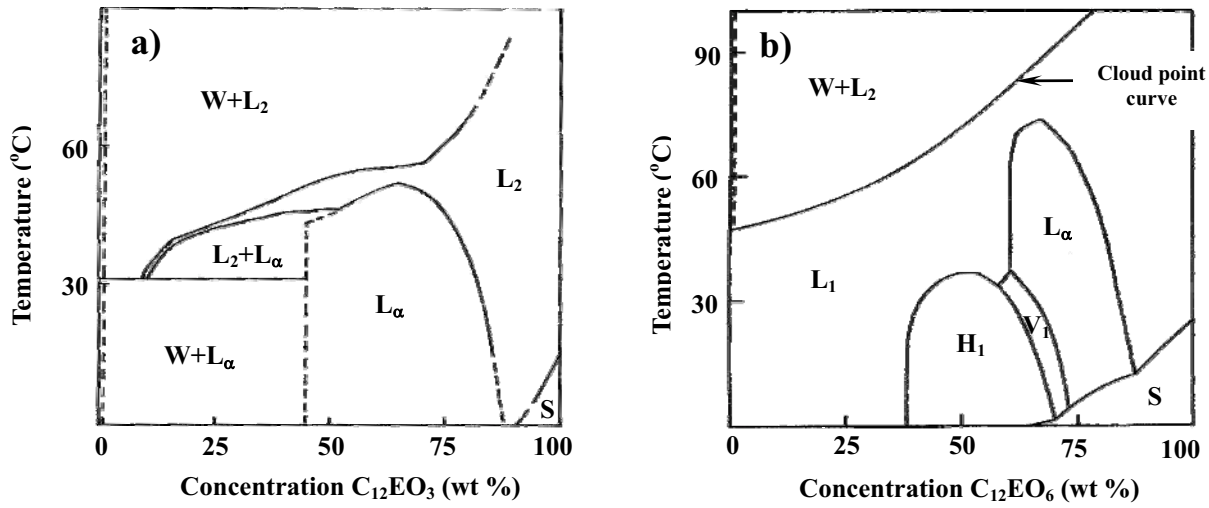


Figure I-5. *Phase diagrams of $C_{12}EO_3$ system (a) and $C_{12}EO_6$ system (b) in water [7]. L_1: Direct micellar solution, H_1: Hexagonal phase, V_1: Bicontinuous cubic phase, L_α: lamellar phase, L_2: reverse micellar solution, W: aqueous solution, S: solid surfactant.*

is characterized by a large dominance of lamellar phase (**Figure I-5** a). For an HLB value above 10, the surfactant is soluble in water. Its diagram looks like to the one reported in **Figure I-5** b, characterized by a liquid crystal domain which is formed by the hexagonal, cubic and lamellar phases. This diagram shows a miscibility curve (or cloud point curve) which is a characteristic of nonionic surfactants. The phase behavior of nonionic surfactants C_nEO_m is sensitive to temperature because of the interactions established between water and oxyethylene chain (EO) (interactions of hydrogen bonds). The appearance of the cloud point is often attributed, in a quite simple way, to a dehydration of oxyethylene groups which causes the demixion. Tiddy et al. [7] proposed that the appearance of the cloud point is related to the balance of intermicellar Van de Waals attractions and hydration repulsion, with the latter decreasing as a function of temperature. For longer EO groups the hydration repulsion is increased and so a higher temperature is required before attractions and repulsions are balanced. Increasing alkyl-chain length increases the attractive force between micelles so lowering the cloud point. At very high temperatures where no mesophases occur at high concentrations, the hydration of EO groups is significantly different from that at lower temperatures.

1.2.2 Solubilization of oil in system based on nonionic surfactants

Nagarajan and Ruckenstein [13] consider two general types of solubilization which are labeled as type I and type II at the beginning of the solubilization process **(Figure I-6)**. For type I solubilization the soluble molecules are located between the surfactant tails in the micelles (penetration effect). For type II solubilization the soluble molecules form a core surrounded by the surfactant molecules as in microemulsions (swelling effect). For nonpolar solutes which would be expected to be located mainly in the hydrocarbon tails region of the micelle, the situation should resemble a mixture of two hydrocarbons.

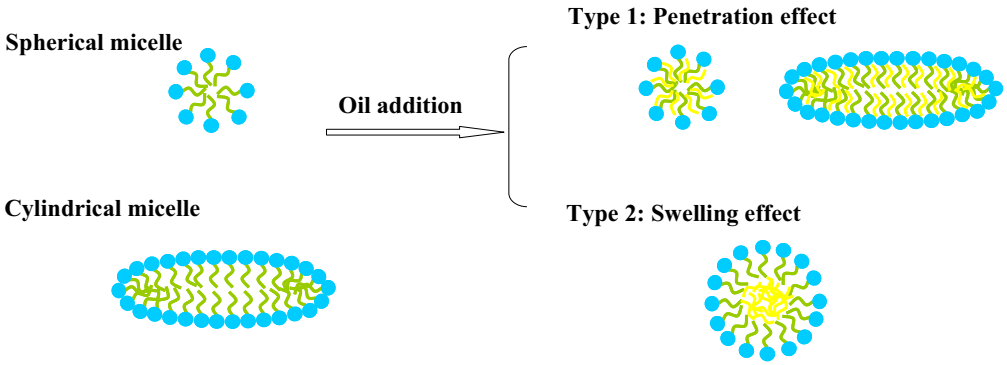


Figure I-6. *Schematic representation of solubilization of oil in micelles [14]*

However, it was noted that the location of the oil molecules can vary with their molecular structure and also with their quantities [15]. For example, at low concentration benzene is solubilized mainly between the chains of micelles, while that beyond a mole fraction of 0.7, a large quantity of these molecules are solubilized in the core of the micelles. It is important to note that the types I and II of solubilization describe ideals cases. Indeed, in practice, the penetration effect and the swelling effect occur often simultaneously.

In a nonionic surfactant/oil/water system, a surfactant can form direct micelles and at low temperature, whereas it forms reversed micelles at higher temperature [16]. The type of emulsion also inverts from O/W to W/O with the increase in temperature. At the transition temperature, there is a three-phase region consisting of water, oil and surfactant phases. Shinoda termed this temperature the **P**hase-**I**nversion **T**emperature (**PIT**) of the emulsion (**HLB** temperature). The PIT is useful index for evaluating the hydrophile-lipophile property of a nonionic surfactant for a given oil: the more hydrophilic the surfactant is, the higher the PIT.

To determine the phase inversion temperature, it is possible to use the method of Friberg [17-19] by drawing a “fish” diagram (so called because of its appearance). To obtain this type of diagram we have to determine the one phase domain labeled as surfactant phase as a

function of temperature and concentration of surfactant for water/oil ratio equals to 1. The concentration of surfactant is plotted on the abscissa and the temperature is on the ordinate (**Figure I-7**). From this diagram we can determine the minimum concentration of surfactant, C* required to solubilize the equal mass of water and oil. The temperature associated with this concentration is the temperature of phase inversion ($\mathbf{T_{HLB}}$). Based on the study of solubilization of hydrocarbon in the hydrogenated nonionic systems, empirical relationships which allow connecting the PIT of the ternary system with the HLB of the surfactant and the molecular structure of oil characterized by **ECN** (**E**quivalent **C**arbon **N**umber) has been established [20, 21]. The **ECN** is identical to the actual number of carbon atoms only for a linear saturated chain. It is defined as the carbon numbers corresponding to the linear saturated oil, which would have the same phase behavior as the considered oil (cyclic, unsaturated or the others). Thus it could be evaluated by measuring experimentally the inversion phase temperature of the system and searching for linear saturated oil which leads to the same **PIT**. Shinoda also determined a relation for calculating the PIT of nonionic surfactant systems [22]. Comparing the values obtained by these two relations, they are in agreement with each other.

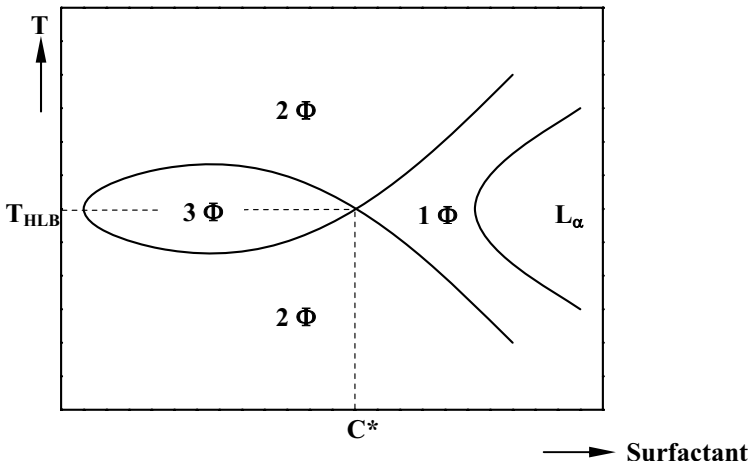


Figure I-7. *Schematic phase diagram plotted as a function of temperature versus concentration of the surfactant [23]*

1.3 Highly concentrated emulsions

Emulsions are heterogeneous mixtures of at least one immiscible liquid dispersed in another in the form of droplets. In most cases, at least one of the liquids will be water or an aqueous solution. Generally, emulsions have average droplet sizes of at least several

micrometers and the droplets have a rather broad size distribution unless special procedures are adopted. Besides, they are metastable and are usually produced by mechanically induced droplet breakup. These systems based of fluorinated composition have been studied in detail by our group and the conclusions have been generalized to the hydrogenated systems. Especially those have been developed by the group of C. Solans. The structure of these emulsions could be determined by optical microscope, small-angle X-ray scattering (SAXS), small-angle neutron scattering (SANS) [24-27] and so on. An emulsion is often described as either-oil-in water (**O/W**) or water-in-oil (**W/O**) where the first phase mentioned refers to the internal (or dispersed) phase. There are three corner-stones guiding practical emulsion formulation which address the type of the emulsions [28]: the Bancroft rule which anticipates the type of the emulsions (direct or reverse) depending on the solubilization of the surfactant in the continuous phase, [29, 30] the Griffin **HLB** scale [11, 31] and the Shinoda phase inversion temperature (**PIT**) concept [32]. If the internal phase volume is higher than 74%, the emulsion belongs to the high internal phase emulsion (**HIPE**) family, also called **highly concentrated emulsions** or **gel-emulsions** [33-37]. The structure of these emulsions resembles that of foams: the water droplets are covered by a very thin layer of continuous phase. Because of their foamlike structure they present a highly viscoelastic behavior that prompted the use of the **gel-emulsion** term to designate these systems [26, 27, 38, 39]. In fact, the volume fraction of the dispersed phase could reach 99%. Optical microscopy of reverse gel-emulsions with water volume fractions near unity revealed a close-packed structure of droplets with polyhedral shape. The shape of the droplets is not spherical but polyhedral because the volume fraction of the internal phase exceeds the limiting value of the close packing of undistorted spheres. The interfacial area is very large although the volume of the continuous phase is very small. As a matter of fact that any further attempt at incorporation above this maximum value brings on a dramatic disruption of the emulsion into two isotropic liquid phases at equilibrium [25]: one phase is a submicellar surfactant solution in water and the other phase is a swollen reverse micellar solution (or water-in-oil (W/O) microemulsion) [40].

Nevertheless, in a reasonable range, gel-emulsions are quite stable despite their low surfactant and oil content, especially some fluorinated emulsions which can be stored for several months without any measurable change in their properties. The nature of the components, the volume fraction of the dispersed phase, the oil/surfactant ratio, the temperature and the presence of additives [41, 42] mainly affect the stability of gel emulsions. The time taken for phase separation can be controlled by appropriate selection of the system

components and temperature [43].

There are different ways to prepare gel-emulsions [44]. One consists of adding the dispersed phase dropwise under gentle stirring to the continuous (microemulsion) phase [27, 38]. Oil-in-water (O/W) gel-emulsions, containing over 90% internal phase by volume, are obtained by adding oil into the direct (L_1) microemulsions whereas W/O gel-emulsions are formed by adding oil into the inverse (L_2) microemulsions [26, 45]. Gel-emulsions may also be formed by the shaking of a closed test tube containing all components (water, surfactant and oil) in the necessary proportions together with small glass beads which trigger the formation of these emulsions [39, 46, 47]. Moreover, highly concentrated emulsion may be prepared through the PIT route from the swollen micellar solution: the highly concentrated water-in-oil emulsions are spontaneously obtained from the oil-in-water micellar solutions (L_1 phase) by a quick increase in the temperature [39, 48, 49], whereas the highly concentrated oil-in-water emulsions are obtained from the L_2 phases by a temperature quench [50, 51]. Gravitational creaming and sedimentation by low speed centrifugation [52-54], ultra-centrifugation [55], or dialysis techniques [56] are used to increase the volume fraction of the internal phase of moderately concentrated emulsions stabilized by nonionic and ionic surfactants. Emulsions with controlled and narrow droplet-size distribution (monodisperse emulsions) are obtained by the steady-state shearing technique [53, 56-59] or by a fractionated crystallization process based on depletion interactions [60, 61].

Owing to their technical applications, highly concentrated emulsions have been extensively investigated and used in a range of common applications, such as pharmaceutics, cosmetic, food technologies and emulsion explosives [62-64]. In addition, it should be noted that they could also be employed as templates for the design of porous materials [65-70].

2. Porous materials

Porous materials have found wide applications in many traditional fields such as catalysis, adsorption, electronics and environmental technology because of their high surface area coupled with many other physical and chemical properties [71-82]. Recently, there has been a rapid growth in emerging areas such as nanotechnology, photonics and bioengineering, which require porous structures with well-defined structural, interfacial, compositional and morphological properties. The famous architect Robert Le Ricolais stated ‘‘the art of structure is where to put the holes’’ [83]. This statement equally applies to the fabrication of porous

architectures, but perhaps it should be rephrased as ‘‘the art of making porous materials is how to control the size and connectivity of the holes’’ [84]. Among the various methods for creating pores, the templating-fabrication strategy can afford a variety of porous networks with a wide range of pore sizes, well-defined morphologies on controllable length scales and various chemical functionalities to match the needs of different applications. Many kinds of porous materials such as (pillared) clays, anodic alumina, carbon nanotubes and related porous carbons and so on, have been extensively described in the literature [85].

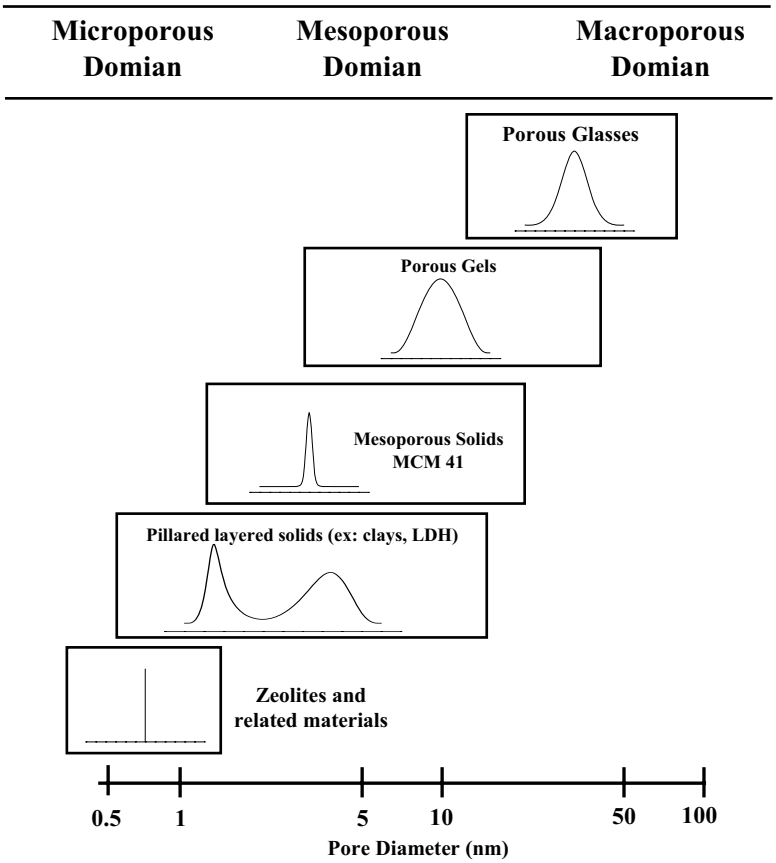


Figure I-8. *Examples of micro-, meso- and macroporous materials, showing pore size domains and typical pore size distributions [82]*

As is well known, porous materials should contain voids as a majority phase, either with random character (disordered pore systems) or with high regularity (ordered pore systems). According to the classification made by IUPAC, porous materials are divided into three classes: microporous (pore size < 2nm), mesoporous (2 – 50nm) and macroporous (>50nm) materials [86]. Some illustrative examples are given in **Figure I-8**. Among the family of microporous materials, the best known members are zeolites which have a narrow and uniform micropore size distribution due to their crystallographically defined pore system.

The structural capabilities at the scale of a few nanometers can meet the demands of the

growing applications emerging in processes involving large molecules, for example, biology and petroleum products. Zeolites or microporous materials, whose pore sizes are less than 2 nm, are far away from these demands. These motivations spark the proliferation of mesoporous and macroporous materials.

In our study, we will focus on mesoporous and/or macroporous silica materials, particularly on hierarchical silica materials. Sol-gel process has been employed to the preparations owing to its economy and the relative simplicity [87].

2.1 Sol-gel process

For introducing what is "**sol-gel process**", we have to expound several definitions first. A **sol** is a stable dispersion of colloidal particles or polymers in a solvent. The particles may be amorphous or crystalline. A **gel** consists of a three dimensional continuous network, which encloses a liquid phase. In a colloidal gel, the network is built from agglomeration of colloidal particles. In a polymer gel the particles have a polymeric sub-structure made by aggregates of sub-colloidal particles. Given all that, the **sol-gel process** may be described as: "Formation of an oxide network through polycondensation reactions of a molecular precursor in a liquid." The idea behind sol-gel synthesis is to "dissolve" the compound in a liquid in order to bring it back as a solid in a controlled manner.

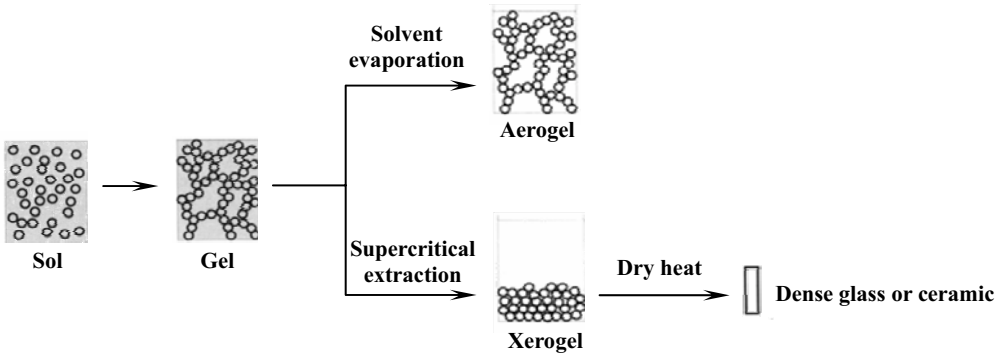


Figure I-9. *Sol-gel processing options*

One of the most widely used routes offering the merits of a low processing temperature with energy savings is using the sol–gel method to prepare nanocomposites. Geffcken and Berger [88] prepared an inorganic oxide film through condensation of nanoparticles using the sol–gel approach in 1939. The sol–gel method became popular in the ceramics industry around the mid-1970s and various types of inorganic glass were manufactured based on this

approach [89]. Philipp and Schmidt [90] and Wilkes et al [91] carried out pioneer works on the preparation of organically modified silicate using various types of alkoxysilane via the sol–gel process. Since then, numerous studies have focused on the preparation of new types of hybrids. Livage and Sanchez et al. [92, 93] reported that they had employed sol-gel processes to prepare Alumina, Titania, Zirconia and Niobium based materials. Factors affecting the final performance of the products include the water/silane ratio, catalyst, reaction temperature and so forth [94].

Silicates easily form gels because it is neither very electropositive nor susceptible to nucleophilic reactions. A typical sol–gel reaction to form silica involves hydrolysis of a tetraalkoxysilane $Si(OR)_4$. The most common ones are tetraethoxysilane ($Si(OCH_2CH_3)_4$) and tetramethoxysilane ($Si(OCH_3)_4$), which are abbreviated in the literature as TEOS and TMOS, respectively.

The elaboration of hybrid materials by bridging organic and inorganic chemistry at a molecular level is now a wide field of investigation. A major appeal of such research activities is probably linked to a synergistic effect carrying advanced properties to the organic-inorganic hybrid materials, which can even be improved in comparison to their own properties. With this respect, the renaissance of sol-gel chemistry [94-96] during the past decade has played a prominent role by providing a versatile method to prepare various solids with well controlled composition, displaying a wide range of attractive properties.

2.2 Material-Templated by Surfactant (MTS)

The first synthesis of an ordered mesoporous material was described in the patent literature in 1969 [97, 98]. However, due to a lack of analysis, the remarkable features of this product were not recognized [85]. In 1992, a similar material was obtained by scientist in Mobil Oil Corporation who discovered the remarkable features of this novel type of silica and leads to a whole field of research [99], meanwhile, the concept of “template” was first postulated in the synthesis of mesoporous silicate materials. In Mobil’s report, quaternary ammonium cationic surfactants such as cetyltrimethyl ammonium bromide ($C_{16}H_{33}N(CH3)_3$-Br, CTAB) were first used as templates to prepare highly ordered mesoporous silicate molecular sieves under hydrothermal, basic conditions. These new family of mesoporous sieves with regular and constant pore diameters in the range of 1.5-10 nm are so called **M41S** [100, 101] which consist on three kinds of materials. MCM-41, which stands

for Mobil Composition of Matter No. 41, shows a highly ordered hexagonal array of unidimensional pores with a very narrow pore size distribution [100, 101]. The walls, however, very much resemble amorphous silica. Other related phases such as MCM-48 and MCM-50, which have a cubic and lamellar mesostructure, respectively, were reported in these early publications as well (**Figure I-10**) [99-101]. At approximately the same time, an alternative, but less versatile approach to prepare mesoporous materials was described by Yanagisawa et al. [102]. Kanemite, a layered silicate, serves as a silica source and the pathway leading to the ordered mesoporous material is thought to proceed via surfactant intercalation into the silicate sheets, warping of the sheets and transformation to the hexagonally packed material. Modifying and optimizing the reaction conditions yields to highly ordered mesoporous silicates and aluminosilicates as well [103, 104]. The obtained materials are designated as FSM-*n*, Folded Sheet mesoporous Materials-*n*, here *n* is the number of carbon atoms in the surfactant alkylchain used to synthesize the material. Since these early discoveries a large research effort has been invested in the synthesis and characterization of a variety of different, although related materials.



Figure I-10. *Representative members of the M41S family [105]*

The emergence of ordered mesoporous materials (**OMMs**) provides not only a series of novel materials that possess large uniform pore sizes (1.5-10 nm), highly ordered nanochannels, large surface areas (~1500 m^2/g) but also an idea of the design of periodic arrangements of inorganic-organic composite nanoarrays. Tremendous research effort was put into the syntheses and applications of these materials. A large variety of mesoporous materials with different mesostructures, such as **HMS** (wormlike) [106], **SBA**-11 (cubic) [107] and **SBA**-3 (hexagonal) [107], etc. and chemical compositions such as silica, metal oxides, [107-114] metal sulfides, [115-117] metals, [118-120] and even polymers and carbons [121, 122], have been synthesized.

2.2.1 Mechanism of formation

A large number of studies have been carried out to investigate the formation and assembly of mesostructures on the basis of surfactant self-assembly. There are two main pathways to synthesize ordered mesostructures: cooperative self-assembly mechanism and "true" liquid-crystal templating process, as shown in **Figure I-11** [123].

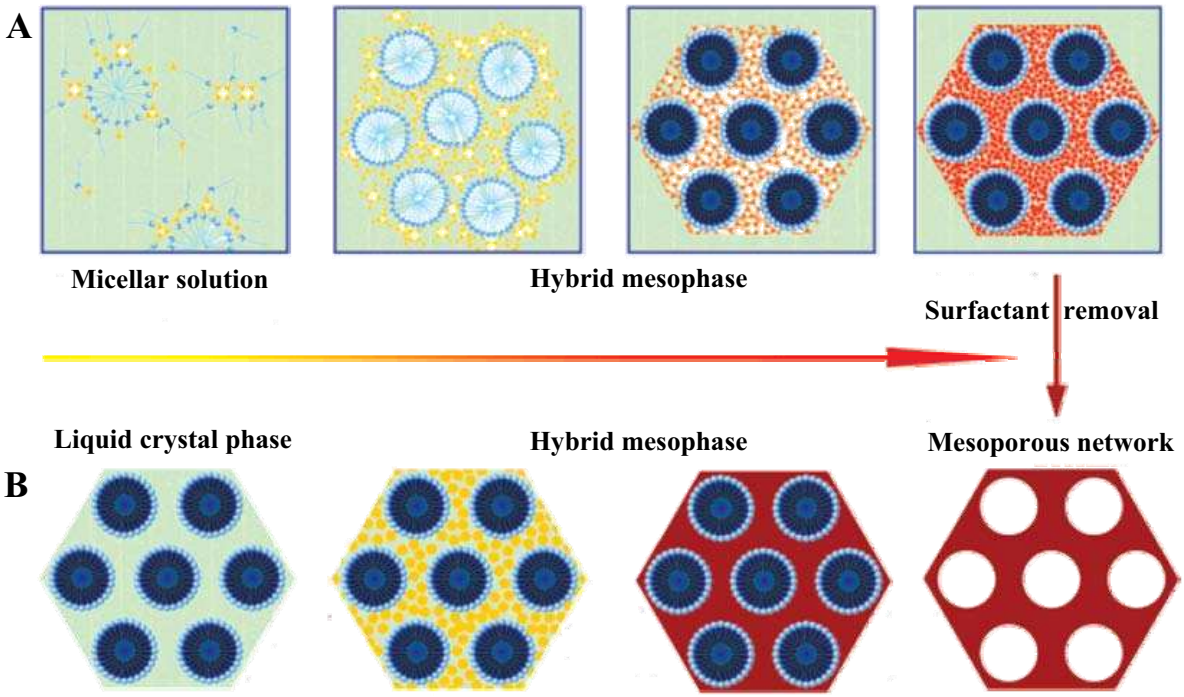


Figure I-11. *Two synthetic strategies of mesoporous materials: (A) Cooperative Self-assembly Templating Mechanism (**CTM**); (B) "True" Liquid-Crystal Templating Mechanism (**LCT**) [123]*

- ***Cooperative Templating Mechanism (CTM)***

In the initial step, the interactions between silica and isolated spherical or cylindrical micelles drive to the formation of an organic-inorganic mesophase. Then, the condensation of the inorganic precursor at the external surface of the micelles occurs. The ordered mesophase is obtained after intermicellar condensation. Finally, the hydrothermal treatment at higher temperature completes the assembly of micelles and the polymerization of the silica source. However, some disagreement concerning the first step of the CTM mechanism appears and numerous investigations were carried out in order to better understand how the surfactant and the inorganic precursor could affect the formation of the hybrid mesophase. Even if the debate concerning the initial step of the CTM mechanism is still opened, it is admitted that the interactions between surfactant and inorganic precursor are responsible for the mesoporous

materials formation.

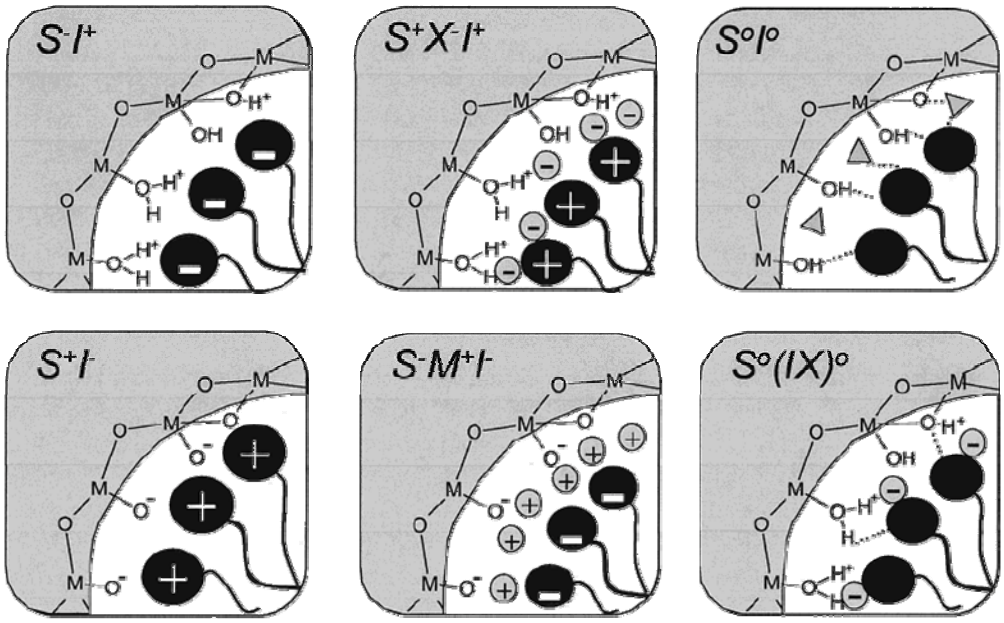


Figure I-12. *Schematic representation of the different types of silica-surfactant interfaces.* ***S*** *represents the surfactant molecule and* ***I****, the inorganic framework.* $\boldsymbol{M^+}$ *and* $\boldsymbol{X^-}$ *represent the corresponding counterions. Solvent molecules are not shown, except for the* $\boldsymbol{I^0S^0}$ *case (triangles); dashed lines correspond to H-bonding interactions [82]*

The cooperative Templating Mechanism is established on a process of cooperative self-assembly, as a result of favorable electrostatic interactions or H-bonding at the inorganic-organic interface. In the case of ionic surfactants, the silicate species in solution play a more active role in directing the formation of the organic-inorganic mesophase through the charge balance with the surfactant ions. The formation of the mesostructured material is mainly governed by electrostatic interactions. In the simplest case, the charges of the surfactant (S) and the inorganic precursor (I) are opposite, in the synthesis conditions (pH). Two main direct synthesis routes have been identified: S^+I^- and S^-I^+ [107]. Two other synthesis paths, considered to be indirect, also yield hybrid mesophases from the self-assembly of inorganic and surfactant species bearing the same charge: counterions get involved as charge compensating species. The $S^+X^-I^+$ path takes place under acidic conditions, in the presence of halogenide anions ($X^- = Cl^-, Br^-$); the $S^-M^+I^-$ route is characteristic of basic media, in the presence of alkaline cations ($M^+ = Na^+, K^+$). The different possible hybrid inorganic-organic interfaces are schematized in **Figure I-12**. Other synthesis routes rely on nonionic surfactants, where the main interactions between the template and the inorganic species are H-bonding or dipolar, giving birth to the so-called neutral path: S^0I^0 [106, 124]. In the case of superacid condition (pH < 2), silica source will charge positively because of the presence of H^+ ($S^0H^+X^-I^+$). **Table I-1** gives different examples of mesostructured inorganic

materials obtained following the abovementioned paths.

Table I-1. *Examples of synthesis route to mesoporous materials [81, 82, 123]*

Surfactant type	Interactions	Route	pH	Template	Examples
Ionic	Direct electrostatic force	S^+I^-	Basic	CTAB	MCM-41 (hex), MCM-48 (cub), MCM-50 (lam) [100, 101]
		S^-I^+	Aqueous	Phosphates sulphates	Mesoporous Al[107]
	Indirect electrostatic force	$S^+X^-I^+$	Acid	CTAB	SBA-1(cub), [107] SBA-2(hex), [125] SBA-3(hex) [126]
		$S^-M^+I^-$	Basic	Phosphates	W, Mo oxides[107, 127]
Nonionic	H bond	S^0I^0	Neutral	Amine surfactants	HMS [106, 128]
	H bond, electrostatic force	$S^0H^+X^-I^+$	Acid	$C_m(EO)_nOH$	MSU[128], CMI [129]
			Super acid pH<2	$C_m(EO)_nOH$	SBA-11 (cub), SBA-12(hex) [130, 131]
				Poly block copolymer	SBA-15 (hex), SBA-16 (cub) [130, 131]
				Sorbitan ester	KIT-5, KIT-6 [132, 133]

- ***Liquid Crystal Templating Mechanism (LCT)***

The second pathway to the preparation of ordered mesostructures utilizes the liquid crystal phase and it is labeled as the direct liquid crystal templating (LCT) mechanism [134, 135]. The inorganic precursors grow around the liquid crystal. After the polymerization and the condensation, the template can be removed, leaving a mesoporous material whose structure, pore size and symmetry are determined by the liquid crystal scaffold. In addition, the high surfactant concentration templating method often leads to monolithic materials rather than powders which are associated with mesostructured silica prepared from micellar solution [136]. Attard and co-workers synthesized mesoporous silicas using high concentrations of nonionic surfactants as templates and TMOS was added as the silica source [134]. Hydrolysis of the alkoxide generated methanol, which would destroy the liquid crystalline phase. Removal of the methanol through gentle vacuum distillation recreated the phase. The condensation of inorganic precursors is improved owing to the confined growth around the surfactants and thus ceramic-like frameworks are formed. After the condensation, the organic templates can be removed by calcination or extraction. The mechanism involved may seem straight forward and the technique is sometimes referred to as **nanocasting** [80]. The inorganic materials “cast” the mesostructures, pore sizes and symmetries from the liquid-crystal scaffolds. It has mainly been used in combination with nonionic surfactants as

templating agents. One interesting aspect of the direct templating method is that it does not require a specific surfactant–silicate interaction, as does the method of synthesis in a micellar solution.

2.2.2 Mesoporous materials via nonionic surfactant templating approach

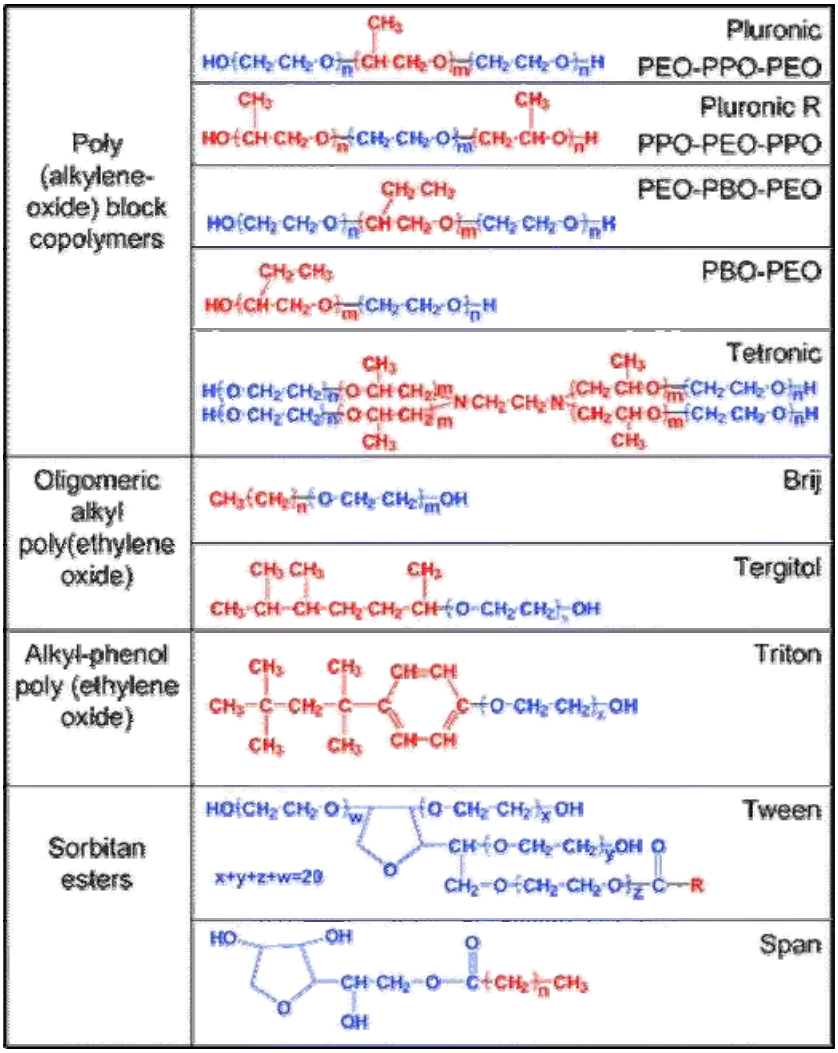


Figure I-13. *Classical commercial nonionic surfactants [137]*

Nonionic surfactants differ from both cationic and anionic surfactants in which the molecules are actually uncharged. The hydrophilic groups are made up of water-soluble moieties (e.g. water-soluble polymer chains). Traditionally, most of nonionic surfactants consist of poly (ethylene oxide) (PEO) chains as hydrophilic groups. They are widely used in industry by reason of attractive characteristics such as low cost, low toxicity and bio-degradation. In addition, nonionic surfactants have a range of ordered micro-scale

aggregates and have become more and more popular and powerful in the synthesis of mesoporous materials. The main classes of nonionic surfactants for synthesizing ordered mesostructures are oligomeric alkyl ethylene oxides, oligomeric alkylphenol ethylene oxides, sorbitan ester surfactants and amphiphilic block copolymers. Commercial nonionic surfactants are frequently used and are listed in **Figure I-13**.

The middle 1990s witnessed efforts to increase the number of mesostructures from a nonionic-surfactant-templating approach [106, 128, 130, 134]. Pinnavaia and co-workers first reported mesoporous silicates templated by organic amines, nonionic oligomeric surfactants and triblock copolymers under neutral conditions and proposed a hydrogen-bonding interaction mechanism, namely N^0I^0 or S^0I^0, where S^0 are amines, N^0 are nonionic surfactants and I^0 are hydrated silicate oligomers derived from tetraethoxy silicate (TEOS) [106, 128]. The products are disordered worm-like mesoporous materials. The pore size distributions are however, uniform and their hydrothermal and thermal stability are high. Attard et al. successfully prepared ordered mesoporous silica structures by using $C_{12}EO_8$ and $C_{16}EO_8$ as structure-directing agents (SDAs) which exhibit pore sizes up to 3.0 nm. Besides, reported by Blin and coworkers [138], well-ordered spherical mesoporous materials with a hexagonal arrangement of channels, analogous to MCM-41, have been directly synthesized by variation of the percentage of $C_{16}EO_{10}$ in aqueous solution. Lately, Wiesner and co-workers [139] conducted illuminating work on the preparation of large pore mesoporous ceramics employing poly(isoprene)-*block*-poly(ethylene oxide) (PI-*b*-PEO) block copolymers as SDAs in an acidic and non-aqueous medium. This suggested that the use of high-molecular-weight block copolymer mesophases instead of conventional low-molecular-weight surfactants provides a simple, easily controlled pathway for the preparation of large-pore silicate mesostructures. Highly ordered mesoporous SBA-15 was then synthesized under strongly acidic conditions by using poly (ethylene oxide) - *block*-poly (propylene oxide)-*block*-poly (ethylene oxide) (labeled as Pluronic) triblock copolymer P123 ($EO_{20}PO_{70}EO_{20}$) as the SDA [130]. The mechanism is most likely via an $S^0H^+X^-I^+$ double-layer hydrogen bonding interaction. Here I^+ are inorganic silicate precursor cations and X^- are counter-anions.

The syntheses of disordered sponge-like or wormholelike mesoporous silica materials templated by nonionic surfactants have also contributed a great deal to the exploiting of organization principles in the surfactant-templating approach. Pinnavaia and co-workers developed disordered MSU mesostructures by using nonionic surfactants as templates under neutral conditions [128, 140]. Acidic and basic solutions are sometimes adopted. Although the mesostructure is disordered, it has uniformly sized mesopores and high surface areas. This

may be one of the reasons for only one broad diffraction peak in the XRD patterns. The pore sizes can be tuned in the range of 2.0–5.8 nm by varying the surfactants. In particular, the pore sizes are very dependent on the synthesis temperature because hydrogen bonds between inorganic species and surfactants under neutral conditions are sensitive to temperature [141-143].

Disordered mesostructures have no unit cell, symmetry and space group. However, the characteristics such as uniform pores, high surface areas and easy modulation offer them good opportunities in catalysis, adsorption, separation and immobilization [144, 145].

2.2.3 Mesoporous materials via nonionic fluorinated surfactant templating approach

As we noted in Part 1 of this chapter, fluorinated surfactants constitute a class of amphiphiles, different from that of hydrogenated surfactants, because of their specific properties [25, 146, 147]. These surfactants have been studied from fundamental standpoint, in terms of physico-chemical and emulsifying, but have been rarely exploited in the field of mesoporous materials until recently. In this context, interest focused on these surfactants is their high thermal stability compared to that of hydrogenated surfactants. Indeed, this property is expected to make hydrothermal treatment at higher temperatures, leading to a better condensation of silica and result in a material with improved hydrothermal stability.

The first mesoporous materials prepared from a fluorinated surfactant were obtained in the laboratory using a nonionic surfactant, $C_8F_{17}C_2H_4(OC_2H_4)_9OH$ [$R^F_8(EO)_9$] provided by DuPont [148]. Mesoporous materials with a hexagonal channel array are prepared at 80 ^oC in a wide range of surfactant contents (5-20 wt.%). The structural and textural analysis shows that these materials have a higher degree of structure compared to those prepared via the hydrogen homologous $C_{16}H_{33}(EO)_{10}$ according to the difference in hydrophobicity of hydrogenated and fluorinated chains ($1CF_2$ = 1.7 CH_2) [149, 150]. This difference may be attributed to the higher volume of fluorocarbon chains. Subsequently, the effect of solubilization of perfluorodecalin (PFD $C_{10}F_{18}$) on the phase behavior of the system $R^F_8(EO)_9$-water and on characteristics of materials has been studied [151, 152].

Kunieda et al. [153] also succeeded in preparing mesoporous materials from fluorinated nonionic surfactant $C_8F_{17}SO_2(C_3H_7)N(C_2H_4O)_nH$ (surfactants provided by Mitsubishi in Japan but not in Europe). By varying the length of the oxyethylene chain (n = 6, 10, 20), the authors followed the degree of structuring of materials prepared at various pH and surfactant

concentrations. The results show that there is an optimal length of the hydrophilic chain (n = 10) for which the hexagonal structures are formed. For values below or above 10, only wormlike materials are obtained. Furthermore, the results show that this fluorinated nonionic surfactants family is suitable for the preparation of materials mesostructures with pore sizes relatively small (between 3.3 and 3.5 nm) and walls thick (greater than 2 nm). Xiao et al. used fluorinated nonionic surfactants with formula $C_5F_{11}C_2H_4(EO)_{10}$ [154] and $C_6F_{13}C_2H_4(EO)_{14}$ [122] to show that it is possible to obtain materials with both, small pore diameter (1.6-4.0 nm) and thick walls (2.5-2.9 nm). A higher degree of structuring material was obtained after the addition of trimethylbenzene without increasing the size of pores. In 2004, Antonietti et al. [155] used mixtures of fluorinated and hydrogenated surfactants. The idea developed from the fact that these two types of surfactants did not mix and form two types of micelles. Thus, condensation of the silica had place on these two types of templates giving rise to mesoporous materials with a bimodal distribution of pore size. Afterward, mixed fluorinated–hydrogenated surfactant-based system $[C_8F_{17}C_2H_4(OC_2H_4)_9–C_{12}H_{25}(OC_2H_4)_8]$ was investigated in the laboratory. Mesostructured silicas with a well hexagonal array of their channels were prepared via a cooperative templating mechanism (CTM) if the loading of fluorinated surfactant is more than 50%. Decreasing the proportion of the fluorinated amphiphile in the mixture leads to the formation of mesoporous silica with a disordered structure. In addition, a study [156] dealing with mixtures of fluorinated $[R_m^F(EO)_n]$ and hydrogenated $[R_m^H(EO)_n]$ surfactants have been done in the laboratory as well. These mixed systems were used as templates for the preparation of mesoporous silica materials via the self-assembly mechanism. Hexagonal mesostructures had been obtained for the ratio between the volumes of the hydrophilic headgroup (V_A) and the hydrophobic part (V_B) in the range of 0.95- 1.78. The main properties of the surfactant which influence the pore ordering in a hierarchical way were also established.

2.3 Hierarchical porous materials

The demand for applications in the encapsulation and separation of proteins, where biomolecules with large molecular weights are involved, drove the development of ordered mesoporous silicas with very large pore sizes, near 30 nm [157, 158]. These practical applications require mesoporous materials having hierarchical pore structures at different length scales in order to achieve highly organized functions, since the limited diffusibility of

substrates through confined nano-channels can be a problem. The development of hierarchical porous materials (**Figure I-14**.) at multiple length scales has attracted much interest over the past few years. The incorporation of ordered mesoporous in macropores materials may be somewhat more interesting and useful for catalysis and for engineering pore systems, in comparison to bimodal mesopore sizes distributions. From the viewpoint of applications, for instance in catalysis, the active sites are often located in the micropores and mesopores, while the macropores favour mass transfer and reduce transport limitations. This becomes particularly important for large molecules (e.g., polymers, biomolecules) or in viscous systems, where diffusion rates are low. For the sake of large performance improvement, such materials should possess adjustable and well-defined macropores and tuneable, interconnected mesopore types of different size in the macropore walls. On all length scales, the larger pores should be connected via smaller pores. Thus, it remains a challenge to fabricate hierarchically bimodal mesoporous–macroporous materials with controlled individual pore sizes and pore structures, although several methods have been reported which combine the individual technologies of mesopore and macropore synthesis, for example, by dual templating of surfactants and colloid crystals [159].

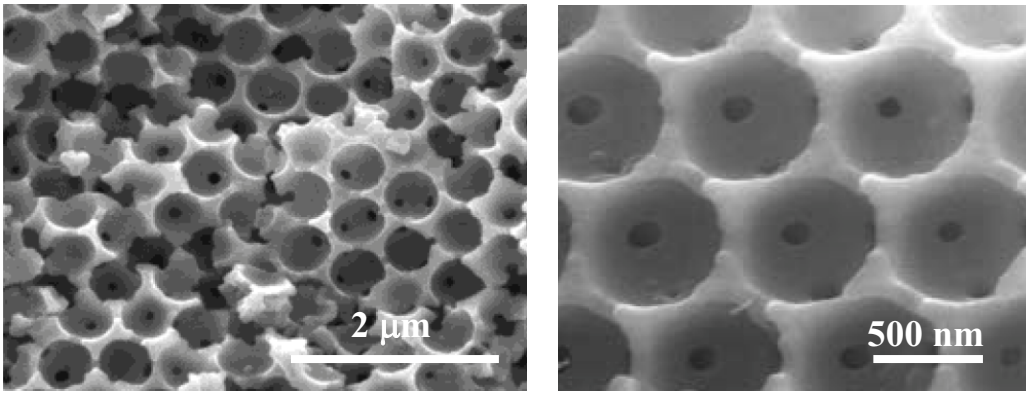


Figure I-14. *SEM of silica material synthesized by using triblock copolymer F127 and cosurfactant butanol. The latex was removed with toluene [160]*

In the synthesis of hierarchical mesoporous–macroporous inorganic oxide-based materials, self-assembled molecular aggregates or supermolecular assemblies are generally employed as the structure-directing agents of mesostructures. Meanwhile, a lot of techniques can be employed for the design of the macroporous network, i.e. emulsions, polymer foams, colloidal crystals, etc. In this section, we will introduce several synthesis strategies of hierarchical meso–macroporous materials mainly, which concern or relate to the present work in the laboratory.

2.3.1 Latex spheres templating

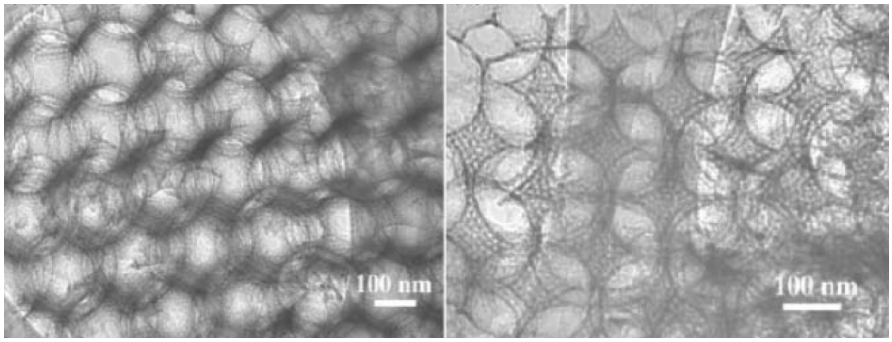


Figure I-15. *TEM images of hierarchical silicas, showing that the framework of the macroporous skeleton is made up of ordered mesoporous silica [159]*

A general procedure of synthesis to generate the macropore network requires the use of latex spheres as templating agents. Colloidal latex spheres, all having the same diameter, are enable to aggregate in a regular way, then the inorganic precursors and surfactant (or copolymer) micellar solution are allowed to infiltrate the spaces between the spheres and this is followed by condensation and crystallization. The removal of the surfactant and colloidal latex spheres, by either high-temperature calcination or solvent extraction, leads to the formation of three-dimensional ordered meso–macroporous materials (**3DOM**) (**Figure I-15**) [159, 161]. More recently, using synthetic latex spheres, Tiddy and co-workers [160, 162] synthesized a series of hierarchically ordered porous silica composites with ordering on three different scales of pore size by using latex spheres and triblock copolymers (Pluronic F127 and P123) as templates in the presence of cosurfactants (n-alcohols) in an acidic medium. The silica materials consist of three-dimensional ordered macropores (200 – 800 nm) with interconnecting, uniform-sized (70 – 130 nm) windows and the walls of these macropores consist of mesostructured pores (3 – 8 nm), as well as a significant microporosity (< 2 nm), presenting a macro-meso-microporous structure with a three-dimensional interconnectivity. The formation of windows is due to the close-packed arrangement of polystyrene spheres (touching points). The meso- and microporosity is generated by the micelle formation of the EO-PO-EO block copolymer in the presence of cosurfactant butanol or pentanol. The surface area and mesopore volume of the materials were low (46 m^2g^{-1}, 0.053 cm^3g^{-1}) when the polystyrene latex was removed by direct calcination at 550 ^oC, while a high total surface area of 531 m^2g^{-1} was obtained after removal of the latex by toluene extraction followed by calcination at 450 ^oC.

2.3.2 Emulsion templating

The method of emulsion templating [163, 164] is perhaps most general and has been used to produce macroporous titania, silica and zirconia with pore sizes from 50 nm to several micrometres, although most of those reported are a disordered macroporous solid without meso- or microporosity. Because the emulsion drops are deformable, macroscopic samples are able to accommodate stresses that arise during gelation and shrinkage. Samples made using rigid spheres, by contrast, tend to break into small pieces that are seldom larger than a few hundred micrometres. In addition, emulsification conditions can be adjusted to produce droplets with different mean sizes which are typically in the micrometre range. Moreover, this can be done to a large extent independently of the self-assembling block copolymer species used to direct the structure of the mesopores. This allows direct and independent control of macro- and mesopore dimensions, so the final pore structures can be tailored to different diffusion and reaction conditions [158].

Introduction of mesoporosity in a macroporous structure has been reported by a surfactant emulsion-mediated synthesis. Tiddy and co-workers [165, 166] use this approach to achieve the room-temperature synthesis of a macro-mesoporous silica material. The formation of macro-cellular foams is explained based on a very simple natural phenomenon of oil-in-water emulsion known as “creaming” which is the migration of the dispersed phase of an emulsion, under the influence of buoyancy. This synthesis was carried out using cetyltrimethylammonium bromide as surfactant and trimethylbenzene as oil. The obtained material has a high surface area (800 m^2g^{-1}) with a narrow pore size distribution center at around 4.0 nm. It is also demonstrated that mesoporous silica could be obtained by using a low oil (mesistylene) concentration, meanwhile under the faster stirring, meso-cellular silica foams will be produced. However, the mesoporous walls adopt a wormhole-like structure.

Cooper and co-workers reported the synthesis of porous emulsion-templated polymer/silica composite beads by sedimentation polymerization of a high internal phase emulsion (**HIPE**) [65]. High surface area silica beads with an average diameter of 1.3 mm, high pore volume of 5.7 cm^3g^{-1} and interconnected macropore structure were obtained by calcination of the composite structures. The **HIPE** structure was retained in the silica beads and the material has high surface area (422 m^2g^{-1}). Indeed, this semi-continuous synthetic procedure could be scaled up to allow the synthesis of significant quantities of beaded materials with a narrow particle size distribution. Carn and co-workers [167] prepared hierarchical inorganic porous monoliths with a double template, i.e. direct emulsion at the macroscale and micellar

templates at the mesoscale. The monolithic materials had typical polymerized high internal phase emulsion (poly-**HIPE**)-type interconnected macroporous network with polydisperse cell and window sizes within the micrometre range. These materials show interconnected macroporosity with disordered structures. The mesopores size varies from 1.2 to 4.0 nm.

As illustrated by these examples the synthesis of well defined macroporous silica with highly ordered mesopores is difficult to perform. However, it was reported in 2006 by the laboratory [168] that the use of oil/water (O/W) fluorinated emulsions to design macroporous-mesoporous silica with well ordered array of mesopores. The emulsion is constituted of fluorocarbon droplets stabilized by the fluorinated surfactant molecules and dispersed in an O/W fluorinated microemulsion. The mesopore size distribution is narrow and centered on about 7.5 nm whereas the size of the macropores varies from 1.0 to 3.0 μm.

2.3.3 Polymerization induced phase separation in the presence of polymers

Chemically induced liquid–liquid phase separation has been applied in the synthesis of siliceous mesoporous materials with co-continuous macropores [169]. This technique is based on the hydrolysis and condensation of inorganic precursors in the aqueous domain, derived from the self-assembly phase of the template used. The earlier the phase separation takes place than the sol-gel transition, the larger the characteristic size of pores and gel skeletons become. A wide variety of water-soluble polymers, such as poly(ethylene oxide), has been used to control the phase separation/gelation kinetics in the preparation of monolithic silica of virtually any shape exhibiting both interconnected macropores and textual mesoporosity. With use of various Si precursors such as tetramethoxysilane, tetraethoxysilane and bis(trimethoxysilyl)-ethane, amorphous or disordered mesopores can be embedded in gel networks which constitute a co-continuous macroporous structure [170, 171].

Nakanishi and co-workers [172, 173] synthesized monolithic pure silica gels with a hierarchical macro-mesoporous structure via a spontaneous sol-gel process and yielded materials with highly ordered 2D-hexagonal arrays of mesopores. The authors explain that the monolithic body with well-defined co-continuous macropores is a result of concurrent phase separation and sol-gel transition induced by the polymerization reaction, whereas the mesopores are templated by the co-operative self-assembly of inorganic species and poly(ethylene oxide)-*block*-poly-(propylene oxide)-*block*-poly(ethylene oxide), as structure-directing agent.

3. Context of study

Based on the work reported in the literatures, we have investigated the preparation and characteristic of hierarchical porous materials by using the concept of the template for creating the macropores and the cooperative template mechanism for the mesopore formation. Majority of the **gel-emulsions** which we have studied in detail are adapted to the preparation of the meso-macroporous materials. In fact, the systems on which we focus consist of oil droplets dispersed in a continuous phase which consists of an O/W microemulsion. If the oil volume fraction is very high, the droplets could be deformed into polyhedra, which are separated by the thin films of the continuous phase. Thus the mesoporous network should be created from the continuous medium, whereas the macropores formed due to the oil droplets. In addition, the high volume of dispersed fraction of oil (>74%) generates numerous droplets which also form the “close packed arrangement” and the “windows” [174].

Thanks to their high chemical and thermal stability, fluorinated surfactants attract more and more interests as template for the preparation of porous materials. However, for the sake of developing preparation method of materials, we had used the hydrogenated system to prepare the concentrated emulsions at first (chapter III), which presented the same structure with the fluorinated ones (chapter IV).

Chapitre II. Partie expérimentale

Pour réaliser le travail présenté dans ce rapport, différentes techniques ont été utilisées dans le but de caractériser les systèmes à base de tensioactif (diagramme de phase et structure des cristaux liquides) et les matériaux poreux (structure, texture et morphologie). Ce chapitre présente la description des produits, les méthodes de caractérisation des molécules de tensioactif et le protocole utilisé pour la synthèse des matériaux poreux. Enfin, les techniques analytiques utilisées dans cette étude sont également décrites.

Chapter II. Experimental part

1. Materials 43
1.1 Surfactants 43
1.2 Hydrogenated compounds 44
1.3 Fluorocarbons 44
2. Phase diagram determination 47
3. Preparation of porous materials 48
3.1 Source of silica 48
3.2 Preparation of the mesoporous materials 49
4. Techniques of characterization 50
4.1 Polarized light microscopy 50
4.2 Small angle X-ray scattering (SAXS) 52
4.3 Nitrogen adsorption-desorption analysis 56
4.4 Dynamic light scattering (DLS) 59
4.5 Scanning electron microscopy (SEM) 60

II. Experimental part

To conduct the work presented in this thesis, several techniques have been used in order to characterize surfactant-based systems (phase diagram and structure of liquid crystals) and porous materials (structure, texture and morphology). This section presents the description of the products, characterization methods of surfactant molecules and the protocol used for the porous materials synthesis. At last, the analytical techniques used in this study are also described.

1. Materials

1.1 Surfactants

This work focuses on the use of nonionic surfactants which are all made of a hydrophilic part consisting of oxyethylene groups (OC_2H_4). The hydrophobic part consists of a linear hydrogenated or fluorinated alkyl chain. **Table II-1** shows their physical-chemical data. In the case of fluorinated surfactant, the presence of a spacer making the link between the hydrophilic and hydrophobic part is necessary. This spacer may consist of one or several methylene groups or by functional groups. For the surfactants studied in this work, the spacer consists of two methylenes.

Table II-1. *Physical-chemical data of used surfactants*

Label	Formula	ρ ($g.ml^{-1}$)*	M ($g.mol^{-1}$)	V_{mol} ($cm^3.mol^{-1}$)	Suppliers
$R^H_{12}A(EO)_9$	$C_{12}H_{25}CO(OC_2H_4)_9OCH_3$	1.00	618	618	Huntsman
$R^H_{12}(EO)_4$	$C_{12}H_{25}$ $(OC_2H_4)_4OH$	0.95	362	381	CECA
$R^F_8(EO)_9$	$C_8F_{17}C_2H_4(OC_2H_4)_9OH$	1.39	870	626	DuPont
$R^F_7(EO)_8$	$C_7F_{15}C_2H_4(OC_2H_4)_8OH$	1.35	744	551	DuPont

** The density is given at 20 °C*

The surfactant $C_{12}H_{25}CO(OC_2H_4)_9OCH_3$ (labeled as $R^H_{12}A(EO)_9$), provided by Huntsman, has an average chemical structure. The hydrophilic chain moiety exhibited a Gaussian chain length distribution and the hydrophobic part is composed of well defined mixture of $C_{11}H_{23}$- and $C_{13}H_{27}$- tails.

The surfactant $C_{12}H_{25}(OC_2H_4)_4OH$ (labeled as $R^H_{12}(EO)_4$) provided by CECA. It should be pointed out that, as a large part of the commercial products, the hydrophobic and hydrophilic chains are not exactly defined. In this case, they are defined by the number-average molecular weight of hydrophobic and hydrophilic chains.

The used fluorinated surfactants $R^F_8(EO)_9$ and $R^F_7(EO)_8$ are provided by DuPont. Concerning the hydrophilic chain moiety, it exhibits a Gaussian chain length distribution. Thus, the subscript of the formula corresponds to an average value. The hydrophobic part is made by the mixture of chains with definite length. The calculation of number-average molecular weight allows us to define the average length of the hydrophobic chains. For

example the average number of fluorinated carbon for $R^F_8(EO)_9$ is 8, whereas for $R^F_7(EO)_8$ it is 7.

1.2 Hydrogenated compounds

A series of alcohols (iso-propanol, butanol and 1-octanol) with different number of carbons are used. Result from their hydropholicity, the solubility of alcohols in water is in the sequence as methanol and isopropanol (miscible) > butanol (7.9 g/100 mL (20 °C)) > 1-octanol (immisible).

Moreover, a series of linear alkanes (octane, decane and hexadecane) with different length of carbon chain is also used in this work. Cyclohexane which comprises a ring molecule with a six-fold symmetrical structure that can adopt either a trans or a cis conformation, is involved as well. **Table II-2** shows the physical-chemical data of hydrogenated compounds.

Table II-2. *Physical-chemical data of used hydrogenated compounds*

Chemicals	Formula	M ($g.mol^{-1}$)	ρ ($g.ml^{-1}$)*	Grade	Suppliers
Methanol	CH_3OH	32	0.79	≥99.9%	VWR
Isopropanol	$(CH_3)_2CHOH$	60	0.785	≥99.8%	Carlo erba
Butanol	C_4H_9OH	74	0.81	≥95%	FLUKA
1-Octanol	$CH_3(CH_2)_7OH$	130	0.82	≥99.5%	Sigma-Aldrich
n-Octane	C_8H_{18}	114	0.70	≥98%	Merck-Shuchardt
Decane	$C_{10}H_{22}$	142	0.73	≥95%	FLUKA
n-Hexadecane	$C_{16}H_{34}$	226	0.77	≥99%	Merck-Shuchardt
Cyclohexane	C_6H_{12}	84	0.779	≥99.5%	PROLAB

** The density is given at 20 ^oC*

Both alcohols and alkanes are used as additives to study their solubilization in the surfactant-based systems. Furthermore the effect of the incorporation of these auxiliaries on the preparation and characteristic of porous materials is also investigated.

1.3 Fluorocarbons

Most of these perfluorinated organic liquids are synthesized for industrial use because of

their value as electrically non conductive, chemically nonreactive and heat stable liquid heat exchangers, leak detectors and hydraulic fluids [175]. Their high solubility for gases, especially oxygen and carbon dioxide [176], has achieved important status because of the possibility of utility in artificial blood and liquid breathing [177]. Due to their oleophobic character, fluorocarbons are unable to solubilize into hydrogenated surfactant systems. On the contrary, they can solubilize into fluorinated surfactant systems, leading to the formation of various structures such as swollen micelles, microemulsions, liquid crystals [147, 149] and concentrated emulsions [26].

Recent works have demonstrated that fluorinated surfactants can be employed for the synthesis of highly ordered mesoporous silica [148, 156, 178]. In our study, different fluorocarbons have been used as oil to prepare microemulsions and emulsions. The effect of the fluorocarbon structure on the properties of the porous materials prepared from the systems has also been examined.

- *The perfluorodecalin*

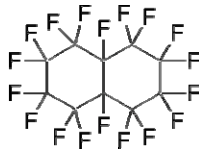


Figure II-1. *Molecular structure of perfluorodecaline*

The perfluorodecalin (labeled as PFD, Aldrich), of molecular formula $C_{10}F_{18}$, consists of a structure in two cycles. The product is constituted by a mixture of isomers cis and trans of composition 45/55 [179].

As the majority of the fluorocarbons, perfluorodecalin has a quite high density at 20°C, almost twice as much as the one of water.

- *The 1-bromo-perfluorooctane*

The 1-bromo-perfluorooctane (labeled as PFOBr, Aldrich), of molecular formula $C_8F_{17}Br$, is a linear molecular, containing a highly polarizable terminal bromine atom. Due to its high polarizability, the bromine atom brings to the molecule a more lipophilic character than the other fluorocarbons [180, 181].

- *The bis (F-butyl)-1,2-ethylene*

The bis (F-butyl)-1,2-ethylene (labeled as F44E, Atochem), of molecular formula

$C_4F_9CH=CHC_4F_9$, is a linear molecule containing an unsaturated double bond CH=CH in the middle of the chain [182]. It was shown that the insaturation brings more lipophilic character to the molecule than a saturated group.

- *The perfluoro-1-Octanol*

Fluorinated alcohols are a class of linear, long-chain, polyfluorinated alcohols (FOHs). They have the generic structure $C_nF_{2n+1}CH_2CH_2OH$. In our study, whereas we used several hydrogenated alcohols such as isopropanol, butanol and octanol as the addictives into our systems, for the sake of comparing to octanol, we chose the perfluoro-1-octanol $C_6F_{13}CH_2CH_2OH$ (Clariant France) as one of the additives to investigate the solubilization effect of different type of alcohols to the fluorinated surfactant based systems.

As we can see from the formula, there is an ethylene group spacer connecting the fluorinated chain and the OH group. The strong increase on hydrophobicity of perfluoro-1-octanol was attributed to the higher fluorocontent of the chain.

Table II-3. *Physical-chemical data of used perfluorocarbons*

Fluorocarbon	**Formula**	**M (g.mol^{-1})**	**ρ (g.ml^{-1})***	**CST_{BrHex} (^oC) [182]**
PFD	$C_{10}F_{18}$	462	1.95	123
F44E	$(C_4F_9CH=)_2$	464	1.62	117
PFOBr	$C_8F_{17}Br$	499	1.93	69
Perfluoro-1-Octanol	$C_6F_{13}C_2H_4OH$	364	1.65	—

** The density was given at 25 ^oC*

After all, fluorochemicals containing halogens or hydrocarbon blocks present a kind of decrease of their lipophilicity who could be evaluated by using a critical solution temperature in n-hexane (CST_{hex}) method [151]. The CST_{hex} is the temperature at which equal volumes of fluorochemical and n-hexane form a single isotropic phase. The lipophilicity of a fluorochemicals increases as the value of CST_{hex} decreases. But the CST value of high lipophilic fluorocarbons cannot be determined in n-hexane directly because of the upper consolute boundary occurring at temperatures is too low to measure. Thus, Weers et al. [182] proposed to another method which measures the CST as a function of n-bromoalkane chain length and extrapolates to n-bromohexane for reference. The CST value using n-bromohexane as the reference are much higher than those observed for n-hexane, thereby moving the CST

for lipophilic fluorochemicals into a measurable temperature range. For example, for PFOBr the CST_{hex} value is evaluated at -24°C, while the CST_{Brhex} value is 69°C. The n-bromoalkane family raises the CST due to increases in the distortion polarizability and isopotential surface area relative to n-alkanes. This method was applied for a great number of fluorocarbons and three of them were used in our study. **Table II-3** shows their CST_{BrHex} and some primary physical-chemical properties.

2. Phase diagram determination

The phase diagrams are established by preparing samples over the whole range of surfactant/water compositions. The required amounts of surfactant, oil and water were introduced into well-closed glass vials to avoid evaporation. They were homogenized by vortex and centrifugation (if necessary). For ternary diagrams, firstly the mixture of surfactant and water were prepared, then the additive was introduced into the system in a successive addition way. The prepared samples were placed in a thermostatic bath and depending on the system, they were allowed to stand from a few hours to several days at the given temperature to reach equilibrium (variable time depending on the sample viscosity). The examination of each sample consists of noting the number of the present phases, their optic properties and their viscosities. Micelle solutions and microemulsions were characterized by visual observation. The average hydrodynamic radius of the microemulsion droplets was measured by dynamic light scattering with a Malvern 300HSA Zetasizer instrument.

The liquid crystal phases were identified by visual inspection with a polarizing light microscope (Olympus BX 50) due to their texture characteristics. The small angles X-ray scattering (SAXS) has been used to delineate precisely the boundary lines of the liquid crystal domains, examining the evolution of the Bragg-distance which is associated to the first peak in the SAXS patterns .

Pseudo-Shinoda diagrams have been established to determine the solubility of the oils in the aqueous solution of surfactant as a function of the temperature, according to the method previously used by Shinoda and Ogawa [183]. These diagrams are drawn for various water/surfactant weight ratios (R) in order to cover the domain of micellar solution domain for the investigated oils.

The appearance of the samples is observed by naked eyes and then by crossed polarizes if necessary. The isotropic phase obtained for each water/surfactant ratio is limited by two

curves. (**Figure II-2**) The lower curve, shown by the open circles, is the solubilization curve above which microemulsions form. The upper curve, shown by the solid circles, is the cloud point curve. When the mixtures were brought at temperatures above this latter curve, they appeared macroscopically biphasic, comprising a lower viscous and whitish phase and an upper fluid and transparent phase. While the equilibrium time to establish the solubilization curve was rather long (in particular at high oil amounts), the cloud point curve was easily obtained and the samples turned opaque instantaneously. This latter phenomenon was reversible and after cooling the mixtures, a single isotropic phase was obtained again, whereas it took a long time before reaching the demixion of the microemulsions by cooling.

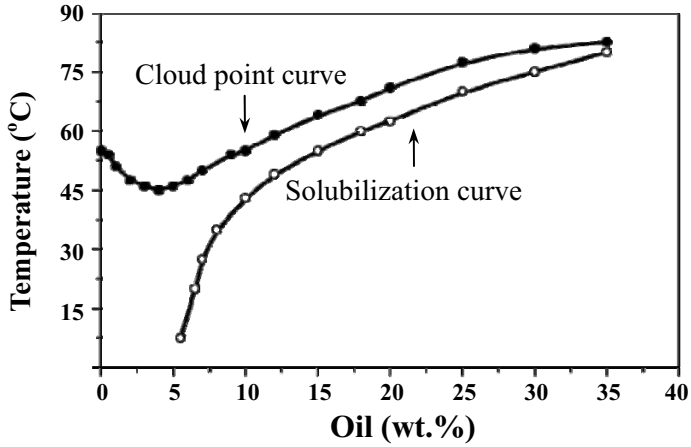


Figure II-2. *Pseudo-Shinoda diagram established for a given water/ surfactant ratio*

3. Preparation of porous materials

3.1 Source of silica

The source of silica used in this work is tetramethoxysilane (labeled as TMOS). Its formula is Si $(OCH_3)_4$. The formation of silica network involves two consecutive reactions [184]:

An initiation reaction, **hydrolysis**, which leads to the formation of hydroxyl groups Si-OH:

$$(CH_3O)_3\text{-Si-}OCH_3 + H_2O \rightarrow (CH_3O)_3\text{-Si-OH} + CH_3OH \quad (1)$$

A successive reaction, **condensation**, which leads to the formation of bridging oxygen:

$$(CH_3O)_3\text{-Si-}OCH_3 + HO\text{-Si-}(CH_3O)_3 \rightarrow (CH_3O)_3\text{-Si-O-Si-}(CH_3O)_3 + CH_3OH \quad (2)$$

$$(CH_3O)_3\text{-Si-OH} + HO\text{-Si-}(CH_3O)_3 \rightarrow (CH_3O)_3\text{-Si-O-Si-}(CH_3O)_3 + H_2O \quad (3)$$

The formation of a gel can take several days or several weeks. To accelerate the reactions, it is possible to vary the pH. Indeed, the reaction condensation of silicates involves

mechanisms with strong pH dependence [184]. Therefore catalysts acidic or basic conditions are often used in sol-gel reactions. The behavior of silicic acid will be considered in different pH regions, **Figure II-3** shows the general relationship between pH and stability of silicic acid or colloidal silica with regard to gelling.

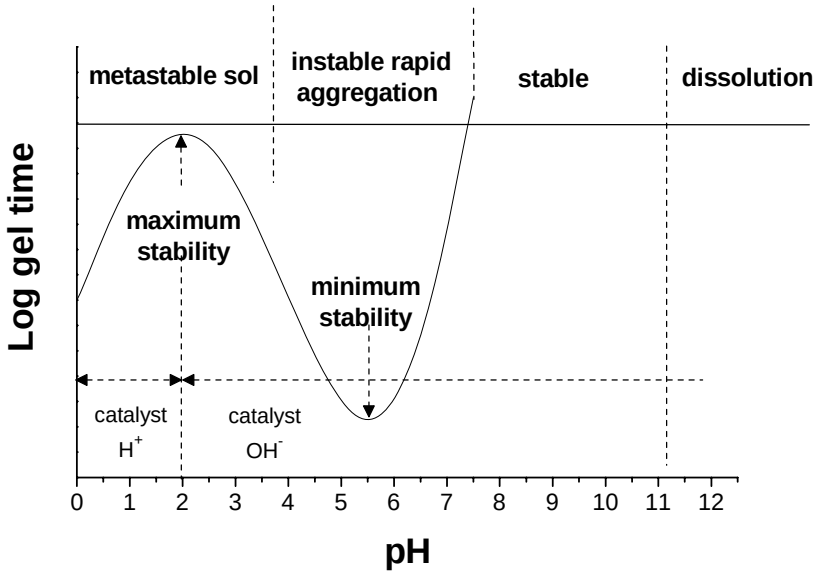


Figure II-3. *Sol stability: relation between log (gel time) vs. pH [184]*

Above about pH 6 or 7, in the absence of soluble salts, silica bears a strong negative charge and gel formation is slow or prevented. Gelling is most rapid at 5 to 6 where the gel occurs rapidly and leads to reactions formation of gels of hydrated amorphous silica [SiO_2,$_x$$H_2O$]. Form about pH 2 to 5, the charge on silica or silicic acid is low, so that presumably the molecules can readily collide. However, in this region the rate of condensation between polysilicic acid molecules depends on the concentration of hydroxyl ions; the OH^- ion is therefore a catalyst for the condensation reaction. At pH values lower (around pH 2), it presents a maximum, that means the system has enough time to complete the hydrolysis of the precursor inorganic silica and the polymerization is progressive. Below pH 2, the rate of polymerization or gelling increases with greater acidity. The rate in this region below pH 2 is proportional to the concentration of H^+.

3.2 Preparation of the mesoporous materials

First, a micellar solution is prepared by dissolving the surfactant in an aqueous solution. The pH value of the solution is adjusted with sulfuric acid. The mixtures are homogenized by stirring (300 rpm) before the addition of tetramethoxysilane (TMOS). Then TMOS is added

dropwise at controlled temperature until reaching a molar ratio surfactant/ TMOS 0.5 while the solutions are kept under stirring for 1 h. Generally speaking, the total amount of solution prepared is 10 g. The obtained mixtures are sealed in Teflon autoclaves (20 ml) and are allowed to undergo hydrothermal treatment at 80 ^{o}C for 24 h. Ethanol extraction is carried out twice with a Soxhlet apparatus for 48 h. The scheme of the preparation is shown in the **Figure II-4**. The addition of oil gives rise either to microemulsion where oil is solubilized in the hydrophobic core of micelles or to emulsions. The oil composition is chosen according to the phase diagram for the preparation of porous materials.

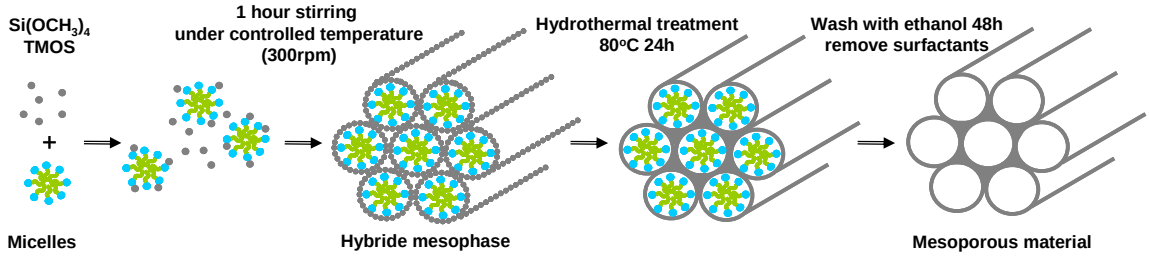


Figure II-4. *Scheme of the method for preparing a mesoporous material with hexagonal structure*

The recovered powder was dried at room temperature and then their characteristics (structure, texture and morphology) are determined by different techniques described below. The structure is determined by Small Angle X-ray Scattering (**SAXS**). The textural properties (i.e. specific surface area, pore size distribution and pore diameter) are obtained by the nitrogen adsorption-desorption analysis. The morphology of the materials is defined by scanning electron microscopy.

4. Techniques of characterization

4.1 Polarized light microscopy

A polarizing microscope is a microscope equipped with two perpendicular polarizing filters named polarizer and analyzer. The polarizer allows the polarization of light in a particular direction. In fact, natural light vibrates in all directions on a perpendicular plane to the direction of propagation. After passing through a polarized filter, it vibrates in a specific direction. The passage of this light polarized through an anisotropic crystal causes a doubling of the light beam initial two rays of different polarizations which propagate at two different speeds. This phenomenon, called birefringence, is due to the difference in index of refraction

anisotropic compounds whose optical properties are different depending on the direction of propagation of light ray. The analyzer, placed after the sample is oriented perpendicular to the polarizer, allows the merger of the two light beams and the image obtained is the result of interference between two rays having different speeds of propagation.

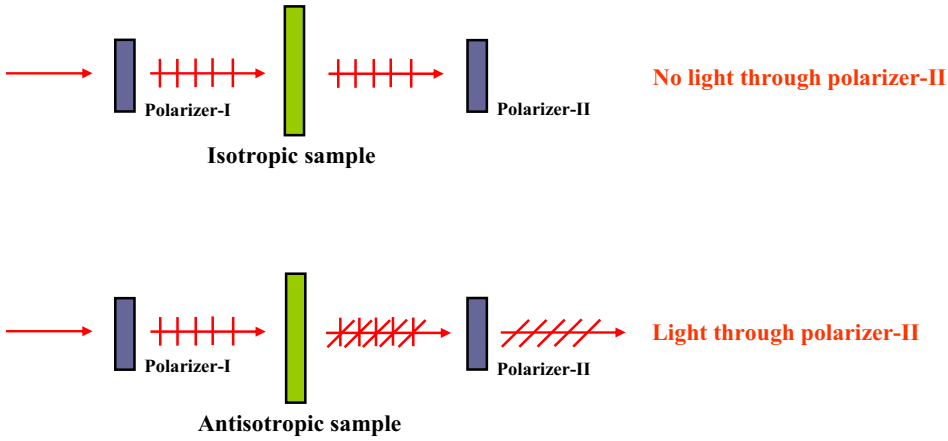


Figure II-5. *Optical properties of isotropic and anisotropic materials under polarized light*

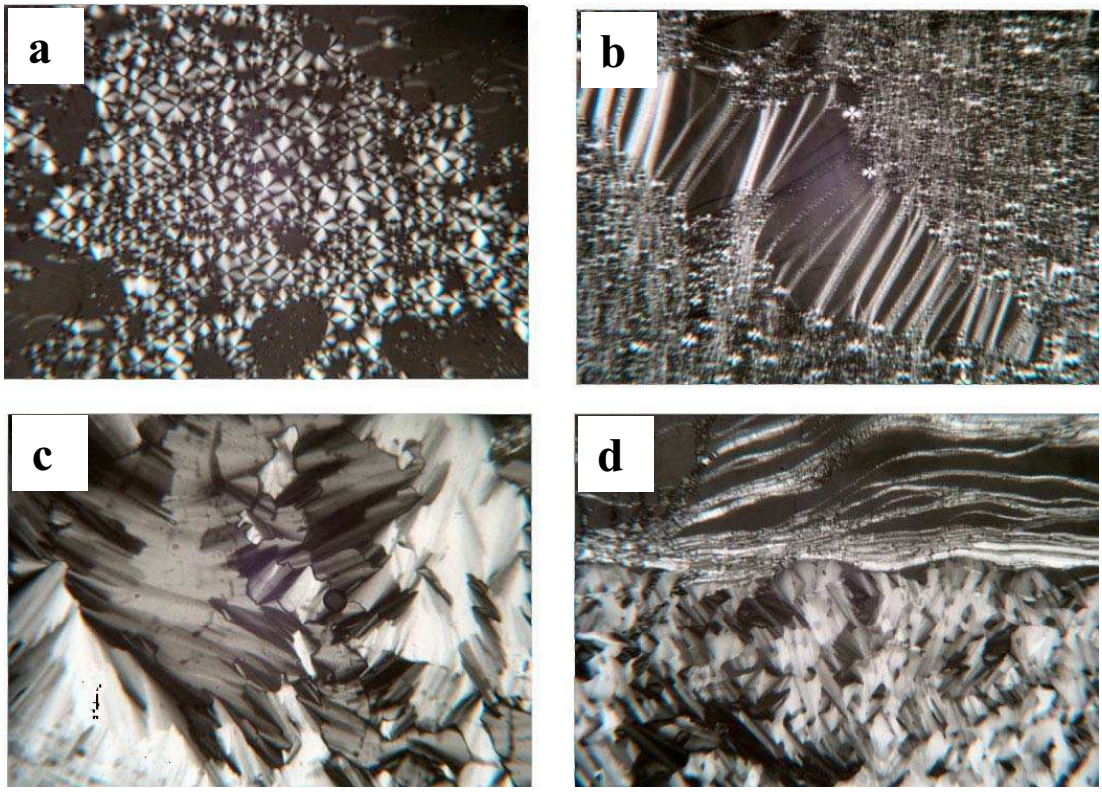


Figure II-6. *Textures of lamellar and hexagonal phases under the polarization microscopy. (a) The L_α phase, texture "Maltese Cross" (b) The L_α phase, oily streaks and "Maltese cross" (c) Hexagonal phase, fanlike texture, (d)Hexagonal phase H_1 coexisting with a phase L_α.*

As it is shown in **Figure II-5**, for isotropic sample, no light passes through the two polarizers, as their polarization plans are rotated 90 degree. Thus, we see nothing under the microscope. On the contrary, for anisotropic sample, the color image is detected due to anisotropic sample reorients the polarization plane of light that could pass through the second polarizer. Observation of liquid crystal phases between two polarizing filters can then distinguish their characteristic birefringent textures (**Figure II-6**). These textures are observable through the microscope because of the defects in liquid crystal phases. Indeed, the liquid properties of these compounds lead to stacking faults at regular intervals to the micrometer scale.

4.2 Small angle X-ray scattering (SAXS)

4.2.1 Principle and structure of SAXS

Small angle X-ray scattering (SAXS) is an analytical method to determine the structure of particle systems in terms of averaged particle sizes or shapes, such as organized molecular systems containing surfactant molecules. This technique is based on the differences in electron densities between the scattering objects and continuous medium. The intensity distribution curves = f (q) of micelles, microemulsions can be accessed using theoretical models of geometry and size of aggregates, as well as among aggregation (number of surfactants per micelle), the conformations of the hydrophilic chains and hydrophobic and other parameters describing the system. For samples with a regular organization, for example liquid crystal phases, the diffraction beam of photons X on different planes of the structure leads to the observation of peaks caused by Bragg geometry characteristics of the system. The repeat distance between these planes diffraction is given by Bragg's law:

$$2d_{h,\,k,\,l}\,Sin\theta = n\lambda$$

$d_{h,\,k,\,l}$: *Bragg distance*
θ : *half-angle diffraction*
n : *order of reflection (integer)*
λ : *wavelength of X-rays*

The relationship between the repeat distances determined from the Bragg reflection reveals the structure of the studied system. According to Bragg's law, in the range of small angle, the greater the distance of repetition is, the smaller the angle between the diffracted

beam and direct beam is. Herein the distances repetition of the studied systems are in the size order of several nanometer, the diffraction angles are small, hereupon in order to detect the diffracted beam, the apparatus requires an important distance between sample and detector.

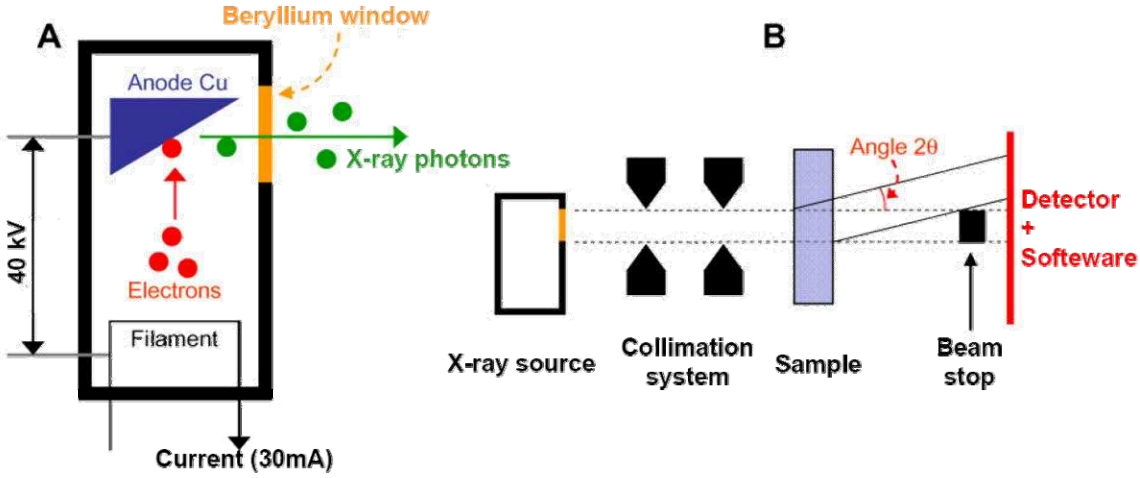


Figure II-7. *The basic design of a sealed tube (A) and the components of a SAXS instrument (B) [185]*

The home built apparatus in the laboratory consists of four main elements:

- An X-ray tube (**Figure II-7**). It contains a filament and an anode (copper) placed in a vacuum housing. Electrical current (30 mV) heats up the filament and electrons are emitted. A high voltage (40 kV) is applied across the filament and the anode, and this high voltage accelerates the electrons towards the anode. When the electrons hit the anode they are decelerated, which causes the emission of X-rays. A fraction of the electrons that hit the atoms of the anode will expel electrons from these atoms, causing emission of characteristic radiation with wavelengths that are typical for the material of the anode. In the case of a copper anode, only the K_α beam, wavelength 1.54 Å is used, the other beams (K_B) with weaker intensities are adsorbed by a nickel filter.
- A curved gold/silica mirror which reflects and focuses the beam.
- A collimation system. It consists of slits for separating the incoming beam from the scattered radiation at small angles.
- A sample holder adapted to employ either a capillary or a cell which to deposit the sample in a thin layer (0.5 mm) between two sheets of mica. A Peltier type temperature control system is associated with the sample holder.
- A detection system composed of a linear detector consists of 1024 channels was immersed in a gas mixture of argon / ethane, which is placed at 530 mm far from the sample.

The range of wave vector q is available from 0.04 to 0.4 $Å^{-1}$ corresponding to repetition distances between 16 and 160 Å.

This apparatus is mainly used for experiments in X-ray diffraction on liquid crystal phases as well as mesoporous powders. We use silver behenate as an angle-calibration reference to determine the origin of *q*.

4.2.2 Detection of lamellar and hexagonal phases

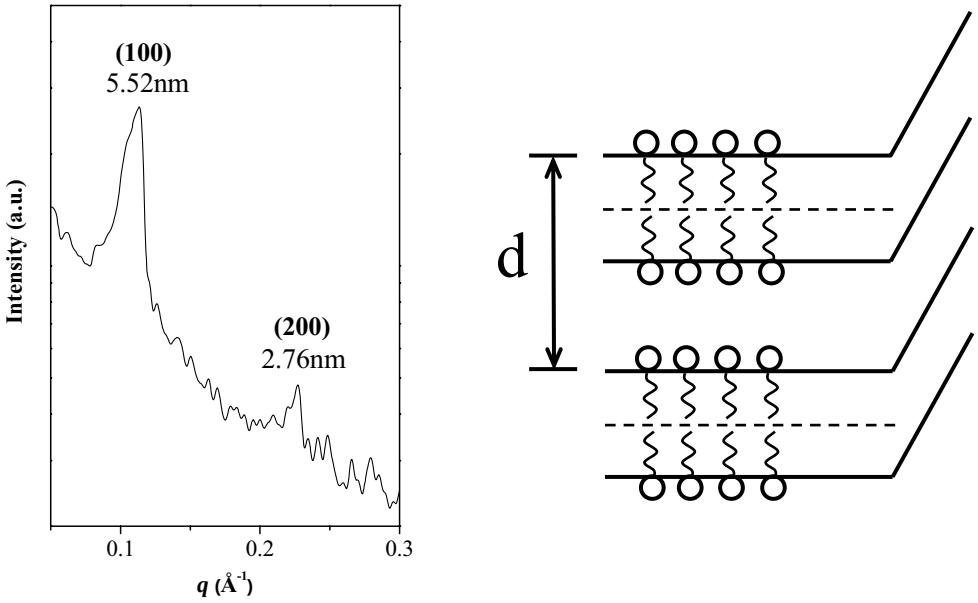


Figure II-8. *Scheme and typical pattern of a lamellar liquid crystal phase (80% $R^{H}_{12}A(EO)_9$ in water)*

The lamellar phase consists of infinitely wide bimolecular layers stacked in a parallel way. The X-ray diffraction on bimolecular layers leads to the appearance of Bragg reflection with decreasing intensity whose positions are defined by q_0, $q_1 = 2\ q_0$, $q_2 = 3\ q_0$ ... where q_0 is the position of the first peak.

The repetition distance corresponds to the layer spacing, while the intensity and width of this peak depend on the regularity of stacking. The diffraction pattern of such a phase exhibits reflections associated to the planes of indices 100, 200……The repeat distance **d** (**Figure II-8**) gives access to determine the structural parameters describing the lamellar phase, such as the cross - sectional area, hydrophilic thickness and hydrophobic thickness (see Chapter III).

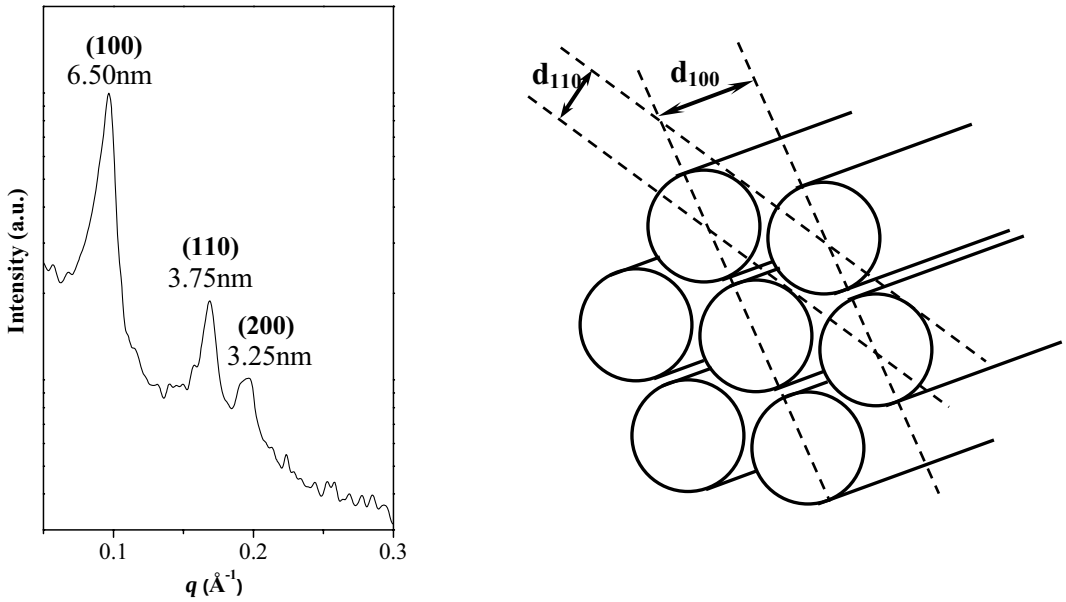


***Figure II-9**. Scheme and typical pattern of a hexagonal liquid crystal phase (50% $R^{H}_{12}A(EO)_9$ in water).*

Hexagonal phase consists of infinitely long cylinders packed in a hexagonal array. The X-ray diffraction on a hexagonal crystal liquid phase leads to the appearance of Bragg reflection with decreasing intensity whose positions are defined by q_0, $q_1 = \sqrt{3}\, q_0$, $q_2 = 2q_0$, $q_3 = \sqrt{7}\, q_0$ ……

These reflections are due to the diffraction of incident beam on different planes (**Figure II-9**). From the geometrical considerations, the composition of system and the partial volumes of hydrophobic and hydrophilic parts of surfactant, it is also possible to calculate the structural parameters from the repetition distance, such as hydrophobic radius and the cross-sectional area. The detail calculation will be developed in chapter III.

4.2.3 Characterization of mesoporous materials

The small angle X-ray scattering is used to identify the structure of mesoporous materials. The ordered materials in this study all have a hexagonal structure similar to MCM-41 (**Figure II-10A**). It has been reported that X-ray diffractograms of powdery hexagonal mesoporous materials exhibit a typical three-peak pattern with a very strong feature at a low angle (100 reflection line) and two other weaker peaks at higher angles (110 and 200 reflection lines). These three reflection lines can be attributed to a hexagonal unit cell ($a_0 = 2d_{100}/\sqrt{3}$), which corresponds to the sum of the pore diameter and the thickness of the pore wall.

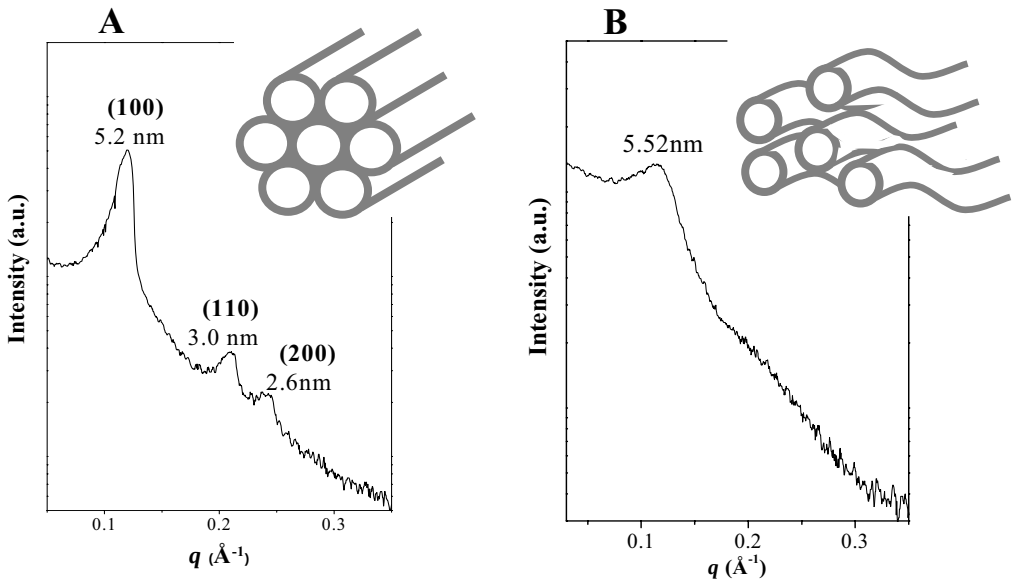


***Figure II-10**. Scheme and RX patterns of hexagonal structure mesoporous materials (A) and worm-like materials (B).*

The absence of the last peaks (**Figure II-10B**) suggests a disordered structure of the mesoporous molecular sieves having wormhole-like channel systems, analogous to MSU-type materials. The broad peak that is observed on the SAXS pattern gives an indication of the average pore-to-pore distance in the disordered wormhole framework which presents a lack of long-range crystallographic order.

4.3 Nitrogen adsorption-desorption analysis

The knowledge of the pore-network texture based on physical adsorption-desorption analyses is fundamental to the characterization of nanometric powders. In our study, we employ this method to determine the pore sizes and specific surface area of the mesoporous materials.

In 1938, by introducing a number of simplifying assumptions, Stephen Brunauer, Paul Emmett and Edward Teller were able to extend the Langmuir mechanism to multilayer adsorption and obtain an isotherm equation (the **BET** equation) [186].

$$\frac{p}{V(p_0 - p)} = \frac{1}{V_m C} + \frac{(C-1)p}{VmCp_0}$$

V : adsorbent volume at pressure p

V_m : volume of monolayer

P_0 : saturation vapor pressure of adsorbent

C : constant

Introducing mathematical algorithms to this method, the differences between adsorption

and desorption isotherms are discussed and the main parameters values were determined, such as specific surface area, pore volume and pores size distribution. The specific surface area is calculated from the monolayer volume at low pressures and molecular area per an adsorbed molecular:

$$S_{BET} = \frac{V_m}{V_{mol}} N_a \sigma$$

σ : molecular area per an adsorbed molecular
(σ = 16.2 Å^2 for N_2 at -196 ^{o}C)
V_{mol} : molar volume of gas
N_a : Avogadro number

The original **BET** treatment involved an extension of the Langmuir kinetic theory of monomolecular adsorption to the formation of an infinite number of adsorbed layers. It would be difficult to overestimate the historical importance of the **BET** theory since for 50 years it has attracted an enormous amount of attention.

Experimental adsorption isotherm recorded in the literature has a wide variety of forms. Nevertheless, the majority of these isotherms which result from physical adsorption may conveniently be grouped into six classes in the IUPAC classification (**Figure II-11**).

- Type I isotherm indicates the existence of micropores in the given system. It rises sharply at low relative pressures and reaches a plateau: the amount adsorbed by the unit mass of solid approaches a limiting value as $p/p_0 \rightarrow 1$.
- Type II isotherm is obtained with non-porous or macroporous adsorbents, which allow unrestricted monolayer-multilayer adsorption to occur at high p/p_0.
- Type III isotherm is not common. This feature is indicative of weak adsorbent-adsorbate interactions.
- Type IV isotherm indicates the existence of mesopores in the given system. Its initial region is closely related to the Type II isotherm, trends to level off at high relative pressures. It exhibits a hysteresis loop, the lower branch of which represents measurements obtained by progressive addition of gas of the adsorbent and the upper branch by progressive withdrawal. The hysteresis loop is usually associated with the filling and emptying of the mesopores by capillary condensation.
- Type V isotherm is relatively rare. As in the case of Type III isotherm, it levels off at high relative pressures, which is indicative of weak adsorbent-adsorbate interactions. In addition, it also exhibits a hysteresis loop which is associated with the mechanism of pore filling and emptying.

- Type VI isotherm is also relatively rare and is associated with layer-by-layer adsorption on a highly uniform surface.

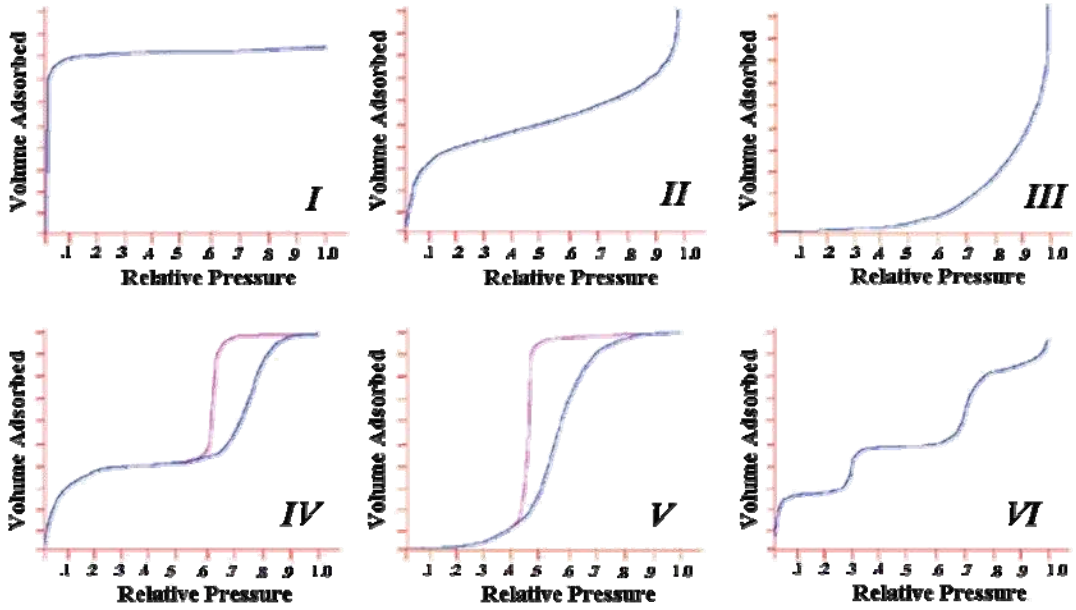


Figure II-11. *The six main types of gas physisorption isotherms, according to the IUPAC classification [187]*

Thanks to its inert and reversible adsorption properties, nitrogen (at -196 °C) is generally considered to be the most suitable adsorptive for standard surface area determination and for this purpose nitrogen adsorption-desorption isotherms were obtained at -196 °C, over a wide relative pressure range from 0.01 to 0.995, with a volumetric adsorption analyzer TRISTAR 3000 manufactured by Micromeritics. The samples were degassed under vacuum for several hours at 320 °C before nitrogen adsorption measurements to remove water and CO_2 physisorbed in the pores of material.

The pore diameter and the pore size distribution were determined by the **BJH** (Barret, Joyner and Halenda) method [188]. Except using a model of the adsorbent as a collection of cylindrical pores, this theory is based on the phenomenon of capillary condensation which appears in the mesopores and the applicability of simple Kelvin equation which involves the assumption of hemispherical meniscus with zero contact angles.

$$\ln\frac{p}{p_0} = \frac{\gamma V_m}{(r_p - t)RT}$$

γ : surface tension at temperature T

r_p : pore radius

t : thickness of an adsorbed layer

This method is applied to the adsorption branch of the isotherm in case of there is interconnected pore network which could induce the desorption branch of the isotherm give incorrect information in the calculation [189]. Based on an iterative calculation, it allows the calculation of the amount of adsorbed gas between a given pressure interval. From the value of pore radius as a function of relative pressure, it is possible to determine the accumulated volume of all these intervals depending on the pore radius. Although it is well-known that this method gives an underestimated pore size around 20% and that some new methods have been developed [190], we used it here for the sake of simplicity and this mathematical algorithm does not significantly affect the results as it is a systematic comparison.

4.4 Dynamic light scattering (DLS)

Dynamic light scattering (DLS) (also known as Photon Correlation Spectroscopy or Quasi-Elastic Light Scattering) is a technique in physics, which is used to determine the size distribution profile of small particles in surfactant solution, such as micelles, microemulsions and emulsions.

Firstly, in order to know the scattered intensity we have to make the optical measurement: temporal fluctuations in intensity of scattered light (wavelength and angle are set by instrument) [191]

$$q = \frac{4\pi n}{\lambda} Sin\theta$$

q : wave vector
n : refractive index
θ : half-angle diffraction
λ : wavelength of X-ray

Analysis of the autocorrelation function decay obtained by DLS from a dilution series of nanodroplets yields information on the effective diffusion coefficient D. Distribution of decay time gives particle size and shape distribution.

$$g(q,\tau) = \frac{\langle I(q,t) I(q,t+\tau) \rangle}{\langle I(q,t) \rangle} \propto 1 + e^{-Dq^2\tau}$$

τ : delay time
I : intensity
D : diffusion constant
t : time

In the limit of infinite dilution, the apparent hydrodynamic radius R_h can be estimated from the Stokes-Einstein equation [192, 193]. Apparently, the apparent hydrodynamic radius includes solvent effects.

$$D = \frac{k_b T}{6\pi\eta R_h}$$

K_b : Boltzmann constant

T : temperature

η : viscosity

R_h : particle radius

In our work, DLS is employed to study droplet size distributions of micelles, microemulsions and emulsions. DLS experiments were carried out using a Zeta 3000HS (Malvern Instruments, Ltd. UK) at 25 ^{o}C. It is equipped with an argon laser (λ = 633 nm) with variable intensity which allows covering the wide size range involved. The hydrodynamic radius measurements were carried out at a scattering angle of 90^0. Almost all the samples were diluted with water which filtered with filter membrane (0.4 μm) before the measurement. The values of droplet size given in this report are those obtained by the CONTIN analysis [193, 194], which is ideal for heterodisperse, polydisperse and multimodal systems.

4.5 Scanning electron microscopy (SEM)

The scanning electron microscope (SEM) is a type of electron microscope that images the sample surface by scanning it with a high-energy beam of electrons in a raster scan pattern. The electrons interact with the atoms that make up the sample producing signals that contain information about the sample's surface topography, composition and other properties such as electrical conductivity. Due to the very narrow electron beam, SEM micrographs have a large depth of field yielding a characteristic three-dimensional appearance useful for understanding the surface structure of a sample. A wide range of magnifications is possible, from about 10 times (about equivalent to that of a powerful hand-lens) to more than 500,000 times, about 250 times the magnification limit of the best light microscopes. Thus we are able to observe the particle morphology closely on a very fine scale.

For conventional imaging in the SEM, specimens must be electrically conductive, at least at the surface, and electrically grounded to prevent the accumulation of electrostatic charge at the surface. Nonconductive specimens are therefore usually coated with an ultrathin coating of electrically-conducting material, commonly gold or graphite, deposited on the sample either by low vacuum sputter coating or by high vacuum evaporation.

The technique of SEM is to focus on a surface of specimen by lens using a condensed electron beam. The interaction between electrons and the material leads to the backscattered

electron emission, X-rays, secondary electrons and so on. These electrons are collected by a detector, converted to a voltage and finally amplified. The apparatus used in this study is microscope HITACHI, S-models 2500 at 15 KeV.

Chapitre III. Préparation et caractérisation de silices poreuses préparées à partir du système à base de $R^{H}_{12}A(EO)_9$

Généralement les matériaux mésoporeux à larges pores sont préparés à partir de microémulsions et dans ce cas l'addition d'huile est relativement faible. Si la concentration en huile est suffisamment importante et en fonction des propriétés du système, en particulier sa TIP, des émulsions concentrées directes peuvent être formées. Du point de vue des matériaux poreux, l'utilisation d'émulsion comme système structurant engendre la formation de macropores voire de matériaux à porosité hiérarchisée.

Dans ce travail, nous avons étudié la préparation de matériaux poreux silicatés à partir de systèmes hydrogénés à base d'un tensioactif non ionique $C_{12}H_{25}CO(OC_2H_4)_9OCH_3$ en présence de différents types d'alcanes. Comme les propriétés des matériaux obtenus, en particulier l'organisation et la taille des pores, peuvent être fortement affectées par le comportement de phase, nous avons examiné la solubilisation de décane, d'hexane et de cyclohexane dans le système $C_{12}H_{25}CO(OC_2H_4)_9OCH_3$/eau. Les micelles de $R^{H}_{12}A(EO)_9$ peuvent incorporer de l'hexadécane, du décane ou du cyclohexane. La détermination des paramètres structuraux des phases cristal liquide montre que le décane peut-être dans les chaînes hydrophobes du tensioactif et forme simultanément un cœur d'huile est formé. La solubilisation de cyclohexane dans les cristaux liquides est limitée à 5 %. Concernant les matériaux mésoporeux l'incorporation de faibles quantités d'hexadécane ou de décane augmente la taille des mésopores, tandis que le cyclohexane ne modifie pas la taille des pores. Ceci signifie que l'hexadécane et le décane forme rien au cœur d'huile dans les micelles. Au contraire, le cyclohexane pénètre entre les chaînes hydrophobes du tensioactif.

Par ailleurs, nous avons mis en évidence que l'hexadécane et le décane permettaient la formation d'émulsions concentrées huile/eau. Lorsque la concentration de ces huiles est supérieure à 40 %, les matériaux présentent des macropores les quels correspondent à l'empreinte des gouttelettes d'huile. Avec le cyclohexane, la formation d'émulsions concentrées n'est pas possible et les matériaux ne présentent pas de macropore. Cette différence de comportement a été relié à la PIT (Température d'Inversion de Phase) du système qui est plus faible dans le cas du cyclohexane.

Chapter III. Preparation and characterization of porous silica templated by $R^{H}_{12}A(EO)_9$ based-system

1. $R^{H}_{12}A(EO)_9$-water system 69
   1.1 Characterization of the $R^{H}_{12}A(EO)_9$-water system **Error! Bookmark not defined.**
   1.2 Characterization of the liquid crystal phases 69
   1.3 Characterization of the mesoporous materials prepared from the $R^{H}_{12}A(EO)_9$-water system 71
2. Solubilization of hydrocarbons in the $R^{H}_{12}A(EO)_9$-water system 73
   2.1 Phase behavior 73
   2.2 Structural parameters of the hexagonal and the lamellar phases 76
   2.3 Influence of the solubilization of oils on the characteristics of materials 78
3. Discussion 88
4. Conclusion 91

III. Preparation and characterization of porous silica templated by $R^{H}_{12}A(EO)_9$ based-system

Generally the large pore mesoporous materials are formed from microemulsions and in that case the amount of oil is relatively low [195, 196]. If the concentration of oil is widely increased, the oil-rich-corner of the phase diagram is reached. Depending on the properties of the systems, in particular its phase inversion temperature (PIT), direct concentrated emulsions can appear [174]. From the porous materials point of view, the use of emulsion as structure-directing surfactant system rather involves the formation of macroporous or hierarchical materials [65-67, 69, 70, 197].

In this study, based on the nonionic hydrogenated $C_{12}H_{25}COO(C_2H_4O)_9CH_3$ surfactant, we have investigated the ability of hydrogenated systems used for the preparation of porous silica materials on the presence of different sorts of alkanes. As the properties of the recovered materials, in particular the organization and pore size, could be strongly affected by the phase behavior. Furthermore a detail study of the effect of the solubilization of decane, hexane and cyclohexane in the $C_{12}H_{25}COO(C_2H_4O)_9CH_3$-water system is carried out. Particularly the ability of the various hydrocarbons to form concentrated O/W emulsions.

1. $R^{H}_{12}A(EO)_9$-water system

1.1 Phase behavior

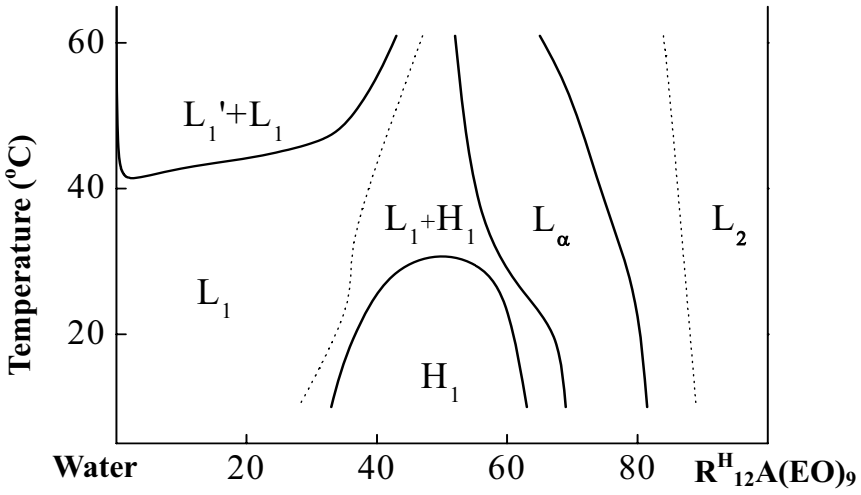


Figure III-1. *Phase diagram of $R^{H}_{12}A(EO)_9$ in water. L_1=micellar solution; L_1'=phase poor in micelles; H_1=hexagonal phase; L_α=lamellar phase; L_2=reverse micelle*

The temperature-composition phase diagram of the $R^{H}_{12}A(EO)_9$-water system is depicted in **Figure III-1.** A direct micellar L_1 phase is detected and its limit varies between 25 to 40 wt.% of surfactant according to the temperature. Above 42°C, two micellar phases are in equilibrium, one is rich in micelles (L_1) and the other one is poor in micelles (L'_1). Indeed, the cloud point is situated at 42°C for 2 wt.% of $R^{H}_{12}A(EO)_9$. At temperature lower than 30°C, the crystal liquid crystal domain is composed of the hexagonal (H_1) and the lamellar (L_α) phases. The existence range of H_1 goes from 35 to 60 wt.% of $R^{H}_{12}A(EO)_9$. If the temperature is increased, the hexagonal phase melts and between 60 to 80 wt.% of surfactant the lamellar phase (L_α) growths.

1.2 Characterization of the liquid crystal phases

The structural parameters of the liquid crystal phases have been determined at 25°C. The hexagonal H_1 phase is characterized by its typical SAXS profile with the relative peak positions, $1 : \sqrt{3} : 2$. The distance *d* associated to the first peak is related to the hydrophobic radius R_H by the relation [198]:

$$\frac{V_B}{V_S + \alpha V_W} = \frac{\sqrt{3}\pi R_H{}^2}{2d^2}$$

where α stands for the number of water molecules per surfactant molecule and V_B, V_S, V_W respectively stand for the molar volumes of the hydrophobic part of the surfactant (V_B = 222.5 cm³/mol), the surfactant (V_S = 618.1 cm³/mol) and water (V_w = 18 cm³/mol). The cell parameter *a* is given by the relation $a = 2d/\sqrt{3}$. The cross-sectional area S can then be deduced from the following relation:

$$S = \frac{2\,V_B}{N\;R_H}$$

N is the number of Avogadro.

Concerning the lamellar phase, as indicated in chapter II, its diffraction pattern exhibits two well resolved reflections associated to the planes of indices 001 and 002. The repetition distance corresponds to the layer spacing between the water and oil films separated by the surfactant bilayer. Based on geometrical considerations the cross sectional area can be calculated from the following formula [198]:

$$S = \frac{2(V_S + \alpha V_W)}{N\;d}$$

The hydrophobic thickness (d_B) is given by: $d_B = \frac{2\,V_B}{S}$. The hydrophobic thickness (L_B) of the surfactant chain is equal to $d_B/2$ and the hydrophilic thickness (d_A) is obtained by subtracting d_B from d_{001} values.

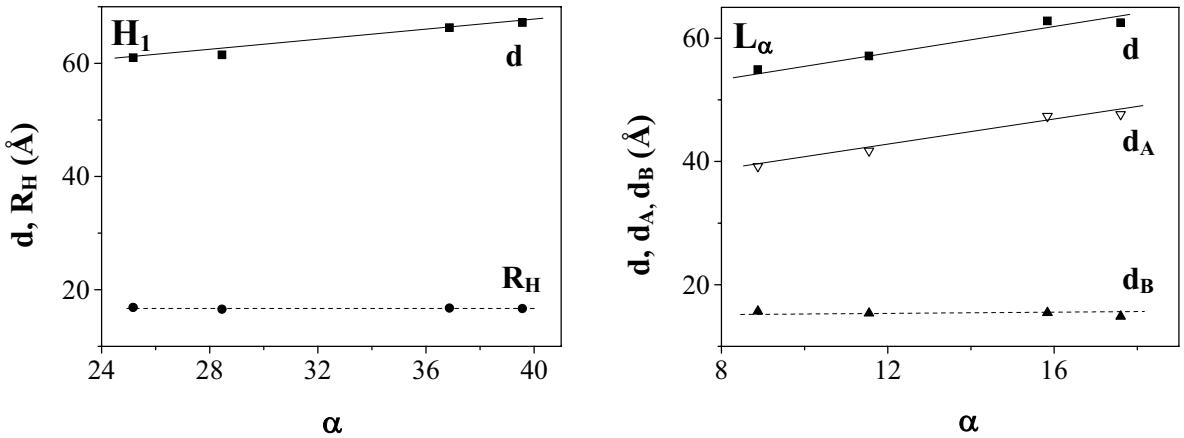


Figure III-2. *Evolution of the structural parameters of the liquid crystal phases. H_1 phase: d (repetition distance), R_H (hydrophobic radius); L_α phase: d (repetition distance), d_A (hydrophilic thickness) and d_B (hydrophobic thickness)*

As shown in **Figure III-2**, for the hexagonal (H_1) and lamellar (L_α) phases, an increase in

the d-spacing is noted with increasing water content. This is due to the hydratation of the head group and water could also form a film between the polar heads of surfactants. The hydrophobic radius (R_H) in the hexagonal phase and the hydrophobic thickness (L_B) in the lamellar phase remain constantly equal to respectively 16.5 and 7.75 Å. These parameters provide direct information about the conformation of the hydrophobic chain. Owing to the length of an extended chain (trans conformation) with 12 carbon atoms is about 16.8 Å and that the thickness of a chain in a folded up conformation is the half of the thickness of a chain in a trans conformation. We can deduce that the hydrophobic chains in the hexagonal phase are completely extended, whereas they adopt a folded up conformation in the L_α domain. These results are in agreement with those obtained for other systems, for example the $C_{12}(EO)_6$/decane/water system [198]. The value of the cross sectional area is 44 ± 1 and 48 ± 1 $Å^2$ respectively for H_1 and L_α, which remains constant in both domains.

1.3 Characterization of the mesoporous materials prepared from the $R^H_{12}A(EO)_9$-water system

Starting from the $R^H_{12}A(EO)_9$-water system, mesoporous materials have been prepared through the self assembly mechanism. As mentioned in the earliest that the building block is a micellar solution, so according to the phase diagram (**Figure III-1**) the concentration of surfactant was varied from 10 to 30 wt.% at 25 °C.

1.3.1 The structural properties

Regarding the SAXS patterns of the sample prepared with a concentration of $R^H_{12}A(EO)_9$ lower than 25 wt.%, in addition to a sharp peak at 5.2 nm, two peaks at 2.9 and 2.6 nm are detected (**Figure III-3**). The three reflections at q ratios $1:\sqrt{3}:2$ are consistent with a hexagonal symmetry. According to the Bragg's law, the unit cell dimension ($a_0=2d_{100}/\sqrt{3}$), which corresponds to the sum of the pore diameter and the thickness of the pore wall, could be calculated and its values is around 6.35 nm. Increasing the surfactant concentration in the solution until 25 wt.%, the position of the sharp peak does not vary on the SAXS pattern. It indicates that a_0 remains constant. However, the secondary reflections, arising from the hexagonal structure are not observed any more. Thus the disorganization of the channel array has begun. The presence of a single reflection indicates the formation of a disordered structure.

If the content of $R^{H}_{12}A(EO)_9$ reaches 30 wt.%, no reflection is detected further by SAXS, which indicates that the channel array is completely disordered.

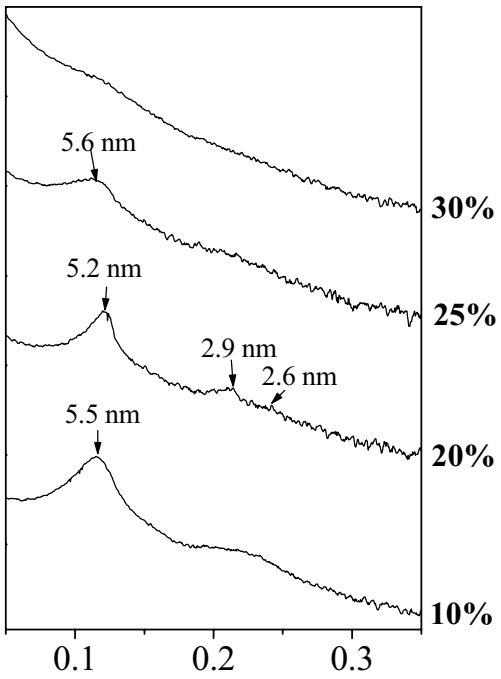


Figure III-3. *SAXS patterns of the material prepared with different concentration of $R^{H}_{12}A(EO)_9$ at 25°C*

1.3.2 The textural characteristics

When the concentration of $R^{H}_{12}A(EO)_9$ is lower than 25 wt.%, a type IV isotherm with a H_1 hysteresis loop is obtained according to IUPAC classification [187] (**Figure III-4**). An H_1 type hysteresis loop is usually obtained from MCM-41 type materials with a very regular arrangement of channels with very homogenous openings [148]. A strong uptake of N_2 adsorption is observed at approximately $p/p_0 = 0.5$, which is the result of the filling of the mesopores due to the capillary condensation. The plateau is reached at approximately $p/p_0 = 0.7$. Beyond this value, the adsorbed volume at the saturation remains constant. Upon the concentration of $R^{H}_{12}A(EO)_9$ increasing, on the isotherm, the capillary condensation is spread out over a larger range of relative pressures, which means that the compound becomes less homogeneous in pore sizes (**Figure III-4**). This is also confirmed by the broader pore diameter distribution, reflecting the transition from a well ordered mesoporous material to a disordered structure with wormhole like channels. While the content of $R^{H}_{12}A(EO)_9$ reaches 30 wt.%, no pore size distribution is evidenced in the mesopore range (**Figure III-4**). The specific surface area and the pore volume vary respectively from 1045 to 537 m^2/g and from

1.2 to 0.2 cm^3/g when the concentration of surfactant is changed from 10 to 30 wt.%.

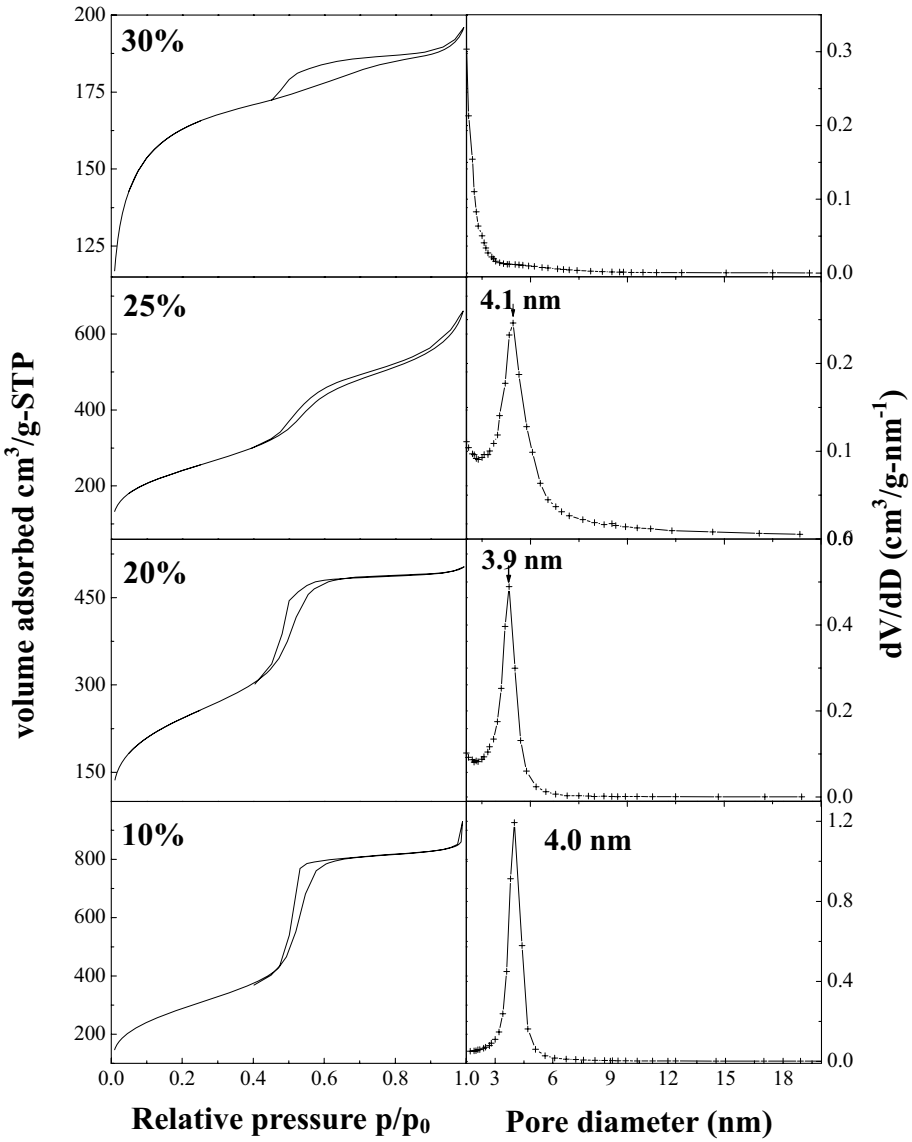


Figure III-4. *Evolution of nitrogen adsorption- desorption isotherm and the corresponding BJH pore size distribution curve with different concentrations of* $R^H_{12}A(EO)_9$

In summary, with system $R^H_{12}A(EO)_9$-H_2O, it is possible to prepare ordered mesoporous materials when the concentration of surfactant less than 20 %.

2. Solubilization of hydrocarbons in the $R^H_{12}A(EO)_9$-water system

2.1 Phase behavior

The solubilization of oils in the system $R^H_{12}A(EO)_9$-H_2O has been studied through the

determination of the Shinoda diagram (see Chapter II p.44). For different water/ surfactant ratios, we determined the microemulsion domain as a function of the temperature. The Shinoda diagrams of hexadecane and decane are reported in the **Figure III-5** at different water/surfactant ratios (R).

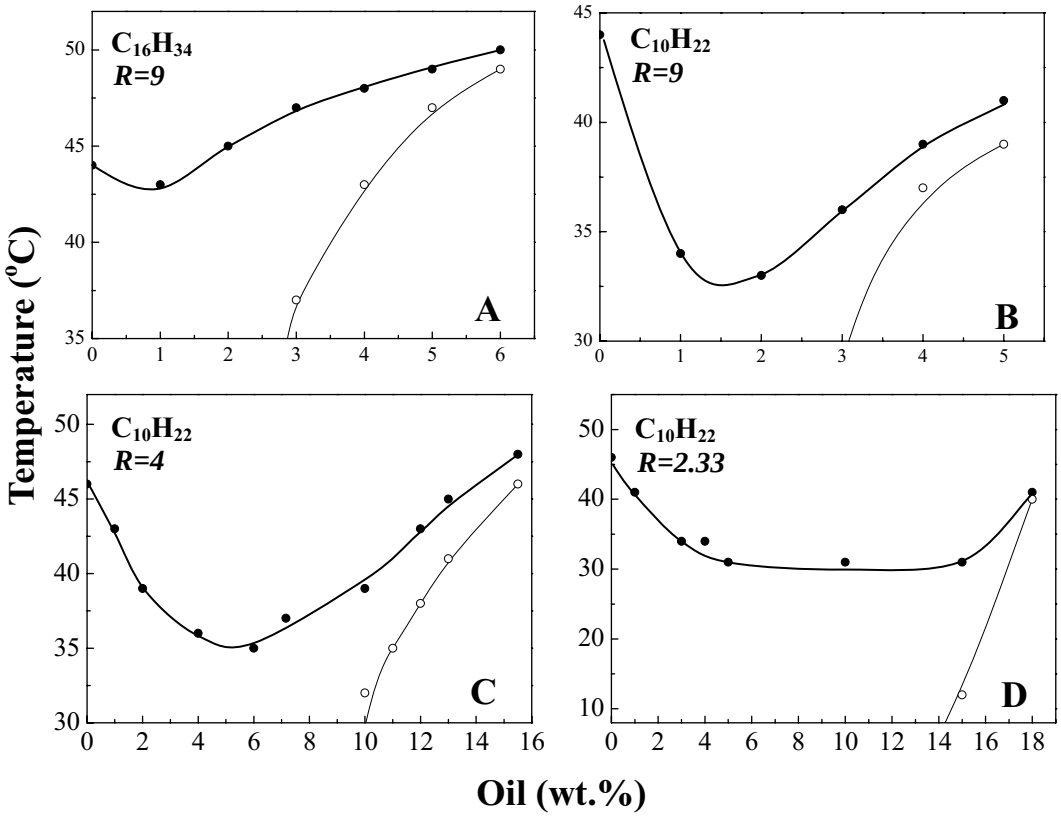


Figure III-5. *Pseudo-Shinoda diagram established with $C_{16}H_{34}$ (A) and $C_{10}H_{22}$ (B, C, D) for different water/surfactant ratios (R)*

Comparing the **Figure III-5 A** and **B**, the increasing solubilization of hexadecane leads to a slight rise of cloud point (limit to 50 °C), meantime the solubilization of decane leads to decrease of the cloud point whose minimum is around 1.5 wt.% (32.5 °C).

The Shinoda diagrams allow us to draw the related ternary diagram at different temperatures. **Figure III-6A** shows the phase diagram of the $R^{H}_{12}A(EO)_9$/hexadecane/water system at 25°C. At this temperature, micelles can incorporate up to 5 wt.% of hexadecane (L_1). If the weight percent of surfactant is raised from 40 up to 60 wt.%, a H_1 phase, which can solubilize up to 10.0 wt.% of $C_{16}H_{34}$ at 25°C is observed. If the $R^{H}_{12}A(EO)_9$ concentration is further increase the hexagonal domain is substituted by the lamellar one (L_α). The existence range of the L_α phase is limited to 12 wt.% of oil. **Figure III-6B and C** show the ternary diagram on the presence of decane and hexadecane respectively. The same sequence of phase

with hexadecane is observed. However, we can note that the incorporation of oil (decane and cyclohexane) is more notable. For the concentration of surfactant at 30 wt.%, it solubilizes almost 20 wt.% of oil. Moreover, with cyclohexane only a lower fraction of oil can be solubilized in the liquid crystal phase, i.e. 3 and 5 wt.% of C_6H_{12} can be incorporated respectively in H_1 and L_α.

For these systems, we examined the formation of concentrated emulsion O/W (oil-rich corner of the phase diagram). These emulsions are prepared by mixing first the surfactant and a small amount of water at the water/surfactant weight ratios between 9 and 2.33. This mixture corresponds to the direct microemulsion denoted L_1. Then, alkanes were added dropwise

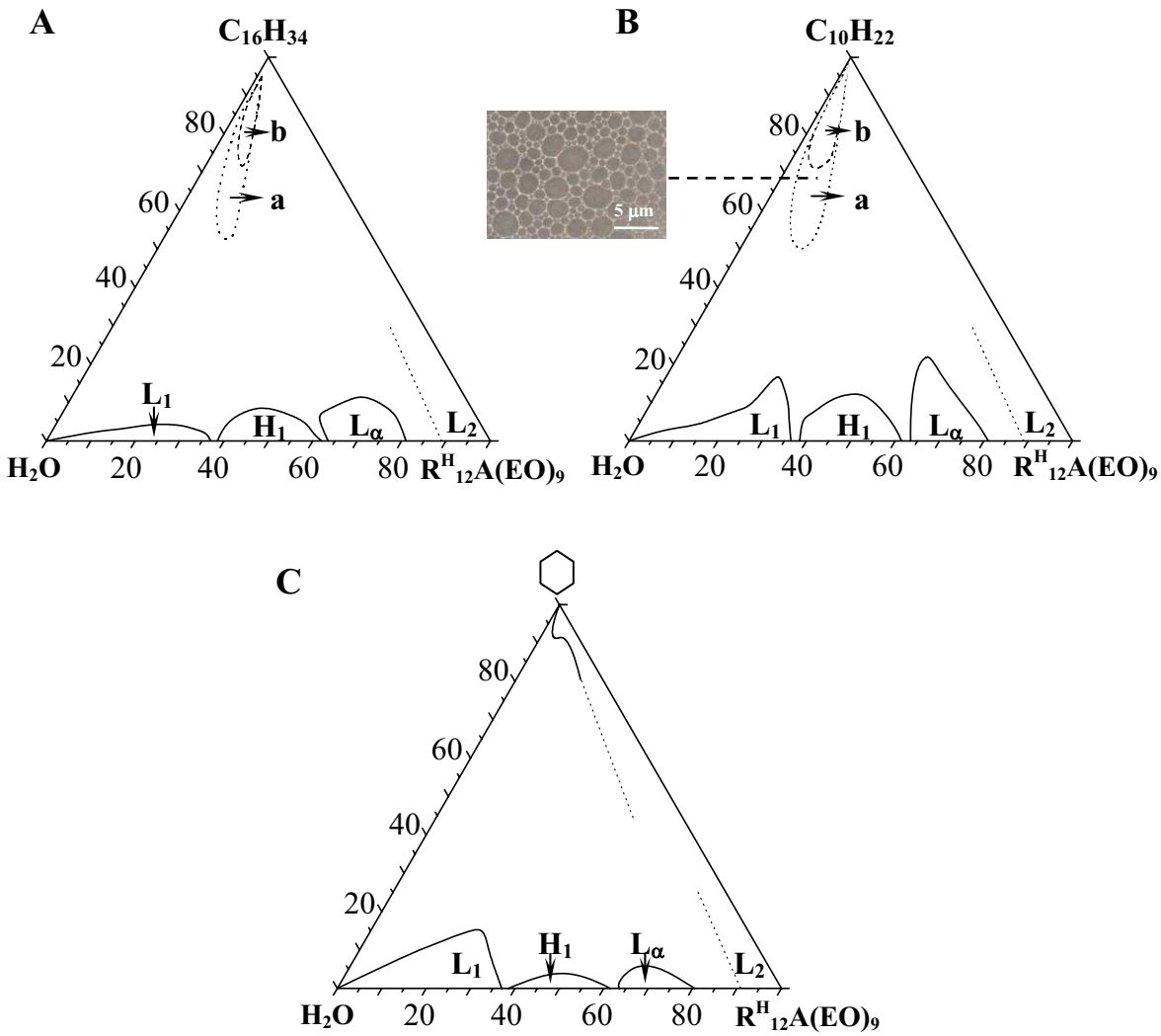


Figure III-6. *Phase diagram (wt.%) of $R^H_{12}A(EO)_9$ /alkane/water system at 25°C A: hexadecane, B : decane and C : cyclohexane. The emulsion is stable for several days (a) and for weeks (b)*

under vigorous stirring by means of a vibromixer. All the samples were kept in the thermostatic bath at 25 °C. For hexadecane and decane amounts larger than 50 wt.%,

oil-in-water concentrated emulsion are formed. Depending on the oil amount they were allowed to stand from a few hours to few weeks. It should be noted that the stability of the emulsion is enhanced when the concentration of hexadecane or decane is increased. Indeed, the samples prepared with an oil loading lower than 70 wt.% are stable for several days (**Figure III-6Aa**), whereas those prepared with concentration of hexadecane or decane higher than 70 wt.% appears to be very stable for weeks (**Figure III-6Ab**). A similar behavior is noted when hexadecane is replaced by decane (**Figure III-6B**). The optical microscope photographs indicate that the droplet size of concentrated emulsion is around 1~2 micrometers (**Figure III-6Ba)**. Upon adding decane more and more, their size could approach to approximately 4 micrometers (**Figure III-6Bb)**. In contrast when cyclohexane is used as oil, the situation is quite different. In the oil-rich corner, except the reverse microemulsion, no domain of concentrated emulsion is observed (**Figure III-6C**).

2.2 Structural parameters of the hexagonal and the lamellar phases

For both the $R^H_{12}A(EO)_9$/hexadecane/water and the $R^H_{12}A(EO)_9$/decane/water systems, we have determined the structural parameters of the H_1 and L_α liquid crystal phases at 25°C. In the ternary system, the values of hydrophobic radius (R_H) and of the cross sectional area (S) in H_1 is deduced from the following equations:

$$\frac{V_B + \beta V_O}{V_S + \alpha V_W + \beta V_O} = \frac{\sqrt{3}\pi R_H^2}{2d^2} \qquad S = \frac{2(V_B + \beta Vo)}{N\ R_H}$$

β and Vo respectively stand for the number of oil molecules per surfactant molecule and for the molar volume of oil. The values of V_O are 293.5 and 194 cm^3/mol respectively for $C_{16}H_{34}$ and $C_{10}H_{22}$.

Concerning the L_α domain, the cross sectional area (S) and the hydrophobic thickness (d_B) in L_α are determined according to the relation:

$$S = \frac{2(V_S + \alpha V_W + \beta V_O)}{N\ d_{001}} \qquad d_B = \frac{2(V_B + \beta V_O)}{S}$$

- *Hexagonal phase*

Looking at the H_1 domain for a given water/surfactant ratio (R) an increase in R_H with the incorporation of oil can be noted for $R^H_{12}A(EO)_9/C_{16}H_{34}$/water and $R^H_{12}A(EO)_9/C_{10}H_{22}$/water systems, we (**Figure III-7**). For example using $C_{10}H_{22}$ as oil a water/surfactant ratio equal to

1.5, R_H is increased from 17.8 to 35.7 Å on increasing β from 0.11 to 2.05. The cross sectional area remains constant with addition of hexadecane (S = 44 ± 1.0 $Å^2$), while it increases from 45.7 to 53.5 ± 1.0 $Å^2$ when decane is incorporated for R=1.50. The values of the cross sectional area suggest that hexadecane molecules are solubilized essentially in the core of the cylinders, whereas decane molecules tend to penetrate also in the palisade layer.

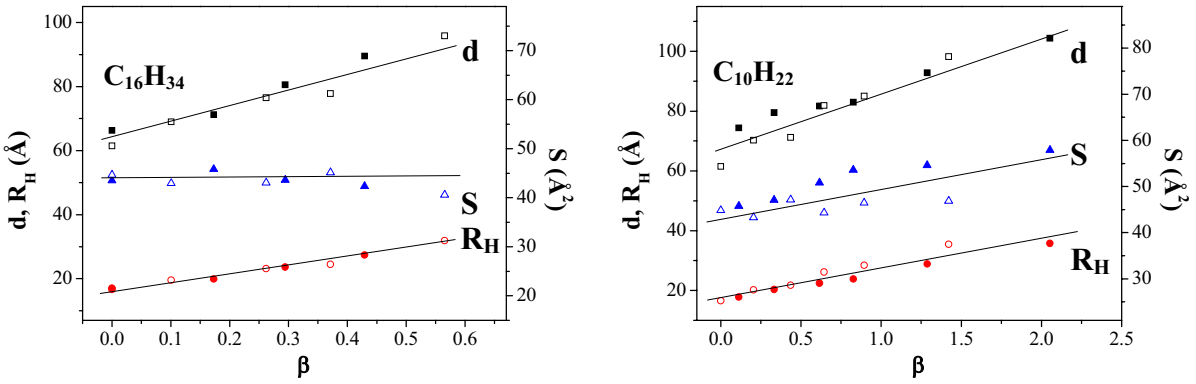


Figure III-7. *Evolution of the structural parameters of the* ***hexagonal*** *liquid crystal phase with $C_{16}H_{34}$ (■, ▲ and ● : R = 1; □, Δ and ○: R = 0.82) and $C_{10}H_{22}$ ((■, ▲ and ● : R = 1.50; □, Δ and ○: R = 0.82) : d (repetition distance), R_H (hydrophobic radius), S (cross-sectional area).*

- *Lamellar phase*

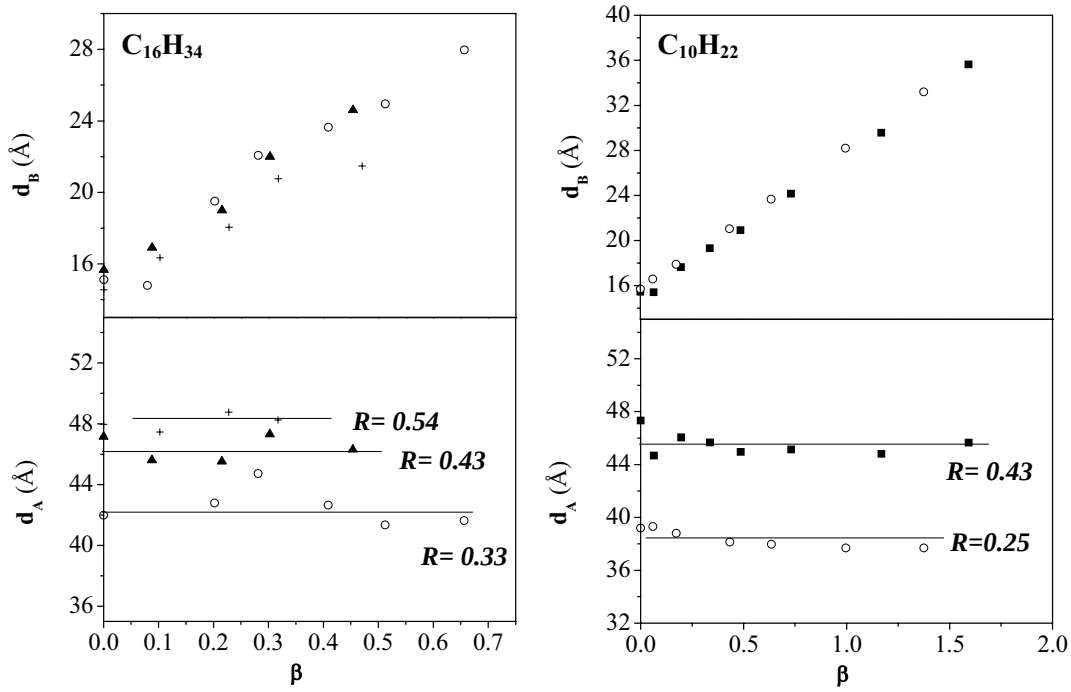


Figure III-8. *Evolution of the structural parameters of the* ***Lamellar*** *liquid crystal phases with $C_{16}H_{34}$ and $C_{10}H_{22}$ for different water/surfactant ratios (R): d_A (hydrophilic thickness) and d_B (hydrophobic thickness).*

Concerning the lamellar phase the two alkanes solubilized in a similar way. As a matter of fact, for a given value of R, from **Figure III-8**, it is observed that d_B values linearly increase with β, whereas d_A remains constant. These results suggest that hexadecane and decane molecules form an interstitial film of oil in the bilayer of the surfactant. Besides, the cross-sectional area almost reminds constant upon the addition of hexadecane. Thus, hexadecane molecules form a free film in the core of the bilayer. In contrast, S increases significantly with β in the decane system, suggesting that decane molecules form an interstitial film of oil in the bilayer of the surfactant fluorinated chains and these molecules are also penetrated between the fluorinated chains.

2.3 Influence of the solubilization of oils on the characteristics of materials

The determination of the phase diagram reveals that the quantity of oil in the microemulsion is related to the molecular structure of each oil. Similarly, the formation of concentrated emulsion also depends on the molecular structure of the added oil.

2.3.1 Effect of oil molecular structure and oil content

The materials from $R^{H}_{12}A(EO)_9$-H_2O based system containing various amounts of hydrogenated oil (hexadecane, decane and cyclohexane) are prepared. TMOS was added into the solution with surfactant / silica ratio 0.5, at room temperature, pH 7 and we chose water / surfactant ratios: R = 9 and R = 3. The procedure for the preparation of the materials was described in Chapter II. Unless otherwise specified, these conditions have always been used in this section. We prepared materials with increasing concentration of oils from 2% to 95%.

The SAXS pattern of the compounds prepared from R=9 micellar solutions and in the presence of hexadecane are depicted in the **Figure III-9**. We can see that the mesopore ordering is enhanced upon the addition of $C_{16}H_{34}$. As a matter of fact when the concentration of $C_{16}H_{34}$ is progressively increased from 0 to 5 wt.% the 110 and 200 become well resolved (**Figure III-9**). The value of unit cell dimension ($a_0=2d_{100}/\sqrt{3}$) varies from 6.2 to 7.6 nm upon the loading of $C_{16}H_{34}$ from 0 to 5 wt.%. Nevertheless, if oil is further added, the intensity of secondary reflections decreases, thus the disorganization of the channel array has begun. Above 10 wt.% of hydrocarbon they are not detected anymore on the SAXS pattern.

The presence of a single reflection indicates the formation of a disordered structure.

The nitrogen adsorption-desorption isotherms of the recovered materials are type IV (**Figure III-10** R=9). The maximum of the pore size distribution is shifted from 4.0 to 5.3 nm when the amount of $C_{16}H_{34}$ varied from 0 to 5 wt.% (**Figure III-10** insert), indicating that in this range of concentration $C_{16}H_{34}$ acts as an expander. As evidenced by **Figure III-14** (R=9) above 5 wt.% of hexadecane, the mean pore diameter remains almost constant.

For the materials prepared from a micellar solution with R=3 (**Figure III-9**), it can also be noted that the first reflection detected on the SAXS pattern is shifted towards lower values of q, i.e. higher value of d-spacing, with the increase of hexadecane concentration. For example, the position of the first peak varies from 5.6 to 9.9 nm when the hexadecane loading reaches 7 wt.%, reflecting the mesopore enlargement. This shift in d-spacing value can be related to the solubilization of oil in micelles. Indeed, it should be reminded that micelles can incorporate up to 6 wt.% of hexadecane. Above 6 wt.%, the oil is in excess and the self assembly mechanism is disturbed. As a matter of fact, as shown in **Figure III-9**, when hexadecane concentration higher than 7 wt.%, only wormhole-like structure are recovered. Upon the addition of hexadecane the shape of the isotherm is also modified for R=3, we can see on **Figure III-10** that the adsorbed volume of nitrogen increases significantly at high relative pressure instead of remaining constant. This phenomenon is attributed to saturation and the isotherm becomes a combination between type IV and type II for 40 wt.% of $C_{16}H_{34}$. In addition, with increase in the $C_{16}H_{34}$ concentration the relative pressure, for which capillary condensation takes place, is shifted toward higher values. Since the p/p_0 position of the inflection point is related to the pore diameter, it can be inferred that an enlargement of the mean pore diameter occurs when the loading of hydrocarbon is raised. This increase in pore diameter is further confirmed by the pore size distribution whose maximum is shifted from 4.0 to 9.8 nm when the content of hexadecane is varied from 0 to 40 wt.% (insert of **Figure III-10** R=3). Moreover, the pore size distribution becomes broader. This indicates that the mesopores become less homogeneous. Concerning the morphology of the materials, several representatives scanning electron micrographs (SEM) of the silicas synthesized with R=3 are shown in **Figure III-13**. When the hexadecane concentration is lower than 40 wt.%, the morphology of the materials can be described as particles with irregular shape, no macropores are obtained. On the contrary, we can see that at $C_{16}H_{34}$ concentrations higher than 40 wt.%, macropores whose diameters are in the range of few microns are formed. Until 80 wt. % of hexadecane added in the system, the collapse of the macropores occurs.

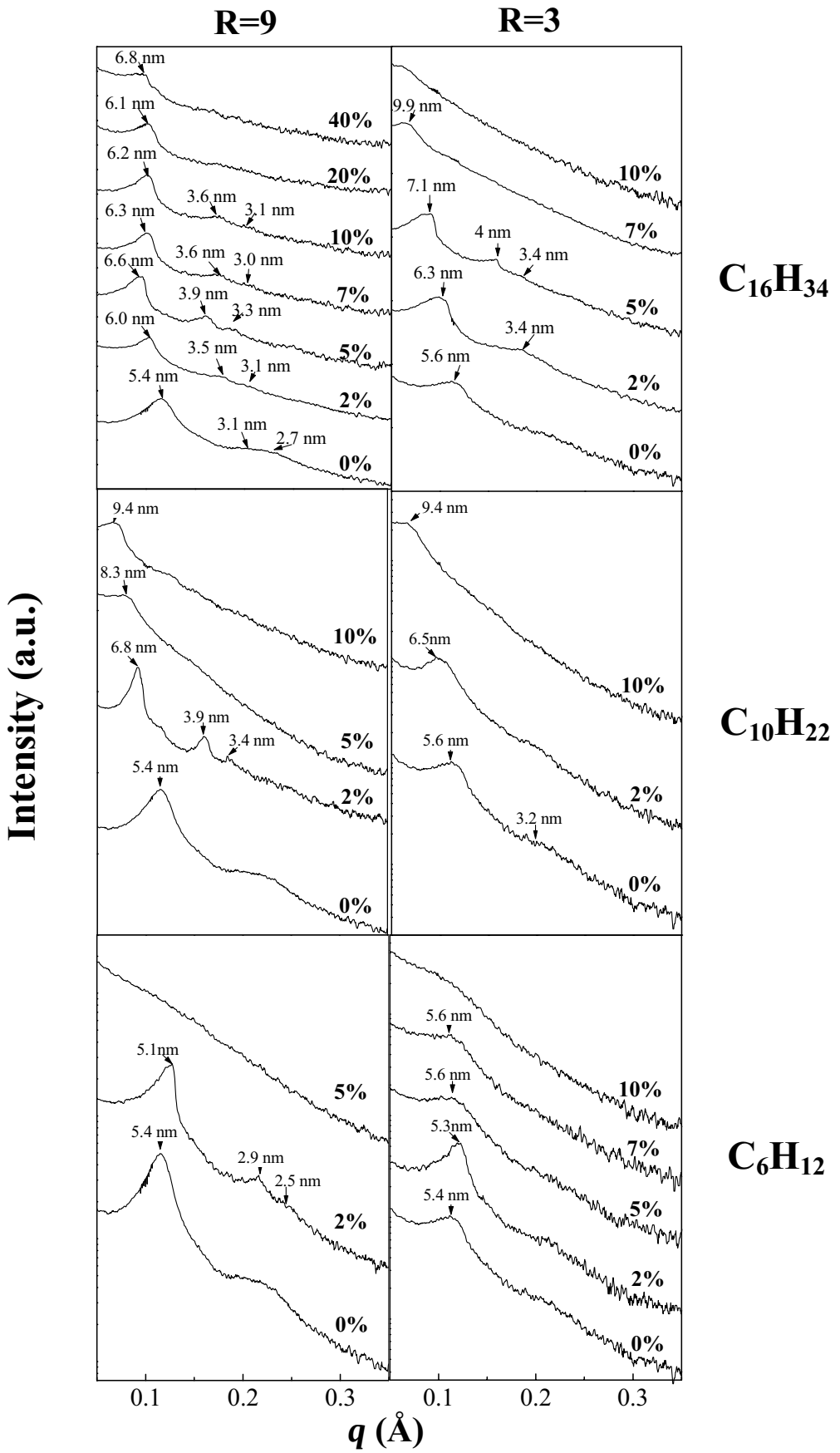


Figure III-9. *SAXS patterns of the material prepared with different concentrations of hexadecane, decane and cyclohexane for R=9 and R=3.*

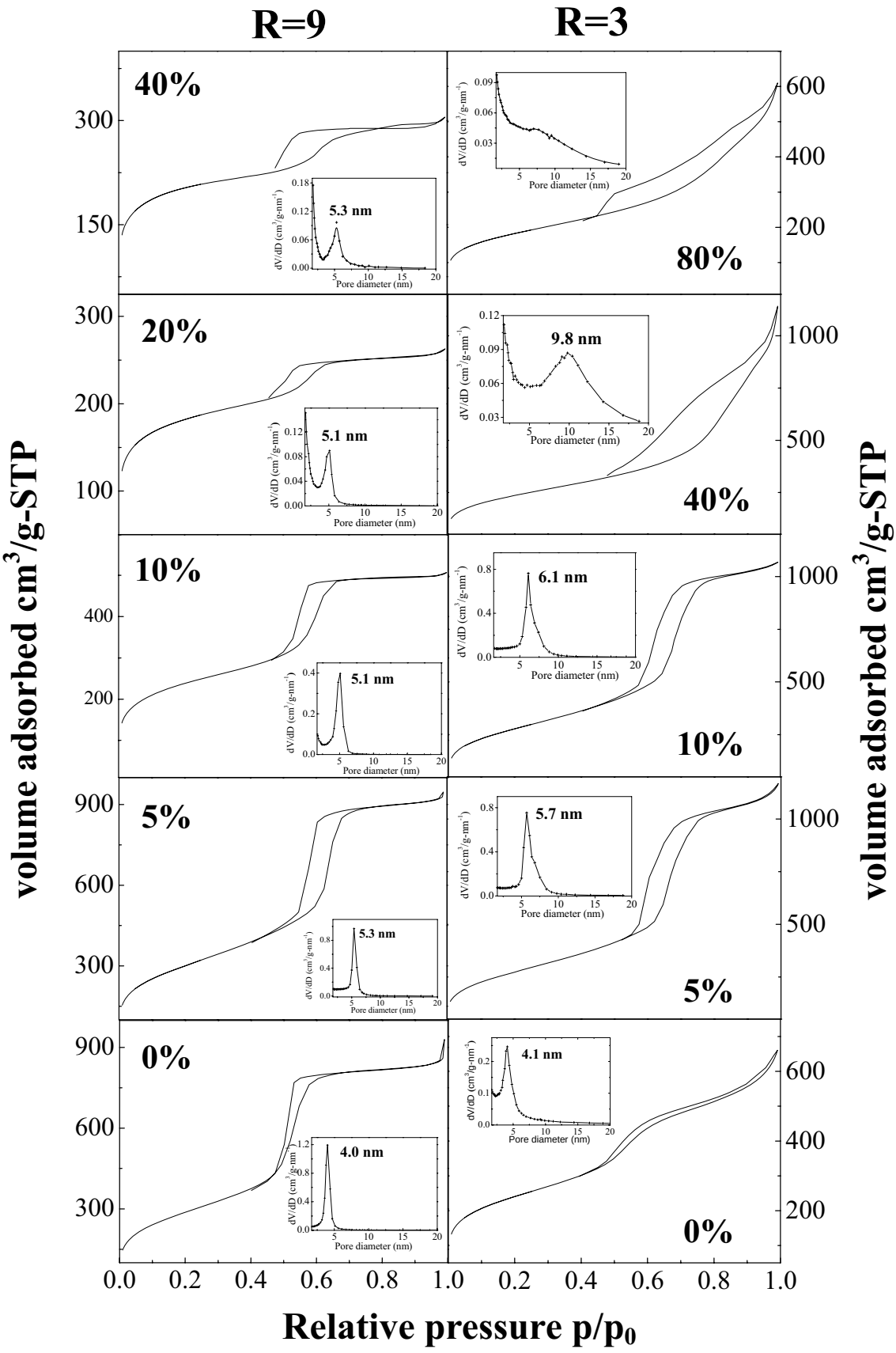


Figure III-10. *Evolution of nitrogen adsorption- desorption isotherm and the corresponding BJH pore size distribution curve (insert) with different concentrations of hexadecane for R=9 and R=3.*

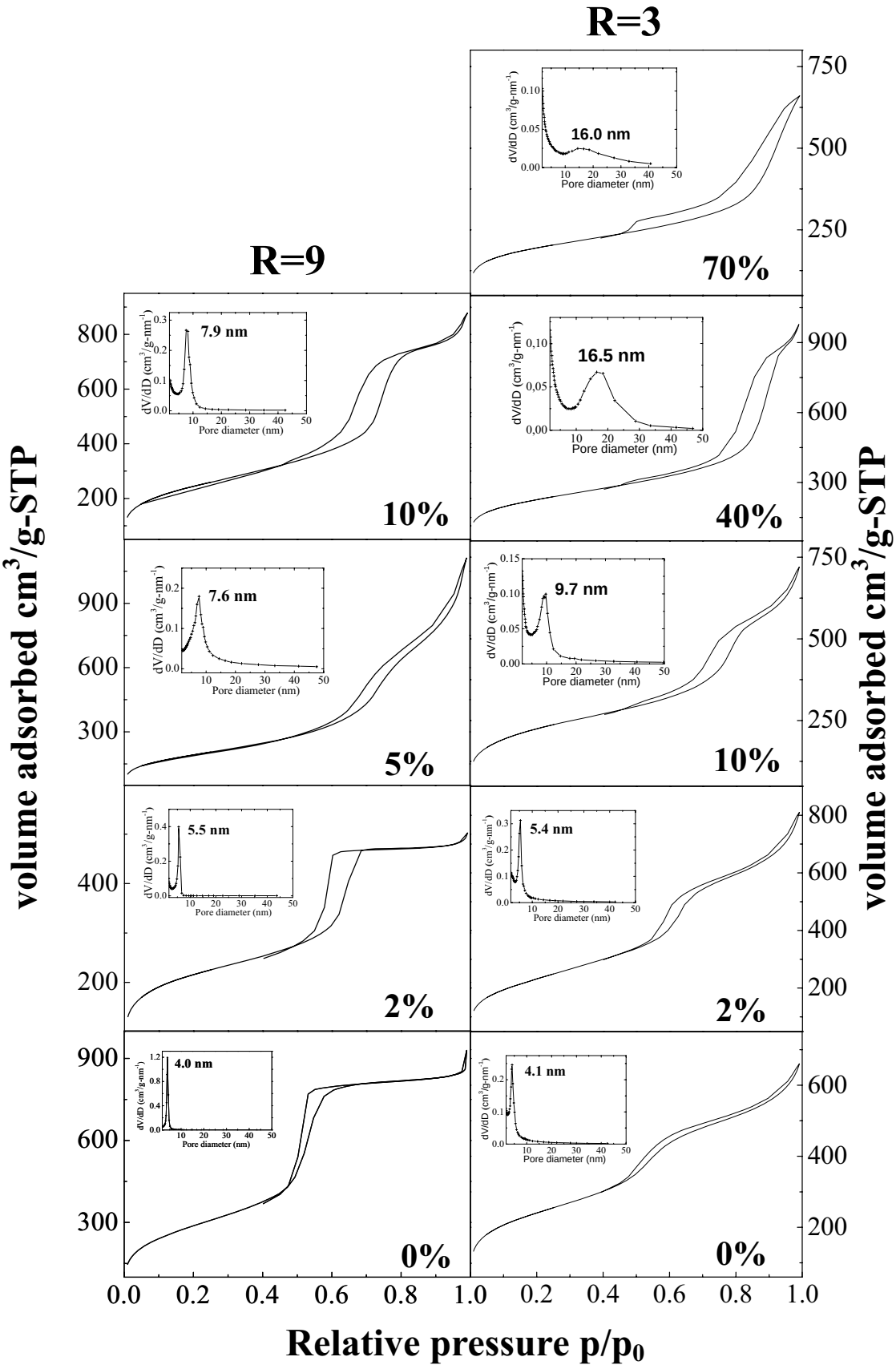


Figure III-11. *Evolution of nitrogen adsorption- desorption isotherm and the corresponding BJH pore size distribution curve (insert) with different concentrations of decane for R=9 and R=3 at pH 7.*

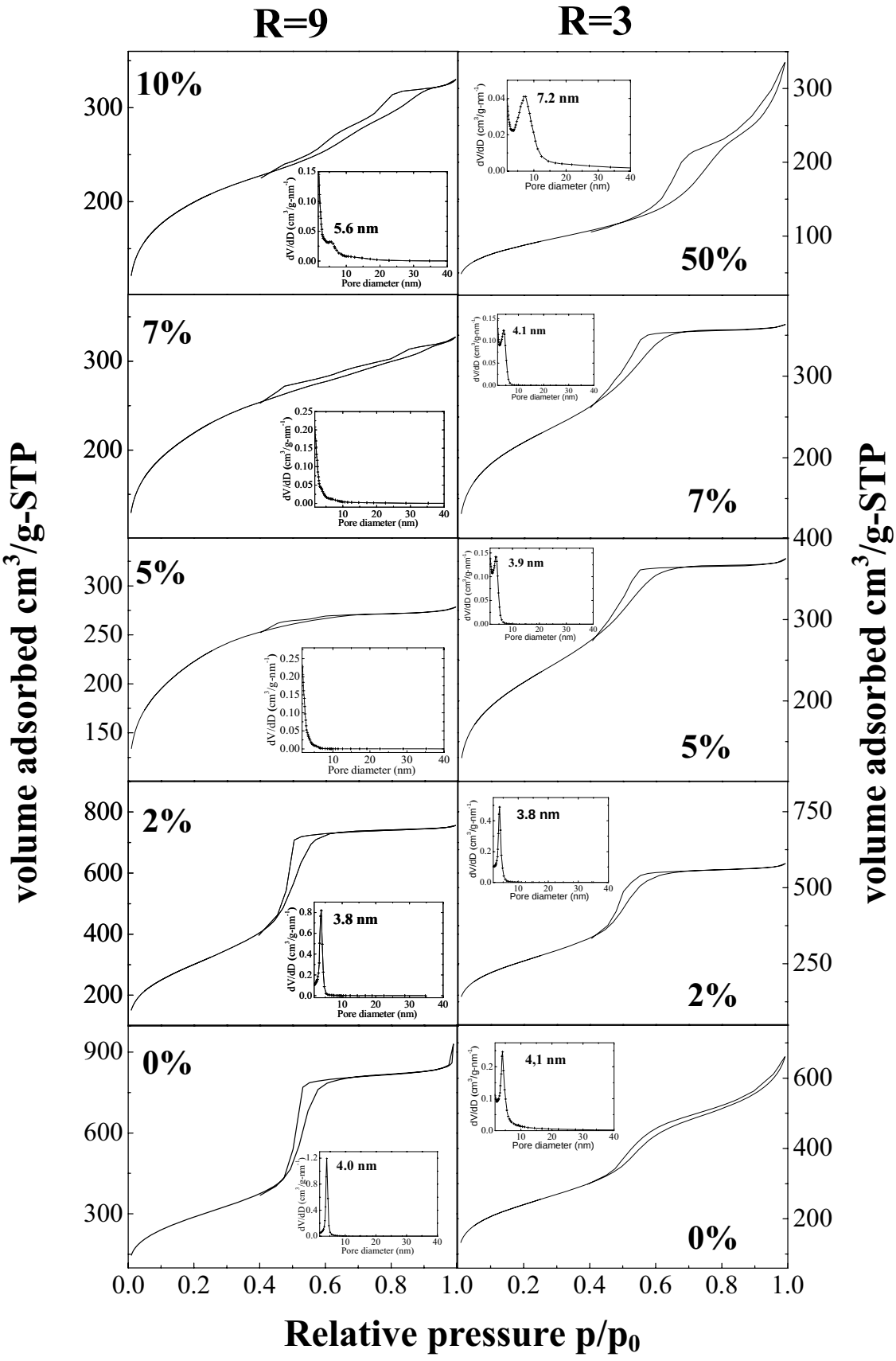
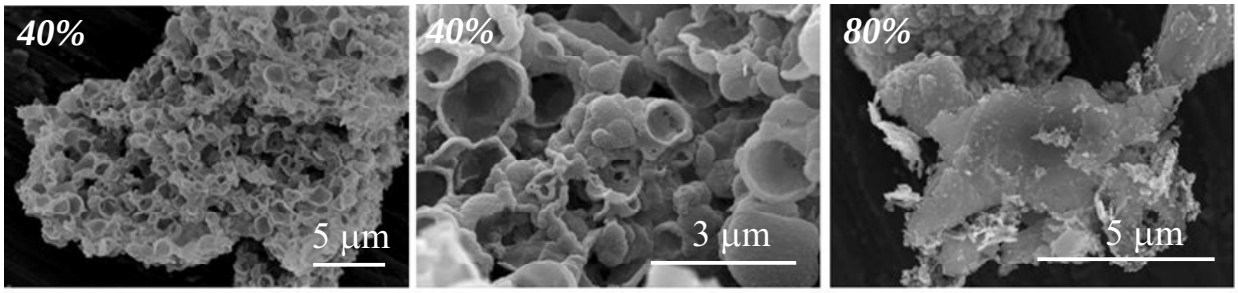
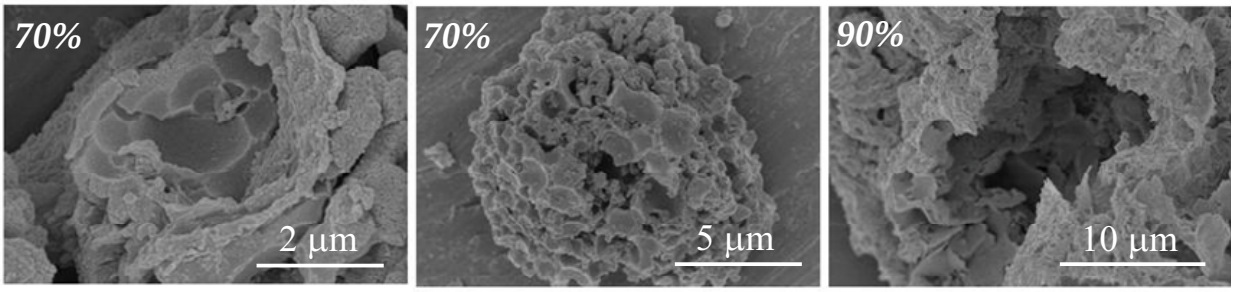


Figure III-12. *Evolution of nitrogen adsorption- desorption isotherm and the corresponding BJH pore size distribution curve (insert) with different concentrations of cyclohexane for R=9 and R=3 at pH 7.*

Hexadecane ($C_{16}H_{34}$)



Decane ($C_{10}H_{22}$)



Cyclohexane (C_6H_{12})

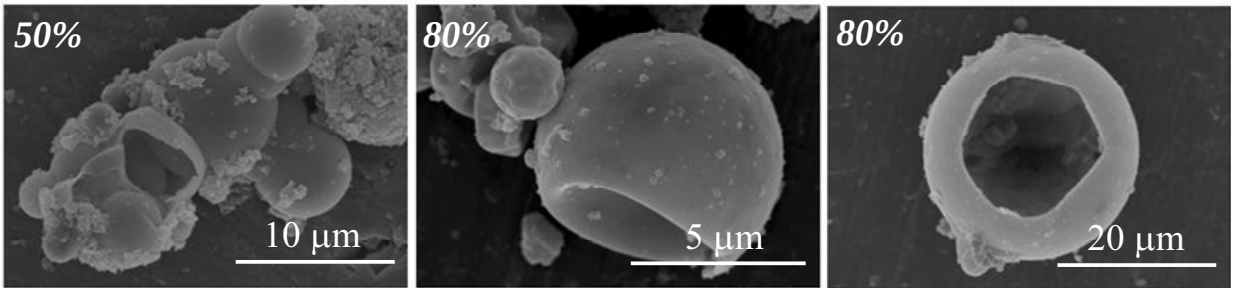


***Figure III-13**. SEM micrographs of materials synthesized with different concentrations of $C_{16}H_{34}$, $C_{10}H_{22}$ and C_6H_{12} at R=3, pH 7.*

Materials obtained from the $R^H_{12}A(EO)_9/C_{10}H_{22}$/water system (**Figure III-11**) exhibit the same characteristics than the ones synthesized from the $R^H_{12}A(EO)_9/C_{16}H_{34}$/water one (**Figure III-9**). The main difference between the two systems is that the lost of mesopore ordering occurs at a lower oil concentration in the case of decane. For example at R=9, upon addition of decane the hexagonal structure is already lost for 5 wt.%, whereas it is preserved until 10 wt.% in the case of $C_{16}H_{34}$.

We can see that with the addition of decane, the adsorbed volume of nitrogen increases significantly at high relative pressures instead remaining constant. The isotherm becomes a combination between type IV and type II at 70 wt.% decane for R=3. Sample synthesized on the presence of decane have a higher pore diameter than the one prepared by using hexadecane as oil. (**Figure III-14**). For the materials obtained, macropores are observed by

SEM for $C_{10}H_{22}$ content higher than 50 wt.% (**Figure III-13**).

Replacing hexadecane or decane by cyclohexane the situation is quite different (**Figure III-9**). Indeed, even if the mesopore ordering is kept in the presence of 2 wt.% of C_6H_{12} for R=9, no line is observed on the SAXS pattern for higher concentrations. This means that a transition from a hexagonal structure to a randomly oriented pore arrangement occurs. For the case of R=3, there are some wormlike mesopores detected on the SAXS pattern until in the presence of 10 wt.% of C_6H_{12} and the 100 reflection is quite flat.

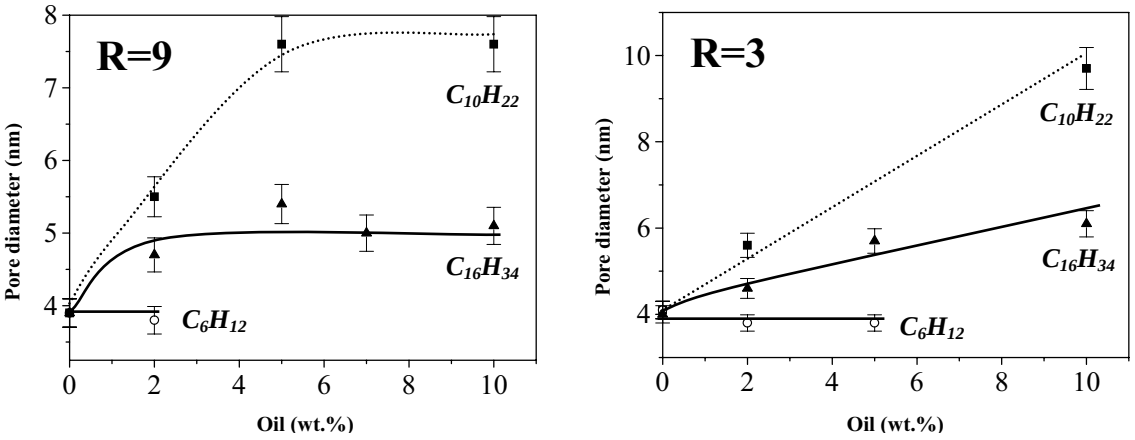


Figure III-14. *Evolution of the mesopore diameter with different concentrations of hexadecane, decane and cyclohexane at R=9 and R=3.*

Whatever the surfactant concentration in the mixture, no swelling of the mesopore is noted (**Figure III-12**). The adsorption- desorption analysis also reveals that no pore size distribution in the mesopore range is obtained for C_6H_{12} loading higher than 2 wt.% for R=9 or higher than 5 wt.% for R=3.

Concerning the morphology of the materials spheres are observed. (**Figure III-13**). Their size varies from several microns even to more than 20 μm with the increase of cyclohexane concentration. The result of the SEM is in accordance with the ternary diagram we have determined above. Since there is no concentrated emulsion formed in the oil-rich domain, balls are obtained.

2.3.2 Effect of reaction medium pH value

So far by now, we have always worked at pH=7 for this system, conditions in which hydrolysis speed of TMOS is minimal. The literature data show that pH plays an important role on the structure of materials [199-201]. In order to understand the influence of medium pH value to the characteristic of porous materials, we changed the reaction medium pH value

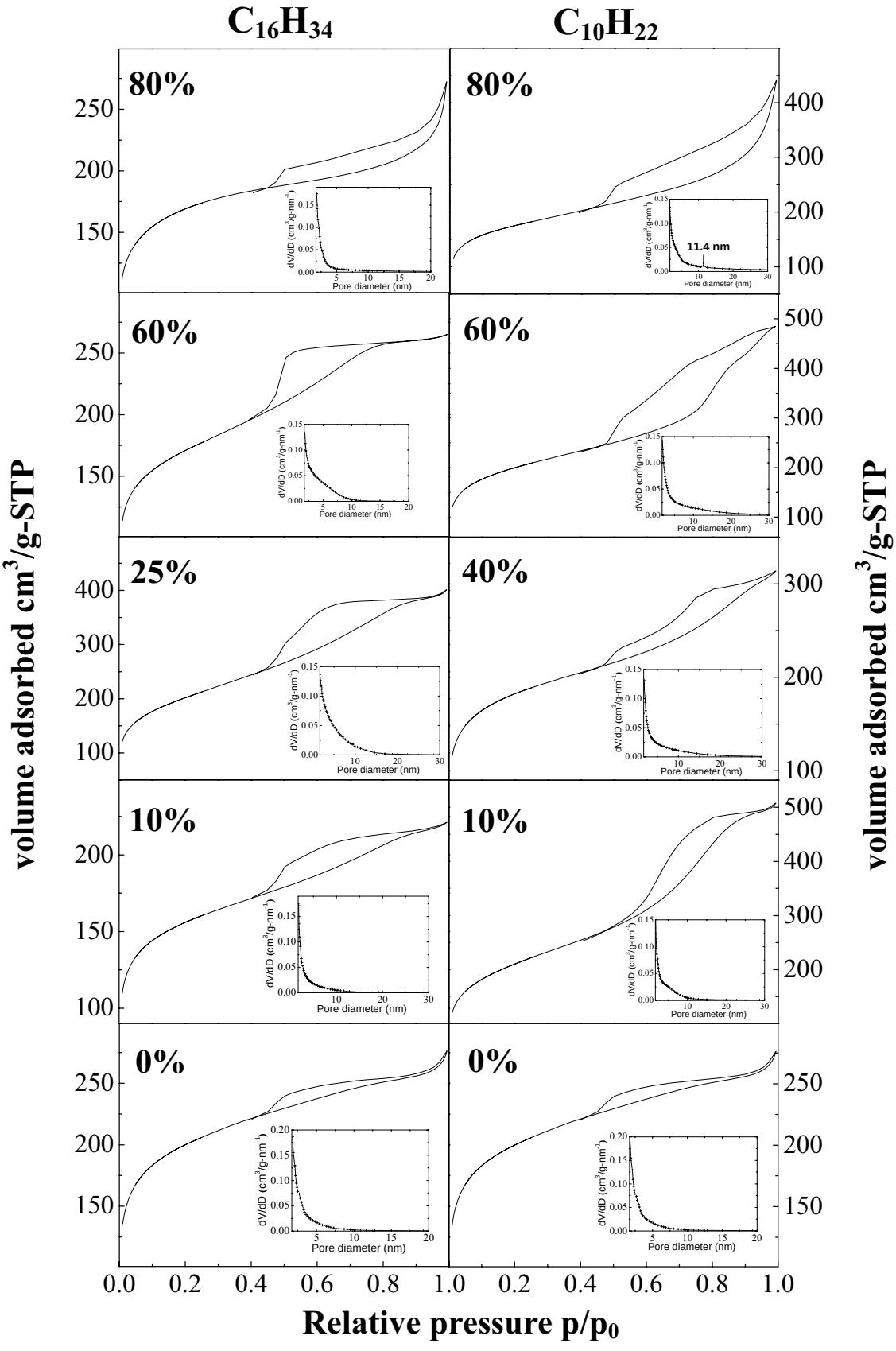


Figure III-15. *Evolution of nitrogen adsorption- desorption isotherm and the corresponding BJH pore size distribution curve (insert) with different concentrations of hexadecane and decane at R=3, pH 0.025.*

to 0.025. The water/surfactant weight ratio is still fixed at 3 and the concentration of oils is varied from 0 to 80 wt.%. TMOS is always added at room temperature.

No matter either which kind of oil or how much amount of oil needs to be added into the $R^{H}_{12}A(EO)_9$-water system since there is no line detected in the SAXS patterns. Obviously, the super-acid medium disfavors the formation of ordered mesopores network, even wormlike structure does not exist at this pH value.

As evidenced by the nitrogen adsorption-desorption measurements (**Figure III-15**), there is no pore size in the mesopore range. Upon the loading of the oils, the isotherms show that an evident quantity of adsorption occurs at high p/p_0, which means that non-porous or macroporous adsorbents existed in the given systems.

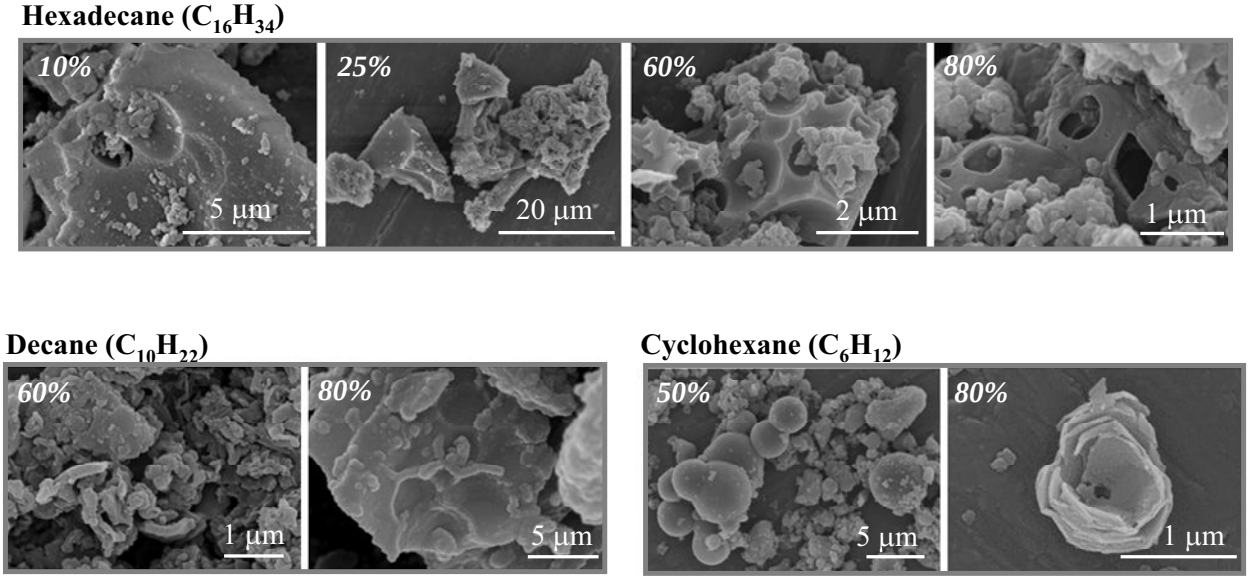


***Figure III-16**. SEM micrographs of materials synthesized with different concentrations of $C_{16}H_{34}$, $C_{10}H_{22}$ and C_6H_{12} at R=3 and pH 0.025.*

The pH conditions have been shown to be an important factor toward controlling the materials morphology. Depending both on the pH value in use during the synthesis and the emulsification process, the morphology of the materials can be drastically changed [167]. However, for the given system, super acid condition does not change the macroporous network. Even if there is no mesopore formation in all three systems, we find a few macropores for hexadecane concentrations between 60 ~ 80 wt. % and the size of the pores is around 1 ~ 2 µm (**Figure III-16**). For the system with decane, undamaged macroporous network is not detected at pH 0.025 and few fragments of macropores is observed at high concentrations of oil (**Figure III-16**). On the contrary, for the materials prepared cyclohexane, there is no difference between pH 0.025 and pH 7 as shown in the **Figure III-16**. Balls still exist even on the super acid medium condition.

3. Discussion

Three main tendencies are drawn from the analysis of the results reported above. The first one deals with the pore size and the swelling of mesopores. Decane and hexadecane act as expanders, while no mesopore enlargement is induced by cyclohexane. Moreover, we can see that mesoporous materials synthesized at water/surfactant ratio R=3 exhibit a higher diameter than the ones prepared from a micellar solution at R=9. To explain the variation of pore diameter with the incorporation of oil, we should have a look at the phase diagram. Indeed, as it can be seen from **Figure III-6**A and B, $C_{16}H_{34}$ and $C_{10}H_{22}$ solubilized in the micelles and the evolution of the structural parameters of both the hexagonal and the lamellar liquid phases evidences that these two hydrocarbons form a real core or film of oil. So we can assume that in L_1 they adopt the same behavior and that are also incorporated in the core of the micelles involving an increase of their volume. In that way, large pore mesoporous materials can be obtained through the CTM-type mechanism after surfactant removal by ethanol extraction (**Figure III-17**). This mechanism is usually considered in order to explain the pore size expansion of mesoporous materials by adding organic auxiliaries as swelling agents [202-205]. For example using non ionic polyoxyethylene surfactant, Bossiere et al. [204] consider a swelling effect of the micelle core to explain the effect of the addition of a swelling agent (TMB) on the pore size of MSU mesoporous silica. Moreover, with the given system here for a given hydrocarbon, as the micelles prepared at R=3 can solubilized a higher amount of hydrocarbon than the one R=9 (**Figure III-6** A and B), the larger swollen micelles gives rise to materials with a higher pore diameter when the synthesis is performed from a solution at R=3. We can also note that for a given surfactant and oil concentration, the mesopore expansion is more notable with decane than with hexadecane. As an example, the pore diameters of the samples prepared at R=3 and with a concentration of alkane equal to 2 wt.% are 5.6 and 4.6 nm when decane and hexadecane are respectively used (**Figure III-14**). This phenomenon can be explained by the fact that the amount oil incorporated in micelles is correlated with the molecular volume of the solubilizates. The number of moles solubilized decrease with the molecular volume of the additive [206]. This is because the equilibrium area of the micelle per surfactant is determined by the interactions at the interface. For this reason it is independent of the size of the solubilizate for a homogeneous family of additives. Consequently the micelles formed are practically identical volume and the volume available

for the solubilizates is fixed and independent of their size. Therefore oil of larger size is solubilized in smaller numbers [206]. This behavior can be related to the phase diagram (**Figure III-6** A and B). Indeed, for a fixed surfactant/water ratio micelles can solubilize a higher quantity of decane than hexadecane. In a paper [207] concerning the modulation of the pore length and the morphological architecture of mesoporous materials by the addition of alkanes, Bao et *al.* also used this argument to explain the variation of the pore size of SBA-15 with the alkane chain length. They reported a change of the mesopore diameter from 12.0 to 15.7 nm by decreasing the alkane chain length from hexadecane to hexane.

Looking at the case of cyclohexane, which is an organic compound that comprises a ring molecule with a six-fold symmetrical structure adopting either a trans or a cis conformation, it appears that even if it is solubilized in the micelles, no swelling effect is noted. In addition if the silica synthesis is performed with a C_6H_{12} concentration higher than 2 wt.% (R=9) or higher than 5 wt.% (R=3), the recovered materials adopt a randomly oriented pore arrangement. These observations led us to conclude that unlike what is observed for the solubilization of cyclohexane by block copolymer micelles such as P123 [206, 208], in the

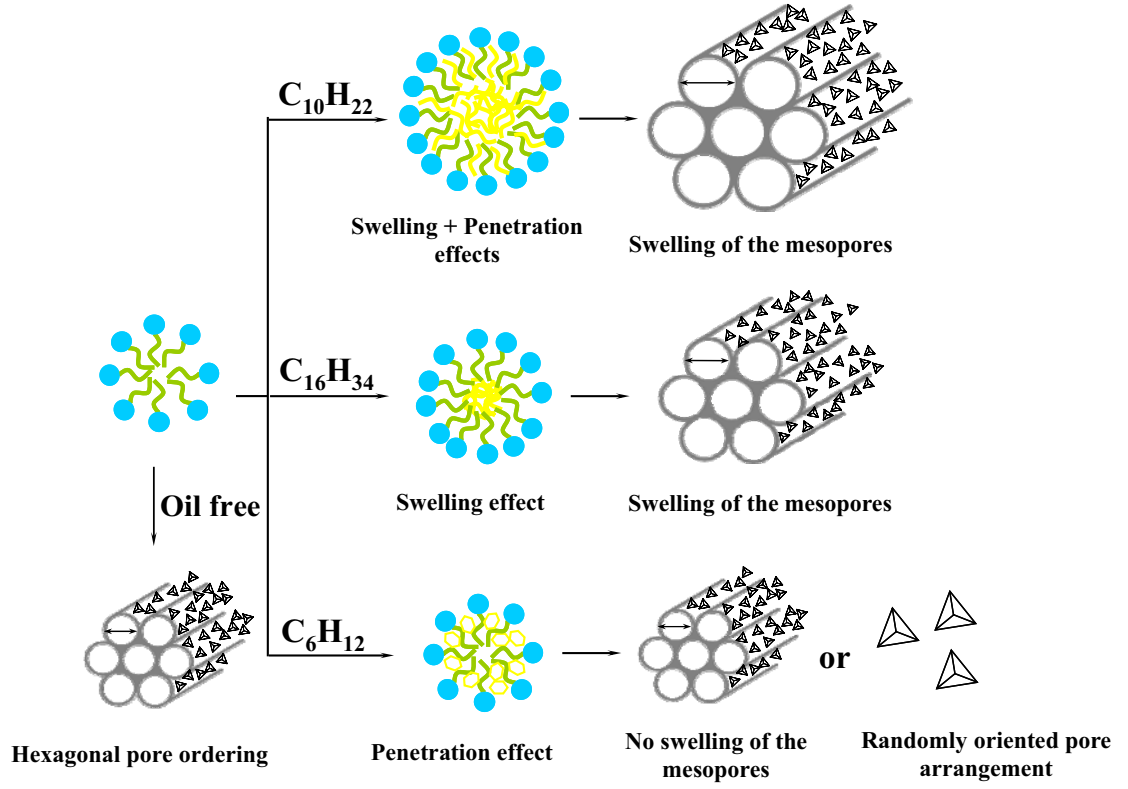


Figure III-17. *Scheme of the hydrocarbon ($C_{10}H_{22}$, $C_{16}H_{34}$ and C_6H_{12}) solubilization in the micelles and of the resulting effect on the mesopore enlargement.*

micelles of $R^H_{12}A(EO)_9$ cyclohexane does not form a core of oil, but it rather penetrate between the hydrophobic chains of the surfactant. Moreover when the concentration of C_6H_{12}

is increased we can assume that due to the presence of the ring steric restriction appears, resulting in a lost of the pore ordering (**Figure III-17**).

The second tendency that can be drawn is that at high concentrations of hexadecane and decane involve the formation of macropores. In contrast, the incorporation of cyclohexane does not lead to this macroporous network. In order to better understand this behavior once again, we have to examine in detail the phase behavior of the $R^{H}_{12}A(EO)_9$/hydrocarbon/water systems. Indeed, the phase behaviors of the ternary systems reported in **Figure III-6** showed that starting at the micellar solution domain, progressive addition of decane or hexadecane until high concentration, concentrated oil-in-water emulsions formed. These emulsions are constituted of oil droplets stabilized by the surfactant molecules. The addition of TMOS into these systems leads to its interaction with the surfactant molecules located at the oil/water interface of droplets, creating casts of the morphological macropores. The hydrothermal treatment at 80°C completes the polymerization of the silica source and after surfactant removal by ethanol extraction the macroporous materials are recovered. In contrast to $C_{10}H_{22}$ and $C_{16}H_{34}$, cyclohexane does not form concentrated emulsions. The solubility of hydrocarbons in aqueous solutions of surfactant has been described in terms of phase inversion temperature (PIT). As mentioned in the introduction part, the PIT corresponds to the temperature at which the transition from direct systems to reverse ones, where the continuous media is non-polar, occurs and it is characterized on the phase diagram by the presence of an island, which joins neither the water nor the oil corner. The PIT of the investigated systems can be calculated according to the following formula [209, 210] :

$$PIT\ (°C) = -160 + 15.5\ HLB + 1.8\ ECN$$

where ECN (equivalent carbon number) characterize the hydrocarbon and depends on its structure, whereas HLB (hydrophilic-lipophilic balance) is 14.23, specific to the surfactant. The PIT of the investigated systems was found to increase in the order C_6H_{12} ~ 62 °C, $C_{10}H_{22}$ ~ 79 °C and $C_{16}H_{34}$ ~ 89 °C. Therefore, as regards the ability to form macroporous materials a possible origin of the peculiar behavior of the $R^{H}_{12}A(EO)_9/C_6H_{12}$/water system could be associated to the fact that C_6H_{12} could not form stable concentrated emulsions due to its too lower PIT. Indeed, to obtain direct concentrated emulsions, the system should exhibit a high value of PIT [32].

The last tendency that can be concluded from the results is that the super acid conditions does not favor the formation of neither mesopore nor macropore in the $R^{H}_{12}A(EO)_9$-based systems with all three kinds of oil. In a study dealing with the relation between the lower consolute boundary and the structure of mesoporous silica materials, it has been evidenced

that the cooperative self assembly mechanism is favored if the lower consolute boundary is shifted toward high temperatures. Moreover, higher is the difference between the phase separation temperature and the temperature at which the silica precursor is added to the surfactant solution, better is the mesopore ordering [196]. Zhao et al. [188] reported the synthesis of silica mesostructures by using the triblock copolymer P85 ($EO_{26}PO_{39}EO_{20}$) and P65 ($E_{20}PO_{30}EO_{20}$) as structuring agent and tetraethyloxysilane (TEOS) as silica precursor. P85 and P65 have a CP value of 82°C in water. The TEOS:P65 (or P85): HCl:H_20 molar composition was : 1:0.0003:6:166. They claimed that ordered mesoporous silicates can only be obtained at a temperature higher than 90°C. To explain this tendency, they assume that the high concentration of H^+ and the ethanol released by the hydrolysis of TEOS have increased the CP of the triblock copolymer to a temperature higher than 100°C. In this study, we have evidenced that for a fluorinated system $R^F_8(EO)_7$/ PFOBr/ water, the mesopore ordering is obtained only if the synthesis is performed at pH 0.025, whereas if it is at pH 2, there is no line detected on the SAXS patterns at all [211]. These results will be discussed in chapter IV in detail. Therefore, we can consider that in the present study the lost of mesopore in strong acidic conditions is not related to a shift of the cloud point curve but it is rather duo to the silica polymerization.

4. Conclusion

Using aqueous solutions of $C_{12}H_{25}CO(C_2H_4O)_9OCH_3$ [$R^H_{12}A(EO)_9$], mesoporous materials with a hexagonal channel array have been prepared at 80°C until 20 wt.% of surfactant through the self assembly mechanism. In order to determine the phase sequence, phase behavior of $R^H_{12}A(EO)_9$ in aqueous solution was first investigated. We have delimited the different phase domains and determined the structural parameters of the H_1 and L_α liquid crystals. We have shown that the hydrophobic chains in the hexagonal phase are completely extended, whereas they adopt a folded up conformation in the L_α region. In both domains no variation of the cross sectional area with the number of water molecules per surfactant molecule is noted.

The effect of the solubilization of hexadecane, decane and cyclohexane into the $R^H_{12}A(EO)_9$-water system was then investigated. Micelles of $R^H_{12}A(EO)_9$ can incorporate $C_{16}H_{34}$, $C_{10}H_{22}$ and C_6H_{12}. The evolution of the structural parameters of the liquid crystal phases with the increase of the alkane concentration show that whatever the liquid crystal phase both the swelling and the penetration effects take place upon addition of decane, while

only the swelling effect occurs with hexadecane.

As regards the porous materials syntheses, the incorporation of low fraction of hexadecane or of decane leads to the formation of large mesoporous silica, whereas no swelling effect is noted with cyclohexane. This indicates that hexadecane and decane form a core of oil in the center of the micelles while cyclohexane is incorporated between the hydrophobic chains of the surfactant. Results also evidence that when hexadecane and decane are used as hydrocarbon, macropores templated by the oil droplets appear if the amount of oil concentration is higher than 40 wt.%. In contrast, due to its low PIT, no macroporous material can be prepared from the $R^{H}_{12}A(EO)_9/C_6H_{12}$/water system.

Chapitre IV. Préparation et caractérisation de matériaux poreux préparés à partir de systèmes à base de tensioactifs fluorés

L'étude des systèmes hydrogène $R^H_{12}A(EO)_9$/alcane/eau a montré que la formation de matériaux macroporeux est favorisée pour les systèmes présentant une TIP élevée. Dans le but de savoir si cette règle peut être généralisée, nous avons étudié des systèmes à base de tensioactifs fluorés. Dans ce chapitre, deux tensioactifs fluorés $C_8F_{17}C_2H_4(OC_2H_4)_9OH$ [$R^F_8(EO)_9$]. et $C_7F_{15}C_2H_4(OC_2H_4)_8OH$ [$R^F_7(EO)_8$]. ont été utilisés pour préparer des matériaux poreux. Nous avons examiné l'effet de la solubilisation de différents fluorocarbures sur les propriétés des matériaux obtenus. Avec le système le plus hydrophile $R^F_8(EO)_9$, la préparation de matériaux qui présentent des macropores est possible avec des émulsion concentrées fluorocarbure/eau qui contiennent plus de 50 % de perfluorodécane ou de perfluorooctybromure (PFOBr).

Avec le système légèrement moins hydrophile $R^F_7(EO)_8$ des matériaux constitués par un réseau de macropores a été obtenu eu utilisant une huile mixte $(C_4F_9CH)_2$= avec une concentration relativement faible de cette huile (15 %) . De plus, ces matériaux présentent un réseau de mésopores qui constitue la paroi des macropores. Lorsque le PFOBr est utilisé, la formation de macropores n'est pas possible. Tout comme pour les systèmes hydrogénés, on constate que la formation de macropores est favorisée si la PIT est élevée.

Chapter IV. Preparation and characterization of porous silica templated by nonionic fluorinated systems

1. The $C_8F_{17}C_2H_4(OC_2H_4)_9OH$ based systems 99

1.1 Phase behavior 99

1.2 Porous silica prepared from $R^F_8(EO)_9$/ PFD/ water $R^F_8(EO)_9$/ PFD/ water systems. 105

2. $C_7F_{15}C_2H_4(OC_2H_4)_8OH$ based systems 113

2.1 Phase behavior 113

2.2 Porous materials prepared from with microemulsions and emulsions. 118

3. Discussion 125

3.1 Macroporous silica 125

3.2 Expansion of the mesopores 126

3.3 Pore ordering in the presence of PFOBr 127

4. Conclusion 128

IV. Preparation and characterization of porous silica templated by nonionic fluorinated systems

The investigation of the $R^{H}_{12}A(EO)_9$/alkane/water system for the preparation of porous materials has revealed that higher PIT of the system favored the formation of macroporous materials. In order to know whether this rule can be generalized, we have considered fluorinated systems. In this study, two fluorinated surfactants $C_8F_{17}C_2H_4(OC_2H_4)_9OH$ and $C_7F_{15}C_2H_4(OC_2H_4)_8OH$ are used for the preparation of porous silica. Herein, we are focused on the effect of the solubilization of various fluorocarbons on the properties of the recovered materials.

1. The $C_8F_{17}C_2H_4(OC_2H_4)_9OH$ based systems

1.1 Phase behavior

This part describes the phase behavior of the surfactant $C_8F_{17}C_2H_4(OC_2H_4)_9OH$ (labeled as $R^F_8(EO)_9$) in water and in presence of two types of oil (perfluorodecalin and perfluorooctyl bromide). These systems are used to prepare meso and/or macroporous materials.

1.1.1 $R^F_8(EO)_9$ in water

The phase behavior of the surfactant $R^F_8(EO)_9$ in water is reported in **Figure IV-1**. Along the investigated temperature range, a direct micellar L_1 phase is detected up to 30 wt.% at 20 ^oC.

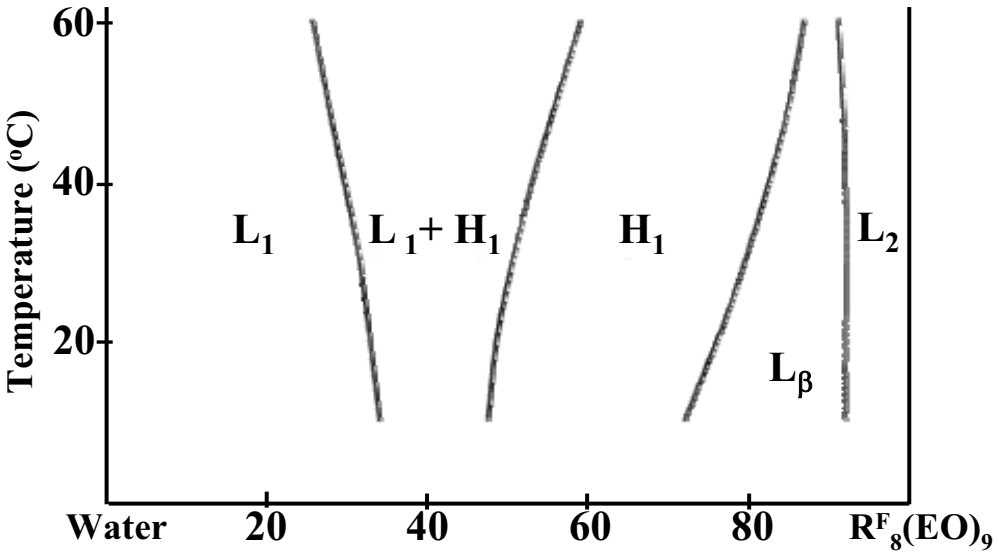


Figure IV-1. *Phase diagram of $R^F_8(EO)_9$ in water [148] L_1= direct micelle; H_1=hexagonal phase; L_β=gel phase; L_2=reverse micelle*

Actually in this domain, only one rather broad peak is observed on the SAXS pattern (**Figure IV-2a**). For example at 10 wt % of $R^F_8(EO)_9$, this peak is a correlation distance to 13.7 nm ($d = 2\pi/q$) which is related to the existence of micelles in the solution. It corresponds to the mean distance between the centers of two micelles. When the surfactant concentration is increased, this peak is shifted toward higher wave vector (**Figure IV-2b**). For a 25 wt % of $R^F_8(EO)_9$, the correlation distance is found to be equal to 9.0 nm because of the decrease of the distance between the center of micelles.

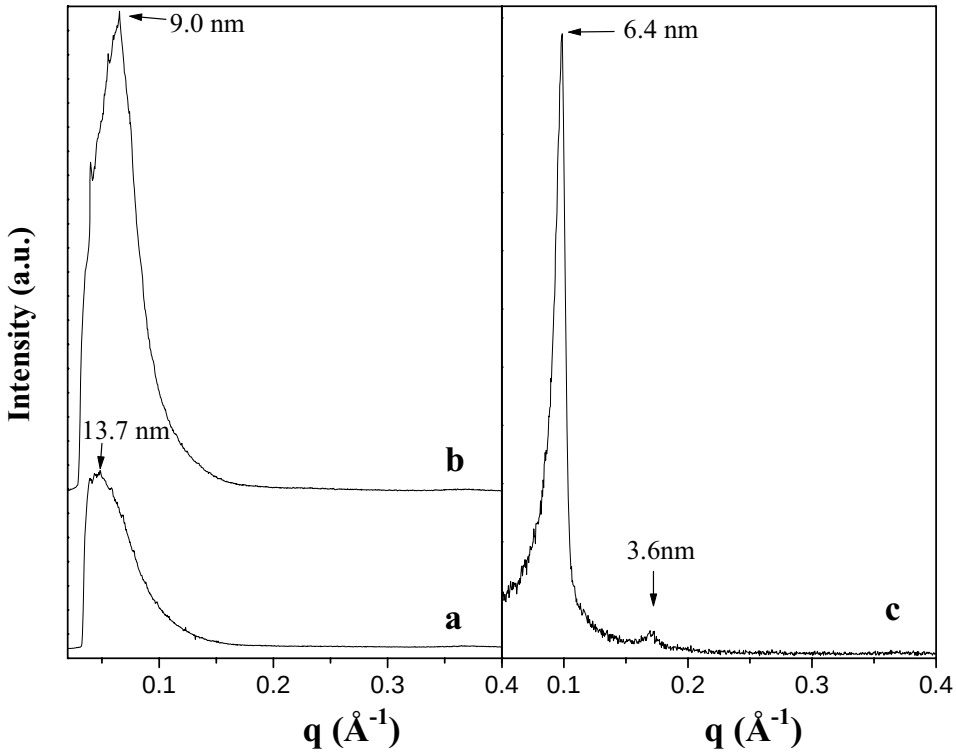


Figure IV-2. *$R^F_8(EO)_9$-water system: Evolution of the SAXS pattern with the concentration (wt %) of $R^F_8(EO)_9$ in water at 25 °C: a, 10% (L_1); b, 25% (L_1); c, 60% (H_1).*



Figure IV-3. *Characteristic texture of the hexagonal liquid crystal.*

When the weight percent of surfactant is increased up to 75, an optically anisotropic phase is detected. The fan-shaped texture (**Figure IV-3**) observed by optical microscopy with polarized light is characteristic of the structure defects of the hexagonal phase. The hexagonal symmetry is confirmed by SAXS measurements. For example, lines located at 6.4 and 3.6 nm for a 60 wt % of $R^F_8(EO)_9$ are detected on the pattern (**Figure IV-2c**). The relative positions of the Bragg reflections are $1:\sqrt{3}$. Consequently, they can be attributed to the (100) and (110) reflections of the hexagonal structure. Contrary to the hydrogenated system, the (200) reflection is generally not observed for fluorinated ones. In this case the extinction is related

to the factor of the form of cylinders which are very weak for the position corresponding to reflection 200. It should be noted that the H_1 phase is separated from L_1 by a two-phase region ($30 \leq$ wt % ≤ 50). The correlation distance obtained from the limit of phase (30 wt %) is close to the Bragg reflection of the hexagonal phase at 50 wt % at low temperature. If the surfactant concentration is further increased (>75 wt %), the texture of the gel phase appears. If the temperature is increased, the limits of the hexagonal phase are shifted toward higher surfactant concentrations.

1.1.2 Haze point of the $R^F_8(EO)_9$/ fluorocarbon systems

"Haze point curve" is a solubilization curve. It is the reverse of cloud point curve, which separates the biphasic zone at low temperature and the one phase zone at high temperature. The haze point of $R^F_7(EO)_8$ – PFOBr system is detected at 35 °C when the concentration of $R^F_7(EO)_8$ is around 2.2 wt.% (**Figure IV-22**). Thus $R^F_7(EO)_8$ is soluble in PFOBr at all the proportions as long as the temperature higher than 35 °C. We tried to determine the haze point of system $R^F_8(EO)_9$ – PFD and $R^F_8(EO)_9$ – PFOBr, but in the scale of the studied temperature, the systems are always two phases owing to their haze points are higher than 100 °C.

1.1.3 Solubilization of perfluorodecalin (PFD)

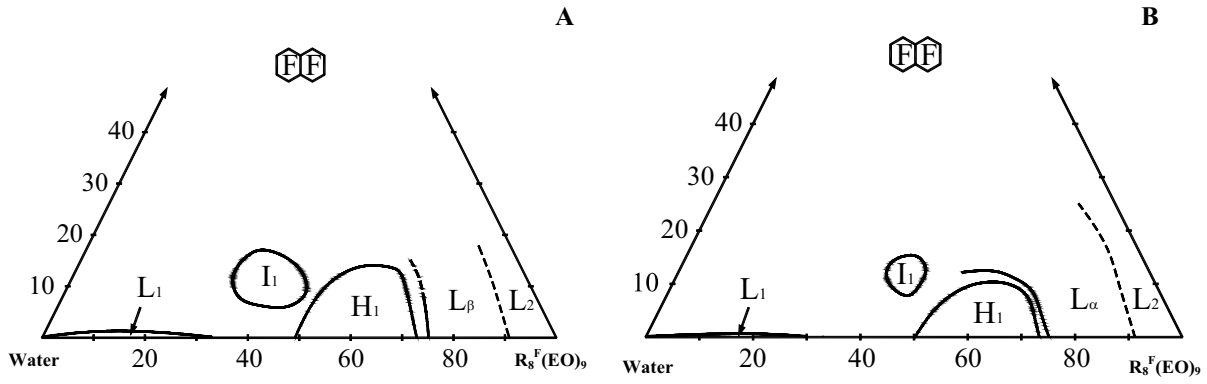


Figure IV-4. *Partial ternary diagram of $R^F_8(EO)_9$/Perfluorodecalin/H_2O at 25 °C (A) and 50 °C (B) L_1=micellar solution; I_1=cubic phase; H_1=hexagonal phase; L_β=gel phase; L_2=reverse micelle [195]*

A partial phase diagram of the ternary $R^F_8(EO)_9$/Perfluorodecalin/water system is reported in **Figure IV-4** at 20 °C and 50 °C. In the investigated temperature range, the liquid crystal domain is composed of the cubic, hexagonal and lamellar phases. At high water

concentration, the existence range of the micellar domain (L_1) is small; only 1 wt % of PFD can be incorporated in micelles. Upon the PFD loading is increasing, a **Winsor I** type solution is obtained.

This terminology corresponds to the one of four general types of phase equilibria identified by Winsor [212]. If the surfactant is preferentially soluble in water, oil-in-water (o/w) microemulsion can be formed and the solubilization of oil in excess induces a biphasic system where the microemulsion coexists with a pure oil phase, namely a Winsor I system. In the case studied here, the upper phase is composed of the swollen micelles, whereas the PFD excess constitutes the lower phase. Between 35 and 50 wt % of $R^F_8(EO)_9$, a cubic phase, which is not observed in the binary system, is formed when the concentration of PFD is located between 8 and 17 wt %. The existence range of the cubic structure is limited. When the weight percent of surfactant is increased from 50 to 72, an optically anisotropic phase is detected. The fan-shaped texture observed by optical microscopy with polarized light is the characteristic of the defects of the direct hexagonal H_1 phase. The hexagonal symmetry is confirmed by SAXS measurements. Indeed, lines located at 6.82 and 3.97 nm, for the sample prepared with 54.5 wt % of $R^F_8(EO)_9$, 9.1 wt % of PFD and 36.4 wt % of water, are detected on the pattern (**Figure IV-5**).

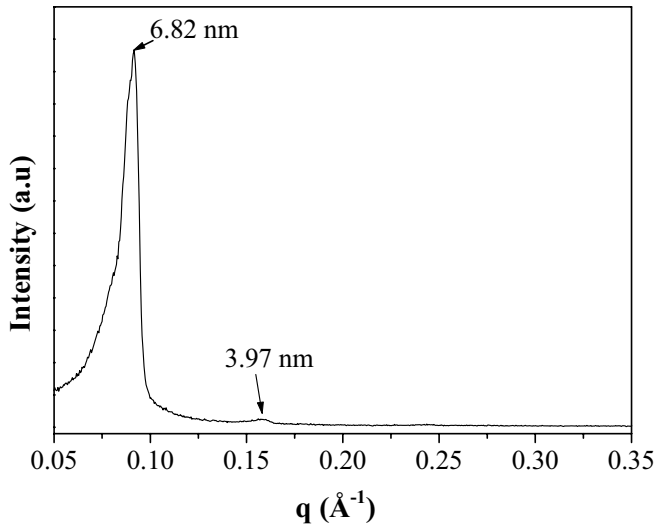


Figure IV-5 *Hexagonal SAXS pattern at 25 °C of sample prepared with 54.5 wt % of $R^F_8(EO)_9$, 9.1 wt % of $C_{10}F_{18}$ and 36.4 wt % of water.*

The relative positions of the Bragg reflections are characteristic of the hexagonal structure. In the ternary system, the (200) reflection is still not observed. The surfactant range composition belonging to H_1 is progressively reduced as the PFD loading is increased. Indeed, as it can be seen in **Figure IV-4**, the perfluorodecalin incorporation rate in the hexagonal

phase is strongly dependent on the water/$R^F_8(EO)_9$ ratio (noted as R) and it reaches a maximum (14.0 wt %) for R = 0.44. The H_1 phase is separated from the cubic one by a two-phase region. If the surfactant concentration is further increased (>73 wt %), depending on the temperature, the lamellar (L_α) or the solid lamellar phase (L_β) appears. The liquid crystal domain is progressively reduced as the temperature increases from 20 to 60 °C and only the lamellar phase remains above 60 °C.

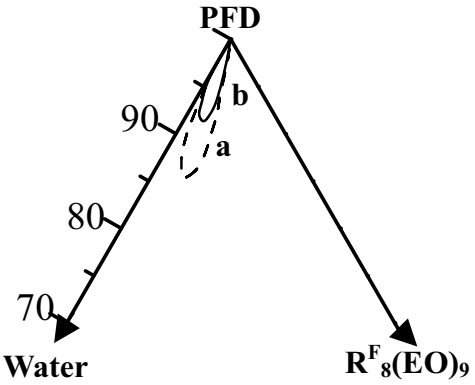


Figure IV-6. *Domain of concentrated emulsions formed by the $R^F_8(EO)_9$ /PFD/water. The emulsion is stable for weeks (a) and for months (b) at room temperature.*

Adding the oils dropwise under gentle stirring to the L_1 phase, oil-in-water concentrated emulsions are obtained for water/ surfactant ratios comprised between 9 and 3 (**Figure IV-6**). It should be noted that the stability of the emulsions is enhanced when the concentration of fluorocarbon is increased. Indeed, the samples prepared with an oil loading lower than 91 wt. % are stable for several weeks (**Figure IV-6**), whereas those preparing with a concentration of PFD higher than 91 wt.% appeared highly viscoelastic and very stable for months (**Figure IV-6b**). The structure of theses emulsions can be described as foams where the oil droplets covered with a surfactant film bathe in the continuous phase, which is constituted by an o/w microemulsion [213].

1.1.4 Solubilization of Perfluorooctyl bromide (PFOBr)

To establish the ternary diagram of $R^F_8(EO)_9$ / Perfluorooctyl bromide /water, we have used the Shinoda method which consists in determining the cloud point curve and the solubilization curve as a function of the temperature (See section 2 of Chapter II). From the binary diagram of $R^F_8(EO)_9$, it was shown that the cloud point is quite high (**Figure IV-1**). Thus, when we were determining the Shinoda diagram, just a part of the solubilization curve

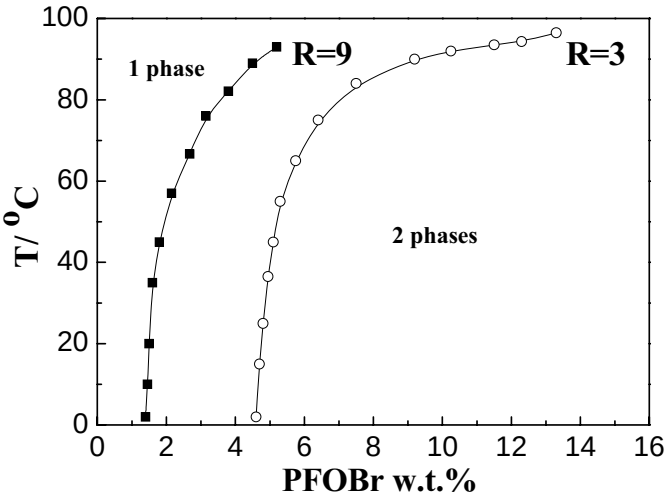


***Figure IV-7**. Part of pseudo-Shinoda diagrams established for a water/surfactant ratios to 9 and 3 (only solubilization curve)*

was detected between 0~100 °C (**Figure IV-7**). Above this solubilization curve, one mere phase is presented. But within this range, we can not reach the cloud point curve.

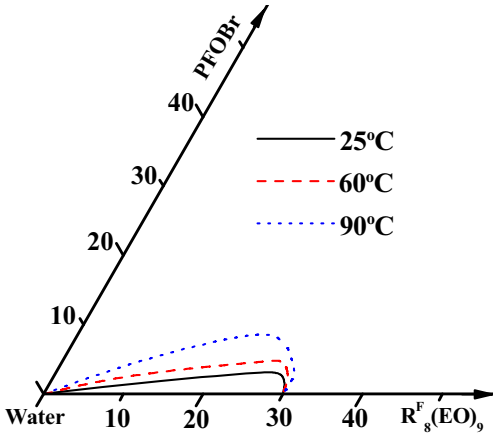


***Figure IV-8.** The zone microemulsion of $R^F_8(EO)_9$/ H_2O /Perfluorooctyl bromide system.*

These data allowed us to determine the subsequent ternary diagram. A partial phase diagram of the ternary $R^F_8(EO)_9/C_8F_{17}Br/H_2O$ system is reported in **Figure IV-8**. The zone of microemulsion is getting larger when the temperature is increased. As we already stated that the PIT is characterized on the phase diagram by the presence of an island, which joins neither the water corner nor the oil corner of the phase diagram. For $R^F_8(EO)_9/C_8F_{17}Br/H_2O$ system, even at 90 °C, the microemulsion domain still joins the water-rich corner of the phase diagram, no island appears. But this domain will be shifted towards higher PFOBr concentrations at temperature higher than 100°C in order to form the island. According to the phase diagram, the PIT value of the system is higher than 100°C.

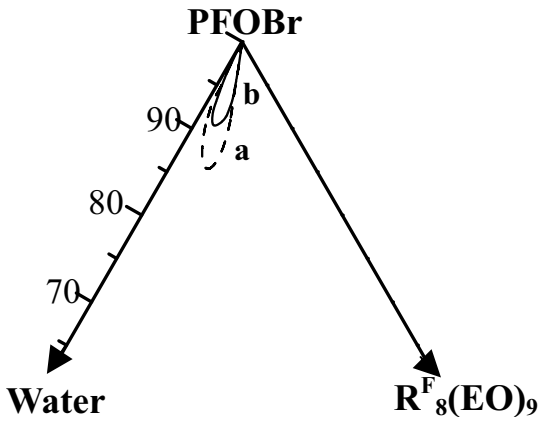


Figure IV-9. *Domain of concentrated emulsions formed by $R^F_8(EO)_9$ /PFOBr/water. The emulsion is stable for weeks (a) and for months (b) at room temperature.*

As observed when PFD is used as oil, at high PFOBr concentration oil-in-water gel emulsions are obtained for R values comprised between 9 and 3 (**Figure IV-9)**.

1.2 Porous silica prepared from $R^F_8(EO)_9$/ PFD/ water $R^F_8(EO)_9$/ PFOBr/ water systems.

1.2.1 Effect of oil molecular structure and oil content

We prepared materials from the $R^F_8(EO)_9$-based system containing various amounts of fluorinated oil at room temperature The water/ surfactant ratios are equal to 9, 4 and 3. The oil concentration varied from 15 to 95 wt.%. . The surfactant /silica molar ratio and the pH are fixed respectively to 0.5 and 2. Silica source was added into the mixture at room temperature. The procedure for the preparation of materials is the same as that used in Chapter II. Unless otherwise specified, same conditions as just mentioned about had always been used in this section.

It was shown previously by our group that PFD can be an effective swelling agent for the design of large pore mesoporous materials while the oil concentration was kept lower than 40 wt.%. The SEM analysis have revealed that no macropore is obtained in the PFD range from 1 to 40 wt.% [195, 196]. That's why in the study reported here we have considered higher PFD concentrations. We prepared materials with increasing concentration of PFD until 95% for R=4 and R=3. As evidenced in **Figure IV-6**, high concentrated emulsion formed in both $R^F_8(EO)_9$/PFD/water and $R^F_8(EO)_9$/PFOBr/water systems. Hence, we used these concentrated emulsions as template to prepare macroporous materials.

When PFOBr is used as oil, considering the comparison with other systems and the facility

to form concentrated emulsions, we mainly focused on R=3 for the preparation of the macroporous materials.

- *The structural properties*

The **Figure IV-10** presents the SAXS patterns of the materials prepared from $R^F_8(EO)_9$/ PDF/ H_2O system. In the investigation range of oil concentration, whatever the water/surfactant ratio, either one broad peak or no reflection is detected on the SAXS pattern. Thus, the recovered materials exhibit no pore ordering and they adopt a wormhole like structure.

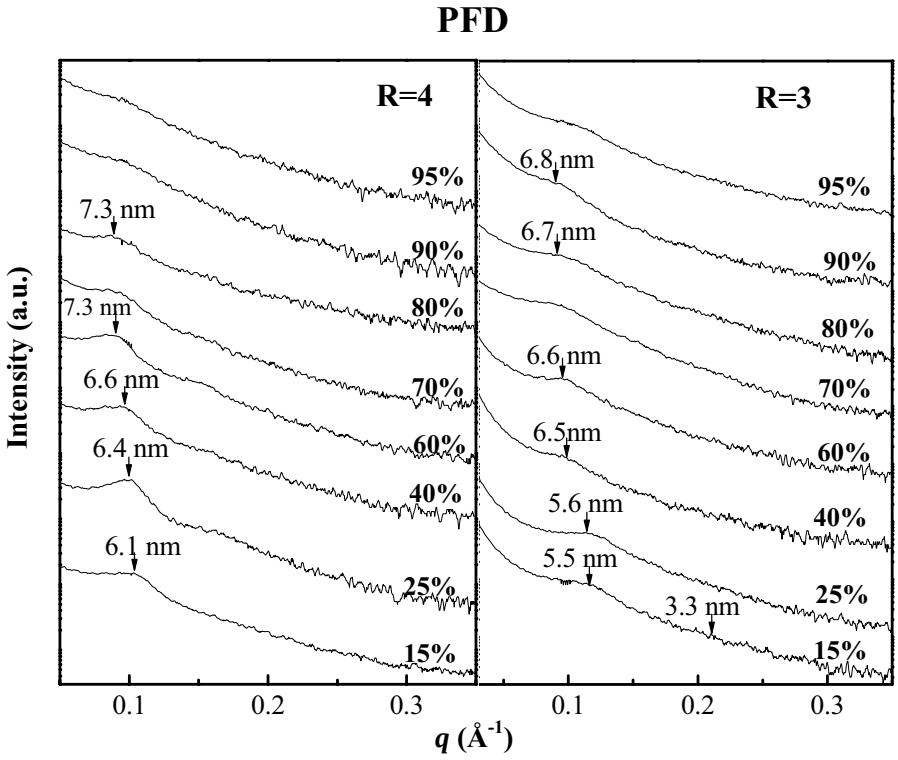


Figure IV-10. *SAXS patterns of the materials prepared from $R^F_8(EO)_9$ with different concentrations of PFD at R=4 and 3, 20°C.*

For the materials prepared with PFOBr, the X-ray patterns of materials are shown in **Figure IV-11**. Firstly, for R=9, the 110 reflection disappeared as soon as we add PFOBr to the system and the Bragg distance is getting larger slightly. Then, we have a look at the progressive addition of PFOBr at R=3 in detail. As regards the material synthesized without oil, in addition to a peak at 5.5 nm, another peak, attributed to the 110 reflection of the hexagonal system, is detected on the SAXS pattern, very weak though. (**Figure IV-11**). However, since the 110 reflection is not well resolved and the 200 peak is not observed, we conclude that the material rather adopts a weakly 2-D hexagonal structure. Upon the addition

of PFOBr, the first reflection is shifted towards lower values of *q*, i.e. higher value of d-spacing. For example, the position of the first peak varies from 5.5 to 7.6 nm when the oil loading is increased from 0 to 30 wt.%.

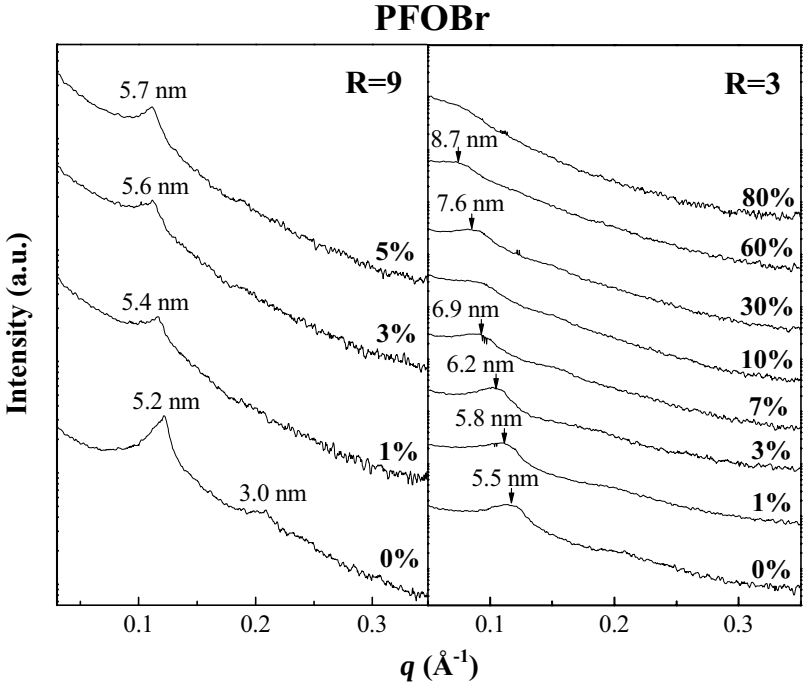


Figure IV-11. *SAXS patterns of the material prepared from $R^F_8(EO)_9$ with different of concentrations of PFOBr for R=9 and 3.*

- *The textural characteristics*

Nitrogen adsorption-desorption isotherms and the corresponding BJH pore size distributions (obtained from an analysis of the adsorption branch of the isotherm) are shown in **Figure IV-12**. According to the IUPAC classification [187], combination isotherms between type IV and type II are obtained from the nitrogen adsorption-desorption analysis.

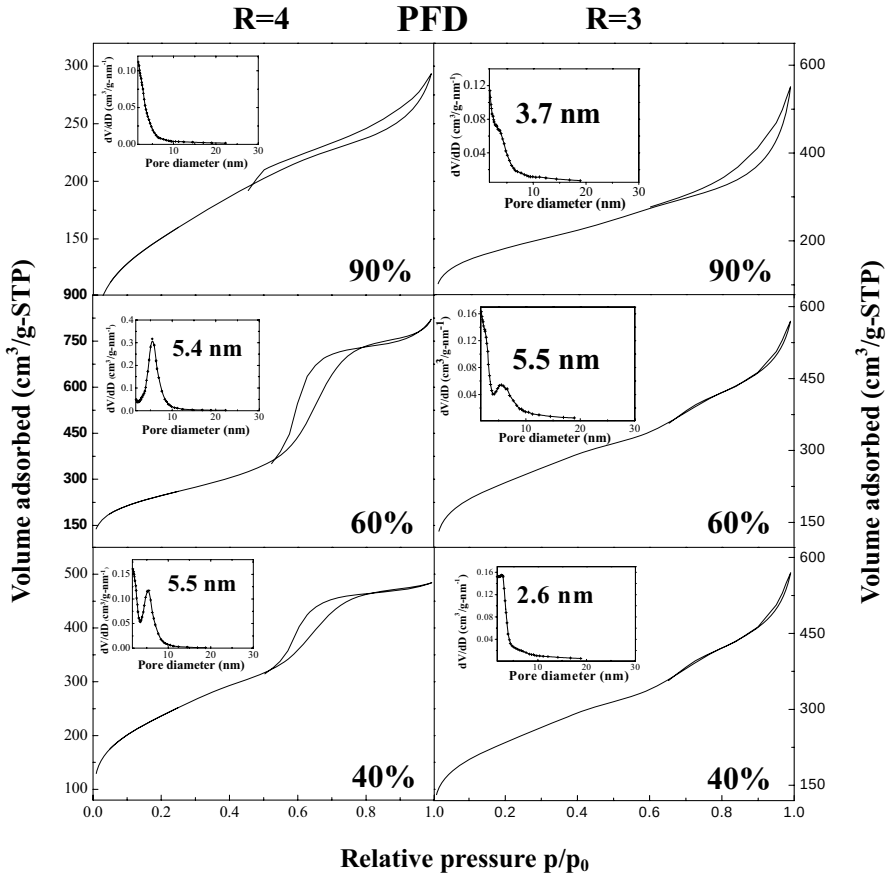


Figure IV-12. *Evolution of the nitrogen adsorption-desorption isotherm and the corresponding BJH pore size distribution curve with the concentration of PFD 40%, 60% and 90 wt.% at R=4 and R=3.*

When 1-bromo-perfluorooctane is used instead of perfluorodecalin, a type IV isotherm, characteristic of mesoporous materials is obtained from the materials prepared without oil and the pore size distribution is narrow and centered at 4.3 nm (**Figure IV-13**). Upon the addition of PFOBr, the shape of isotherm changes. Indeed we can see that the adsorbed volume of nitrogen increases significantly at high relative pressures instead of remaining constant as a result of saturation. It is noted that the isotherm becomes a combination between type IV and type II at 80 wt. % of PFOBr. Moreover, the maximum of the pore size distribution is shifted from 4.3 to 5.4 nm when the amount of oil varied from 0 to 30 wt. %, indicating that in this range of concentration PFOBr acts as an expander.

As evidenced by **Figure IV-14B**, above 30 wt.% of fluorocarbon, the mean pore diameter remains almost constant, but the pore size distribution becomes broader (inserts of **Figure IV-13**). As it can be noted from **Figure IV-14A**, whatever the PFOBr concentration, the specific surface area is high (> 800 m²/g).

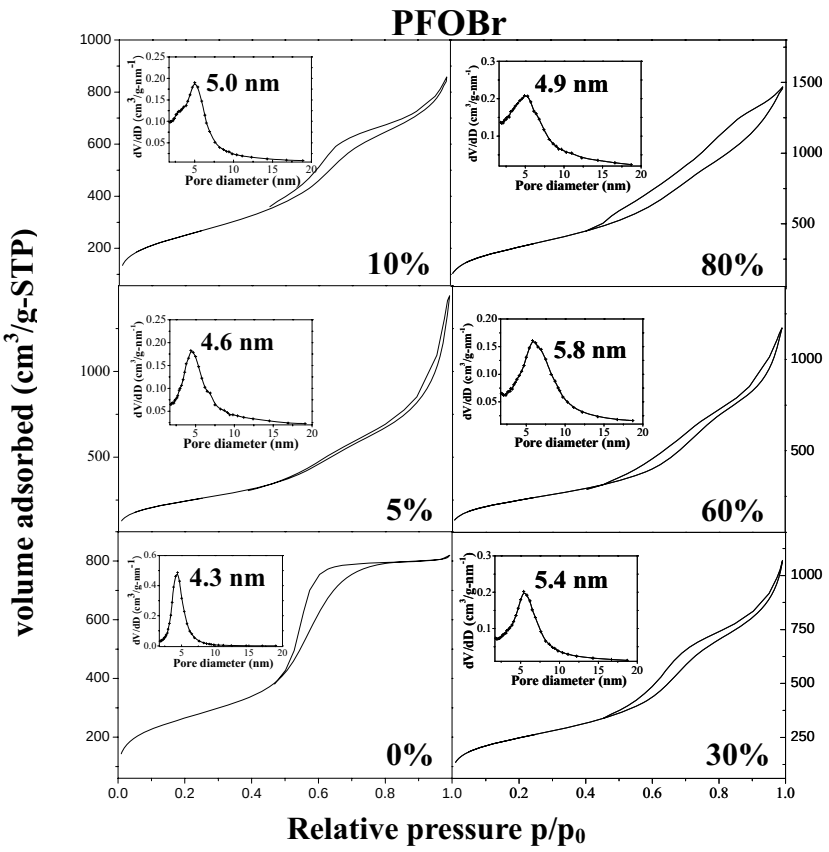


Figure IV-13. *Evolution of the nitrogen adsorption-desorption isotherm and the corresponding BJH pore size distribution curve (insert) with the concentration of PFOBr 0%, 5%, 10%, 30%, 60% and 80 wt.%, R=3.*

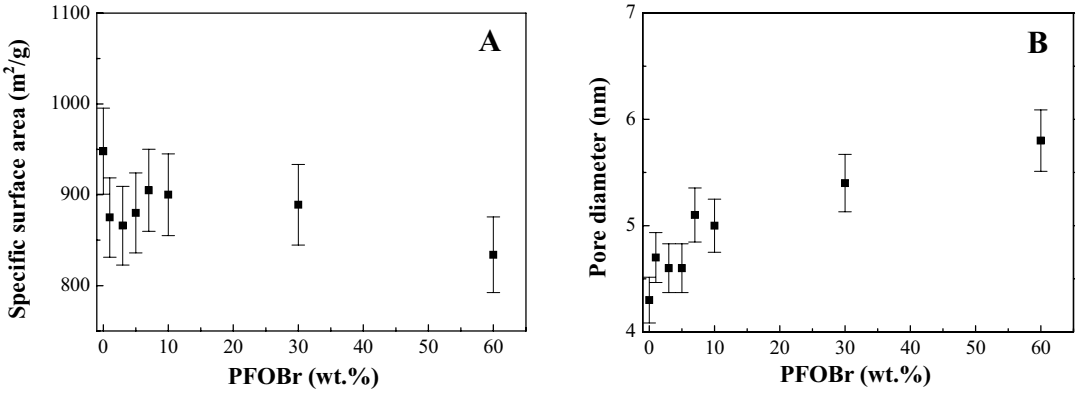


Figure IV-14*. Variation of the specific surface area (A) and of the pore diameter (B) as a function of the concentration of PFOBr.*

- *Morphology*

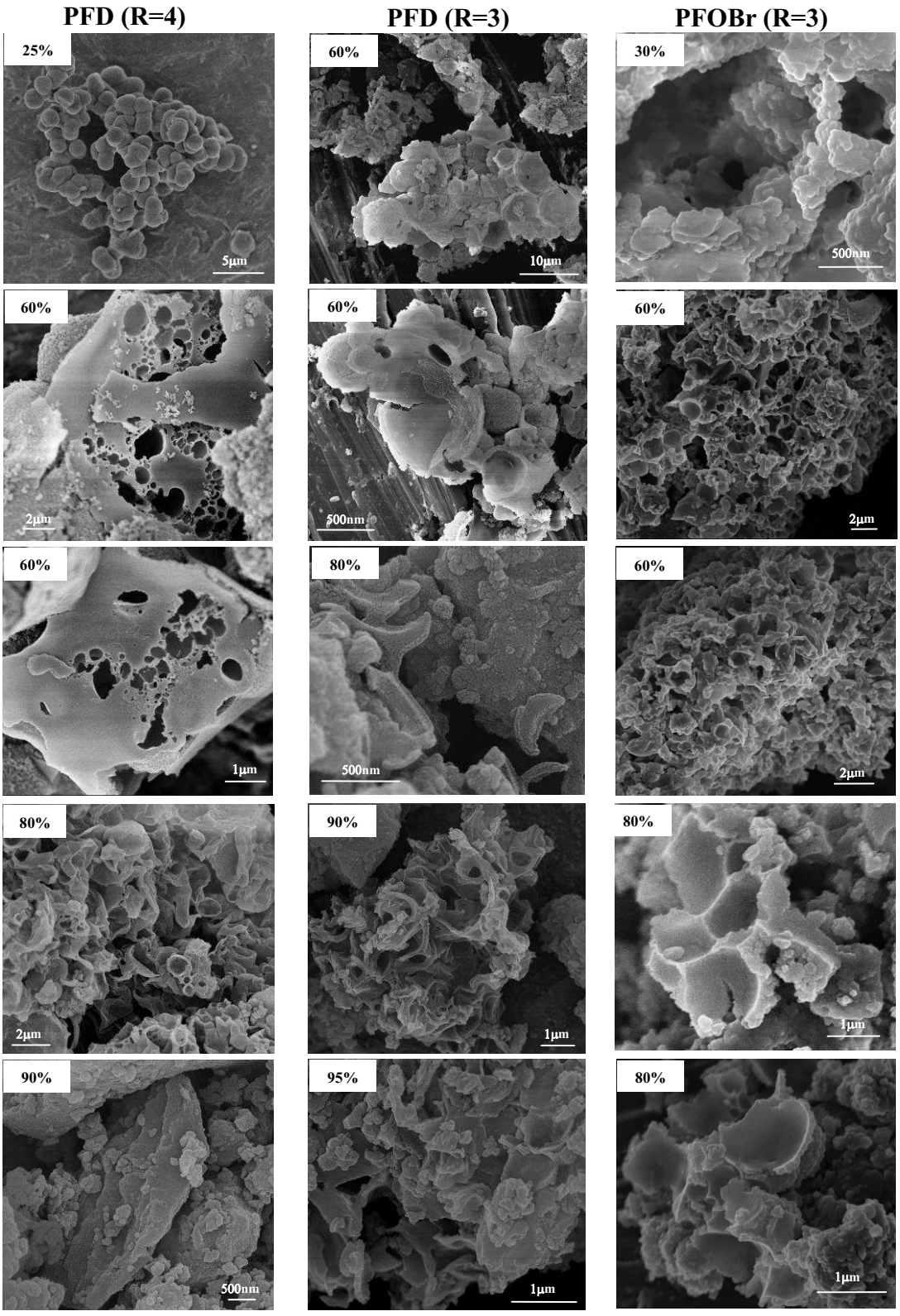


Figure IV-15. *SEM micrograph of samples prepared with the different concentrations of PFD and PFOBr*

From **Figure IV-15**, which depicts several representatives scanning electronic micrographs (SEM) of the synthesized silicas, we can see that either for PFD or PFOBr,

macroporous materials are recovered at oil concentrations at least higher than 50 wt.%. Indeed hollow spheres with apertures whose size is around 1 ~ 2 μm are formed. Upon the oil content higher and higher, these hollow spheres are broken, thus after surfactant and oil removal the collapse of their structure has occurred. Besides, when fluorocarbon concentrations lower than 50%, the morphology of the materials can be described as an agglomerate of silica particles (**Figure IV-15** top left corner), no macropores are obtained.

1.2.2 Effect of reaction medium pH value

As done for the $R^{H}_{12}A(EO)_9$/ alkane/ water system, we examined the effect of the pH on the properties of the materials. The TMOS is always added at room temperature.

- *The structural properties*

The pattern of X-ray diffraction of samples prepared at pH 0.025 with PFD and PFOBr are presented in **Figure IV-16**. Comparing the structure of the materials prepared at pH 2 and pH 0.025, we can see that the superacid condition does not favor the mesopore ordering. Moreover, the first reflection also has been shifted towards lower values of q, thus d-spacing is getting larger upon the addition of oils.

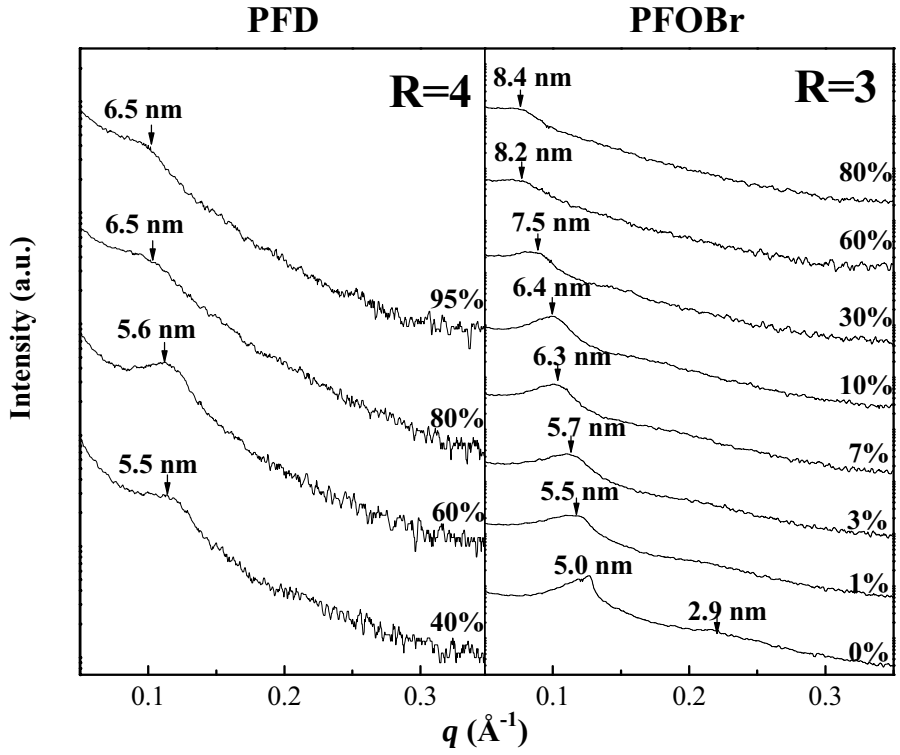


Figure IV-16. *SAXS pattern of the materials prepared with PFD and PFOBr at pH 0.025*

- *The textural characteristics*

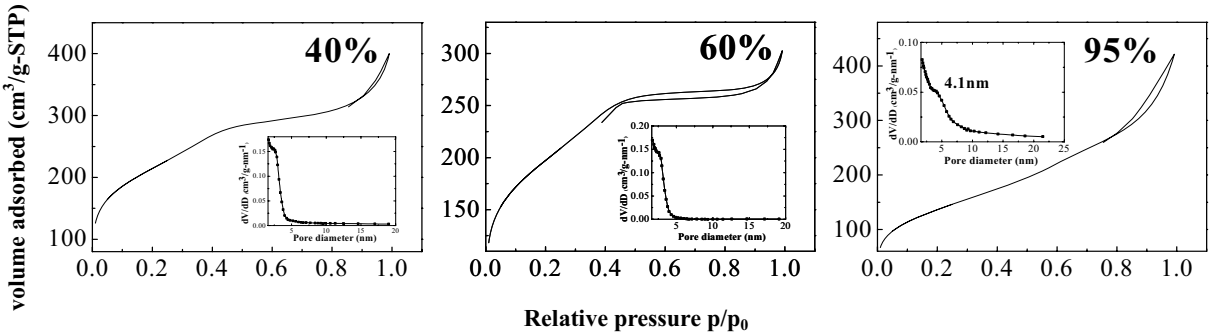


Figure IV-17. *Evolution of the nitrogen adsorption-desorption isotherm and the corresponding BJH pore size distribution curve with the concentration of PFD 40%, 60% and 95 wt.% at R=4, pH0.025.*

From the nitrogen adsorption-desorption analysis (**Figure IV-17**), it appears that the molecular sieves obtained with content of PFD higher than 40 wt.% exhibit isotherm intermediates between type II and type IV.

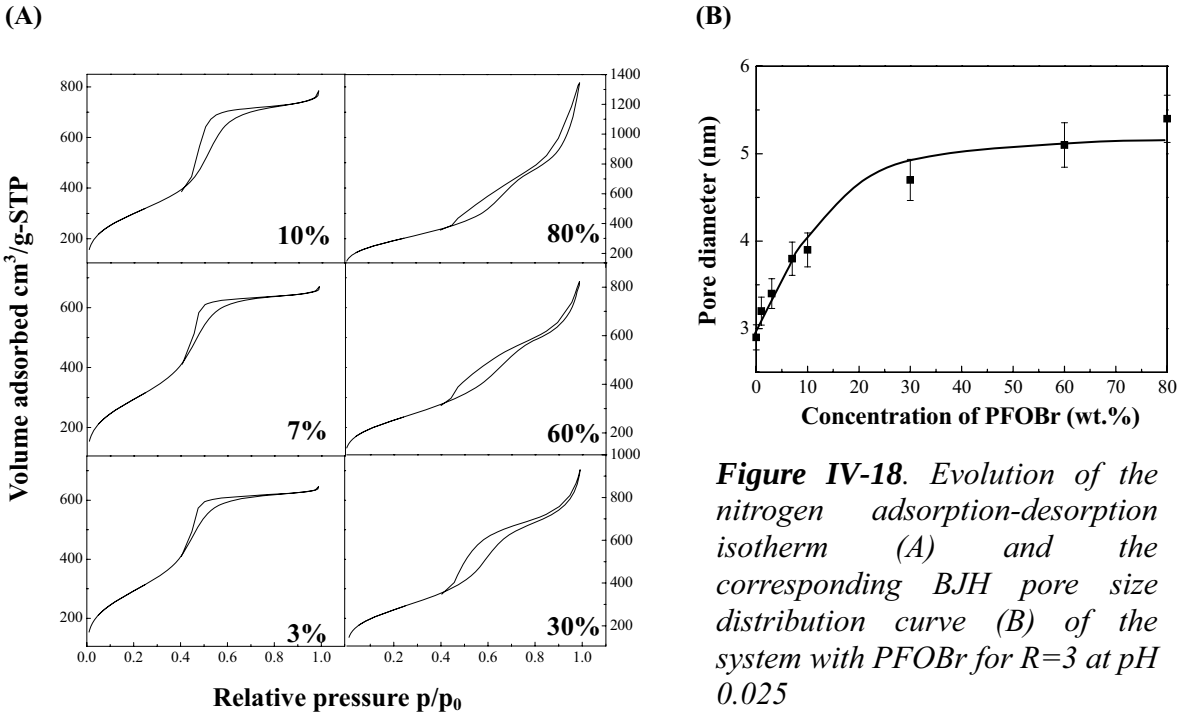


Figure IV-18*. Evolution of the nitrogen adsorption-desorption isotherm (A) and the corresponding BJH pore size distribution curve (B) of the system with PFOBr for R=3 at pH 0.025*

Concerning the case of PFOBr, the textural characteristics of the recovered materials show the same tendency than the one prepared at pH 2 (**Figure IV-18**).

- *Morphology*

Only damaged macroporous network is detected for these systems at pH 0.025. Indeed, super

acid condition does not favor the formation of macroporous network as we expected. Nevertheless, few fragments of macropores are observed at 60 wt.% of oil concentration (**Figure IV-19**).

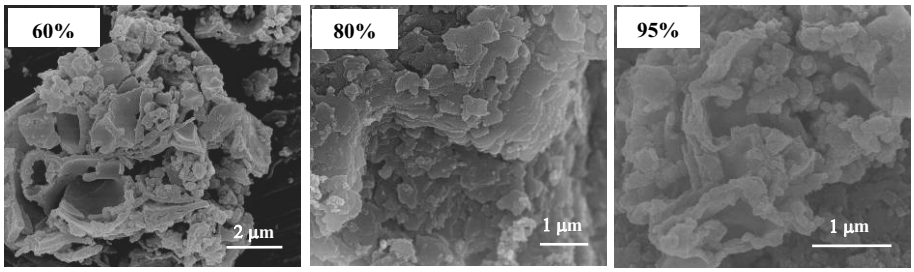


Figure IV-19. *SEM micrograph of samples prepared with the different concentration of PFD for R=4 at pH 0.025.*

Besides, after ethanol extraction, materials prepared at pH 0.025 were recovered as monoliths which are dozen millimeters in length (**Figure IV-20**). On the contrary, there is not monolith observed at pH 2.



Figure IV-20 *Photograph of a monolith prepared at 7% PFOBr, R=3, pH=0.025.*

2. $C_7F_{15}C_2H_4(OC_2H_4)_8OH$ based systems

2.1 Phase behavior

This part describes the phase behavior of surfactant $C_7F_{15}C_2H_4(OC_2H_4)_8OH$ (labeled as $R^F{}_7(EO)_8$) in water and in presence of three types of oil (perfluorodecalin, bis (F-butyl)-1,2-ethylene and perfluorooctyl bromide), which is used to prepare meso and / or macroporous materials.

2.1.1 $R^F{}_7(EO)_8$ in water

The binary surfactant - water phase diagram (**Figure IV-21**), which has been established

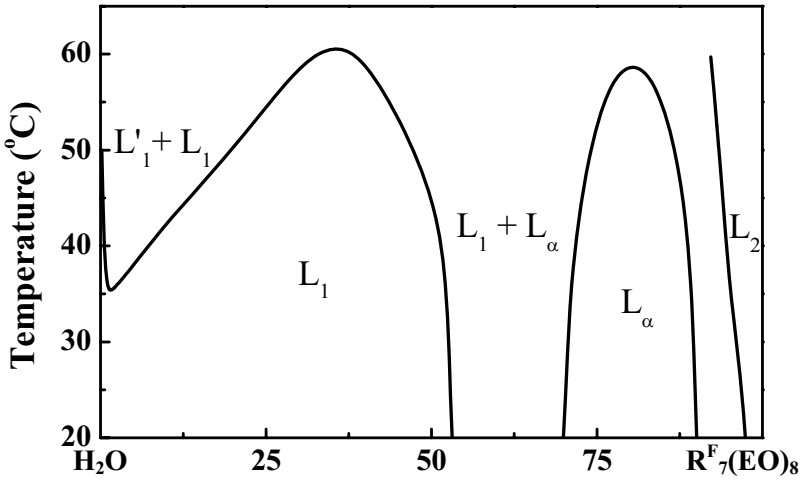


***Figure IV-21**. Temperature-composition phase diagram of $R^F_7(EO)_8$ in water [174].*

between 20°C and 65°C, evidenced that the system presents a cloud point at 35°C for 1 wt. % of surfactant. Below the miscibility curve, the system presents a micellar phase (L_1), whereas above this curve the phase separation occurs and the system separates in two phases: one phase rich in micelles (L_1) and the other one poor in micelles of surfactant (L'_1). The micellar phase L_1 is found to be present over a wide range of surfactant compositions going up to 52.5 wt% at 20°C. The liquid crystal domain contains only a lamellar (L_α) phase which is stable over a temperature range going up to 57.5°C.

The micellar solutions prepared at 25 wt% of surfactant showed flow birefringence, while remaining isotropic at rest. When the micelles were characterized by dynamic light scattering, big size particles in the micellar solution were determined, which is incompatible with the length of the chains of the surfactant.

2.1.2 Haze point of the $R^F_7(EO)_8$/ fluorocarbon systems

The haze point of $R^F_7(EO)_8$ – PFOBr system is detected at 35 °C when the concentration of $R^F_7(EO)_8$ is around 2.2 wt.% (**Figure IV-22**). Thus $R^F_7(EO)_8$ is soluble in PFOBr at all the proportions as long as the temperature higher than 35 °C. We also tried to determine the haze point of the other oils, such as PFD and F44E. But in the scale of the studied temperature, the systems are always two phases owing to their haze points are higher than 100 °C.

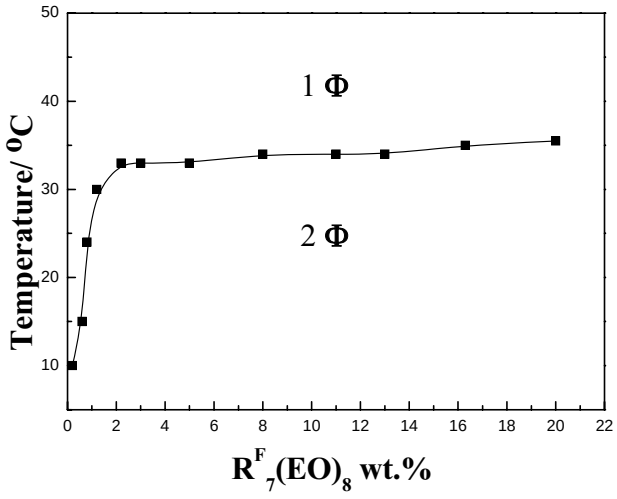


Figure IV-22. *Solubilization of $R^F_7(EO)_8$ in PFOBr.*

2.1.3 Solubilization of PFD, F44E and PFOBr in the system $R^F_7(EO)_8$-water

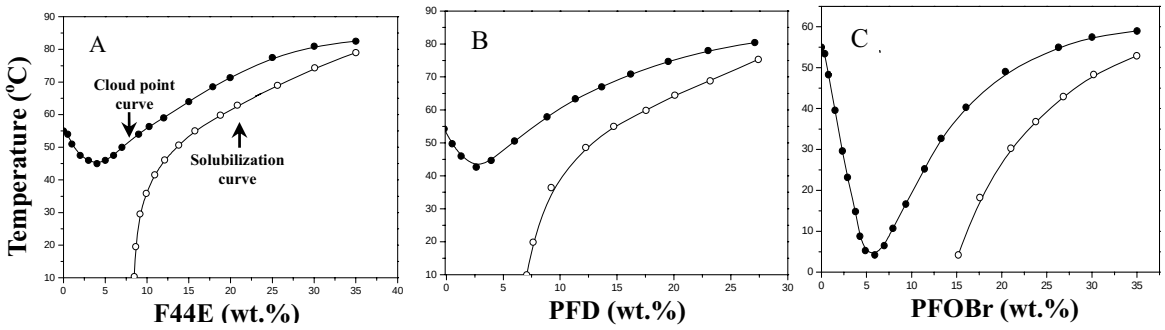


Figure IV-23. *Pseudo-Shinoda diagrams established for a water/ $R^F_7(EO)_8$ ratio (R) equals to 3 and with A : PFD, B : F44E and C : PFOBr.*

The solubilization of oil in the $R^F_7(EO)_8$-based system has been studied through the determination of the Shinoda diagram (see Chapter II). For different water/ surfactant ratios, we determined the microemulsion domain as a function of the temperature, solubilizing of perfluorodecalin, PFOBr and a mixed oil labeled as F44E ($C_4F_9CH{=}CHC_4F_9$). The Shinoda diagrams of the three oils are reported in the **Figure IV-23** for R=3.

By comparing the three diagrams, a shift of the cloud point curve to higher temperatures is observed following the sequence: PFOBr < F44E < PFD. This suggests that compared to PFD and F44E, PFOBr interacts more strongly with the oxyethylene groups and as a consequence the system becomes more “hydrophilic”. Such a behavior could be explained by the presence of either the highly polarizable terminal bromide atom which brings a higher degree of “hydrophilicity” [214].

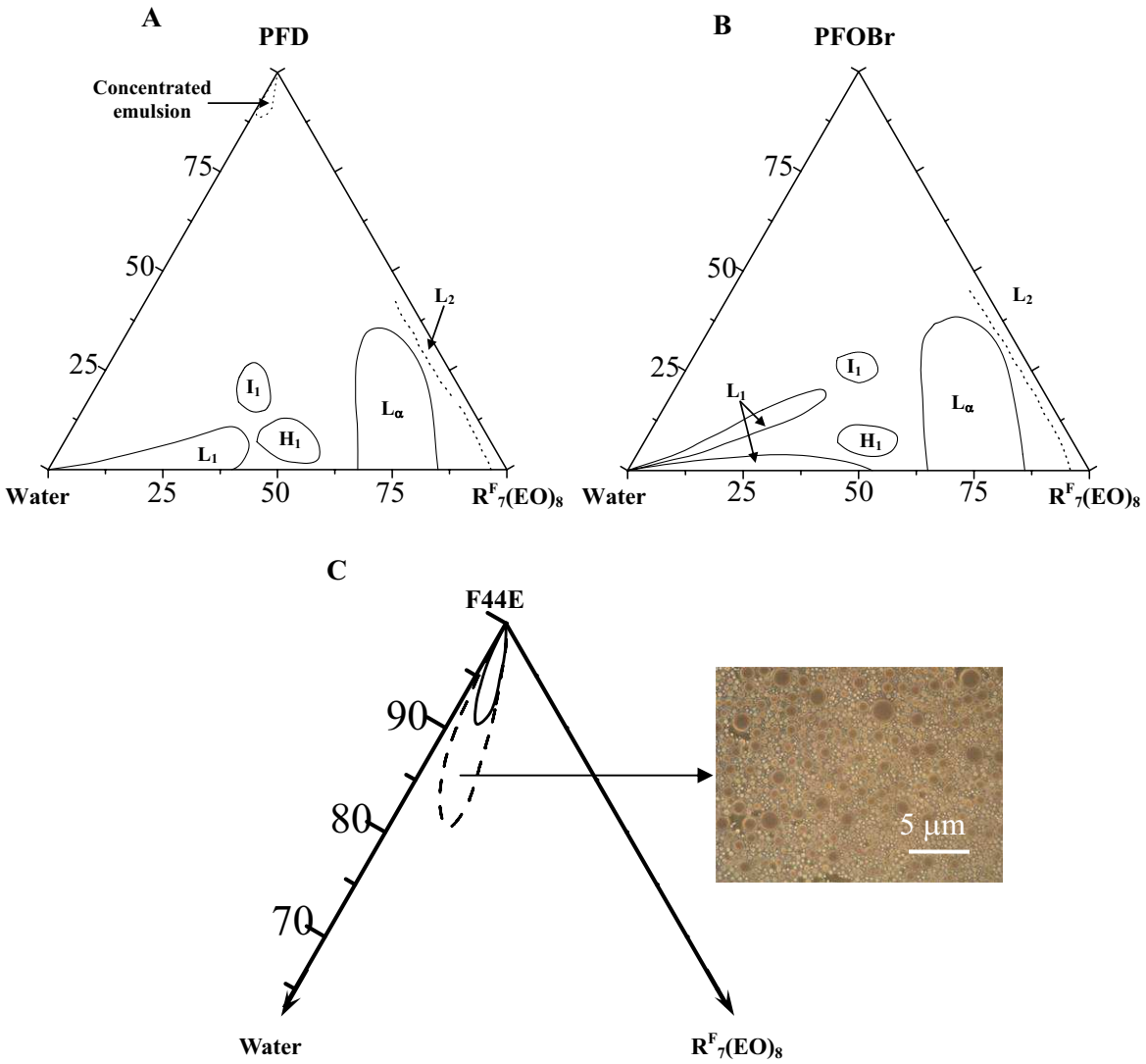


Figure IV-24. *Phase diagram (wt %) of $R^F_7(EO)_8$ /fluorocarbon/water system: PFD (A); PFOBr (B); Domain of concentrated emulsions formed by the $R^F_7(EO)_8$/F44E/water (C). The emulsions are stable for weeks (dash) and for months (solid) at 20 °C.*

The ternary diagrams at 20 °C is established from the Shinoda diagrams (**Figure IV-24**). At this temperature, micelles can incorporate up to 12 wt. % of PFD for R=1.63 (**Figure IV-24A**). Concerning PFOBr the situation is quite different: 4 wt.% of oil can be incorporated in the micelles and for higher concentration of PFOBr a domain of microemulsion, which joined the water corner, is also detected (**Figure IV-24B**). These microemulsions can incorporate up to 21 wt. % of PFOBr at 20°C. Whatever the type of oil, hexagonal (H_1) and micellar cubic (I_1) phases appear only upon addition of oil whereas the L_α phase, which exists in the binary system, swells.

On the other hand, at high oil amounts (oil-rich corner of the phase diagram), very stable concentrated emulsions are formed with the PFD and F44E-based systems at 20 °C, whereas

PFOBr does not form concentrated emulsions at this temperature. For example, the samples prepared at R = 5.7 with 95 wt% of PFOBr were relatively fluid and split into two phases, whereas those preparing with PFD appeared highly viscoelastic and very stable for months. PFOBr is therefore not an efficient fluorocarbon to form stable concentrated emulsions with the surfactant $R^F_7(EO)_8$.

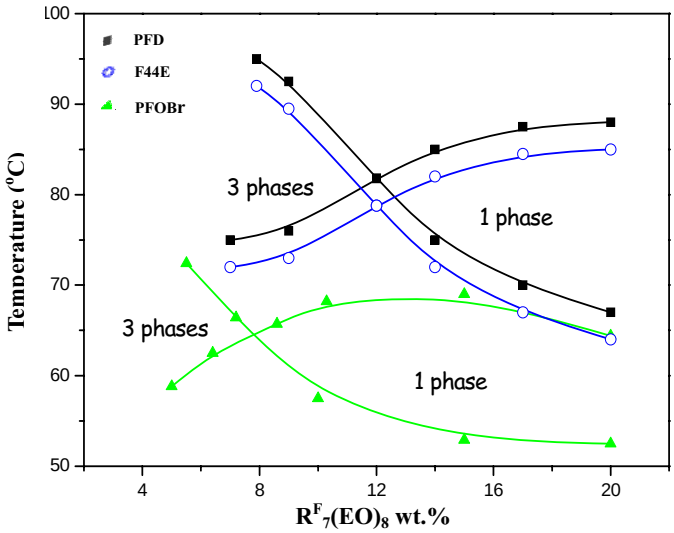


Figure IV-25. *PIT determination: Minimum surfactant requirement to obtain an isotropic solution containing fluorocarbon and water in equal weight*

In order to have a better understanding of the key for the concentrated emulsion formation, according to the results obtained by Solans C. et al [46], we have to introduce the PIT which has been determined by the fish diagram (**Figure IV-25**). Indeed, as indicated previously, PIT can be determined from the temperature at which the minimum concentration of surfactant is used to solubilize equal weights of water and oil in a single isotropic phase [22]. The PIT of the investigated systems were determined from the diagrams represented in **Figure IV-25** and were found to increase in the order PFOBr ~ 65 °C, F44E ~ 78 °C and PFD > 82 °C. These values are in good agreement with the empirical formula established to predict the PIT value in fluorinated systems [150]:

$$PIT\ (°C) = 31\ HLB + 1.7\ ECN - 225$$

where ECN (equivalent carbon number) characterize the fluorocarbon and depends on its structure, whereas HLB (hydrophilic-lipophilic balance) is specific to the surfactant. Indeed, with a HLB value of 9.6 for $R^F_7(EO)_8$ the calculated PIT are found to be equal to 67 °C for PFOBr , 83 °C for PFD and F44E (Table IV-1).

Table IV-1. *The ECN (Equivalent Carbon Number) values and PIT (Phase Inverse Temperature) estimates of the three fluorocarbons.*

	PFD	F44E	PFOBr
ECN	6	6	-2
Experimental PIT	82	78	65
Calculated PIT	83	83	67

To sum up, we conclude that higher PIT value favors the formation of high concentrated emulsions. On the contrary, $R^F_7(EO)_8$ / PFOBr system could not form stable concentrated emulsions due to its very low PIT.

2.2 Porous materials prepared from with microemulsions and emulsions.

Whatever the concentration of $R^F_7(EO)_8$ in the micellar solution and the temperature of the reaction, the spectra are at best only a broad line, characteristic of a worm-like structure, similar to MSU-type materials. Their nitrogen adsorption- desorption analyses displays type IV isotherms which characterize mesoporous materials [215].

2.2.1 Effect of molecular structure and content of oils

In this section, we discuss the properties of the materials prepared from the $R^F_7(EO)_8$/Oil/H_2O systems containing various amounts of fluorinated oil. The oil compositions were chosen in order to be either in the microemulsion domain or in the emulsion region and the concentration of oil was varied from 0 to 60 wt. %. The silica precursor was added at 40°C at pH 2 and the water/surfactant weight ratio was fixed at 3. The procedure for the preparation of materials is the same as that used in Chapter II.

- *The structural properties*

For the materials prepared with PFD, three reflections at q ratios $1:\sqrt{3}:2$, consistent with a hexagonal symmetry, are observed on the SAXS pattern until to 12 wt. % (**Figure IV-26**). According to the Bragg's law, the unit cell parameter ($a_0=2d_{100}/\sqrt{3}$) varies from 6.5 to 7.4 nm upon the loading of PFD from 0 to 12 wt.%. If the PFD concentration is further increased, the position of the first peak varies from 6.4 to 6.9 nm when the oil loading reaches 30 wt.%.

Nevertheless, the second reflections disappear, meaning that the regular channel array is lost.

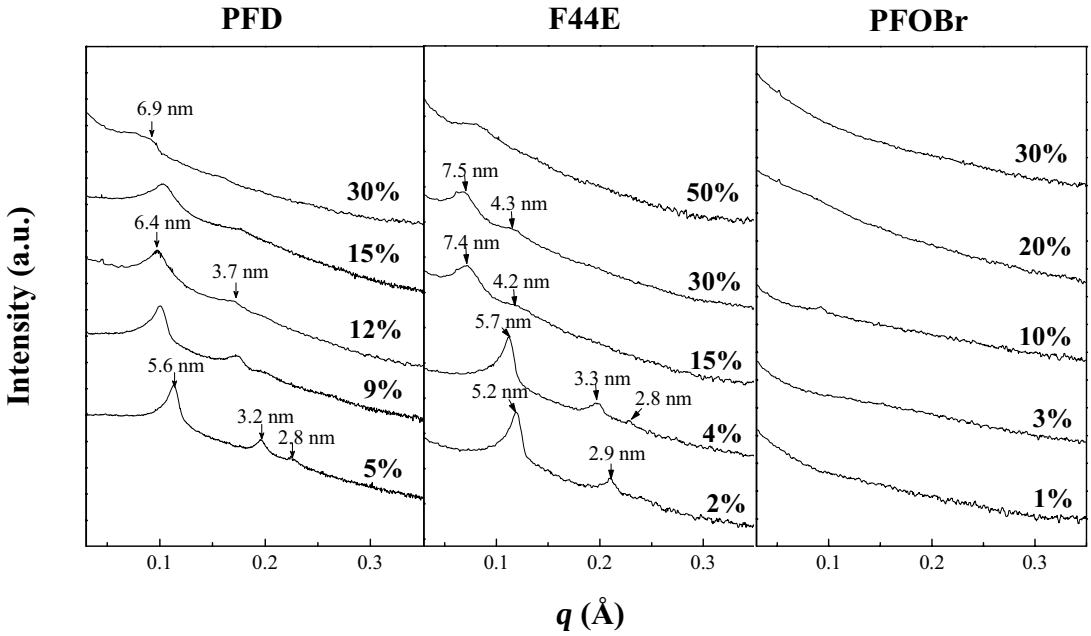


Figure IV-26. *SAXS patterns of the material prepared from $R^F_7(EO)_8$ with different concentrations of PFD, F44E and PFOBr at R= 3*

The presence of a single reflection indicates the formation of a disordered structure.Similar results are obtained with the incorporation of F44E (**Figure IV-26**). Meanwhile, the situation is quite different in the PFOBr system (**Figure IV-26**), where no line is observed, indicating a further loss of ordering as compared to the samples prepared from the $R^F_7(EO)_8$-water binary system [215]. In that case the obtained materials adopt a complete randomly pore structure.

- *The textural characteristics*

A type IV isotherm with a H_1 hysteresis loop by BDDT classification [216] is obtained for the samples prepared from the $R^F_7(EO)_8$ / PFD/ water or $R^F_7(EO)_8$ / F44E / water systems with a low concentration of oil (**Figure IV-27**). A strong uptake of N_2 adsorption is observed at approximately p/p_0 = 0.50~0.65 (PFD) and p/p_0 = 0.4~0.60 (F44E) when the concentrations of oil are lower than 20 wt.%, which is a result of the filling of the mesopores due to the capillary condensation. When the PFD or F44E loading is increased up to 30 wt.%, the relative pressure for which capillary condensation takes place is shifted toward higher values. Since the p/p_0 position of the inflection point is related to the pore diameter, it can be inferred that an enlargement of the mean pore diameter occurs when the loading of oil is raised. This increase in pore diameter is further confirmed by the pore size distribution whose maximum is shifted from 5.3 nm to 6.9 nm (PFD) and from 4.1 nm to 5.4 nm (F44E), when the PDF concentration is changed from 3 to 20 wt.% while the concentration of F44E varies from 2 to

15 wt.% (**Figure IV-27**). This confirms the swelling effect of PFD and F44E but the pore size

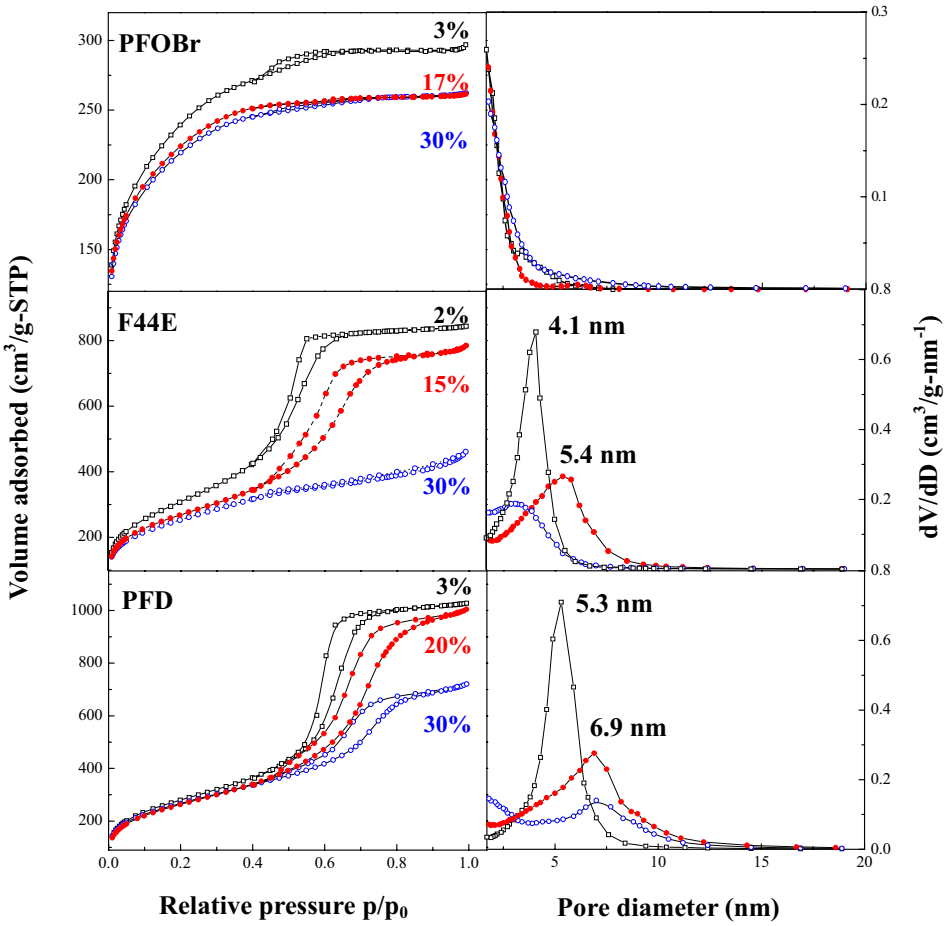


***Figure IV-27**. Porous materials : adsorption-desorption isotherms and pore size distribution of compounds prepared from $R^F_7(EO)_8$ with PFD, F44E and PFOBr*

expansion is accompanied by a broadening of the pore size distribution. The plateau is reached at approximately p/p_0 = 0.70~0.80. Beyond this value the adsorbed volume at the saturation remains constant. Above 30 wt.% of PFD or F44E at high relative pressure (beyond $p/.p_0$=0.9), the adsorbed volume of nitrogen does not remain constant any more (**Figure IV-27**). Whatever the oil and its loading, the specific surface area is rather high (> 900m^2/g). However, its value slowly decreases with the incorporation of oil.

As compared to PFD and F44E, the materials obtained from the PFOBr based-system exhibit a different behavior (**Figure IV-27**). Indeed, isotherms are intermediates between type I and IV. According to Dubinin [217], these kinds of isotherms are characteristic of supermicroporous materials, i.e. the pore size is located at the limit between the micro and mesoporous domain. This phenomenon is further confirmed by the analysis of the pore size distribution, whose maximum is lower than 1.7 nm.

- *Morphology*

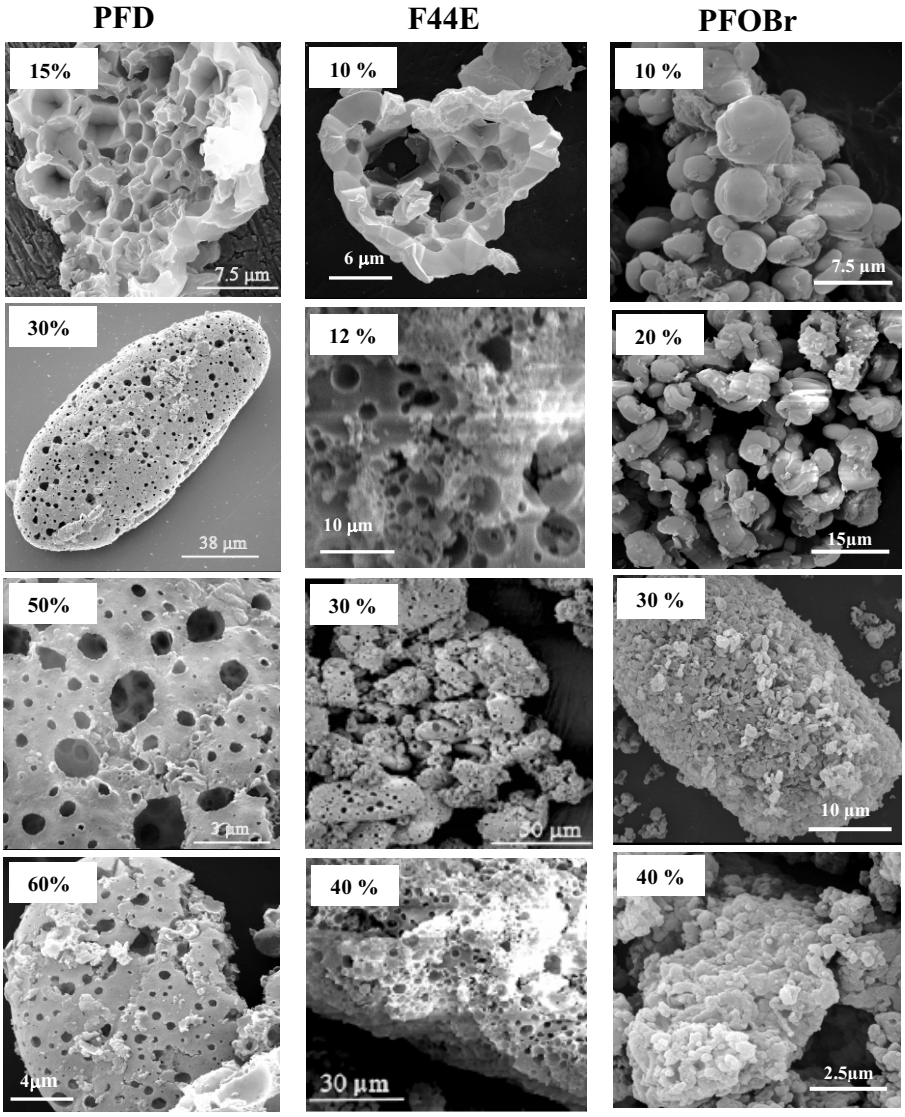


***Figure IV-28**. SEM micrograph of materials prepared from $R^F_7(EO)_8$ with different concentrations of PFD, F44E and PFOBr*

From **Figure IV-28** which shows several representatives scanning electron micrographs (SEM) of the synthesized silica, it appears that both $R^F_7(EO)_8$/ PFD/ water and $R^F_7(EO)_8$/ F44E/ water systems provide a macroporous network. Indeed, highly porous particles are clearly evidenced. Depending on the fluorocarbon amount, PFD gives rise either to macro-mesoporous structures with polyhedral cells without any interconnecting window (15% PFD), or to big particles of *ca.* 30 - 130 µm in length with oval shapes (30 - 60% PFD). In any case, the macropores are not well-ordered and typically the pore size is in the range of few microns.

Depending on the fluorocarbon concentration, F44E gives rise not only to

macro-mesoporous structures with spherical shapes without any interconnecting window (10% - 12% F44E), but also to big particles of *ca.* 30 - 60 µm in length with oval shapes (30% - 40% F44E). Anyway, as observed for the materials prepared from the $R^F_7(EO)_8$/ PFD/ water system, the macropores are not well-ordered and the pore size is typically in the range of few microns. In addition, we can see that for the $R^F_7(EO)_8$/ F44E/ water system, the macropores are obtained at low amount of oil 10 wt.%. Thus, this system is very favorable for the formation of macroporous materials.

Concerning the system with PFOBr, whatever the synthesis condition, the system does not give rise to the formation of macropores. The morphology of the materials can be described as an agglomerate of rods, gyroids and toroids when the concentration of PFOBr is lower than 40 wt.%.

2.2.2 Effect of reaction medium pH value.

Once again we have investigated the effect of pH value on the properties of the materials for these systems.

- *The structural properties*

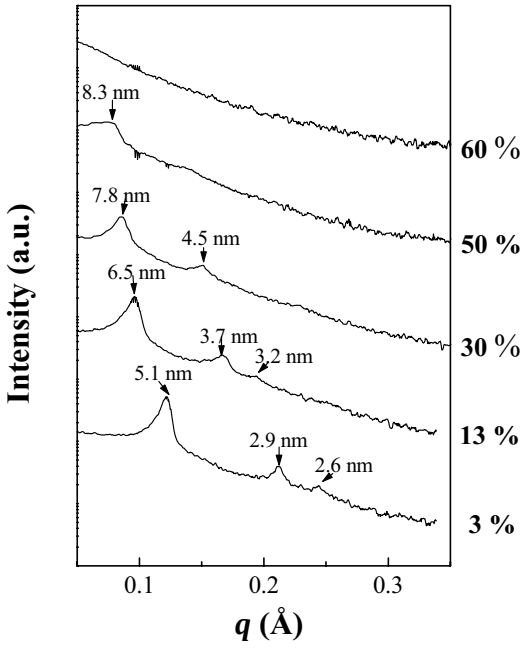


***Figure IV-29**. SAXS pattern of the material prepared from $R^F_7(EO)_8$ with PFOBr at pH 0.025 and 20 °C*

The SAXS patterns of the samples prepared at pH 0.025 with PFOBr are depicted in **Figure IV-29**. Decreasing the pH to 0.025, the appearance of a reflection line situated at 7.4 nm for the material prepared with a concentration of PFOBr equals to 10 wt. %, shows the formation of a wormhole-like structure. This means that when the pH value is decreased to 0.025, the transition from a randomly oriented pore arrangement to a wormhole like structure occurs and the pore ordering enhances. Indeed, it should be reminded that there is no line observed at pH 2 and 40 ^{o}C.

Concerning materials synthesis in the presence of PFD and F44E, we note that beyond 20 wt.% of fluorocarbon, a better mesopore ordering is generally obtained at pH 0.025 compared to at pH2.

As indicated previously the $R^{F}_{7}(EO)_{8}$-water system exhibits a cloud point at 35 ^{o}C. In a paper dealing with the relation between the lower consolute boundary and the structure of mesoporous silica, our group has shown that bigger the difference between the phase separation temperature and the temperature at which the silica precursor is added into the micellar solution, better is the mesopore ordering. So in this part, TMOS was added at 20 ^{o}C instead of 40 ^{o}C. By this way, the mesopore ordering should be enhanced due to the effect of pH and the shift of the cloud point.

Under these conditions, it is interesting to note that up to 40 wt.% of PFOBr, three reflections at q ratios $1:\sqrt{3}:2$, consistent with a hexagonal symmetry are observed on the SAXS pattern (**Figure IV-29**). On these conditions, the mesopores ordering occurs. Above 40 wt.% of PFOBr, only disordered structures are recovered (**Figure IV-29**)

- *The textural characteristics*

Compared to materials prepared at pH=2, there is no change in the nitrogen adsorption-desorption isotherms noted with PFD and F44E. Concerning PFOBr the situation is different. Indeed, at pH=0.025 when the TMOS is added at 20 ^{o}C, a type IV isotherm is obtained by nitrogen adsorption-desorption analysis (**Figure IV-30A**) and the pore diameter increases from 3.5 to 7.2 nm (**Figure IV-30B**). Above 40 wt.% of PFOBr, the shape of the isotherms changes and the pore diameter remains constant to 7.2 nm.

This observation evidences the role played by the pH and the temperature at which the silica precursor is added on the properties of the recovered materials. Indeed, it should be remind that at pH=2 when TMOS is added at 20 ^{o}C, only supermicroporous materials are obtained.

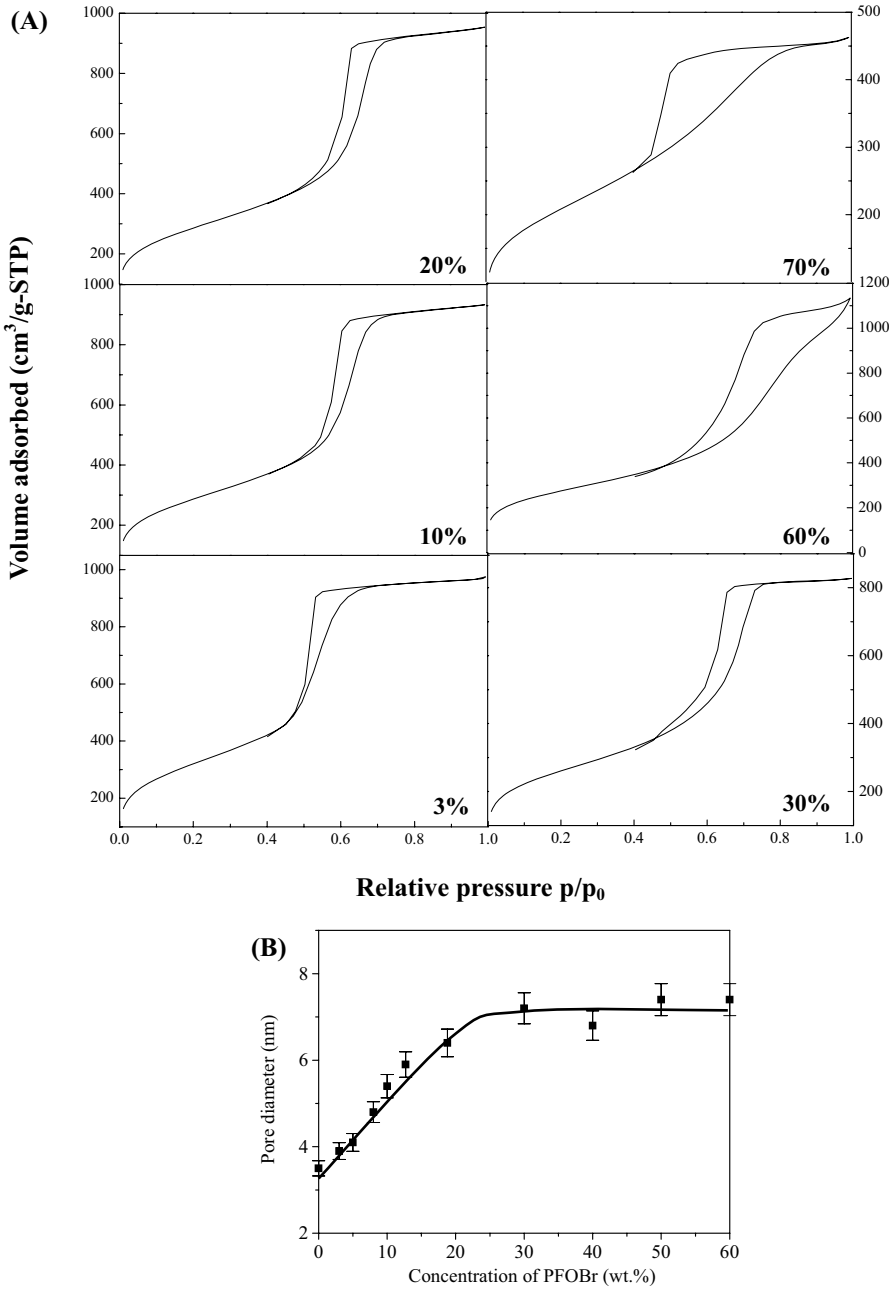


Figure IV-30*. Evolution of the nitrogen adsorption-desorption isotherm (A) and the corresponding BJH pore size distribution curve (B) of the system with PFOBr at 20°C, pH 0.025.*

- *Morphology*

From **Figure IV-31** which shows several micrographs of the materials prepared with different fluorinated oils, it appears that changing the synthesis conditions does not involve any change on the morphology. As a matter of fact, macropores are obtained with both the $R^F_7(EO)_8$/ PFD/ H_2O and $R^F_7(EO)_8$/ F44E/ H_2O system whereas no macropore is formed with

the $R^F_7(EO)_8$/ PFOBr/ H_2O one. If the concentration of PFOBr is lower than 40 wt.%, the morphology of the materials is described as an agglomerate of rods, gyroids and toroids (**Figure IV-31**). In creasing the PFOBr concentration, regular edge-shaped large particles with variable sizes and forms are obtained (**Figure IV-31**).

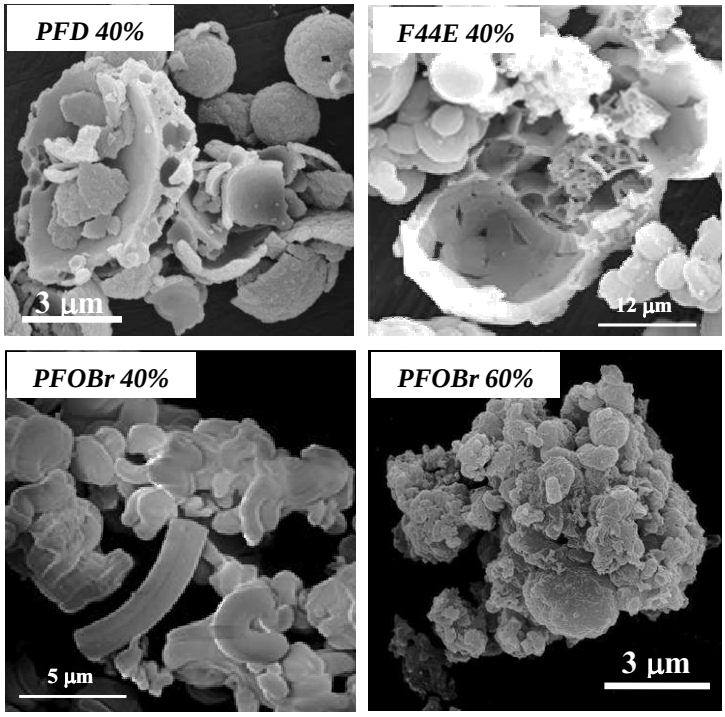


***Figure IV-31**. SEM micrograph of samples prepared from $R^F_7(EO)_8$ with PFD, F44E and PFOBr, respectively at 20 °C, pH0.025*

3. Discussion

3.1 Macroporous silica

Using the $R^F_7(EO)_8$ surfactant, at pH=2 when the silica precursor is added at 40°C, 1-bromo-perfluorooctane neither leads to well ordered mesostructures nor to macroporous materials. On the contrary, in the same condition macroporous materials are formed from the $R^F_8(EO)_9$/ PFOBr/ water system. For understanding this behavior, we must have a look at the phase behavior of the $R^F_m(EO)_n$/fluorocarbon/water systems in relation to the formation of concentrated emulsions (**Figure IV-9** and **Figure IV-24**). As evidenced in **Figure IV-6**, the $R^F_8(EO)_9$/PFD/water system gives rise to oil-in-water concentrated emulsion for water/ surfactant ratios comprised between 9 and 3. It should be noted that the stability of the emulsion enhances when the concentration of fluorocarbon increases. Therefore, as regards the ability to form macroporous materials a possible origin of the peculiar behavior of the

$R^F_7(EO)_8$ / PFOBr / water system could be associated to the fact that PFOBr could not form stable concentrated emulsions with $R^F_7EO_8$ due to its very low PIT. Indeed, to obtain direct concentrated emulsions, the system should exhibit a high value of PIT.

3.2 Expansion of the mesopores

The second tendency is that the various fluorinated systems which are investigated can be used for the preparation of large pore mesoporous materials. Nevertheless, depending on the surfactant we have to consider two different swelling mechanisms. As a matter of fact the investigation of the $R^F_m(EO)_n$/ fluorocarbon/ water diagram has revealed that when $R^F_8(EO)_9$ is used as surfactant only a small fraction of PFOBr or PFD can be incorporated in micelles at 20°C (**Figure IV-4** and **Figure IV-8**). The liquid crystal phase domain is constituted of cubic, hexagonal and lamellar phases. The existence range of these phases depends on the temperature, the surfactant/water ratio and oil loading [195]. Thus, for the $R^F_8(EO)_9$ surfactant-based system the swelling effect of the mesoporous pore diameter observed with PFD and PFOBr can not be attributed to the formation of a core of oil in the micelles. Nevertheless, when TMOS is added to the surfactant, water and oil mixture, a hexagonal hybrid mesophase, whose features are analogous to the H_1 liquid crystal, is formed through a CTM (Cooperative Templating Mechanism).

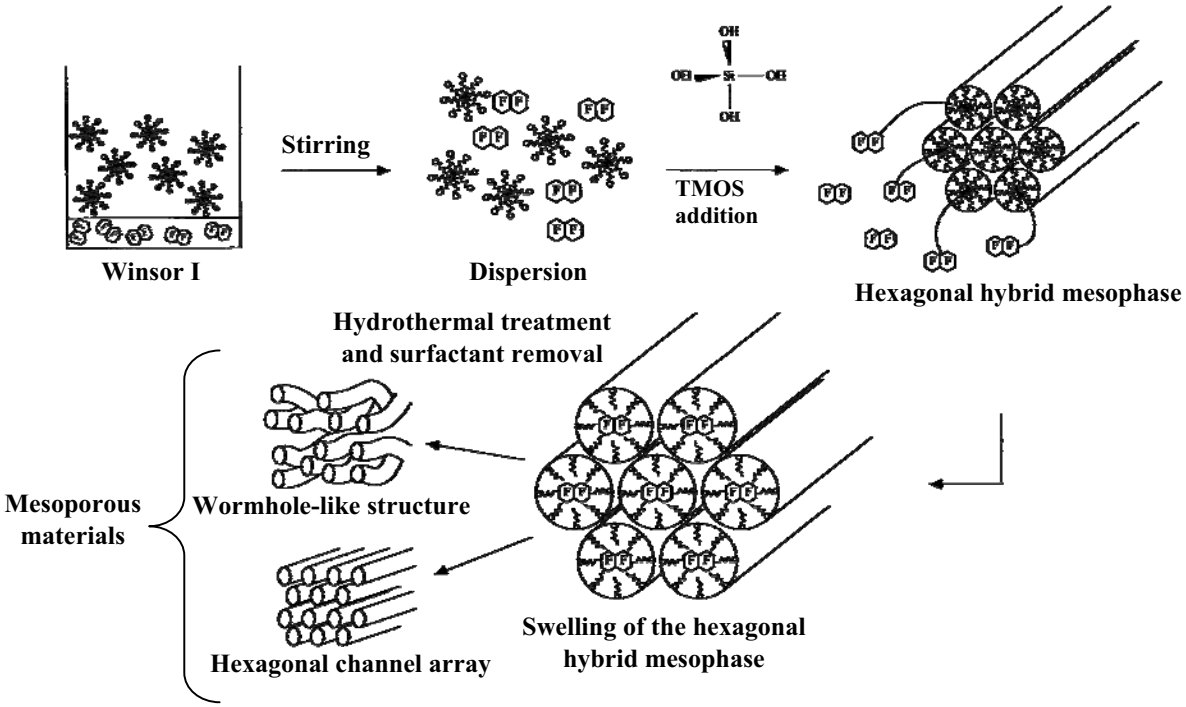


Figure IV-32. *Scheme of the proposed swelling mechanism of mesoporous materials pore size [195]*

So concerning the swelling mechanism of mesoporous materials we propose that oil can be incorporated in this hybrid hexagonal mesophase, involving a channel-swelling (**Figure IV-32**). However, at higher loading of solubilizer, the expansion of the pore size still occurs but the recovered materials adopt a wormhole-like structure.

On the contrary, for the $R^F_7(EO)_8$ surfactant based system, the oil molecules are solubilized in the core of the micelles and their volume is increased. In that way, large pore mesoporous materials can be obtained through the CTM-type mechanism after surfactant removal by ethanol extraction. In that case the swelling mechanism is the same than the one determine in the chapter III for the large mesoporous materials obtained from the $R^H_{12}A(EO)_9$/ alkane/ water system.

3.3 Pore ordering in the presence of PFOBr

Finally for the $R^F_8(EO)_7$/PFOBr/water system, the mesopore ordering is obtained only if the synthesis is performed at pH 0.025, beside this the silica precursor has to be added at 20°C. This phenomenon can be related to the influence of the cloud point curve on the self assembly mechanism. Indeed, the investigation of the binary $R^F_7(EO)_8$-water phase diagram evidenced that $R^F_7(EO)_8$ presents a cloud point at 35°C (**Figure IV-21)** and as mentioned previously in our group, it has been evidenced that the cooperative self assembly mechanism is disturbed if the lower consolute boundary is not shifted toward high temperatures. Moreover, higher the difference between the phase separation temperature and the temperature at which the silica precursor is added to the surfactant solution is, better the mesopore ordering becomes. It should also be reminded that Zhao and coworkers [199] have reported the synthesis of silica mesostructures by using the triblock copolymer P85 ($EO_{26}PO_{39}EO_{20}$) and P65 ($E_{20}PO_{30}EO_{20}$) as structuring agent and tetraethyloxysilane (TEOS) as silica precursor. P85 and P65 have a CP value of 82°C in water. The TEOS : P65 (or P85): HCl : H_2O molar composition was : 1 : 0.0003 : 6 : 166. These authors claim that ordered mesoporous silicates can only be obtained at a temperature higher than 90°C. To explain this tendency, they assume that the high concentration of H^+ and the ethanol released by the hydrolysis of TEOS have increased the CP of the triblock copolymer to a temperature higher than 100°C. Therefore, we consider that in the present study the mesopore ordering in strong acidic conditions is due to a shift toward high temperatures of the cloud point curve, when the synthesis is performed at pH 0.025 and the TMOS is added at 20°C.

4. Conclusion

In this study two fluorinated surfactants $R^F_8(EO)_9$ and $R^F_7(EO)_8$ are used for the preparation of porous silica. We investigate the effect of the solubilization of various fluorocarbons on the properties of the recovered materials. Looking at the $R^F_8(EO)_9$-based system, large pore mesoporous materials are obtained with PFOBr. The investigation of the phase diagram reveals that only a small fraction of the fluorocarbon is incorporated into the micelles, so, the mesopore size expansion occurs through a swelling of the hybrid mesophase. At oil concentrations higher than 50 wt.% both PFOBr and PFD give rise to macroporous silica. Concerning the $R^F_7(EO)_8$ surfactant, the results obtained by SAXS, nitrogen adsorption-desorption analyses evidence that F44E is an effective expander to enlarge the pore size of mesoporous materials through a swelling of the micelles. In addition, the $R^F_7(EO)_8$/F44E/water system is very favorable for the design of a macropore network. Indeed, macroporous materials are recovered as soon as the F44E concentration is higher than 10 wt.%. On the contrary, when PFOBr is incorporated instead of F44E, the situation is quite different. As a matter of fact, the mesopore ordering is obtained only if the synthesis is performed at pH 0.025 and if the silica precursor is added at 20°C. Moreover, due to the low PIT value, whatever the synthesis conditions, the $R^F_7(EO)_8$/PFOBr/water system does not lead to the formation of macropores.

Comparing this behavior and the one reported for hydrogenated emulsions in chapter III, we can conclude that both hydrogenated and fluorinated systems obey to the same rule i.e. the formation of macroporous materials templated by emulsions is favored with systems, which exhibit a high value of the PIT.

Chapitre V. Effet de l'addition d'alcool dans le système à base de $R^F_8(EO)_9$ sur les caractéristiques des matériaux poreux silicatés

Il a été montré que le méthanol et l'éthanol issus de l'hydrolyse des précurseurs silicatés, respectivement le tétraméthoxysilane (TMOS) et le tétraéthoxysilane (TEOS), peuvent influencer le paramètre d'empilement ou compact déplacer la courbe de point de trouble et modifié la structure des matériaux mésoporeux. En fait, il est bien connu que le comportement de micelles de tensioactif dans l'eau est modifié eu présence d'alcool. Plus la chaîne de l'alcool est longue, plus son comportement se rapproche de celui d'une vraie huile. Cela signifie que l'alcool se place au cœur des micelles et augmente ainsi la taille des micelles. Les alcools à courtes chaînes jouent plutôt le rôle de co-solvant. Enfin, les alcools à chaînes intermédiaires peuvent jouer le rôle de co-solvant ou de co-tensioactif en fonction de la longueur de la chaîne. Les effets de l'addition d'alcools dans des solutions aqueuses de tensioactif ioniques et non ioniques sur la structure de silices mésoporeuses avec des tensioactifs ioniques et non ioniques ont déjà été étudiés. Avec les tensioactifs non ioniques, les alcools peuvent favoriser la formation de mésostructures en modifiant la courbure des micelles. Dans ce travail, nous avons étudié les effets de l'addition d'alcools hydrogénés à différentes longueurs de chaînes méthanol, d'isopropanol, n-butanol et 1-octanol et du fluoro-octanol sur les caractéristiques des matériaux mésoporeux préparés à partir du système à base de $C_8F_{17}C_2H_4(OC_2H_4)_9OH$ [$R^F_8(EO)_9$].

Pour conduire cette étude, nous avons tout d'abord examiné la solubilisation de chacun de ces alcools dans le système $R^F_8(EO)_9$/Eau et déterminé les paramètres structuraux de la phase cristal liquide hexagonale. Nous avons pu ainsi démontrer que le méthanol, l'isopropanol et le butanol se comportaient comme co-solvants dans le domaine de concentrations étudiées. Au contraire, l'octanol et le fluore-octanol joue le rôle de co-tensioactif. Concernant les matériaux silicatés, la présence de ces alcools ne modifie pas la taille des pores, ce qui signifie que les composés ne sont pas des agents gonflants. Les alcools à courte chaîne interagissent avec la tête des tensioactifs en induisant leur déshydratation tandis que l'octanol fluoré et hydrogéné en tant que co-tensioactif perturbent le mécanisme d'auto-assemblage et une perte de structuration des matériaux est obtenue.

Chapter V. The effect of the alcohols addition in the $R^F_8(EO)_9$-based system on the characteristics of mesoporous silica

1. Solubilization of methanol and iso-propanol in the $R^F_8(EO)_9$-water system 135
   - 1.1 Ternary diagram 135
   - 1.2 Structural parameters of hexagonal crystal liquid phase 136
   - 1.3 Mesoporous materials prepared from system $R^F_8(EO)_9$-water with methanol or isopropanol 138
   - 1.4 Discussion 143
2. Solubilization of butanol in the $R^F_8(EO)_9$-water system 143
   - 2.1 Ternary diagram 144
   - 2.2 Structural parameters of the hexagonal crystal liquid phase 144
   - 2.3 Mesoporous materials prepared from the system $R^F_8(EO)_9$/water in the presence of butanol 151
3. Solubilization of octanol in the $R^F_8(EO)_9$-water system 156
   - 3.1 Ternary diagram 156
   - 3.2 Structural parameters of hexagonal crystal liquid phase 156
   - 3.3 Mesoporous materials prepared from system $R^F_8(EO)_9$-water with octanol 159
   - 3.4 Discussion 162
4. Solubilization of fluorinated octanol in the $R^F_8(EO)_9$- water system 163
   - 4.1 Ternary diagram 163
   - 4.2 Structural parameters of hexagonal crystal liquid phase 164
   - 4.3 Mesoporous materials prepared from the system $R^F_8(EO)_9$-water in the presence of fluorinated octanol 166
   - 4.4 Discussion 170
5. Conclusion 170

V. The effect of the alcohols addition in the $R^F_8(EO)_9$-based system on the characteristics of mesoporous silica

It has been shown that methanol and ethanol formed during the hydrolysis of the silicate source tetramethoxysilane (TMOS) or tetraethoxysilane (TEOS) respectively, can influence the structure of mesoporous silica by altering the surfactant packing parameter or shifting the cloud point curve [218, 219]. Indeed, it is well known that the behavior of surfactant micelles in water can be influenced by the presence of alcohols [220-223]. Moreover, it has been shown especially with the Brij35-water system that the structural properties of micelles are sensitive to the addition of alcohols [224]. Longer the chain of the alcohol, more it behaves like a real oil. It means that the alcohol locates in the core of the micelle which results in an increase of the micelle size. When the chain of the alcohol is short, the alcohol acts as a co-solvent. At last, for the medium chain, depending on the alcohol chain length, they can behave either as co-solvent or as co-surfactant on the function of the length of the chain.

Till now the effects of alcohol in the synthesis of mesoporous silica with ionic and nonionic surfactants as templates have been roundly studied [225-232]. For mesoporous silica synthesis using nonionic surfactant, alcohol could tune the mesostructure efficiently through modifying surface curvature of the micelles [231]. It was also proposed that alcohol can change the polarity of the synthesis solution and reduce the hydrolysis and condensation rates of silicate species [232].

In this study, we have mainly investigated the effect of the addition of alcohol having various hydrogenated chain length on the characteristics of mesoporous materials prepared from the $C_8F_{17}C_2H_4(OC_2H_4)_9OH$ [$R^F_8(EO)_9$] fluorinated surfactant based system. As micelles, mesoporous materials should be influenced by the molecular structure of the alcohol added into the surfactant solution. We have considered in particular the incorporation of methanol, iso-propanol, n-butanol and 1-octanol. Owing to the strong oleophobicity of the fluorinated chains, the choice of octanol is especially interesting. In fact, formation of mixed system could be considered. To compare to 1-octanol, we have chosen the fluorinated alcohol $C_6F_{13}C_2H_4OH$ which contains two hydrogenated methylene groups due to the synthesis limit. It can be noted as $R^F_6(EO)_0$ by analogy with the label of $C_8F_{17}C_2H_4(OC_2H_4)_9OH$.

1. Solubilization of methanol and iso-propanol in the $R^F_8(EO)_9$-water system

1.1 Ternary diagram

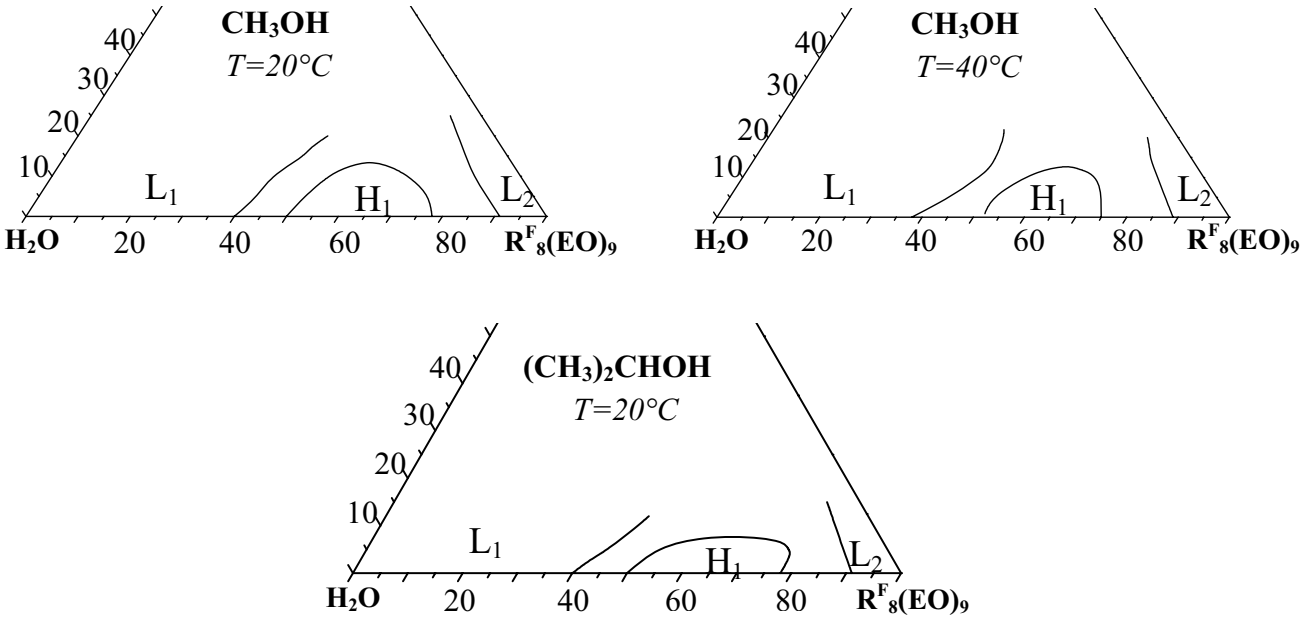


Figure V-1. *Phase diagrams (wt %) of $R^F_8(EO)_9$/CH_3OH/water systems at 20 °C and 40 °C, and $R^F_8(EO)_9$/$(CH_3)_2CHOH$/water system at 20 °C.*

Addition of methanol or iso-propanol into the $R^F_8(EO)_9$-water system favors the formation of an isotropic phase. As shown on the phase diagrams of **Figure V-1**, this micellar domain (L_1) detected for $R^F_8(EO)_9$ content lower than 40 wt %, without alcohol, is progressively expanded toward the higher surfactant concentrations with the addition of either methanol or iso-propanol. This domain is isotropic, but these structural properties have not been determined in detail. For example, at 20°C the isotropic domain is extended up to 57 wt % of $R^F_8(EO)_9$ for a weight percent of methanol equal to 20. Similarly the limit of this domain is extended up to 55 wt % of $R^F_8(EO)_9$ for a weight percent of iso-propanol equal to 10.

When the loading of surfactant is increased from 50 to 78 wt. %, a direct hexagonal H_1 phase is observed. The methanol and iso-propanol solubilization rate in the hexagonal phase is strongly dependent on the water/$R^F_8(EO)_9$ ratio (R). Indeed, upon the addition of methanol or iso-propanol, the surfactant range of composition belonging to H_1 is progressively reduced and the hexagonal liquid crystal phase is completely melted when the methanol concentration

reaches 15 wt % and the iso-propanol concentration reaches 7 wt %. These liquid crystal phases disappear in aid of less ordered ones.

If the water/$R^F_8(EO)_9$ mass ratio is decreased under 0.11 the reverse micellar phase (L_2) is maintained in the presence of methanol and iso-propanol at 20 °C. The same sequence is observed when the temperature is raised to 40 °C (**Figure V-1**).

1.2 Structural parameters of hexagonal crystal liquid phase

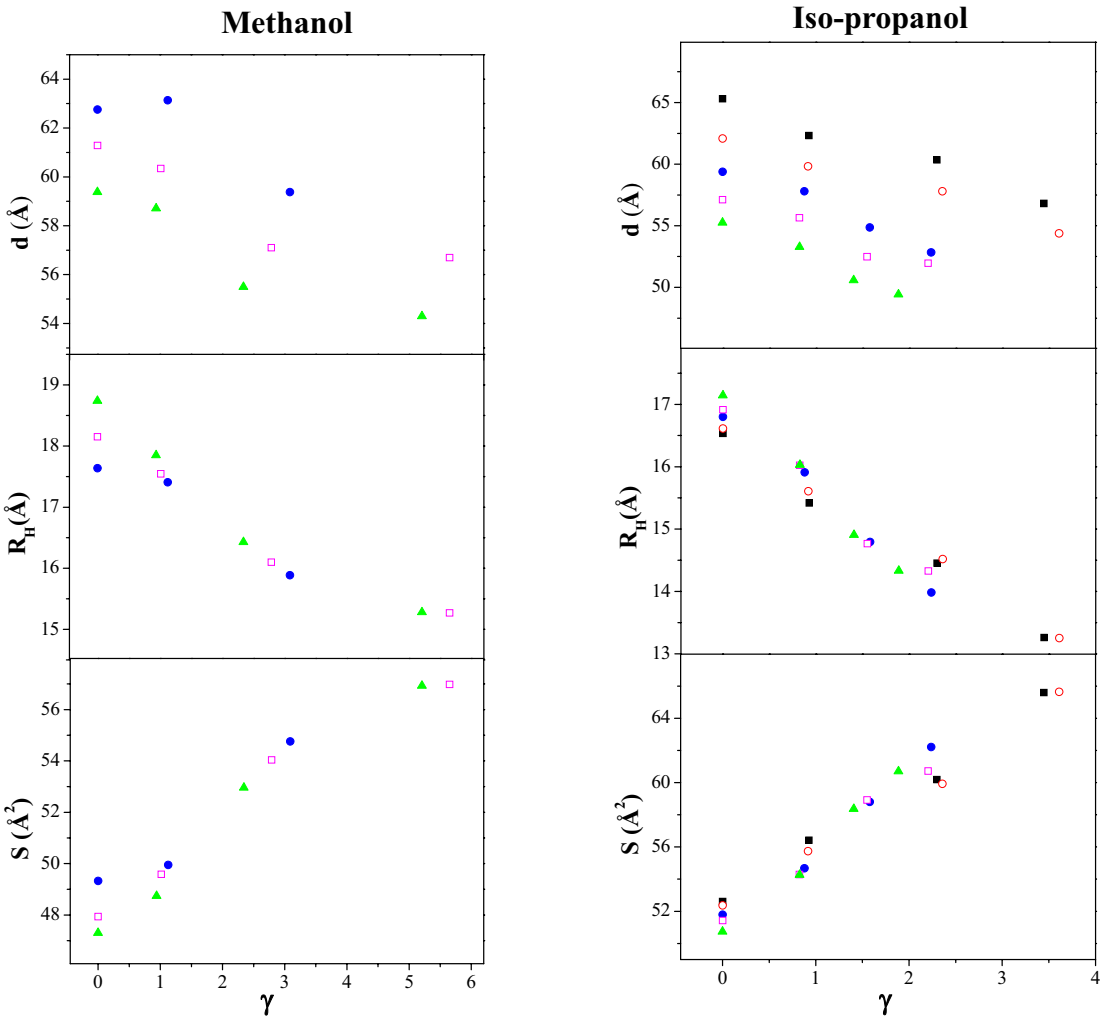


***Figure V-2**. Evolution of the d-spacing (d), hydrophobic radius (R_H) and cross sectional area (S) as a function of the number of alcohol molecules per surfactant molecule (γ) in H_1 for different water/ $R^F_8(EO)_9$ (R) with methanol and iso-propanol. : R = 1.00; ○: R = 0.82; : R = 0.67; □: R = 0.54; ▲ : R = 0.43.*

The hexagonal H_1 phase is characterized by SAXS measurements. The effect of alcohol addition is investigated by considering the evolution of the Bragg distance d for different water/surfactant ratios (R). The results indicate that the Bragg distance decreases linearly as a

function of the number of alcohol molecules per surfactant molecule (γ) (**Figure V-2)**. Considering the geometry of a hexagonal phase (see p. 7), the Bragg distance is related to the hydrophobic radius of the cylinders R_H by the relation:

$$d = \left(\frac{\sqrt{3}\pi}{2\Phi_B} \right)^{1/2} R_H$$

where Φ_B is the hydrophobic volume fraction.

Assuming that methanol or iso-propanol is soluble only in water, the hydrophobic volume fraction for one mole of surfactant is given by the following relation:

$$\Phi_B = \frac{V_B}{V_S + \alpha V_W + \gamma V_{al}}$$

where α stands for the number of water molecules per surfactant molecule; γ stands for the number of methanol or iso-propanol molecules per surfactant molecule; V_B and V_S, respectively correspond to the molar volumes of the hydrophobic part of the surfactant (V_B = 261 cm³/mol) and the surfactant (V_S = 626 cm³/mol); V_W is the molar volumes of water (V_W = 18 cm³/mol); V_{al} corresponds to the molar volumes of methanol (V_{al} = 40 cm³/mol) or iso-propanol (V_{al} = 76 cm³/mol). In these conditions, the calculated values of hydrophobic radius decrease linearly with the addition of alcohol (**Figure V-2**). In the binary system the value of hydrophobic radius R_H is 17 ~ 18 Å. This value means that the hydrophobic chains are completely extended. Since the length of an extended chain with 10 carbon atoms is about 14 Å. The values of R_H are higher than 14 Å, as the surfactant is composed of fluorinated chains with different lengths this can be due to the contribution of the longer tails. **Figure V-2** shows the evolution of R_H as a function of γ at 20°C, for different values of R. Upon addition of 15 wt.% of methanol or 10 wt.% of iso-propanol, the R_H value is equal respectively to 15 and 13 Å. So the addition of these alcohols involves a shrinkage of the hydrophobic core of the cylinders, which can explain the decrease of the d-spacing value. For example, in the case of methanol for R=0.43, d decreases from 59 to 54 Å, while R_H varies from 18.7 to 15.3 Å. Likewise for iso-propanol, for R=0.43 the values of d and R_H are respectively changed from 55 to 47 Å and from 17 to 14 Å when γ is varied from 0 to 1.9. The cross-sectional area S, which can be related to the hydrophobic radius by the relation:

$$S = \frac{2V_B}{N \; R_H}$$

linearly increases with the loading of alcohol (**Figure V-2**). For example, S varies from 47 to 56 Å^2 with addition of 12 wt. % of methanol for R = 0.43, meanwhile S varies from 52 to 64.5

$Å^2$ with addition of 12 wt. % of iso-propanol for R = 0.82. The variation of S likely links to the partial dehydration of the oxyethylene chain for the benefit of the penetration of alcohol molecules in the interfacial film which has larger molar volume than just in the water.

1.3 Mesoporous materials prepared from system $R^F_8(EO)_9$-water with methanol or isopropanol

After investigating the phase diagram and evaluating the liquid crystal structural parameters of the ternary $R^F_8(EO)_9/CH_3OH$/water and $R^F_8(EO)_9/(CH_3)_2CHOH$/water systems, mesoporous silica materials have been prepared from the CTM mechanism. The preparation of silica materials through the CTM mechanism requires a micellar solution. The concentrations of surfactant, which have been fixed at water/$R^F_8(EO)_9$ mass ratio R=9, belong to the L_1 domain. The TMOS has been added to the surfactant solution at 20 ^oC for methanol system or 40 ^oC for iso-propanol system and the solutions were kept stirring for 1 hour. The molar ratio of surfactant/TMOS is fixed to 0.5. The obtained mixtures were sealed in Teflon autoclaves and allowed to undergo hydrothermal treatment at 80 ^oC for 24 hours. Ethanol extraction was carried out with a Soxhlet apparatus for 48 hours. Unless otherwise specified, same conditions of preparation have always been used in this section. In these conditions the hydrolysis of TMOS produces 3 wt% of CH_3OH for the silicas prepared by using the $R^F_8(EO)_9$ surfactant.

1.3.1 The structural properties

The SAXS patterns of the materials prepared from micelles of $R^F_8(EO)_9$ with a methanol concentration lower than 10 wt % exhibit three peaks at 5.3, 3.1 and 2.7 nm (**Figure V-3**). The presence of the two last peaks is suggestive of a hexagonal organization of the channels. According to Bragg's law, the unit cell dimension ($a_0=2d_{100}/\sqrt{3}$), which corresponds to the sum of the pore diameter and the thickness of the pore wall, can be calculated and its value is found equal to 6.1 nm. If methanol is further added into the micellar solution no secondary reflections are detected any longer (**Figure V-3**). Thus, the regular channel array is lost and the presence of a single reflection indicates the formation of a disordered structure.

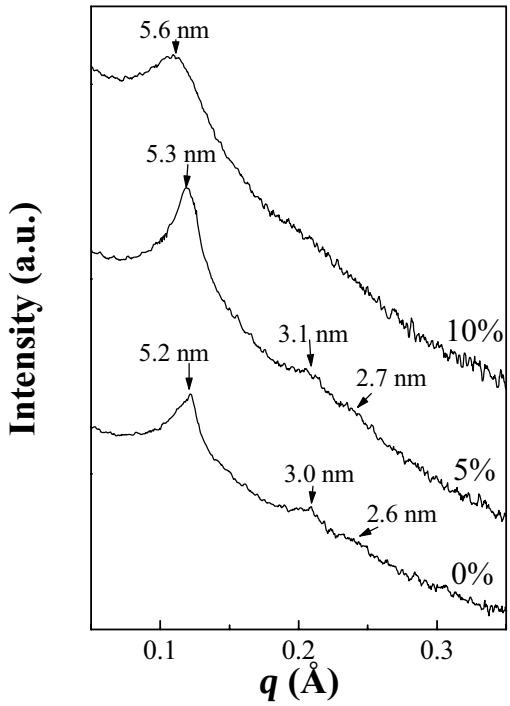


Figure V-3. *SAXS patterns of the materials prepared from the $R^F_8(EO)_9/CH_3OH$/water system; the concentration of the added methanol is equal to a : 0, b : 5 and c : 10 wt.% for R=9 at pH 2 and 20 °C.*

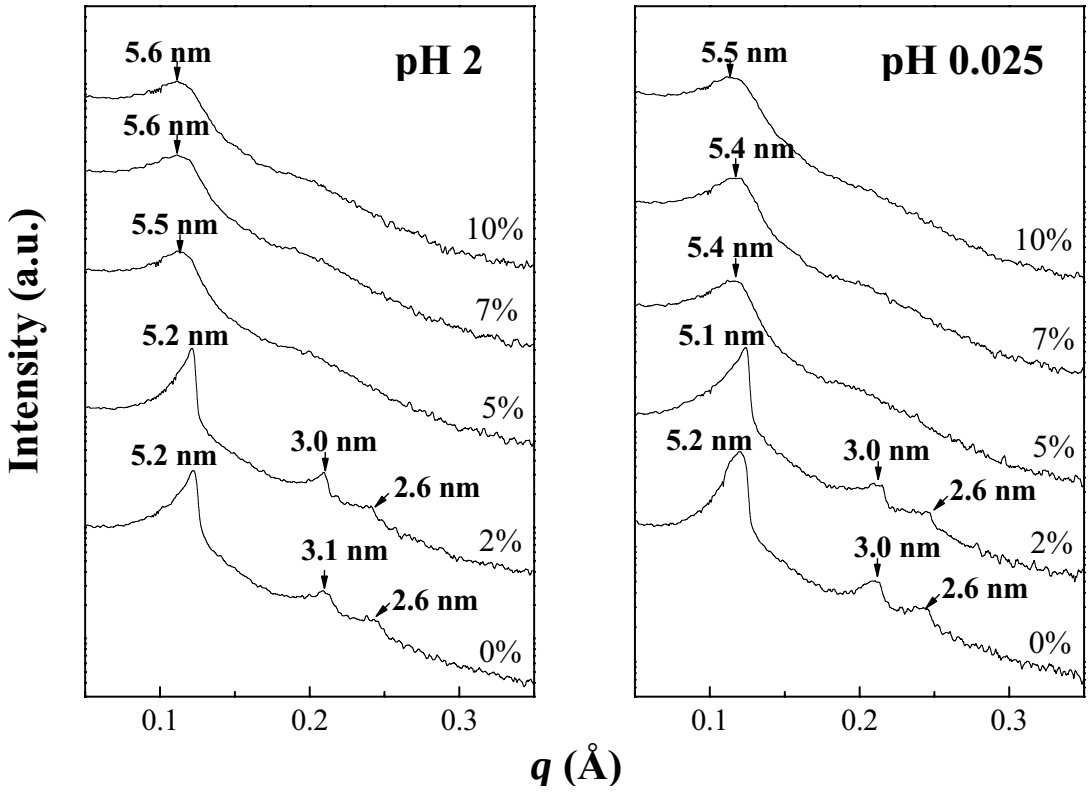


Figure V-4. *SAXS patterns of the materials prepared from the $R^F_8(EO)_9$-based system with different concentrations of $(CH_3)_2CHOH$ for R=9 at 40 °C.*

Similarly we observed the same change trend for the materials prepared on the presence of iso-propanol at pH 2 and pH 0.025 (**Figure V-4**). The materials are ordered if the concentration of the added alcohol is lower than 5 wt.%. From this concentration, the recovered materials exhibit a wormhole-like channel system.

1.3.2 The textural characteristics

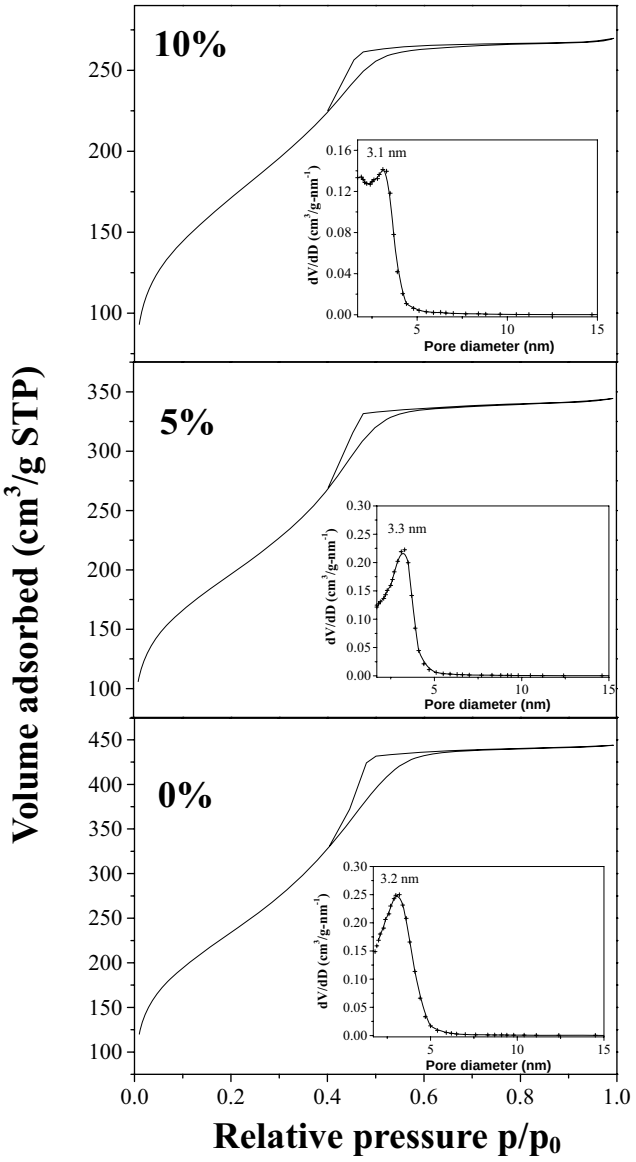


Figure V-5. *Evolution of nitrogen adsorption-desorption isotherm and the corresponding BJH pore size distribution curve (insert) with different concentrations of CH_3OH: 0, 5 and 10 wt.% for R=9 at pH 2 and 20 °C.*

Nitrogen adsorption-desorption isotherms and the corresponding BJH pore size distributions (insert), obtained from an analysis of the adsorption branch of the isotherm are

shown in **Figure V-5** and **Figure V-6**. No matters how many methanol and the iso-propanol contents are, the type IV isotherms, characteristic of mesoporous materials, are obtained.

Table V-1. *Structure properties of the samples prepared with methanol (20 °C)*

CH_3OH added (wt%)	CH_3OH overall (wt%)	structure	**d** [1] (nm)	$\mathbf{a_o}$ [2] (nm)	$\mathbf{S_{BET}}$ [3] (m^2/g)	∅ [4] (nm)	Wall thickness (nm)
0	3	hexagonal	5.2	6.0	860	3.2	2.8
5	7.8	hexagonal	5.3	6.1	709	3.3	2.8
10	12.8	wormlike	5.6	6.5	619	3.1	3.4

1.**d**: repetition distance; 2.$\mathbf{a_o}$: unit cell; 3.$\mathbf{S_{BET}}$: specific surface area; 4.∅: pore diameter.

From **Table V-1** and **Table V-2**, we can observe that the progressive incorporation of alcohol does not modify significantly the maximum of the pore size distribution. In the case of methanol, a decrease of the specific surface area is noted (**Table V-1**). Its value drops from 860 to 619 m²/g when about 10 wt% of methanol is added to the micellar solution. For iso-propanol, whatever the concentrations, the specific surface area is rather high (> 950 m^2/g) (**Table V-2**).

Table V-2. *Structure properties of the samples prepared with iso-propanol (40 °C)*

pH	wt%	structure	**d** [1] (nm)	$\mathbf{a_o}$ [2] (nm)	$\mathbf{S_{BET}}$ [3] (m^2/g)	∅ [4] (nm)	Wall thickness (nm)
2	0	hexagonal	5.2	6.0	1045	3.6	2.4
	2	hexagonal	5.2	6.0	994	4.1	1.9
	5	wormlike	5.5	6.4	1029	4.0	2.4
	7	wormlike	5.6	6.5	1019	3.9	2.6
	10	wormlike	5.6	6.5	953	3.8	2.7
0.025	0	hexagonal	5.2	6.0	1043	3.4	2.6
	2	hexagonal	5.1	5.9	1027	3.8	2.1
	5	wormlike	5.4	6.2	1022	3.6	2.6
	7	wormlike	5.4	6.2	988	3.6	2.6
	10	wormlike	5.5	6.4	981	3.6	2.8

1. **d**: repetition distance; 2.$\mathbf{a_o}$: unite cell; 3.$\mathbf{S_{BET}}$: specific surface area; 4.∅: pore diameter.

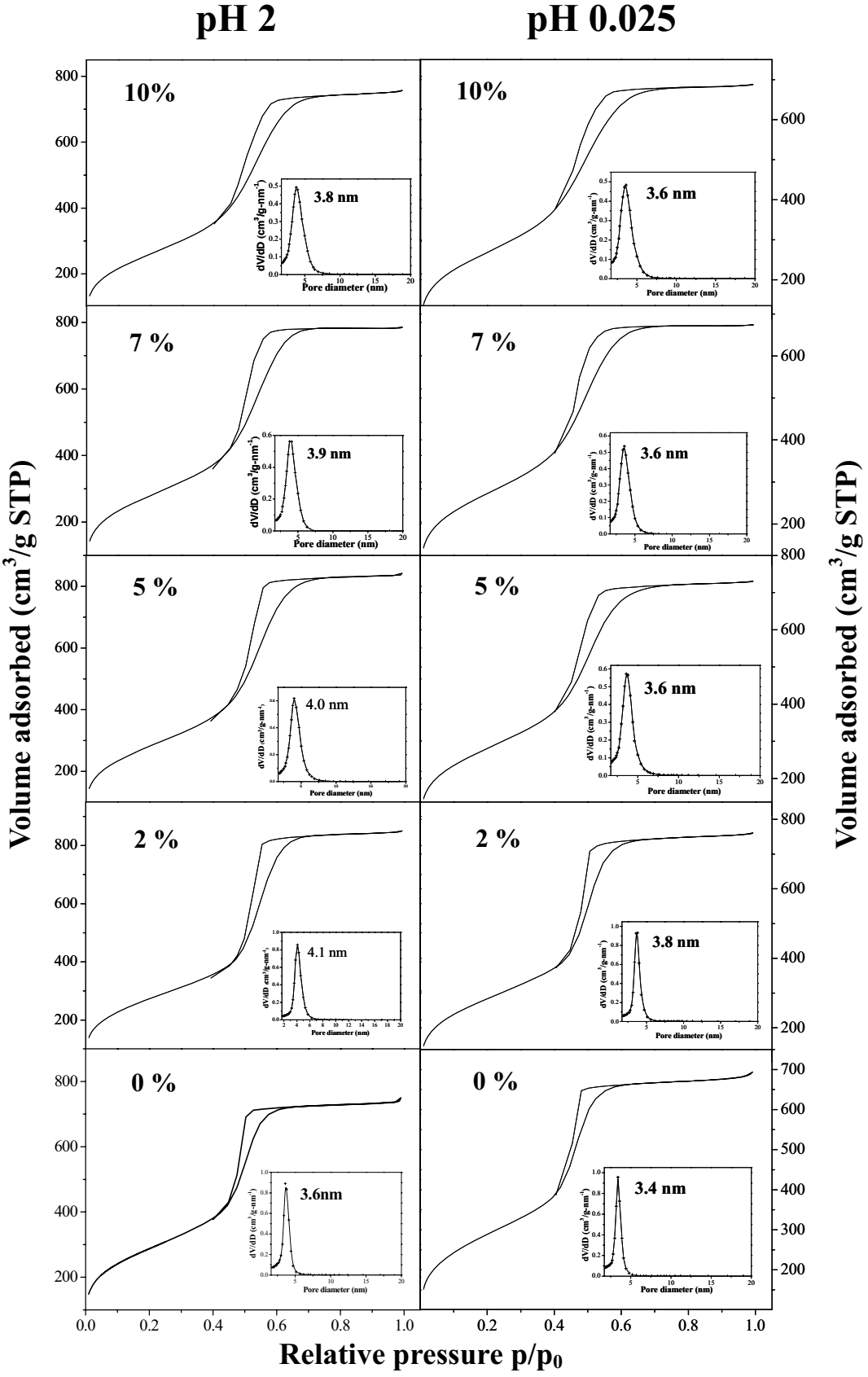


Figure V-6. *Evolution of nitrogen adsorption-desorption isotherm and the corresponding BJH pore size distribution curve (insert) with different concentrations of $(CH_3)_2CHOH$ for ratio R=9 at 40 °C.*

1.4 Discussion

By comparison of the channel arrangement of the mesostructured silica prepared with and without the addition of alcohol we can see that the regular array of the materials obtained from $R^F_8(EO)_9$ is lost when 10 wt % of CH_3OH and 5 wt % of $(CH_3)_2CHOH$ are respectively added. In the case of methanol, this corresponds to an overall concentration of CH_3OH in the blend equal to 12.8 wt %. It is the sum of the methanol released during the TMOS hydrolysis and methanol that is added to the micellar solution during the material synthesis. So, the methanol produced only during the hydrolysis of TMOS, about 3 wt%, does not disturb the CTM mechanism. A similar behavior is also noted with the addition of iso-propanol up to 2 wt.%. Above this concentration the mesopore ordering is lost. As explained above, methanol and iso-propanol are totally solubilized in water and they interact with the micelles via oxyethylene units. Thus from 10 wt. % of methanol or 5 wt. % of iso-propanol the hydrogen bonds between alcohols and the EO groups disfavored the ones between the hydrolyzed TMOS and the surfactant. Besides, it is reported in literature that the addition of these short chain alcohols in the micellar solution also results in a micelle breaking effect [224]. The destruction of micelles makes the surfactant solubilize simply in water and alcohol as monomers. As a consequence the self-assembly mechanism is disturbed and wormhole-like structures are recovered. Moreover, this observation is in good agreement with the evolution of the phase diagram (**Figure V-1**). Indeed, we have evidenced that the surfactant range composition belonging to H_1 is progressively reduced with CH_3OH or $(CH_3)_2CHOH$ addition. The presence of alcohol also has a destruction effect of H_1 as in the case of micelles, it participates into the solubilization of surfactant in water. Thus, it can be assumed that the hexagonal hybrid-mesophase is disorganized if the methanol or iso-propanol content is increased, as observed for the H_1 liquid crystal, which can incorporate at the most 15 wt.% CH_3OH and 10 wt.% $(CH_3)_2CHOH$ respectively at 20°C.

2. Solubilization of butanol in the $R^F_8(EO)_9$-water system

n-butanol could be considered as a medium chain length alcohol [221]. Its solubility in water is 7.9 g/100 mL (20 °C), conversely, the solubility of water in n-butanol is 20.1 g/100 mL (20 °C) [233]. In this part, we will study the effect of n-butanol addition into the $R^F_8(EO)_9$-water system.

2.1 Ternary diagram

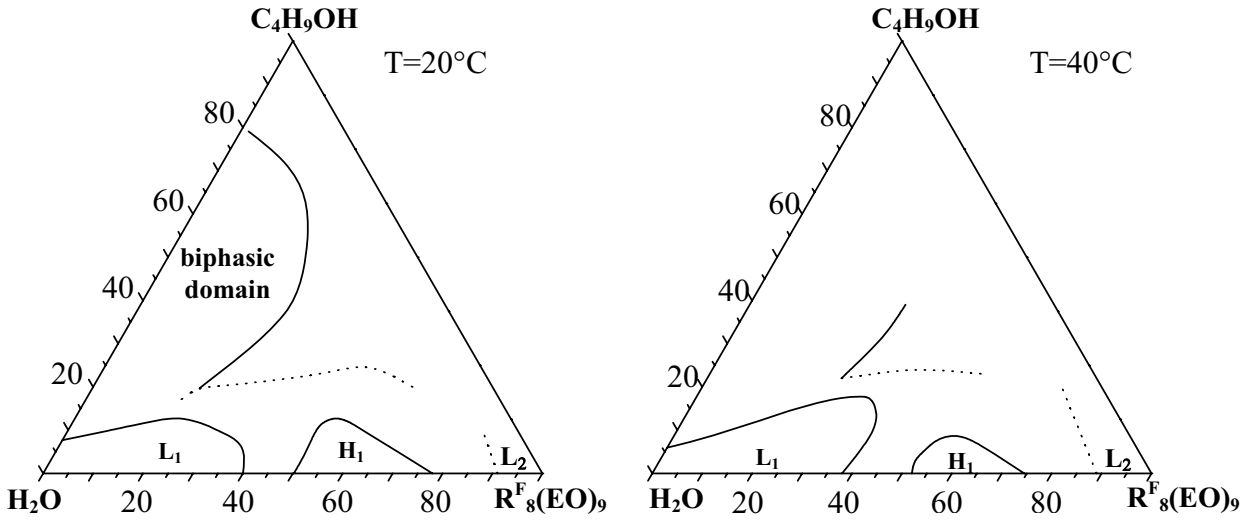


Figure V-7. *Phase diagram (wt %) of $R^F_8(EO)_9/C_4H_9OH$/water system at 20 °C and 40 °C.*

In contrast to methanol and iso-propanol which make the isotropic domain larger, upon addition of n-butanol, the micelles can incorporate up to 12 wt % at 20 °C (**Figure V-7**). From 50 to 78 wt. % of surfactant, a direct hexagonal H_1 phase is observed. The n-butanol solubilization rate in the hexagonal phase is strongly dependent on the water/$R^F_8(EO)_9$ mass ratio (R). Indeed, upon the addition of n-butanol, the surfactant range of composition belonging to H_1 is progressively reduced and the hexagonal liquid crystal phase is completely melted when the n-butanol concentration reaches 15 wt % at 20 °C. On the other hand, $R^F_8(EO)_9$ is soluble in all proportion in n-butanol and depending on the $R^F_8(EO)_9/C_4H_9OH$ ratio (labeled as R_S), the system can solubilize a large quantity of water. For instance, if the value of R_S is equal to 0.82, 50 wt. % of water can be solubilized in the system. The same phase sequence is observed at 40 °C, but the limits of the phases are shifted (**Figure V-7**). The isotropic phase is getting larger while the liquid crystal domain is reduced.

2.2 Structural parameters of the hexagonal crystal liquid phase

We determined the Bragg distance for two independent series of experiments:

- From different water/surfactant ratios (R) covering the hexagonal liquid crystal domain, the n-butanol is incorporated progressively (**Figure V-8** pathway A). The samples corresponding to each addition of n-butanol are examined by the SAXS.
- From different ratios of R_S = surfactant/n-butanol (between 6.1 and 13.3), a

minimum quantity of water is added in order to reach the hexagonal liquid crystal phase. Subsequently, successive additions of water are carried out in order to cover the whole hexagonal liquid crystal domain and each sample is examined by the SAXS (**Figure V-8** pathway B). This method allows us to consider that the alcohol forms a mixed system with the surfactant. Thus, each ratio R_S corresponds to a well defined mixed system and the incorporation of water is investigated for each mixed system.

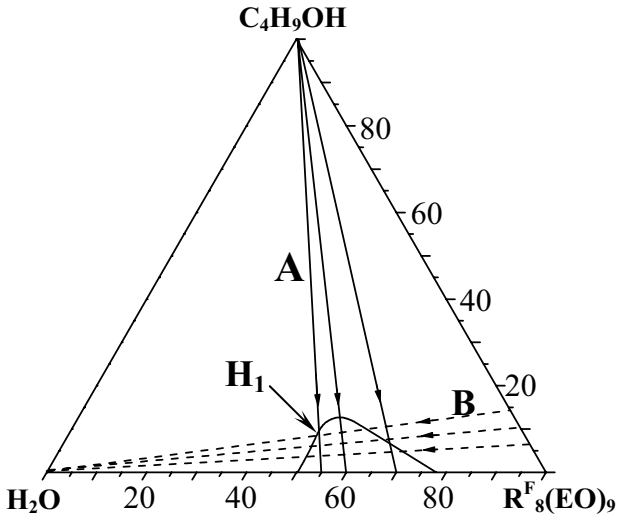


***Figure V-8**. Schema of two independent series of experiments (pathway A and B) for the hexagonal liquid crystal phase domain of $R^F_8(EO)_9$/ n-butanol /water system*

➢ **Results obtained from pathway A**

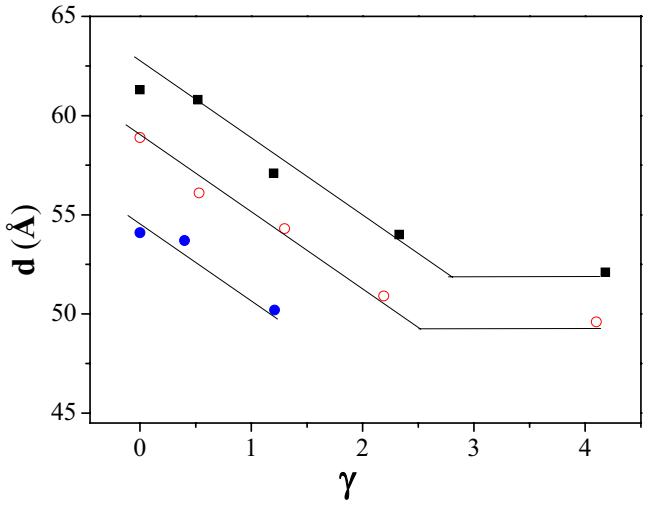


***Figure V-9.** Evolution of the d-spacing (d) as a function of γ (the number of n-butanol molecules per surfactant molecule) in H_1 for ■ : R = 0.79; ○: R = 0.61; ● : R = 0.39.*

From the results obtained by considering the incorporation of n-butanol in the binary

system water/surfactant, the Bragg distances are reported as a function of the number of n-butanol molecules per surfactant molecule (γ) for each value of R.

For a given water/surfactant ratio (R), the Bragg distance (d) is deceasing linearly with the incorporation of n-butanol (**Figure V-9**). In addition, higher the value of R, higher the value of d. For example, if γ=1.2, d varies from 50.0 to 52.5 Å, when R is changed from 0.39 to 0.79. To explain these results, two models can be taken into account.

The first one consists in considering that the n-butanol molecules are located in the hydrophobic core of the micelles, but they may also penetrate into the hydrophobic chains. We design this model as "**Oil model**". According to the relation established for the hexagonal phase (see p. 64), the hydrophobic radius can be calculated by reconsidering the hydrophobic volume fraction. Thus, the relation can be written as:

$$\frac{V_B + \gamma V_{But}}{V_S + \alpha V_W + \gamma V_{But}} = \frac{\sqrt{3}\pi R_H^2}{2d^2}$$

where γ stands for the number of n-butanol molecules per surfactant molecule and V_{But} stands for the molar volume of n-butanol (V_{But}=91 cm^3/mol).

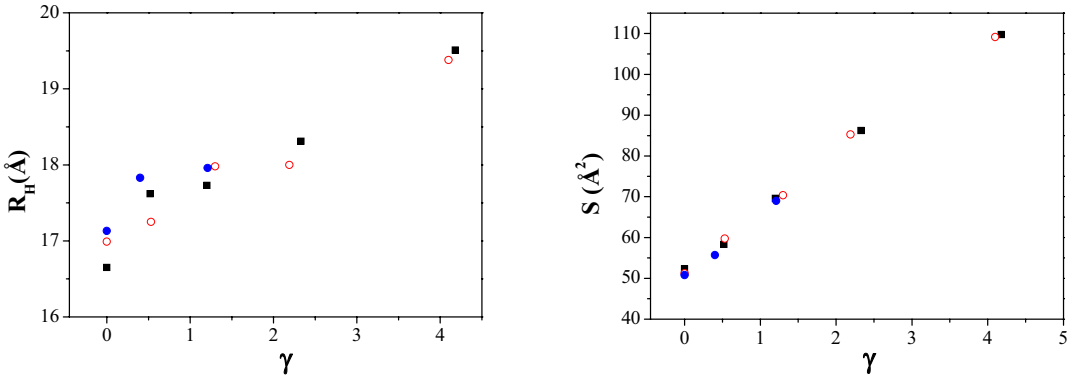


Figure V-10. *Evolution of the hydrophobic radius (R_H) and cross sectional area (S) as a function of γ in H_1 for ■ : R = 0.79; ○: R = 0.61; ● : R = 0.39.*

As shown in **Figure V-10**, the hydrophobic radius is increasing as a function of γ for different R. The values of the cross sectional area (S) in H_1 are deduced from the following equation:

$$S = \frac{2(V_B + \gamma V_{But})}{N\ R_H}$$

where N is the number of Avogadro. The values of cross-sectional area increase linearly from 50 to 110 Å^2 as a function of γ (**Figure V-10**). For a fixed value of γ, no variation of S with R is noted.

The second model considers that n-butanol solubilizes in water and behaves as a

co-solvent, which is the same way like methanol and isopropanol. This model is also designed as "co-solvent model". Considering that the hydrophobic volume is constituted only by the hydrophobic part of the surfactant, the values of hydrophobic radius (R_H) in H_1 are deduced from the following equation:

$$\frac{V_B}{V_S + \alpha V_W + \gamma V_{But}} = \frac{\sqrt{3}\pi R_H^2}{2d^2}$$

It is revealed in **Figure V-11** that the hydrophobic radius is decreasing almost linearly as a function of γ. For a given γ, the hydrophobic radii remain almost constant when the value of R varies.

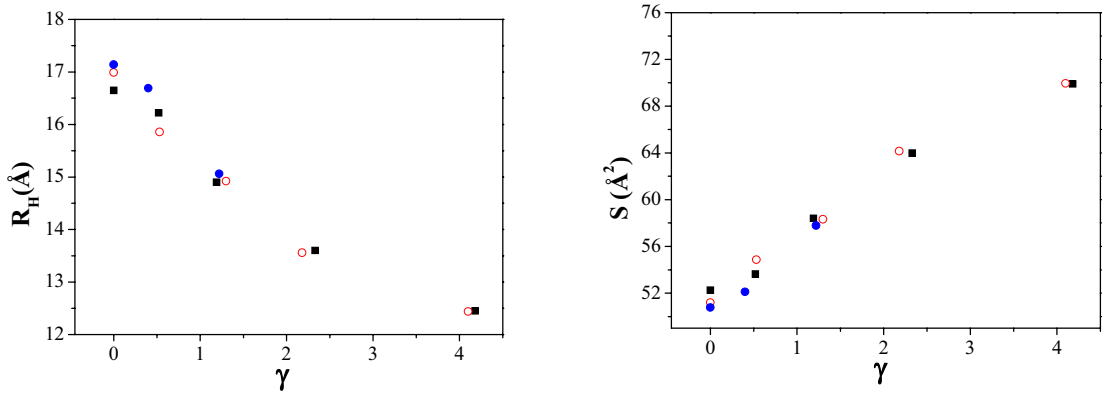


Figure V-11. *Evolution of the hydrophobic radius (R_H) and cross sectional area (S) as a function of γ in H_1 for ■ : R = 0.79; ○: R = 0.61; ● : R = 0.39.*

The values of the cross sectional area (S) in H_1 are given by:

$$S = \frac{2V_B}{NR_H}$$

The values of cross-sectional area increase from 52 to 70 $Å^2$ as a function of γ for different R (**Figure V-11**). Once again we do not observe significant variation as a function of R.

➢ **Results obtained from pathway B**

For the second set of experiments, we have to consider that n-butanol and surfactant form a real mixed amphiphile system whose characteristics depend on the ratio between the two components. Thus, in that case the system is reduced to a binary mixed surfactant-water system and to determine the structural parameters of the liquid crystal phase, the **co-surfactant model** is employed. Each surfactant/n-butanol ratio (R_S) corresponds to a mixed surfactant and the swelling of the hexagonal liquid crystal phase by water is followed

by the determination of Bragg distance (d). The results depicted in **Figure V-12** show that the d linearly increases with the incorporation of water in each of mixed entities (**Figure V-13**).

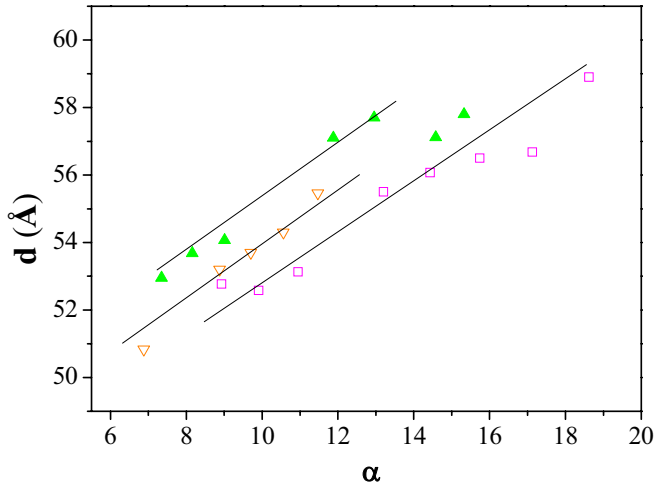


Figure V-12. *Evolution of the d-spacing (d) as a function of α in H_1 for various mixed entities □ : R_S = 32.3; ▲ : R_S = 8.1; ▽ : R_S =6.1.*

The molecular weight M^m, the density d^m and the molar volume of mixed surfactant V^m are calculated as follow:

$$M^m = \frac{n_{But}M_{But} + n_S M_S}{n_{But} + n_S}\ ;\quad d^m = 1/\left(\frac{x_S}{d_S} + \frac{1-x_S}{d_{But}}\right)$$

where n_{But} and n_S respectively stands for the mole number of n-butanol and $R^F_8(EO)_9$; x_S is the mass fraction of surfactant in the mixed amphiphile entity (surfactant-butanol); M_{But} and M_S correspond to the molar weight of n-butanol and $R^F_8(EO)_9$; d_S and d_{But} correspond to the density of surfactant and n-butanol, respectively. Considering the mixed molar volume of the hydrophobic part of the surfactant V_B^m and of the mixed entity V_S^m which depend on the molar ratio between n-butanol and $R^F_8(EO)_9$, the distance d associated to the first peak is related to the hydrophobic radius R_H by the relation:

$$\frac{V_B^m}{V_S^m + \alpha V_W} = \frac{\sqrt{3}\pi R_H^2}{2d^2}$$

where α stands for the number of water molecules per mixed amphiphile entity. From **Figure V-13**, we can observe that for the various mixed systems, the hydrophobic radii decrease slightly with the incorporation of water.

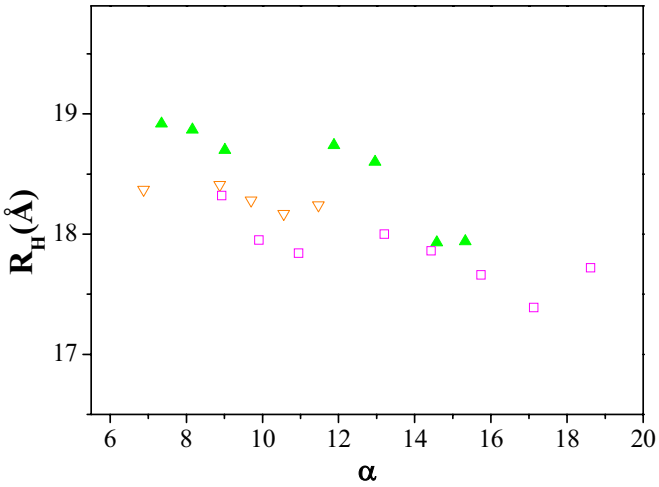


Figure V-13. *Evolution of the hydrophobic radius (R_H) as a function of α in H_1 for different R_S, □ : R_S = 32.3; ▲ : R_S = 8.1; ▽ : R_S =6.1.*

The cross-sectional area S can then be deduced from the relation as below:

$$S = \frac{2V_B^m}{NR_H}$$

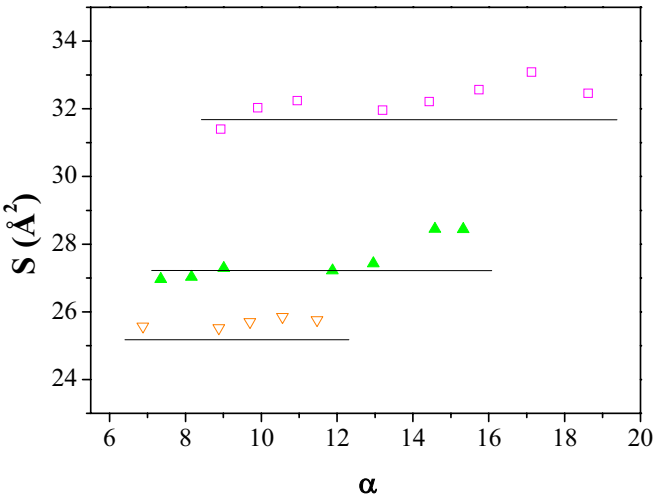


Figure V-14. *Evolution of the cross sectional area (S) as a function of α in H_1 for □ : R_S = 32.3; ▲ : R_S = 8.1; ▽ : R_S =6.1.*

For a given mixed system, S remains almost constant with the variation of α (**Figure V-14**). Nevertheless, From **Figure V-14**, we can note that the value of the cross-sectional area is raised when the proportion of $R^F_8(EO)_9$ in the mixed system is increased. For example, S varies from 25 to 33 Å^2 when the $R^F_8(EO)_9$ content in the mixed system is changed from 86% to 97%.

The results obtained from the **oil model**, which consider that n-butanol is located in the hydrophobic core of the cylinders, lead to high value of S for the highest loading of n-butanol

(up to 110 Å). These values do not seem to be realistic. As a matter of fact, in the binary system, the hydrophobic chains are totally extended, thus the increase of hydrophobic radius should be attributed to the solubilization of n-butanol in the core of the cylinders and there is no reason at all for cross-sectional area increasing so strongly. Hence, we can conclude that that the **oil model** does not correspond for the description of the studied system.

If we consider that n-butanol acts as a co-surfactant now, the **co-surfactant model** has to be applied. But once again R_H and S do not match well with the reality. Indeed, the values of the hydrophobic radius which vary from 18 to 19 along R_S=32.3 are higher than the size of the hydrophobic chain adopting an extended conformation. The value of the cross-sectional area are surprising low. For example, for a $R^F_8(EO)_9$/n-butanol ratio equals to 6.1, S is only around 25 $Å^2$. This value should be compared to 47 $Å^2$, which is obtained from the pure $R^F_8(EO)_9$ system. Thus, we can conclude that the **co-surfactant model** does not adapt to the given system either.

At last, we should have a look at the situation where n-butanol is solubilized in water; this corresponds to the **co-solvent model** (**Figure V-11**). In this case, no matter how much is the ratio R, the hydrophobic radius R_H decrease from around 17 to 12.5 Å with the addition of 15 wt. % of n-butanol. As the case of methanol and iso-propanol, the hydrophobic chains fold up and at the same time, the cross-sectional area is growing up (52 to 70 $Å^2$). Thus, once again we can explain this phenomenon by a dehydration of the oxyethylene units. This scenario seems to be quite probable.

In addition, in the micellar solution domain, the micelle size has been measured by dynamic light scattering (**Figure V-15**). The concentration of n-butanol is raising from 0 to 5 wt % for water/$R^F_8(EO)_9$ ratios equal to 19. The size of the micelles in water is quite monodisperse and centered at around 7.5 nm. Upon the addition of n-butanol, the distribution of micelle size curve becomes broader and slightly shifts toward to a higher diameter. These results are in agreement with the penetration of n-butanol into the palisade layer. Consequently, micelles probably will become more polydisperse due to the fact that the number of n-butanol molecules which penetrate between the hydrophilic chains is not precise. Therefore, we can assume that for the investigated n-butanol range of concentrations, the n-butanol molecules are rather solubilized in water and they interact with the surfactant polar headgroup. Thus, it seems to be more reasonable that the co-solvent model adapts to the given system.

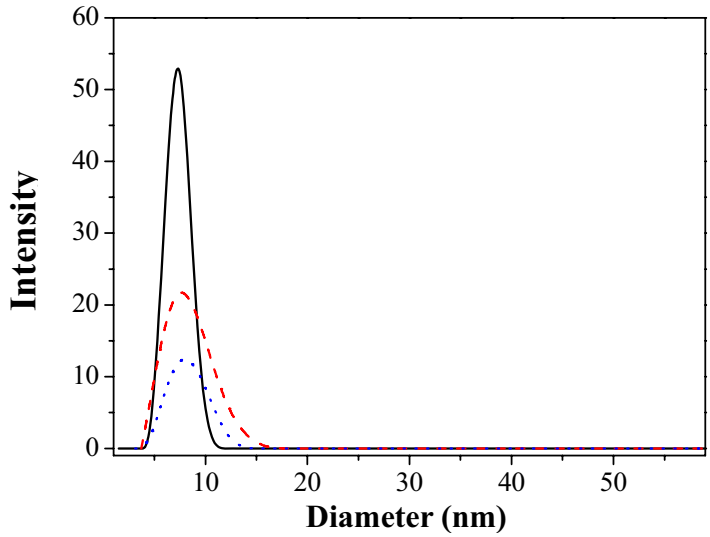


Figure V-15. *Hydrodynamic diameter (D) distributions of $R^F_8(EO)_9$/water system with 0, 2 and 5 wt % concentrations of n-butanol at 20 °C.*

2.3 Mesoporous materials prepared from the system $R^F_8(EO)_9$/water in the presence of butanol

Mesoporous silica materials have been prepared from the CTM mechanism. Micellar solutions are prepared with R=9 and 4. Then, n-butanol is added at 40 °C. For R=9, four samples with n-butanol concentrations equal to 2, 5, 10 and 20 wt.% are prepared. For R=4, two samples are prepared, namely, 2 and 5 wt.% n-butanol. The TMOS has been added to the surfactant solution at 40 °C with surfactant/TMOS molar ratio of 0.5 at pH 2 or pH 0.025. The solutions were kept stirring for 1 hour. The obtained mixtures were sealed in Teflon autoclaves and allowed to undergo hydrothermal treatment at 80 °C for 24 hours. Ethanol extraction was carried out with a Soxhlet apparatus for 48 hours.

2.3.1 Materials prepared at pH 2

- *The structural properties*

Upon addition of n-butanol, the hexagonal structure is kept until the concentration of n-butanol remains lower than 5 wt% (**Figure V-16** left**)**. When the n-butanol amount reaches 5 wt.%, the secondary reflections are almost disappeared and a wormlike structure is observed. It means that the disorganization of the channel array has begun. If the content of n-butanol is further increased, no reflection is detected anymore (**Figure V-16)**. Thus, the regular channel

array is completely lost in this case. Referring to the phase diagram reported in **Figure V-7**, we can see that for these n-butanol concentrations, i.e. 10 and 20 wt. %, no micellar domain is observed. Since there is no micelle formed, the self assembly mechanism can not occur and only disordered materials can be recovered.

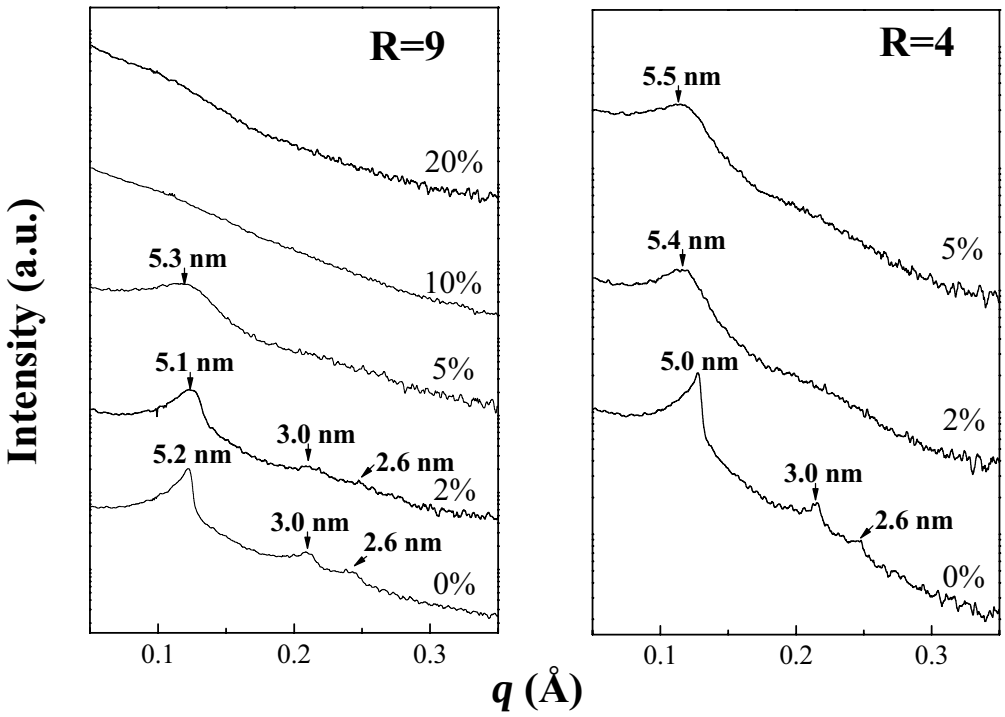


Figure V-16. *SAXS patterns of the materials prepared from the $R^F_8(EO)_9$/water system with different concentrations of n-butanol for R=9 and 4 at pH 2 and 40 °C.*

As regard the materials prepared with a water/ $R^F_8(EO)_9$ ratio equals to 4 (**Figure V-16**), the loss of the mesopore ordering occurs as soon as n-butanol is added to the surfactant solution and for the investigated range of n-butanol concentrations only wormhole like structures are obtained. This observation strengthen our hypothesis that n-butanol rather solubilizes in water. To explain the formation of the wormhole like structure we can use the same arguments than the ones developed for methanol and iso-propanol.

- *The textural characteristics*

Whatever the butanol concentration and the water/surfactant ratio, a type IV isotherm is obtained by nitrogen adsorption-desorption analysis (**Figure V-17**). Nevertheless when the n-butanol concentration reaches 20 wt.%, the capillary condensation is spread out over a larger range of relative pressures, meaning that the compound becomes less homogeneous in

pore sizes (**Figure V-17**). This is also confirmed by the broader pore diameter distribution. In addition, the pore size distribution is centered on about 3.4 nm and 4.0 nm for R=9 and R=4, respectively. These values which are very close to the one obtained for the mesostructured silica prepared without the addition of n-butanol. Thus, there is no swelling effect of n-butanol. Once again this observation supports the choice of the co-solvent model.

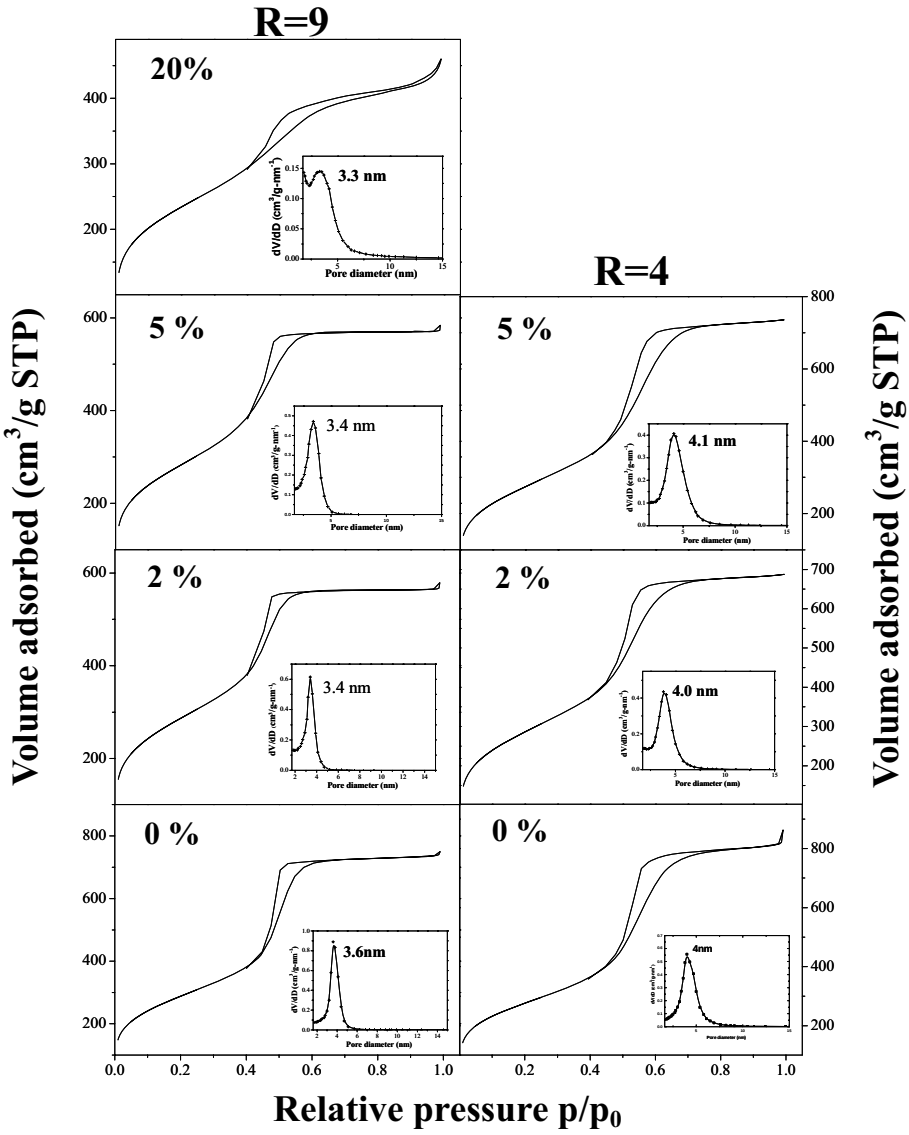


Figure V-17. *Evolution of nitrogen adsorption-desorption isotherm and the corresponding BJH pore size distribution curve (insert) with different concentrations of n-butanol for R=9 and R=4 at pH 2 and 40 °C*

- *Morphology*

From **Figure V-18**, which depicts several representatives scanning electron micrographs (SEM) of the synthesized silicas, we can see that spherical silica particles with around 3 μm size are formed at 5 wt. % n-butanol. Subsequently, they agglomerate when the n-butanol

concentration has been raised to 20 wt. %.

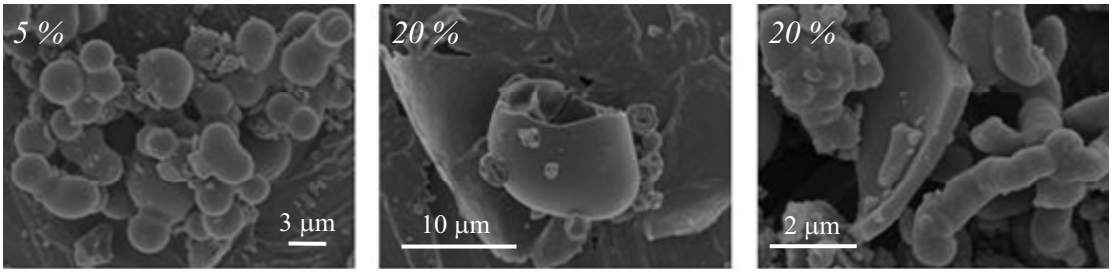


Figure V-18. *SEM micrograph of samples prepared from $R^F_8(EO)_9$-water system with 5 and 20 wt.% of n-butanol at pH 2 and 40 °C.*

2.3.2 Materials prepared at pH 0.025

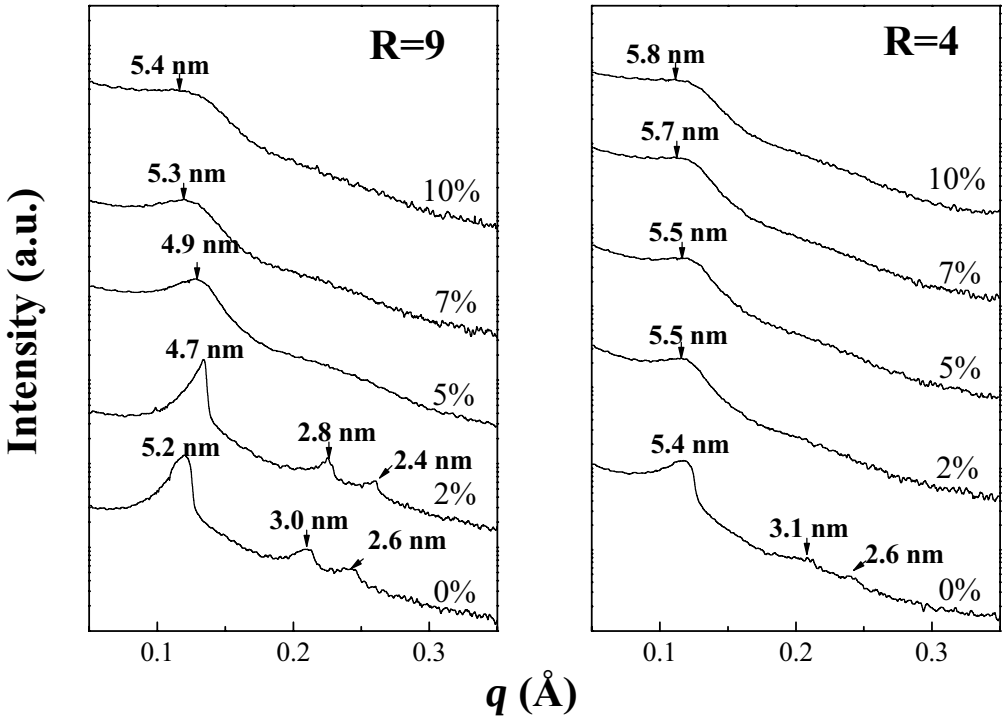


Figure V-19. *SAXS patterns of the materials prepared from the $R^F_8(EO)_9$-water system with different concentrations of n-butanol for R=9 and 4 at pH 0.025 and 40 °C.*

So far by now, we have always worked at pH 2 for this system. As we quoted in the Chapter III (p.81) [199-201], the medium pH value is a significant parameter to the structure of the materials. Thus, we examined the effect of medium pH value 0.025 on the properties of the materials prepared from the $R^F_8(EO)_9$/n-butanol/water system. The other preparation conditions are same. Whatever the value of R, we can see from **Figure V-16** and **Figure V-17** that changing the pH does not modify the characteristic of the recovered materials. Indeed, a lost of mesopore ordering is noted upon the addition of n-butanol. In addition, the mesopore

size distribution becomes broader.

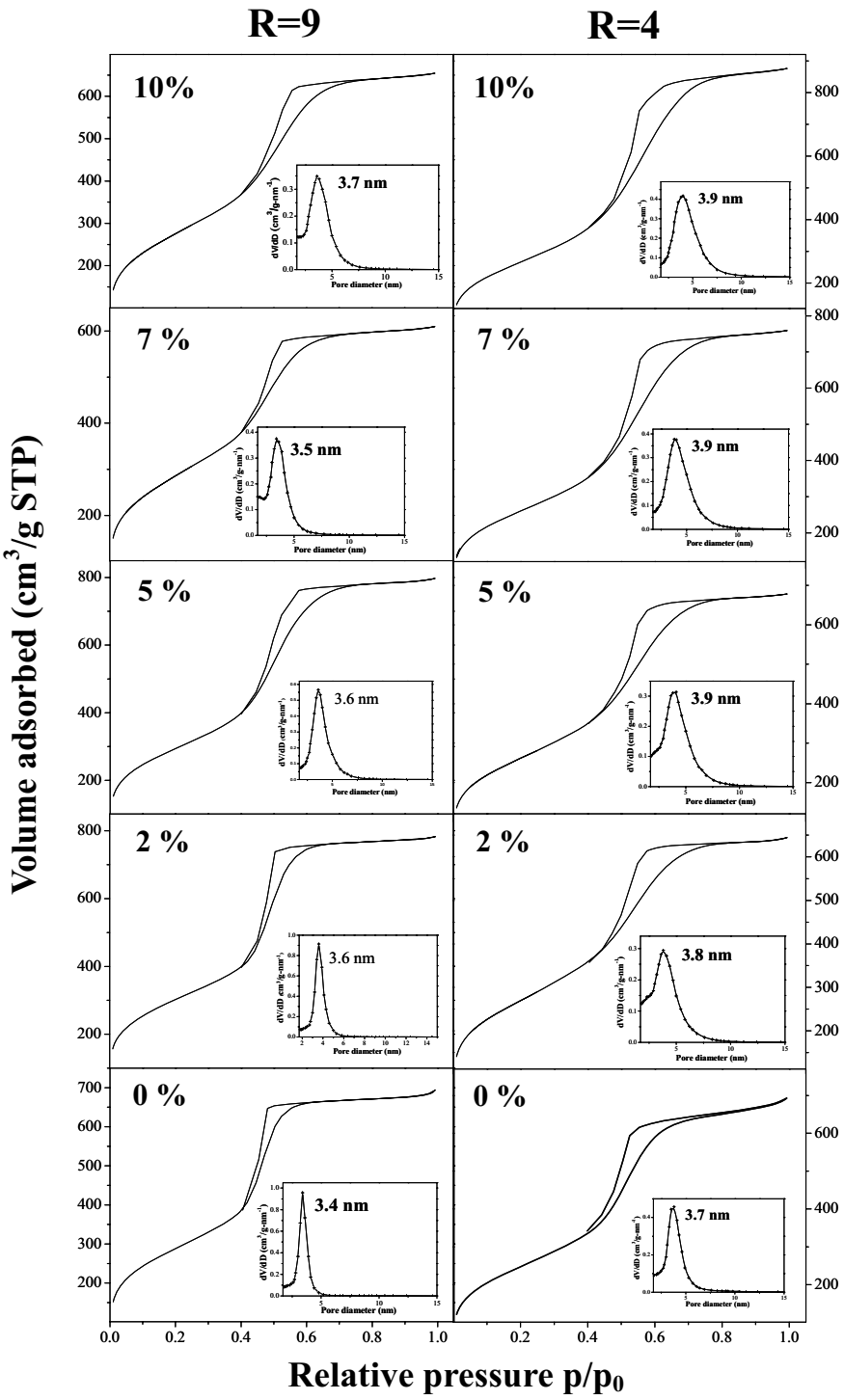


Figure V-20. *Evolution of nitrogen adsorption-desorption isotherm and the corresponding BJH pore size distribution curve (insert) with different concentrations of n-butanol for R=9 and R=4 at pH 0.025 and 40 °C.*

To conclude this part, the results of the materials characterization are in accordance with the conclusion obtained from the investigation of the structural parameters of the hexagonal

liquid crystal phase. In the investigation range of concentrations, the n-butanol acts as a co-solvent and it solubilizes in water.

3. Solubilization of octanol in the $R^F_8(EO)_9$-water system

1-octanol (noted as octanol for short) could be considered as a long chain length alcohol. It is immiscible with water.

3.1 Ternary diagram

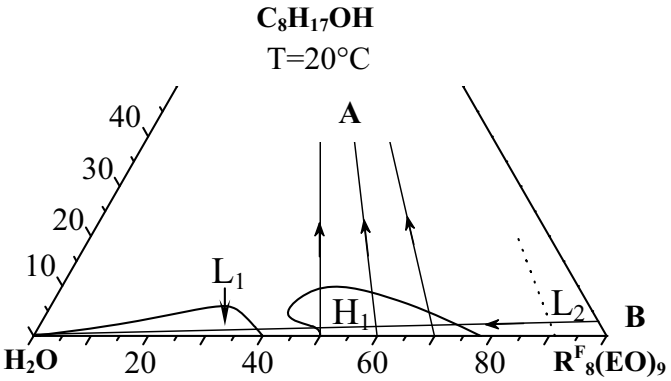


Figure V-21. *Phase diagram (wt %) of $R^F_8(EO)_9$/**$C_8H_{17}OH$**/water system at 20 °C.*

The ternary diagram depicted in **Figure V-21** shows that the solubilization of octanol increased when the concentration of surfactant rises. However, at the most only 6 wt. % of $C_8H_{17}OH$ for R=1.86 can be solubilized. Increasing the $R^F_8(EO)_9$ concentration from 50 to 78 wt. %, a direct hexagonal phase which can incorporate a slightly higher amount of octanol up to 10 wt.% for R=0.82 is detected. We can also note that upon the addition of octanol, the H_1 domain is shifted toward the water rich part of the diagram.

3.2 Structural parameters of hexagonal crystal liquid phase

The same procedure with the one used in the case of the addition of n-butanol has been applied to determine the Bragg distance. Therefore, we have led two set of independent experiments. First, for different values of R, octanol is incorporated in binary systems (pathway A). Second, the octanol is mixed with the surfactant along different ratios R_S and the formation of the hexagonal phase is obtained through the addition of water (**Figure V-21**). The evolution of water swelling into the liquid crystal phase is examined by the determination

of Bragg distance. (pathway B)

➢ **Results obtained from pathway A**

As octanol is completely insoluble in water, the co-solvent model, i.e. the solubilization of octanol molecules in water has not been considered. Therefore, only the oil model that means the location of the octanol molecules in the hydrophobic core of the rods has been taken into account.

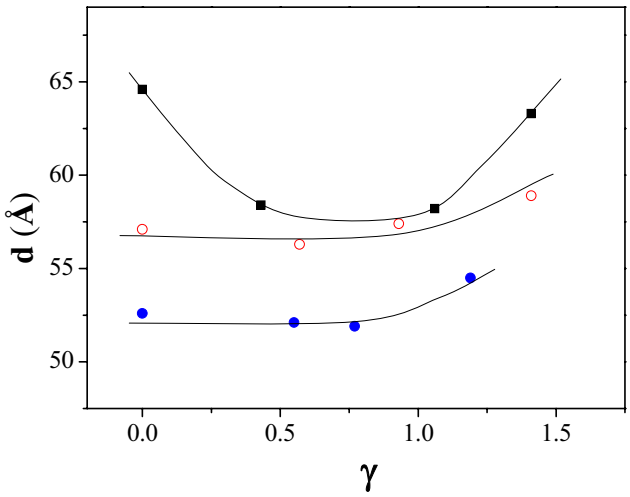


Figure V-22. *Evolution of the d-spacing (d) as a function of γ in H_1 for ■ : R =1.00; : R = 0.67; ● : R = 0.43*

For the system containing the higher content of water (R=1), we can see that the variation of the Bragg distance as a function of γ exhibits a minimum, while for the other ratios, it remains constant at the beginning of the octanol addition (**Figure V-22**). Then the further solubilization of alcohol involves a slight increase of Bragg distance. For example, for R=0.43, d remains constant to 52.2 Å until γ=0.77, then its value is increased to 54.5 for γ=1.19.

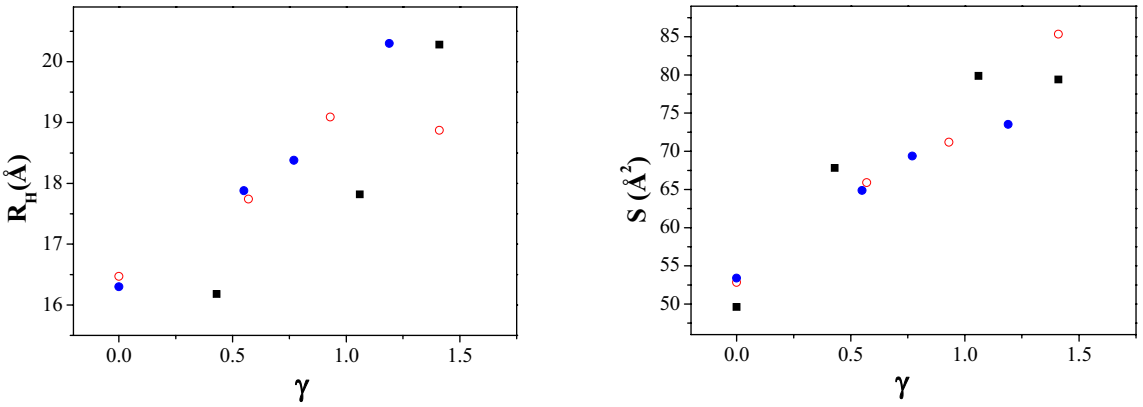


Figure V-23. *Evolution of the hydrophobic radius (R_H) and cross sectional area (S) as a function of γ in H_1 for ■ : R =1.00; ○: R = 0.67; ● : R = 0.43*

Both the hydrophobic radius and the cross-sectional area increase respectively, from 16 to 20 Å and from 50 to 82 $Å^2$ when γ is changed from 0 to 1.41 (**Figure V-23)**. Nevertheless, looking carefully at the values of S, the variation of the cross-sectional area does not correspond to a real physical state. So the oil model does not seem to fit well to explain the solubilization of octanol in the H_1 phase.

- **Results obtained from pathway B**

In this case, each mixed entities is characterized by an average molar mass and molar volume. According to these considerations, we plotted the Bragg distance as a function of the water quantity that is progressively added into the various mixed-systems (**Figure V-24**). For example, for R_S= 32.3, d increases linearly from 55 to 60 Å when α is varied from 16.9 to 28.7. Moreover, we can see that the enrichment of octanol in the mixed amphiphile does not significantly affect the values of the Bragg distance.

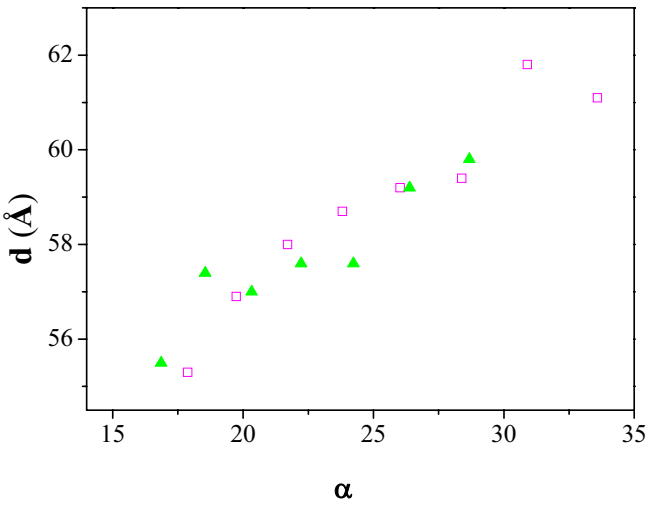


Figure V-24. *Evolution of the d-spacing (d) as a function of α in H_1 for R_S = 32.3(▲) and the pure surfactant (□)*

The hydrophobic radius slightly varies from 18 to 17 Å with α (**Figure V-25**). As this variation is in the dubiousness of the measurement, we can assume that it is not significant and that R_H remains constant. Upon the incorporation of water, the cross-sectional areas enlarge slightly. In addition, the increase of the octanol content involves a decrease of S (**Figure V-25**). For example, S varies from 49, value obtained for the pure surfactant, to 40 $Å^2$ value calculated upon the addition of 8 wt.% of octanol. The variations of S obtained by considering pathway B are quite coherent. Therefore, we retain this model and we can conclude that octanol is incorporated in the palisade layers and behaves like a co-surfactant.

This conclusion is in good agreement with the results reported by Strey et al. [234]. Indeed, in a paper dealing with general patterns of phase behavior of mixtures of H_2O, alkanes, alkyl glucosides and alcohols, the authors also considered that octanol is mixed in the surfactant layer.

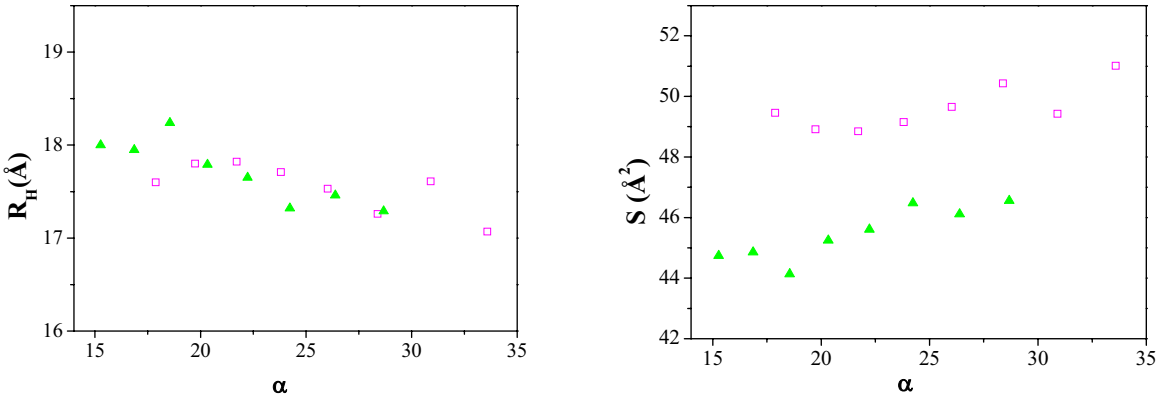


Figure V-25. *Evolution of the hydrophobic radius (R_H) and cross sectional area (S) as a function of α in H_1 for R_S = 32.3(▲) and the pure surfactant (□)*

3.3 Mesoporous materials prepared from system $R^F_8(EO)_9$-water with octanol

According to the phase diagram, mesoporous silica materials have been prepared from the CTM mechanism. Micellar solutions are prepared for the water/$R^F_8(EO)_9$ mass ratio R=9 and 4. Then, octanol is added in the range from 1 to 20 wt.%. The TMOS has been added to the surfactant solution at 40 °C with a surfactant/TMOS molar ratio = 0.5 and at pH = 2. The solutions were kept under stirring for 1 hour. The obtained mixtures were sealed in Teflon autoclaves and allowed to undergo hydrothermal treatment at 80 °C for 24 hours. Ethanol extraction was carried out with a Soxhlet apparatus for 48 hours.

3.3.1 The structural properties of materials

As soon as the octanol is incorporated into the system, the ordered structure starts losing. For example, when 1 wt.% octanol is added into the system, it is found that the first peak is still keep sharp but the 110 and 200 reflection and are not well resolved. We can conclude that the material rather adopts a weakly 2D hexagonal structure. In addition, the first reflection is not shifted by the addition of octanol. If the octanol amount is further increased, no reflection is detected any more when the octanol concentration reaches 2 wt.% (**Figure V-26**). Thus, the regular channel array is completely lost in this case.

Looking at the materials prepared with a water/ $R^F_8(EO)_9$ ratio equals to 4, the same tendency with the one described for R=9 is noted. However, the hexagonal pore ordering is maintained for higher alcohol concentrations. For example, the hexagonal channel array is still observed at 2 wt.% of octanol for R=4, but it is totally lost for R=9 in the same conditions (**Figure V-26)**. When the octanol amount reaches 5 wt.%, the secondary reflections are almost disappeared and a wormlike structure is observed. It means that the disorganization of the channel array has begun. If the content of octanol is further increased, no reflection is detected anymore (**Figure V-26)**. Thus, the regular channel array is completely lost.

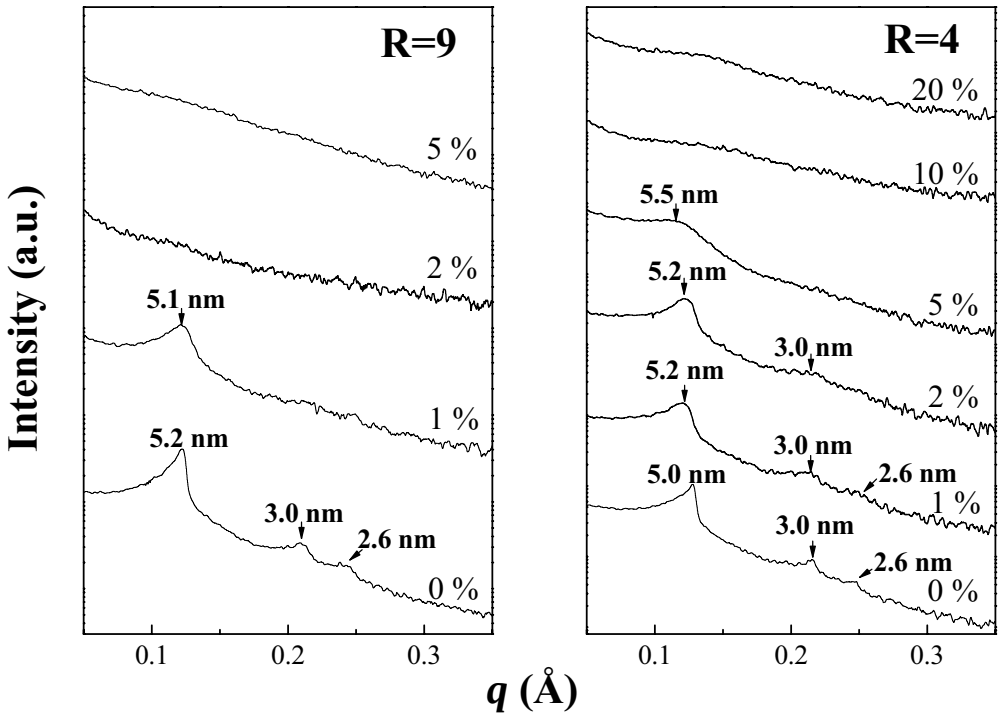


Figure V-26. *SAXS patterns of the materials prepared from the $R^F_8(EO)_9$-based system with different concentrations of octanol for R=9 and 4 at pH 2 and 40 °C.*

3.3.2 The textural characteristics

When the concentrations of octanol are lower than 2 wt.% and 7 wt.% respectively for R=9 and R= 4, a type IV isotherm is obtained (**Figure V-27**). A strong uptake of N_2 adsorption is observed at approximately $p/p_0 = 0.5$, which is the result of the filling of the mesopores due to the capillary condensation. Moreover, that the beginning position of the uptake of N_2 adsorption is staying at the same point tells us that the maximum of the pore size distribution keeps constant, which is also confirmed by the analysis of the pore size distribution curves (**Figure V-27**). The mesopore size distribution is centered on about 3.6 nm for R=9 and 4.2 nm for R=4. These values are very close to the ones obtained for the

mesostructured silica prepared without addition of octanol. Thus, octanol does not act as a

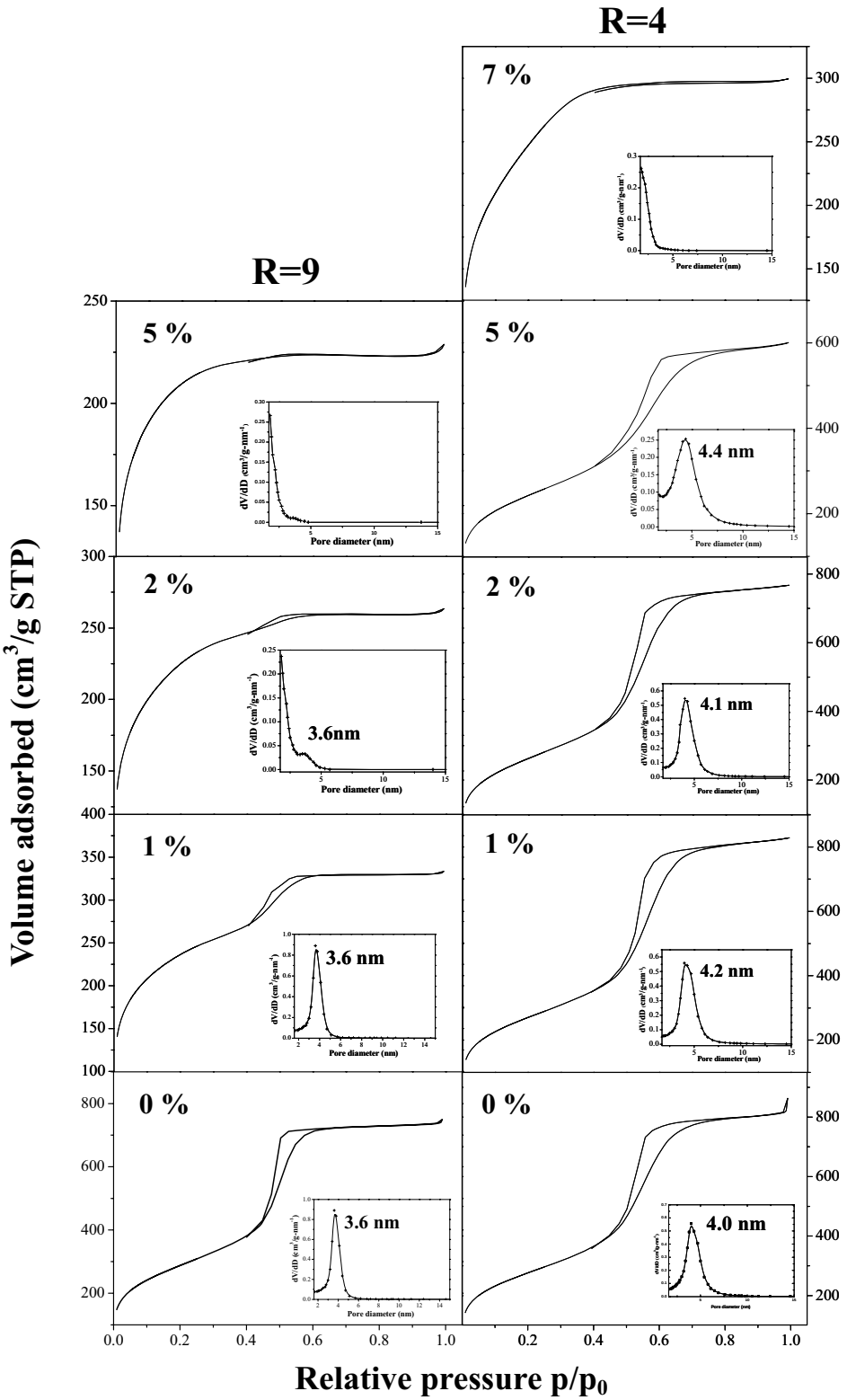


Figure V-27. *Evolution of nitrogen adsorption-desorption isotherm and the corresponding BJH pore size distribution curve (insert) with different concentrations of octanol for R=9 and R=4 at pH 2 and 40 °C.*

swelling agent. Upon the further addition of octanol, the systems exhibit a different behavior.

Isotherms are intermediates between type I and IV. According to Dubinin [217], these kinds of isotherms are characteristic of supermicroporous materials, that is, the pore size is located at the limit between the micro and the mesoporous domain. This phenomenon is further confirmed by the analysis of the pore size distribution, whose maximum is lower than 1.7 nm.

3.4 Discussion

The results concerning the characterization of the mesoporous materials have revealed that octanol does not act as a swelling agent. This observation supports the choice of the co-surfactant model. Moreover, the pore diameter remains constant. This is in good accordance with the fact that in the hexagonal liquid crystal phase hydrophobic radii remain constant upon the addition of octanol.

During the preparation of mesoporous materials, the structural characteristics of materials are strongly depending on the ratio R. Specifically, for R=9, 1 wt.% of octanol can be solubilized in the micellar solution which allows us to prepare ordered mesoporous materials with maximum 1 wt.% of this addition, whereas for R=4, 5 wt.% of octanol can be solubilized in the micellar solution which allows us to obtain ordered mesoporous materials with until maximum 5 wt.% of this alcohol. As the self assembly mechanism requires micelles in the solution, the loss of the mesopore ordering noted with the incorporation of the octanol concentration in the surfactant solution might be attributed to the absence of micelles.

To complete this work, we have performed some experiments to investigate the effect of octane addition in the $R^F_8(EO)_9$-water system. Compare to octanol, the phase behavior is different, as octane can not be incorporated into the micelles at all. Indeed, the absence of the hydroxyl group does not allow them act like co-surfactant. By contrast, hexagonal liquid crystals have been detected until 4 wt.% of octane. The Bragg distances have been determined in the H_1 phase and the results evidence a slight increase with the addition of octane. As an example for R=0.53, d increases from 55 to 60 Å when the octane concentration varies from 0 to 3.6 wt.%. Materials have also been synthesized in the presence of octane. The characterization results show that the mesopore ordering is kept until the addition of 15 wt.% of octane for R=9 and until 5 wt.% of octanol for R=4. Nevertheless, no variation of the mesopore diameter is noted. So no swelling effect occurs. Indeed, despite that octane can not be solubilized into the $R^F_8(EO)_9$ micelles, its incorporation in the H_1 liquid crystal phase allows us to think about a mesopore size expansion through a swelling of the hybrid

mesophase as observed for materials prepared from the $R^F_8(EO)_9$/ PFD/ water system. But in this last case, there is a variation of the pore size, which does not exist in the materials prepared with octane. Thus, such a mechanism does not occur. However, octane does not affect the self assembly mechanism, furthermore, it does not change the materials characteristics either.

4. Solubilization of fluorinated octanol in the $R^F_8(EO)_9$-water system

The fluorinated alcohol $C_6F_{13}C_2H_4OH$ is not soluble in water. It has a similar molecular structure with the surfactant $R^F_8(EO)_9$, but its polar head is limited to a hydroxyl functional group and it can be noted as $R^F_6(EO)_0$.

4.1 Ternary diagram

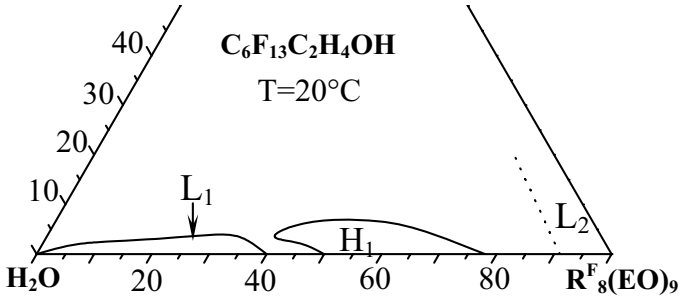


Figure V-28. *Phase diagram (wt %) of $R^F_8(EO)_9$/**$C_6F_{13}C_2H_4OH$**/water system at 20 °C.*

The ternary diagram of the $R^F_8(EO)_9$/ $R^F_6(EO)_0$/ water (**Figure V-28**) system at 20 °C is similar to the $R^F_8(EO)_9$/ octanol/ water one (**Figure V-21**). Depending on the water/surfactant ratios, micelles can incorporate between 1 and 4 wt.% of fluorinated octanol. The further addition of fluorinated octanol does not lead to a Winsor I system. In fact the biphasic domain consists in water and an anisotropic phase which is probably the hexagonal phase. Upon the addition of $R^F_6(EO)_0$ the limit of hexagonal of the liquid crystal phase is shifted toward the water-rich part of the diagram. At the most, 7 wt.% of fluorinated octanol can be incorporated into H_1.

4.2 Structural parameters of hexagonal crystal liquid phase

The determination of Bragg distance has been done with the samples prepared from different ratios R to cover the over all liquid crystal domain. By this way, we have considered only the **oil model**, i.e. the $R^F_6(EO)_0$ molecules are solubilized in the hydrophobic core of the cylinders. As the fluorinated octanol is completely insoluble in water, the co-solvent model has not been taken into account.

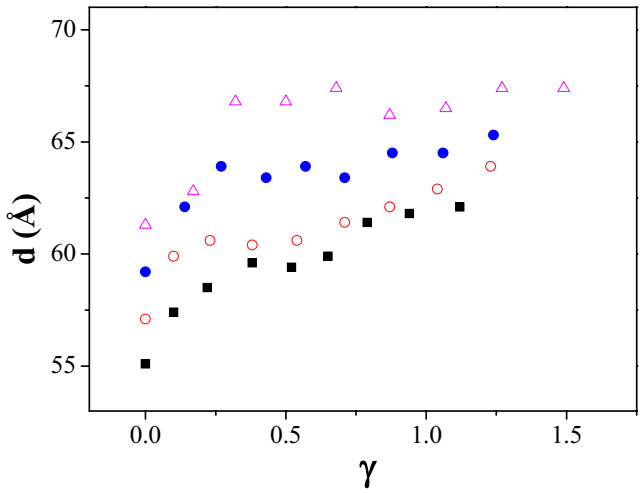


Figure V-29. *Evolution of the d-spacing (d) as a function of γ in H_1 for ■ : R =0.43; ○: R = 0.54; ● : R = 0.67; Δ: R = 0.82*

Results show that the Bragg distance increases with the addition of $R^F_6(EO)_0$ (**Figure V-29**). Nevertheless, whatever the value of R, a change of the slope is noted when 1.5 wt.% of fluorinated octanol are incorporated in the system. This corresponds to a value of γ (molecule number of $R^F_6(EO)_0$ per surfactant) equal to 0.3.

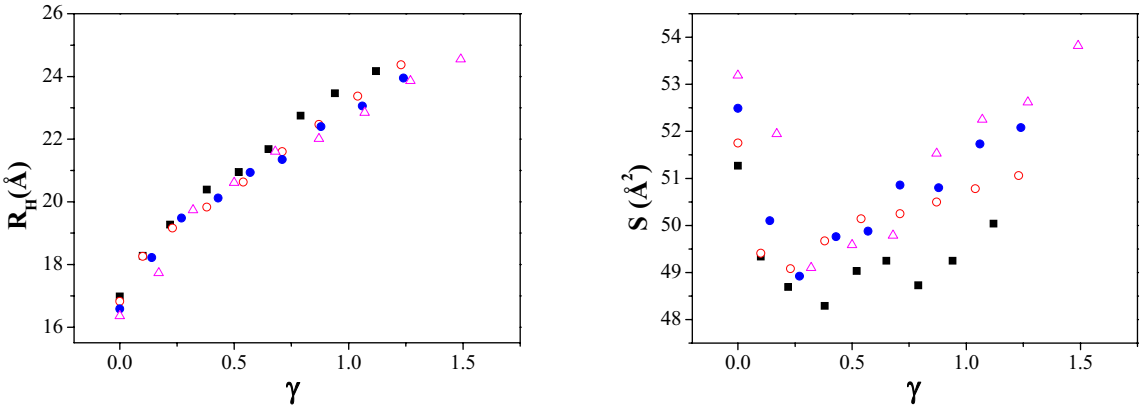


Figure V-30. *Evolution of the hydrophobic radius (R_H) and cross sectional area (S) as a function of γ in H_1 for ■ : R =0.43; ○: R = 0.54; ● : R = 0.67; Δ: R = 0.82.*

Assuming that the hydrophobic volume fraction corresponds to $V_B + \gamma V_{FO}$, where V_{FO} is the molar volume of the fluorinated octanol, the hydrophobic radius (R_H) and the cross sectional area (S) have been calculated following the relations given by page 126. Results depicted in **Figure V-30** show that R_H increases from 17 to 24 Å as a function of γ, meanwhile, S drops from 53 to 48 $Å^2$ when γ is changed from 0 to 0.3, then its value raises again. This change of behavior could be explain by considering that at first the alcohol molecules penetrate between the hydrophobic chains of the surfactant and then they form a core in the center of the cylinders. But this scenario does not completely satisfy the given system.

Since the molecular structure of the fluorinated octanol is very similar to the one of the surfactant, we have considered the formation of a mixed palisade layer which corresponds to the **co-surfactant model**. In this case, the evolution of the Bragg distance as a function of the water content for various $R^F_8(EO)_9$/ $R^F_6(EO)_0$ ratios (R_S) have been deduced from the experimental values obtained from the samples prepared with different water/ surfactant ratio (R). Once again, the mixtures of surfactant/fluorinated octanol are considered as a mixed entity. The molecular weight (M^m) and the molar volume V^m of the mixed surfactant are calculated for each mixture corresponding to different ratios R_S. The evolution of the Bragg distance as a function of water incorporation is given in **Figure V-31**.

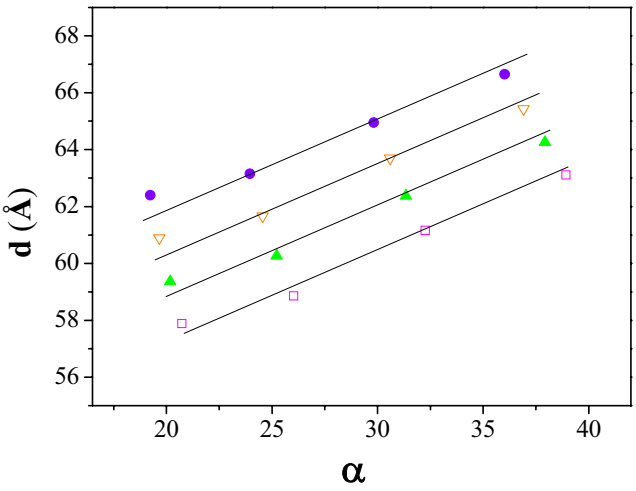


Figure V-31. *Evolution of the d-spacing (d) as a function of α (molar number of water per surfactant) in H_1 for □ : R_S = 0.02; ▲ : R_S = 0.04; ▽ : R_S =0.06; ● : R_S =0.09.*

The Bragg distances are increasing monotonically upon the addition of water for different R_S (**Figure V-31**). Besides, we observe on **Figure V-32** that the hydrophobic radii trend to diminish whereas the cross-sectional area rises with the incorporation of water for the different mixed entities. The point to emphasize here is that for different ratios R_S, the whole parameters vary monotonically. The incorporation of water in each mixed entity leads the

hydrophobic chains to be folded. In the meantime, these folded hydrophobic chains result in the enlargement of the cross-sectional area. Moreover, the increase of the Bragg distance can be attributed to the incorporation of water between the cylinders of the hexagonal phase. To sum up, this **co-surfactant model** considering that the fluorinated octanol molecules associate with the surfactants to form a palisade layer seems to be reasonable to fit the given system.

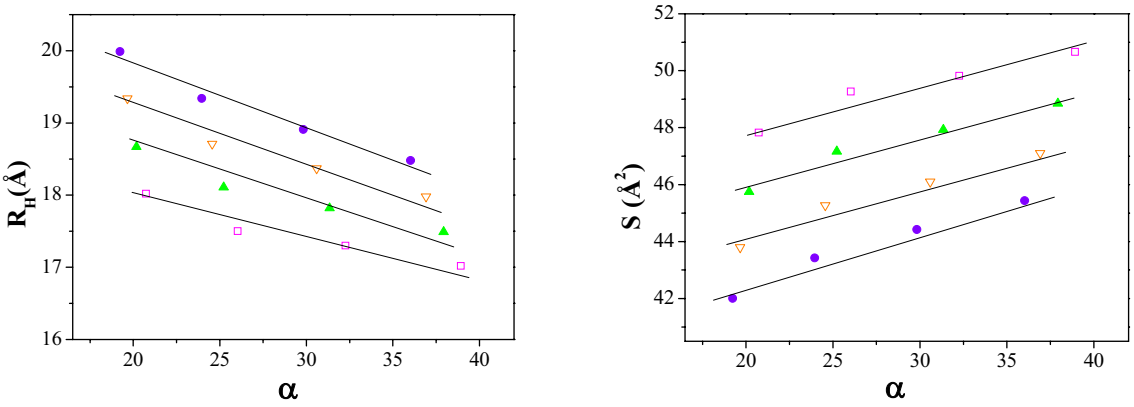


Figure V-32. *Evolution of the hydrophobic radius (R_H) and cross sectional area (S) as a function of α in H_1 for □: R_S =0.02; ▲ : R_S =0.04; ▽: R_S =0.06; ● : R_S =0.09.*

4.3 Mesoporous materials prepared from the system $R^F_8(EO)_9$-water in the presence of fluorinated octanol

According to the phase diagram, mesoporous silica materials have been synthesized from the CTM mechanism. Micellar solutions are prepared for the water/$R^F_8(EO)_9$ mass ratio R=9 and 4. The concentration of fluorinated octanol is fixed to 1, 2, 5, 10 and 20 wt.%. The TMOS has been added to the surfactant solution at 20 °C or 40 °C at pH 2 with the surfactant/TMOS molar ratio equal to 0.5 and the solutions were kept stirring for 1 hour. The obtained mixtures were sealed in Teflon autoclaves and allowed to undergo hydrothermal treatment at 80 °C for 24 hours. Ethanol extraction was carried out with a Soxhlet apparatus for 48 hours.

4.3.1 The structural properties

Whatever the synthesis conditions, the mesopore ordering is kept only until the addition of 1 wt.% of $R^F_6(EO)_0$. Except there is a wormlike structure observed for R=4 at 40 °C, no reflection is detected anymore when the alcohol amount reaches 2 wt.%. Thus, the regular channel array is completely lost in this case. In addition, as we can see on the SAXS patterns the first reflections are not shifted by the addition of fluorinated octanol.

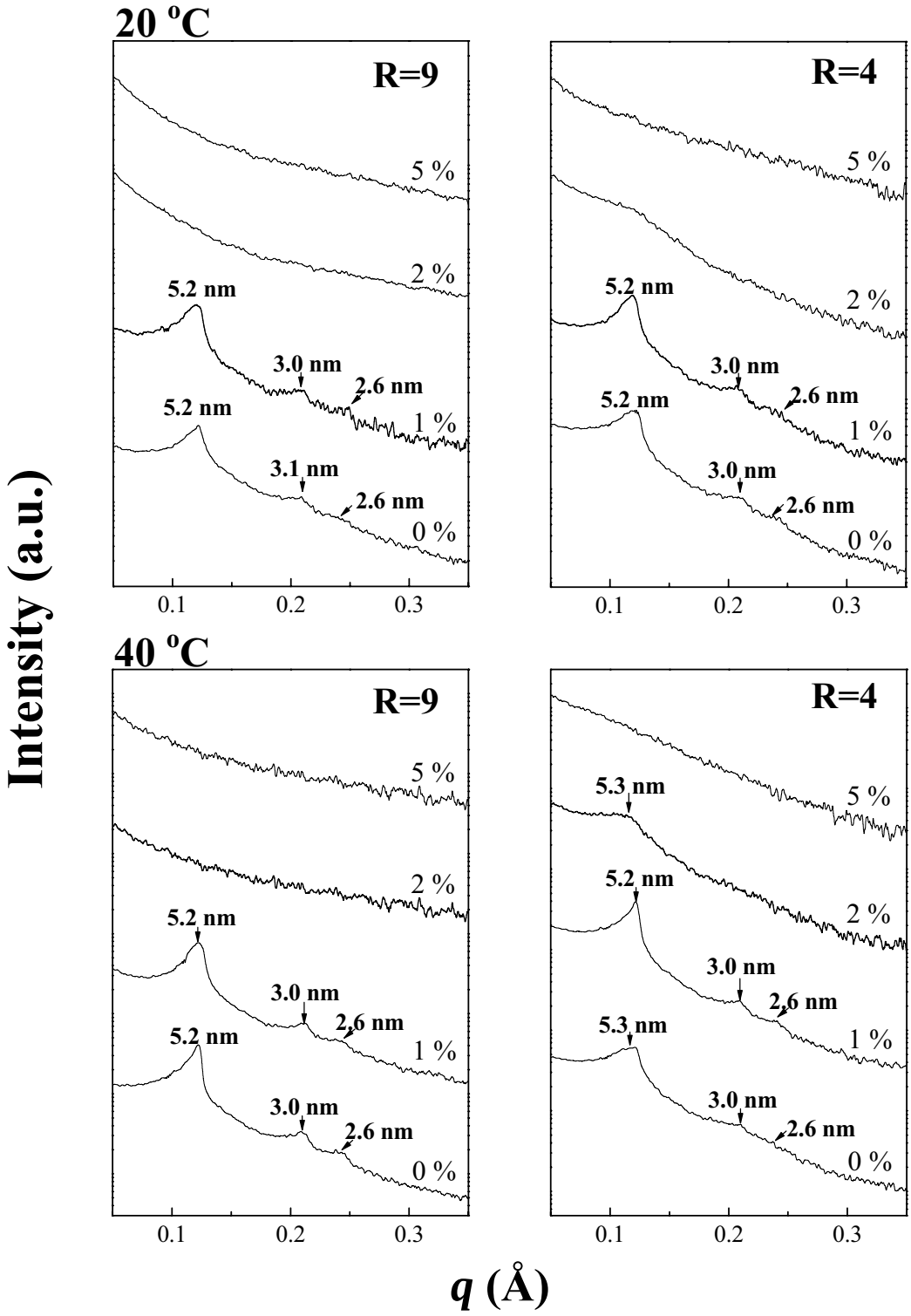


Figure V-33. *SAXS patterns of the materials prepared from the $R^{F}_{8}(EO)_{9}$-based system with different concentrations of fluorinated octanol for R=9 and R=4; TMOS is added at 20 °C or 40 °C at pH= 2*

4.3.2 The textural characteristics

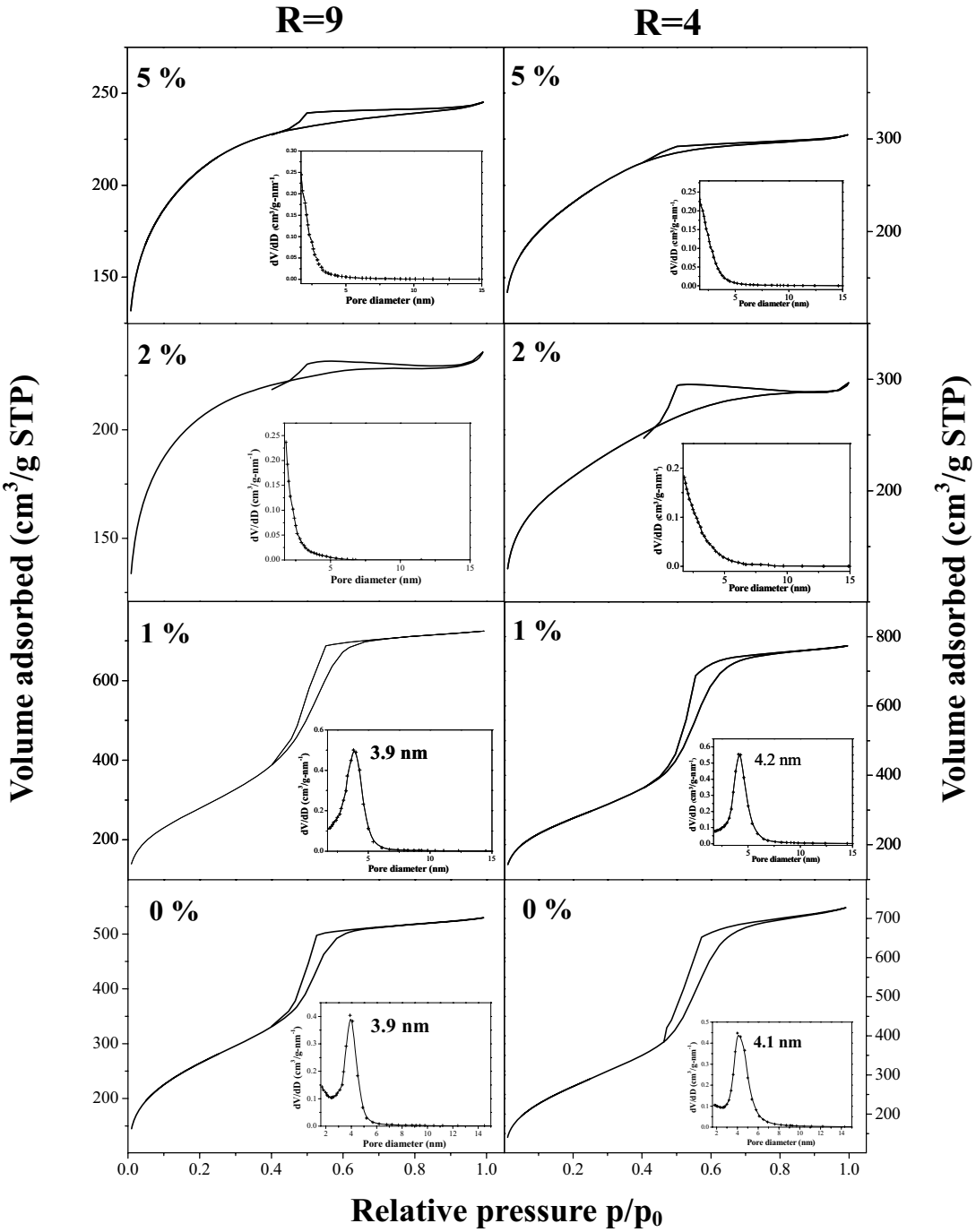


Figure V-34. *Evolution of nitrogen adsorption-desorption isotherm and the corresponding BJH pore size distribution curve (insert) with different concentrations of fluorinated octanol for R=9 and R=4; TMOS is added at 20 °C and pH= 2*

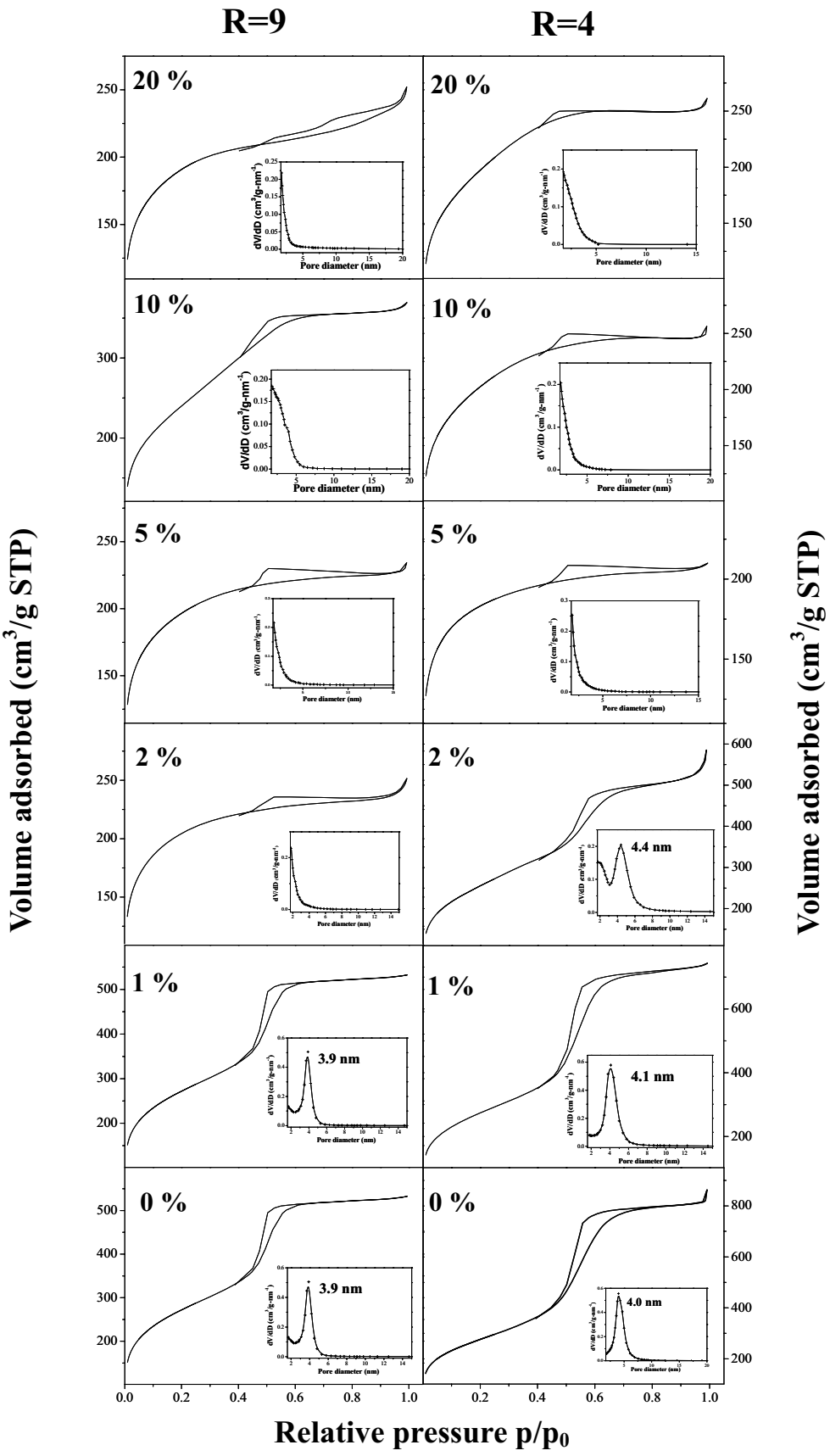


Figure V-35. *Evolution of nitrogen adsorption-desorption isotherm and the corresponding BJH pore size distribution curve (insert) with different concentrations of fluorinated octanol for R=9 and R=4; TMOS is added at 40 °C and pH= 2*

Nitrogen adsorption-desorption isotherms and the corresponding BJH pore size distributions are displayed in **Figure V-34** for the materials prepared at 20 °C. A type IV isotherm is obtained when the concentration of $R^F_6(EO)_0$ is lower than 2 wt.%. Moreover, the maximum of the pore size distribution does not vary (**Figure V-34 insert**). Whatever the value of R, upon the further addition of fluorinated alcohol, the isotherms are intermediates between type I and IV at 2 and 5 wt.% of fluorinated octanol. The same tendency is noted when the TMOS is added at 40 °C (**Figure V-35**).

4.4 Discussion

The incorporation of the fluorinated octanol in the micelles is limited to 4 wt.% whereas in the hexagonal liquid crystal phase up to 7 wt.% of $R^F_6(EO)_0$ can solubilize into the system. The investigation of the structure parameters shows that the fluorinated octanol rather behaves as a co-surfactant. It is located in the palisade layer and the hydrophobic radius of the cylinders decreases with the addition of $R^F_6(EO)_0$.

Concerning the materials prepared from this system, whatever the values of R and the synthesis conditions, the materials adopt a disordered structure as soon as the $R^F_6(EO)_0$ concentration reaches 2 wt.%. No mesopore enlargement is noted upon the addition of the fluorinated octanol. This result fits well with the structure data of the hexagonal liquid crystal phase. Indeed, the results evidence that $R^F_6(EO)_0$ rather acts as a co-surfactant instead of an oil. The complete lost of the mesopore ordering can be related to the absence of micelles beyond the phase limit (cf. diagram represented in **Figure V-28**). Indeed, it should be reminded that when the concentration of fluorinated octanol is higher than 2 and 3 wt.% respectively for R=9 and R=4 at 20 °C, no micellar phase is observed anymore.

5. Conclusion

In this study, we have used hydrogenated alcohols (**Table V-3**) with different chain lengths and one fluorinated alcohol (**Table V-3**) as additives to determine their effect on the characteristics of mesoporous materials. For this, we have first examined the effect of the solubilization of each alcohol on the $R^F_8(EO)_9$ phase behavior in water and we have investigated the corresponding hexagonal liquid crystal phase by the determination of the structural parameters. By this way, we have demonstrated that short chain alcohols (methanol

and iso-propanol) and the medium chain alcohol (n-butanol) in the considered range of concentrations behave like a co-solvent. By contrast, the long chain alcohol (octanol) and the fluorinated octanol act as a co-surfactant.

Table V-3. *Behavior of the alcohols in the $R^F_8(EO)_9$ based-system [233]*

Alcohol	Methanol CH_3OH	Iso-propanol $(CH_3)_2CHOH$	1-butanol C_4H_9OH	1-octanol $C_8H_{17}OH$	Fluorinated octanol $C_6F_{13}C_2H_4OH$
Solubility in 100g water /g	∞	∞	7.9	~0	~0
Effect	co-solvent	co-solvent	co-solvent	co-surfactant	co-surfactant

Looking at the silica materials prepared in the presence of these alcohols, whatever the alcohol, no real pore size expansion is noted. This means that these alcohols are not swelling agents for the given system. The short chain alcohols are solubilized in water and they interact with the surfactant headgroup involving their dehydration. The addition of fluorinated or hydrogenated octanol does not provoke a change in the curvature of the palisade layer. This change could have involved the formation of crystal phase with different structure and the preparation of mesoporous materials, for example, with a cubic pore arrangement. In our study, these alcohols rather act as a co-surfactant and they induce a loss of the pore ordering. As a matter of fact, even at low concentration, the incorporation of the fluorinated or hydrogenated octanol gives rise to wormhole like structure or to a randomly pore arrangement.

Conclusion

Le principal objectif de cette étude était d'établir les relations entre les propriétés des tensioactifs hydrogénés et fluorés non ioniques et leur capacité à être utilisés comme empreinte pour la synthèse de matériaux mésoporeux, macroporeux ou à porosité hiérarchisée. Par conséquent, différents systèmes, binaires, ternaires ou mixtes en présence d'additifs ont été examinés. L'effet de la solubilisation d'hexadecane, de décane et de cyclohexane dans le système $R^{H}_{12}A(EO)_9$-eau a été étudiée. Les micelles de $R^{H}_{12}A(EO)_9$ peuvent incorporer $C_{16}H_{34}$, $C_{10}H_{22}$ et C_6H_{12}. L'évolution des paramètres structuraux des cristaux liquides a mis en évidence que le décane à la fois pénètre dans les chaînes hydrophobes du tensioactif et forme un coeur d'huile ; tandis que l'addition d'hexadécane n'interagit pas avec les chaînes hydrophobes et forme seulement un cœur huileux. Concernant les synthèses des matériaux poreux, l'incorporation de faibles fractions d'hexadecane ou de décane conduit à la formation de silices mésoporeuses aux larges pores ; tandis qu'aucune augmentation de la taille des pores n'est observée avec le cyclohexane. Ainsi ; l'hexadecane et le décane forment un coeur d'huile dans le centre des micelles alors que le cyclohexane est pénètre plutôt entre les chaînes hydrophobe du tensioactif. Les résultats mettent également en évidence que l'utilisation d'hexadecane et de décane comme hydrocarbure conduit à la formation de macropores, pour des concentrations supérieures à 40 % pour lesquelles des émulsions concentrées huile / eau sont formées. Les macropores correspondant à l'empreinte des gouttes d'huile. Au contraire, à cause de sa faible TIP, aucun matériau macroporeux ne peut être préparé à partir du système $R^{H}_{12}A(EO)_9/C_6H_{12}$/eau. Des matériaux poreux silicatés ont aussi été préparés à partir de deux tensioactifs fluorés $R^{F}_{8}(EO)_9$ et $R^{F}_{7}(EO)_8$ afin de les comparer aux systèmes à base de tensioactif hydrogéné. Les effets de solubilisation de différents fluorocarbures sur les propriétés des matériaux ont été examinés. Pour le système à base de $R^{F}_{8}(EO)_9$, des diamètres de pores plus larges sont obtenus lorsque l'on utilise PFOBr au lieu de PFD. La détermination du diagramme de phase a révélé que seule une faible fraction de fluorocarbure peut être incorporée dans les micelles. Par conséquent, l'expansion des mésopores se produit dans la mésophase hybride. Pour des concentrations en huile supérieures à 50% les ajouts de PFOBr ou de PFD donnent lieu à la formation de silice macroporeuse. Pour le système à base de $R^{F}_{7}(EO)_8$, les résultats obtenus par SAXS, adsorption-désorption d'azote ont démontré que l'addition de F44E conduit à la formation de mésopores plus larges et que le gonflement a lieu à partite des micelles. De plus, le système

$R^F_7(EO)_8$/F44E/eau a été très favorable vis-à-vis de la formation de macropores. En effet, des macropores ont été obtenus aussitôt que la concentration en F44E est supérieure à 10%. Au contraire, lorsque PFOBr est incorporé à la place de F44E, la situation est différente. L'organisation des mésopores est seulement obtenue si la synthèse est réalisée à pH 0.025 et si le précurseur silicaté est ajouté à 20°C. De plus, à cause de la faible valeur de TIP, le système $R^F_7(EO)_8$/PFOBr/eau ne conduit pas à la formation de macropores. En comparant ce comportement à celui observé pour les tensioactifs hydrogénés, nous pouvons conclure que les systèmes à base de tensioactif hydrogéné et fluoré obéissent aux mêmes règles ; i.e. la formation de macropores à l'aide d'émulsions est favorisée avec des systèmes qui présentent une TIP élevée.

Enfin, la dernière partie de ce travail a été consacrée à l'utilisation d'alcools hydrogénés et fluorés avec différentes longueurs de chaînes comme additif pour évaluer leur impact sur les caractéristiques des matériaux. Afin de mieux comprendre leur influence sur les propriétés des matériaux mésoporeux, nous avons tout d'abord examiné l'effet de la solubilisation de chaque alcool sur le comportement de phase du tensioactif dans l'eau et les paramètres structuraux de la phase hexagonale ont été examinés eu détail. Nous avons démontré que les alcools à courtes chaînes (méthanol et isopropanol) et à chaînes intermédiaires (n-butanol) jouent le rôle de co-solvant dans le domaine de concentration considéré. Au contraire, les alcools à longues chaînes (octanol et fluoro-octanol) jouent le rôle de co-tensioactif. Nous avons montré que, quel que soit l'alcool utilisé, les matériaux préparés ne présentent pas d'augmentation significative de la taille des pores. Cela signifie que ces alcools ne jouent pas le rôle d'agent gonflant pour les systèmes étudiés. D'un coté, les alcools à courtes chaînes sont solubilisés dans l'eau et interagissent avec les têtes polaires des tensioactifs conduisant à leur déshydratation. De l'autre, l'addition d'octanol fluoré ou hydrogéné ; qui agit plutôt en tant que co-tensioactif ; engendre une perte d'organisation des pores. Par conséquent, même à faible concentration, l'incorporation d'octanol fluoré ou hydrogéné conduit à la formation de structure vermiforme ou même à la perte complète de l'homogénéité de la taille des pores.

Conclusion

The main objective of this study was to establish relationships between the properties of fluorinated and hydrogenated nonionic surfactants and their abilities to be used as template for the preparation of mesoporous, macroporous and even hierarchical materials. Thus, various systems, such as binary, ternary and mixed ones in presence of additives, were taken into account. The effect of the solubilization of hexadecane, decane and cyclohexane into the $R^{H}_{12}A(EO)_9$-water system have been studied. Micelles of $R^{H}_{12}A(EO)_9$ can incorporate $C_{16}H_{34}$, $C_{10}H_{22}$ and C_6H_{12}. The evolution of the structural parameters of the liquid crystal phases with the increase of the alkane concentration showed that whatever the liquid crystal phase both the swelling and the penetration effects took place upon addition of decane, while only the swelling effect occurred with hexadecane. As regards the porous material syntheses, the incorporation of low fraction of hexadecane or of decane leads to the formation of large mesoporous silica, whereas no swelling effect was noted with cyclohexane. This indicates that hexadecane and decane formed a core of oil in the center of the micelles while cyclohexane was incorporated between the hydrophobic chains of the surfactant. Results also evidenced that when hexadecane and decane were used as hydrocarbon, macropores templated by the oil droplets appeared if the amount of oil concentration was higher than 40 wt.% because of the formation of concentrated emulsions. By contrast, due to its low PIT, no macroporous material could be prepared from the $R^{H}_{12}A(EO)_9/C_6H_{12}$/water system.

To compare to the hydrogenated surfactant-based system, we also considered two fluorinated surfactants $R^{F}_{8}(EO)_9$ and $R^{F}_{7}(EO)_8$ which were used for the preparation of porous silica. We had studied the effect of the solubilization of various fluorocarbons on the properties of the recovered materials. Looking at the $R^{F}_{8}(EO)_9$-based system, higher pore diameters are obtained when perfluorooctyl bromide (PFOBr) is used as oil instead of perfuorodecalin (PFD). The determination of the phase diagram revealed that only a small fraction of the fluorocarbon could be incorporated into the micelles, so, the mesopore size expansion occurred through a swelling of the hybrid mesophase. At oil concentrations higher than 50 wt.% both PFOBr and PFD gave rise to macroporous silica. Concerning the $R^{F}_{7}(EO)_8$ surfactant, the results obtained by SAXS, nitrogen adsorption-desorption analyses evidence that $C_4F_9CH{=}CHC_4F_9$ (F44E) was an effective expander to enlarge the pore size of mesoporous materials through a swelling of the micelles. In addition, this

$R^F_7(EO)_8$/F44E/water system was very favorable for the design of a macropore network. Indeed, macroporous materials were recovered as soon as the F44E concentration was higher than 10 wt.%. On the contrary, when PFOBr was incorporated instead of F44E, the situation was quite different, neither mesopore nor macropore is obtained. The only way to prepare organized materials from PFOBr system is to perform the syntheses at pH 0.025 and at 20°C. Moreover, due to the low PIT value, whatever the synthesis condition the $R^F_7(EO)_8$/PFOBr/water system did not lead to the formation of macropores. Comparing this behavior and the one reported for hydrogenated emulsions, we could conclude that both hydrogenated and fluorinated systems obey to the same rule i.e. the formation of macroporous materials template by emulsions is favored with systems which exhibit a high value of the PIT.

Finally, the last part of this work had been devoted to use hydrogenated alcohols with different chain length and a fluorinated alcohol as additives to tune the characteristics of the recovered materials. To better understand their influence on the properties of mesoporous materials, at first, we have examined the effect of the solubilization of each alcohol on the surfactant phase behavior and the corresponding hexagonal liquid crystal phase by the determination of the structural parameters. We have demonstrated that short chain alcohols (methanol and iso-propanol) and the medium chain alcohol (n-butanol) in the considered range of concentrations behave like a co-solvent. On the contrary, the long chain alcohol (octanol) and fluorinated octanol act as a co-surfactant. Afterward, we found that no matter the silica materials prepared in the presence of which kind of alcohol, there is no significant pore size expansion. It means that these alcohols are not swelling agents for the studied system. On one hand, the short chain alcohols are solubilized in water and they interact with the surfactant headgroup involving their dehydration. On the other hand, the addition of fluorinated or hydrogenated octanol rather acts as a co-surfactant and they induce a loss of the pore ordering. As a matter of fact, even at low concentration, the incorporation of the fluorinated or hydrogenated octanol gives rise to wormhole like structure or to a randomly pore arrangement.

Outlooks

Surfactant based systems can be used for design of porous materials. In this work, we have seen that mesoporous and macroporous materials can be respectively synthesized from micelles and emulsions. Another template that can be employed for the preparation of this kind of compound deals with nano-emulsions.

Nano-emulsions [235-239] are emulsions consisting of small quite monodisperse droplets, typically in the 20-200 nm size range, who are often referred to in the literature also as miniemulsions, ultrafine emulsions, submicron emulsions and so on. The major publications and applications of nano-emulsions are concerned with those of the O/W type. Although they could have similar size like microemulsion droplets and appear transparent or translucent, they are in fact distinctly quite different from true microemulsions. Nano-emulsions are thermodynamically unstable and their formation generally requires energy input. The properties of nano-emulsions depend not only on thermodynamic conditions (i.e., composition, temperature and pressure) but also on the preparation method and crucially, on the order of component addition [240].

After all, the kinetic stability of nano-emulsions and their transparent or translucent appearance due to the presence of nanometer-sized droplets, makes these systems of interest for fundamental studies and practical applications, such as agrochemical applications [241], food technology [242], pharmaceutical [243] and cosmetic [244] fields. Recently, more and more publications on nano-emulsion applications deal with the preparation of polymeric nanpoparticals using a monomer as the disperse phase (also called miniemulsion polymerization method) [245, 246].

To obtain nanodroplet emulsions, significant amounts of mechanical energy are needed, making high-energy preparation methods be unfavorable for industrial applications [247]. Therefore, the preparation of nano-emulsions with reproducible properties and small droplet sizes using low-energy methods has been a field of growing interest [243, 248, 249]. Thereinto, C. Solans research group has published lots of work in this domain [243, 246, 248, 250-261].

Low-energy methods make use of accessible phase transitions occurring during the emulsification process as a result of changes in surfactant film spontaneous curvature. On these conditions, studies on phase behavior for optimization of nano-emulsion properties are

important. The aim is to obtain nano-emulsions of small droplet size and low polydispersity.

The need of bicontinuous or lamellar liquid crystal phases during emulsification is described in detail in a few publications [253, 262, 263]. Besides this, some works have proved that the formation of nano-emulsions is obtained by the phase inversion temperature method (**PIT**) [251, 255, 260, 264], phase inversion composition method (**PIC**) [254, 258], or self-emulsifying method [241, 264-267]. To make use of these approaches, it is necessary to study the relationship between the phase behavior of the initial system and the resulting nanoemulsions. For example, with the **PIT** method, emulsions are obtained with a system containing nonionic surfactant by increasing or lowering the temperature quickly to pass through the **PIT**. In particular, if the initial system is located in a bicontinuous microemulsion region (D phase) or a two phase (W + D) system, from the **PIT**, nanoemulsions can be readily generated (**Figure O-1** [251]**)**. On the contrary, for the phase inversion composition method (**PIC**), the continuous phase is added to the dispersed phase at constant temperature until phase inversion occurs and the intended emulsion type is formed. For self-emulsifying method, the type of initial emulsion is that of the desired emulsion. So the dispersed phase is simply added to the continuous phase under intensive agitation. In some literature [264], however, self-emulsification is also attributed to a simultaneous mixing of all the emulsion components in the mixing chamber.

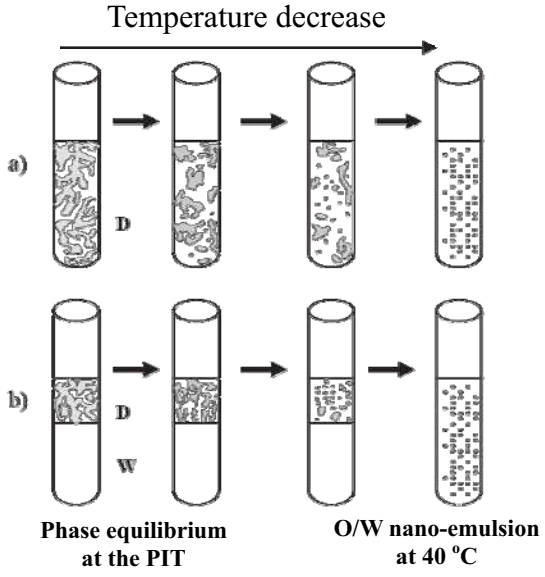


Figure O-1. *Schematic representation of a possible mechanism for O/W nano-emulsion formation by the PIT method. The curvature of the surfactant interfacial film is changed by cooling, and the D bicontinuous phase is disrupted, forming nanodroplets. a) An oil-swollen D microemulsion phase is the initial equilibrium phase; b) two phases, W+D, are the initial equilibrium, and the water excess is not participating in the nanodroplet formation but as a dilution medium. [250]*

However, no direct evidence has yet been put forward to clarify these issues. Further efforts are required in order to fully understand the mechanism of nanoemulsion formation and therefore, optimize nanoemulsification processes.

Therefore, taking advantage of the monodispersity of nano-emulsion, we are interested in introducing **nano-emulsion** as the template for preparing porous materials. Concerning the formation of nano-emulsion, we have used a low-energy method proposed by C. Solans' research group, which are facile put in practice. From the work developed by Forgiarini, A. et al [250]. We investigated the system based on commercial surfactant remcopal supplied by CECA. The formula of this surfactant consists of a hydrogenated carbon chain with 12 carbons and the average number of oxyethylene is 4. It is noted as $R^{H}_{12}(EO)_4$. We have examined the co-solubilization of water and decane with this surfactant.

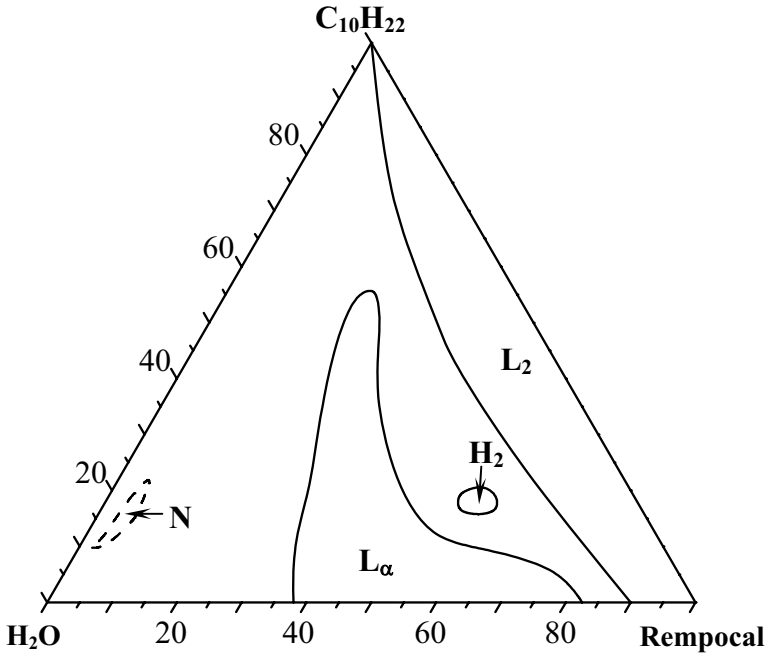


Figure O-2. *Phase diagram (wt.%) of $R^{H}_{12}(EO)_4$ /decane/water system at 25°C . N= domain of nano-emulsion; L_α=lamellar phase; H_1=hexagonal phase; H_2=reverse hexagonal phase; L_2=reverse micelle*

The ternary diagram is shown in **Figure O-2.** In addition to the liquid crystal phases (lamellar and reverse hexagonal), only reverse micellar phase is obtained. For 5 wt. % concentration of surfactant, we prepared nano-emulsions which are bluish and containing between 10 wt.% and 20 wt.% of water. The result of dynamic light scattering (**DLS**) measurements also confirms the existence of the nano-emulsions (**Figure O-3**). The samples are diluted with water which filtered with filter membrane (0.4 μm) before the measurement. These samples are stable during the measurements, but an increase of the particle size is observed upon the time. The hydrodynamic diameter distributions exhibit two peaks at 40 and 220nm, respectively. The first tiny one can be due to the micelles which are presented in the

aqueous media; the second sharp one results from the formation of the nano-emulsions.

After investigating the phase diagram of the ternary $R^H_{12}(EO)_4$ /decane/ water system, which gives rise to nano-emulsions, we have performed some preliminary experiments to synthesize porous materials. We have prepared nano-emulsions containing 80 wt.% of water with a $R^H_{12}(EO)_4$/ decane ratio equals to 0.25. The TMOS has been added to the mixture at 25 ^oC at pH= 2. The surfactant/TMOS molar ratio is fixed to 0.5. The obtained mixtures were sealed in Teflon autoclaves and allowed to undergo hydrothermal treatment at 80 ^oC for 48 hours. Ethanol extraction was carried out with a Soxhlet apparatus for 48 hours.

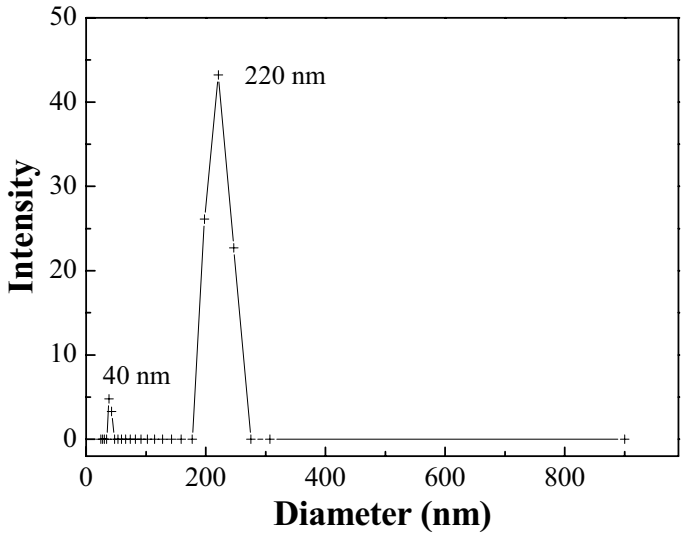


Figure O-3. *Hydrodynamic diameter (D) distributions obtained after the dilution of the sample containing 80 wt.% of water with a $R^H_{12}(EO)_4$/ decane ratio equals to 0.25 at pH 2 and 25 ^oC.*

Unfortunately, we do not succeed in obtaining mesoporous materials. As a matter of fact, no value is noted in the mesopore range on the pore size distribution represented in **Figure O-4**. In addition, no pore ordering is detected on the SAXS pattern (***Figure O-4*** A).

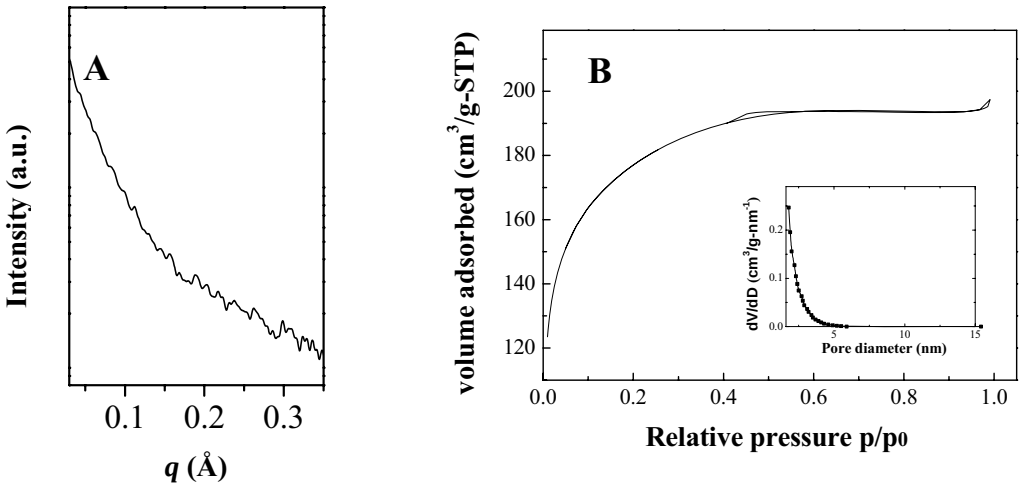


Figure O-4. *(A) SAXS pattern and (B) evolution of nitrogen adsorption-desorption isotherm and the corresponding BJH pore size distribution curve (insert) of the materials prepared from the $R^{H}_{12}(EO)_4$/ decane/ water system at pH 2 and 25 °C*

Concerning the morphology of the materials, several representatives scanning electron micrographs (SEM) are shown in **Figure O-5**. We can see that, macropores whose diameters are in the range of few microns are formed from the given system. Thus we can assume that the addition of TMOS has destroyed the nano-emulsions and give rise to an emulsion. The observed macropores correspond to a fingerprint of the droplets of the emulsions.

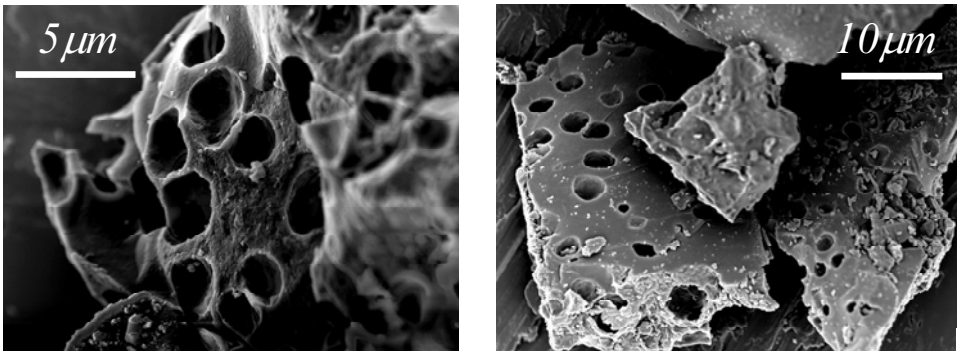
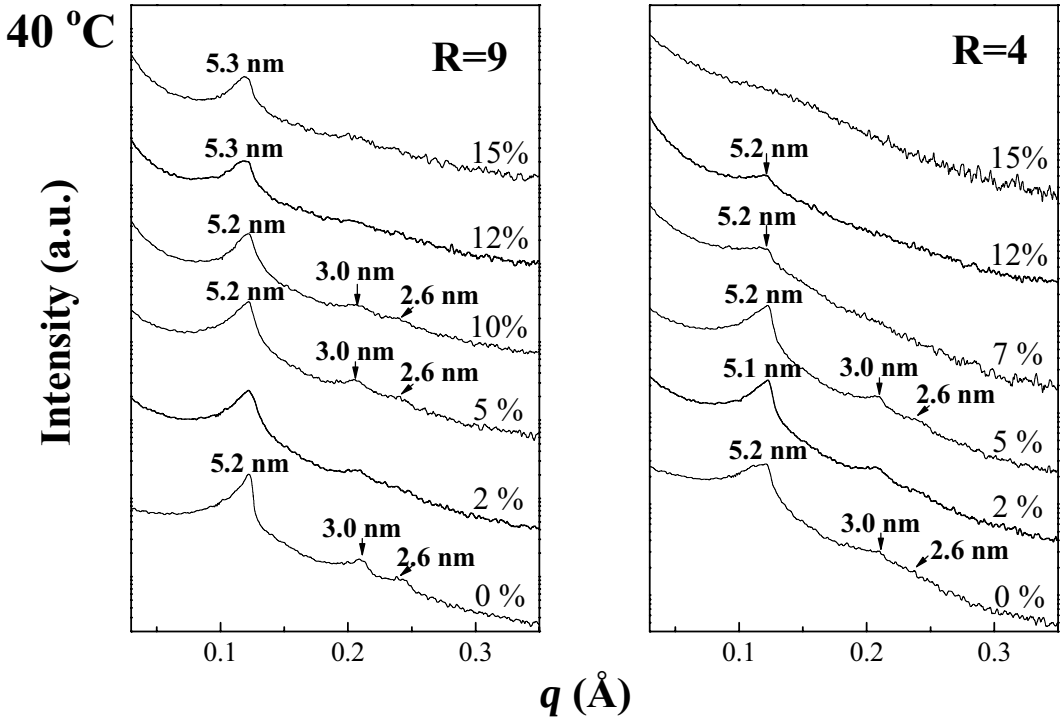


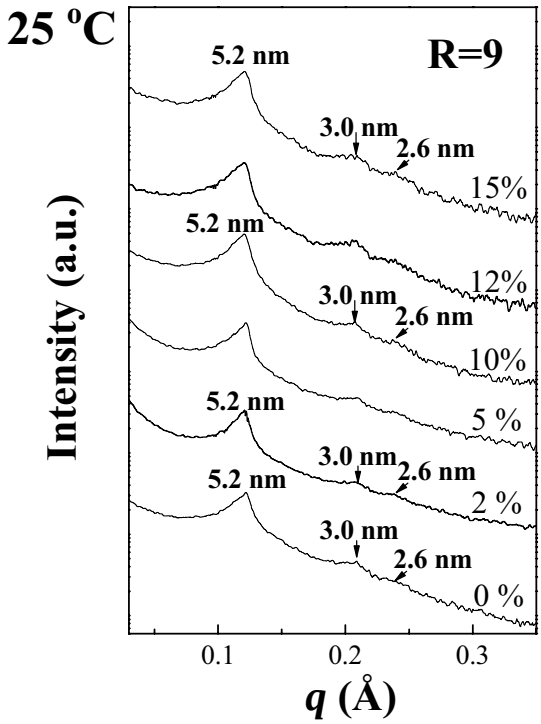
Figure O-5. *SEM micrograph of materials prepared from the $R^{H}_{12}(EO)_4$/ decane/ water system at pH 2 and 25 °C*

Complementary studies are required in order to optimize the synthesis procedure to design porous materials by using nano-emulsions as template.

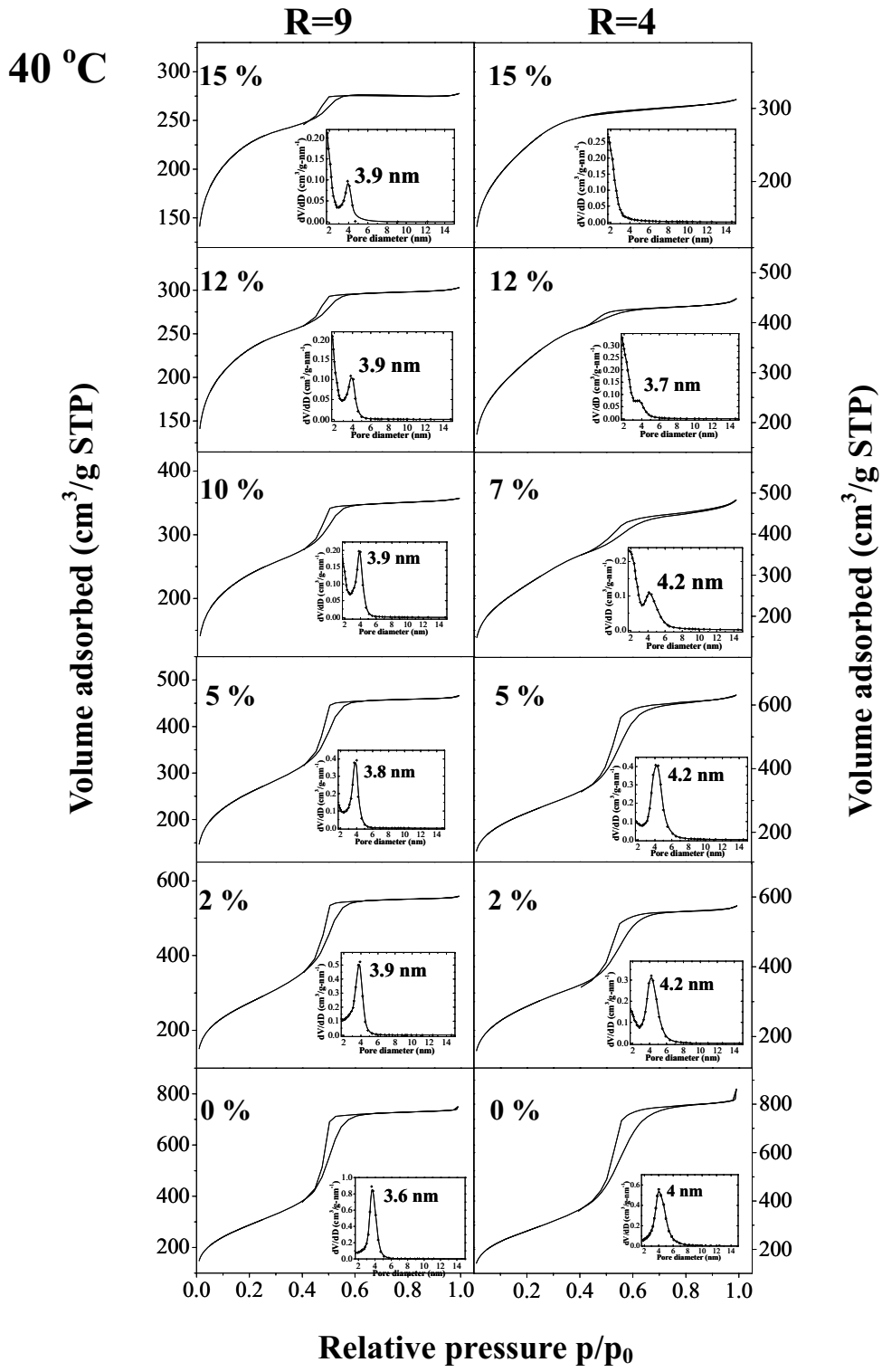
Appendix

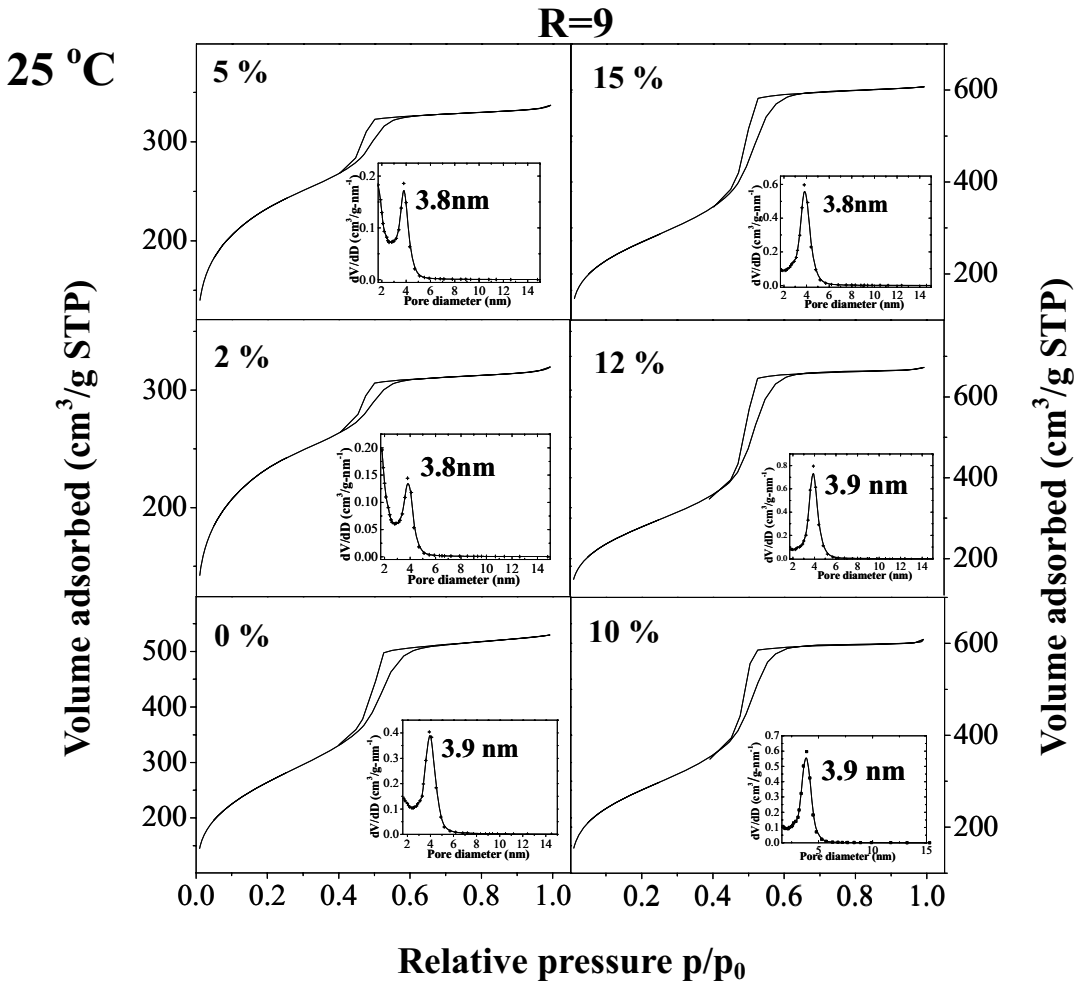
Appendix 1 : *SAXS pattern of the materials prepared from the $R^F_8(EO)_9$/ octane/ water system at pH 2*





Appendix 2 : *Evolution of nitrogen adsorption-desorption isotherm and the corresponding BJH pore size distribution curve (insert) of the materials prepared from the $R^F{}_8(EO)_9$/ octane/ water system at pH 2*




R=9
25 °C
5 %
15 %
2 %
12 %
0 %
10 %
3.8nm
3.8nm
3.8nm
3.9 nm
3.9 nm
3.9 nm
Pore diameter (nm)
dV/dD (cm³/g-nm⁻¹)
Volume adsorbed (cm³/g STP)
Volume adsorbed (cm³/g STP)
Relative pressure p/p0

References

[1] Rosen, M. J., *Surfactants and Interfacial Phenomena, 3rd Edition.* John Wiley & Sons Chichester, UK, 2004; p 464.

[2] Fairhurst, C. E.; Fuller, S.; Gray, J.; Holmes, M. C.; Tiddy, G. J. T., in: *Handbook of Liquid Crystals*, Demus, D., (Ed.) Wiley-VCH Verlag GmbH Weinheim, Germany, 1998; Vol. 3, p 341-392.

[3] Laughlin, R. G., *The Aqueous Phase Behavior of Surfactants*. Academic, London, UK London, UK, 1996; p 558.

[4] Boden, N.; Corne, S. A.; Holmes, M. C.; Jackson, P. H.; Parker, D.; Jolley, K. W., *Dep. Phys. Chem.* **1986,** *47*, 2135-2144.

[5] Safinya, C. R.; Roux, D.; Smith, G. S.; Sinha, S. K.; Dimon, P.; Clark, N. A.; Bellocq, A. M., *Physical Review Letters* **1986,** *57*, 2718.

[6] Charvolin, J.; Sadoc, J. F., *Journal de Physique (Paris)* **1987,** *48*, 1559-1569.

[7] Mitchell, D. J.; Tiddy, G. J. T.; Waring, L.; Bostock, T.; McDonald, M. P., *J. Chem. Soc., Faraday Trans.* **1983,** *79*, 975-1000.

[8] Karlstroem, G., *J. Phys. Chem.* **1984,** *88*, 4769.

[9] Kunieda, H.; Shigeta, K.; Ozawa, K.; Suzuki, M., *J. Phys. Chem. B* **1997,** *101*, 7952.

[10] Kunieda, H.; Shigeta, K.; Ozawa, K.; Suzuki, M., *The Journal of Physical Chemistry B* **1997,** *101*, 7952-7957.

[11] Griffin, W. C., *J. Soc. Cosmet. Chem.* **1949,** *1*, 311.

[12] Davies, J. T.; Rideal, E. K., *Interfacial Phenomena*. New York, 1963; p 371-383.

[13] Nagarajan, R.; Ruckenstein, E., *Separation Science and Technology* **1981,** *16*, 1429-1465.

[14] Sjoblom, J.; Stenius, P., in: *Surfactant science series*, Schick, M. J.; Marcel, D., (Eds.) New York, 1987; Vol. 23, p 369-434.

[15] Mukerjee, P.; Cardinal, J. R., *The Journal of Physical Chemistry* **1978,** *82*, 1620-1627.

[16] Shinoda, K.; Satio, H., *J. Colloid Interface Sci.* **1968,** *26*, 70.

[17] Shinoda, K.; Friberg, S., *Adv. Colloid Interface Sci.* **1975,** *4*, 281-300.

[18] Friberg, S. E.; Mandell, L.; Larsson, M., *j. Colloid Interface Sci.* **1969,** *29*, 155-156.

[19] Shinoda, K.; Friberg, S., in: John Wiley and Sons New York, 1986; p 95.

[20] Buzier, M.; Ravey, J.-C., *Journal of Colloid and Interface Science* **1983,** *91*, 20-33.

[21] Buzier, M.; Ravey, J. C., *J. Colloid Interface Sci.* **1985,** *103*, 594-596.

[22] Kunieda, H.; Shinoda, K., *Journal of Colloid and Interface Science* **1985,** *107*, 107-121.

[23] Kahlweit, M.; Strey, R.; Busse, G., *Journal of Physical Chemistry* **1990,** *94*, 3881-3894. .

[24] Ravey, J. C.; Stébé, M. J., *J. Physica B* **1989,** *156-157*, 394.

[25] Ravey, J. C.; Stébé, M. J., *J. prog. Colloid Polym. Sci.* **1990,** *82*, 218-228.

[26] Ravey, J. C.; Stébé, M. J.; Sauvage, S., *Colloids Surfaces A* **1994,** *91*, 237-257.

[27] Pons, R.; Erra, P.; Solans, C.; Ravey, J. C.; Stébé, M. J., *The Journal of Physical Chemistry* **1993,** *97*, 12320-12324.

[28] Kabalnov, A.; Wennerstrom, H., *Langmuir* **1996,** *12*, 276-292.

[29] Bancroft, W. D., *J. Phys. Chem.* **1913,** *17*, 501.

[30] Bancroft, W. D., *J. Phys. Chem.* **1915,** *19*, 275.

[31] Griffin, W. C., *J. Soc. Cosmet. Chem.* **1954,** *5*, 249.

[32] Shinoda, K.; Frieberg, S., *Emulsions and Solubilization*. J. Wiley & Sons New York,

1986.
[33] Solans, C.; Azermar, N.; Parra, J., in: *Trends in Colloid and Interface Science II*, 1988; p 224-227.
[34] Cameron, N. R.; Sherrington, D. C., in: *Advances in Polymer Science*, Springer Berlin/ Heidelberg 1996; Vol. 126, p 163-214.
[35] Ravey, J. C.; Stébé, M. J., *Colloids Surfaces A* **1994,** *84*, 11-31.
[36] Princen, H. M., *Journal of Colloid and Interface Science* **1983,** *91*, 160-175.
[37] Zhang, H.; Cooper, A. I., *Soft Matter* **2005,** *1*, 107-113.
[38] Ravey, J. C.; Stébé, M. J.; Sauvage, S., *J. Chim. Phys.* **1994,** *91*, 259.
[39] Pons, R.; Carrera, I.; Erra, P.; Kunieda, H.; Solans, C., *Colloids and Surfaces A: Physicochemical and Engineering Aspects* **1994,** *91*, 259-266.
[40] Rocca, S.; Garcia-Celma, M. J.; Caldero, G.; Pons, R.; Solans, C.; Stébé, M. J., *Langmuir* **1998,** *14*, 6840-6845.
[41] Solans, C.; Dominguez, J. G.; Parra, J. L., *Colloids Polym Sci* **1988,** *266*, 570.
[42] Kunieda, H.; Yano, N.; Solans, C., *Colloids and Surfaces* **1989,** *36*, 313-322.
[43] Solans, C.; Pinazo, A.; Calderó, G.; Infante, M. R., *Colloids and Surfaces A: Physicochemical and Engineering Aspects* **2001,** *176*, 101-108.
[44] Babak, V. G.; Stébé, M. J., *J. Dispersion Sci. Techol.* **2002,** *23*, 1-22.
[45] Ravey, J. C.; Stébé, M. J., *Physica B* **1994,** *157*, 394-397.
[46] Kunieda, H.; Solans, C.; Shida, N.; Parra, J. L., *Colloids and Surfaces* **1987,** *24*, 225-237.
[47] Solans, C.; Pons, R.; Zhu, S.; Davis, H. T.; Evans, D. F.; Nakamura, K.; Kunieda, H., *Langmuir* **1993,** *9*, 1479-1482.
[48] Kunieda, H.; Fukui, Y.; Uchiyama, H.; Solans, C., *Langmuir* **1996,** *12*, 2136-2140.
[49] Förster, T.; Von Rybinski, W.; Wadle, A., *Advances in Colloid and Interface Science* **1995,** *58*, 119-149.
[50] Ozawa, K.; Solans, C.; Kunieda, H., *Journal of Colloid and Interface Science* **1997,** *188*, 275-281.
[51] Taisne, L.; Cabane, B., *Langmuir* **1998,** *14*, 4744-4752.
[52] Princen, H. M.; Aronson, M. P.; Moser, J. C., *Journal of Colloid and Interface Science* **1980,** *75*, 246-270.
[53] Aronson, M. P., *Langmuir* **1989,** *5*, 494-501.
[54] Aronson, M. P.; Petko, M. F., *Journal of Colloid and Interface Science* **1993,** *159*, 134-149.
[55] Sonneville-Aubrun, O.; Bergeron, V.; Gulik-Krzywicki, T.; Jonsson, B.; Wennerstrom, H.; Lindner, P.; Cabane, B., *Langmuir* **2000,** *16*, 1566-1579.
[56] Mason, T. G.; Lacasse, M.-D.; Grest, G. S.; Levine, D.; Bibette, J.; Weitz, D. A., *Physical Review E* **1997,** *56*, 3150.
[57] Mason, T. G.; Bibette, J., *Physical Review Letters* **1996,** *77*, 3481.
[58] Mabille, C.; Schmitt, V.; Gorria, P.; Leal Calderon, F.; Faye, V.; Deminière, B.; Bibette, J., *Langmuir* **1999,** *16*, 422-429.
[59] Perrin, P., *Langmuir* **2000,** *16*, 4774-4778.
[60] Bibette, J., *Journal of Colloid and Interface Science* **1991,** *147*, 474-478.
[61] Bibette, J., *Journal de Physique: JP* **1992,** *2*, 401.
[62] Sagitani, H.; Hattori, T.; Nagai, M., *Nippon Kagaku Kaishi* **1983,** *10*, 1399.
[63] Atwood, D.; Florence, A. T., in: Chapman & Hall New York, 1983.
[64] Becher, P., in: Marcel Dekker New York, 1988.
[65] Zhang, H.; Hardy, G. C.; Rosseinsky, M. J.; Cooper, A. I., *Advanced Materials* **2003,** *15*, 78-81.
[66] Binks, B. P., *Advanced Materials* **2002,** *14*, 1824-1827.

[67] Oh, C.; Chung, S.-C.; Shin, S.-i.; Kim, Y. C.; Im, S.-S.; Oh, S.-G., *Journal of Colloid and Interface Science* **2002,** *254*, 79-86.
[68] Zhao, C.; Danish, E.; Cameron, N. R.; Kataky, R., *Journal of Materials Chemistry* **2007,** *17*, 2446-2453.
[69] Zhang, S.; Chen, J., *Polymer* **2007,** *48*, 3021-3025.
[70] Blin, J. L.; Grignard, J.; Zimny, K.; Stébé, M. J., *Colloids and Surfaces A: Physicochemical and Engineering Aspects* **2007,** *308*, 71-78.
[71] Davis, M. E., *Nature* **2002,** *417*, 813-821.
[72] Schüth, F., *Angewandte Chemie International Edition* **2003,** *42*, 3604-3622.
[73] Stein, A., *Advanced Materials* **2003,** *15*, 763-775.
[74] López, C., *Advanced Materials* **2003,** *15*, 1679-1704.
[75] Holmberg, K., *Journal of Colloid and Interface Science* **2004,** *274*, 355-364.
[76] Cundy, C. S.; Cox, P. A., *Chemical Reviews* **2003,** *103*, 663-702.
[77] Kyotani, T., *Carbon* **2000,** *38*, 269-286.
[78] Hentze, H. P.; Antonietti, M., *Current Opinion in Solid State and Materials Science* **2001,** *5*, 343-353.
[79] Bommel, K. J. C. v.; Friggeri, A.; Shinkai, S., *Angewandte Chemie International Edition* **2003,** *42*, 980-999.
[80] Polarz, S.; Antonietti, M., *Chemical Communications* **2002,** 2593-2604.
[81] Linssen, T.; Cassiers, K.; Cool, P.; Vansant, E. F., *Advances in Colloid and Interface Science* **2003,** *103*, 121-147.
[82] Soler-Illia, G. J. d. A. A.; Sanchez, C.; Lebeau, B.; Patarin, J., *Chemical Reviews* **2002,** *102*, 4093-4138.
[83] Hollister, S. J., *Nat Mater* **2005,** *4*, 518-524.
[84] Zhao, X. S.; Su, F.; Yan, Q.; Guo, W.; Bao, X. Y.; Lv, L.; Zhou, Z., *Journal of Materials Chemistry* **2006,** *16*, 637-648.
[85] Taguchi, A.; Schüth, F., *Microporous and Mesoporous Materials* **2005,** *77*, 1-45.
[86] Sing, K. S. W.; Everett, D. H.; Haul, R. A. W.; Moscou, L.; Pierotti, R. A.; Rouquerol, J.; Siemieniewska, T., *Pure Appl. Chem.* **1985,** *57*, 603.
[87] Ye, F.; Collinson, M. M.; Higgins, D. A., *Physical Chemistry Chemical Physics* **2009,** *11*, 66-82.
[88] Geffcken, W.; Berger, B., *Ger. Pat.* **1939,** *736*, 411.
[89] Levene, L. T., I. M. 1972.
[90] Philipp, G.; Schmidt, H. J., *Non-Cryst Solids* **1984,** *63*, 283.
[91] Wilkes, G. L.; Orler, B.; Huang, H., *Polym Prepr* **1985,** *26*, 300.
[92] Diré, S.; Babonneau, F.; Sanchez, C.; Livage, J., *J. Mater. Chem.* **1992,** *2*, 239-244.
[93] Griesmar, P.; Papin, G.; Sanchez, C.; Livage, J., *Chemistry of Materials* **1991,** *3*, 335-339.
[94] Brinker, C. J.; Scherer, G. W., in: *Sol-Gel Science*, San Diego, 1990.
[95] Livage, J.; Henry, M.; Sanchez, C., *Prog. Solid State Chem.* **1988,** *18*, 259.
[96] Hench, L. L.; West, J. K., *Chem. Rev.* **1990,** *90*, 33.
[97] Chiola, V.; Ritsko, J. E.; Vanderpool, C. D. 1971.
[98] Di Renzo, F.; Cambon, H.; Dutartre, R., *Micropor. Mater.* **1997,** *10*, 283.
[99] Beck, J. S.; Chu, C. T. W.; Johnson, I. D.; Kresge, C. T.; Leonowicz, M. E.; Roth, W. J.; Vartuli, J. W. 1991.
[100] Kresge, C. T.; Leonowicz, M. E.; Roth, W. J.; Vartuli, J. C.; Beck, J. S., *Nature* **1992,** *359*, 710.
[101] Beck, J. S.; Vartuli, J. C.; Roth, W. J.; Leonowicz, M. E.; Kresge, C. T.; Schmitt, K. D.; Chu, C. T. W.; Olson, D. H.; Sheppard, E. W.; McCulle, S. B.; Higgins, J. B.; Schlender, J. L., *J. Am. Chem. Soc.* **1992,** *114*, 10834.

[102] Yanagisawa, T.; Shimizu, T.; Kuroda, K.; Kato, C., *Bull. Chem. Soc. Jpn.* **1990,** *63*, 988.
[103] Inagaki, S.; Fukushima, Y.; Kuroda, K., *J. Chem. Soc. Chem. Commun.* **1993,** 680.
[104] Inagaki, S.; Koiwai, A.; Suzuki, N.; Fukushima, Y.; Kuroda, K., *Bull. Chem. Soc. Jpn.* **1996,** *69* 1449.
[105] Carreon, M. A.; Guliants, V. V., *European Journal of Inorganic Chemistry* **2005,** *2005*, 27-43.
[106] Tanev, P. T.; Pinnavaia, T. J., *Science* **1995,** *267*, 865.
[107] Huo, Q. S.; Margolese, D. I.; Ciesla, U.; Feng, P. Y.; Gier, T. E.; Sieger, P.; Leon, R.; Petroff, P. M.; Schuth, F.; Stucky, G. D., *Nature* **1994,** *368*, 317.
[108] Sun, T.; Ying, J. Y., *Nature* **1997,** *389*, 704.
[109] Tian, Z. R.; Tong, W.; Wang, J. Y.; Duan, N. G.; Krishnan, V. V.; Suib, S. L., *Science* **1997,** *276*.
[110] Yang, P. D.; Zhao, D. Y.; Margolese, D. I.; Chmelka, B. F.; Stucky, G. D., *Nature* **1998,** *396*, 152.
[111] Zou, X. D.; Conradsson, T.; Klingstedt, M.; Dadachov, M. S.; O'Keeffe, M., *Nature* **2005,** *437*, 716.
[112] Tian, B. Z.; Liu, X. Y.; Tu, B.; Yu, C. Z.; Fan, J.; Wang, L. M.; Xie, S. H.; Stucky, G. D.; Zhao, D. Y., *Nat. Mater.* **2003,** *2*, 159.
[113] Grosso, D.; Boissiere, C.; Smarsly, B.; Brezesinski, T.; Pinna, N.; Albouy, P. A.; Amenitsch, H.; Antonietti, M.; Sanchez, C., *Nat. Mater.* **2004,** *3*, 787.
[114] Corma, A.; Atienzar, P.; Garcia, H.; Chane-Ching, J. Y., *Nat. Mater.* **2004,** *3*, 394.
[115] MacLachlan, M. J.; Coombs, N.; Ozin, G. A., *Nature* **1999,** *397*, 681.
[116] Braun, P. V.; Osenar, P.; Stupp, S. I., *Nature* **1996,** *380*, 325.
[117] Trikalitis, P. N.; Rangan, K. K.; Bakas, T.; Kanatzidis, M. G., *Nature* **2001,** *410*, 671.
[118] Attard, G. S.; Bartlett, P. N.; Coleman, N. R. B.; Elliott, J. M.; Owen, J. R.; Wang, J. H., *Science* **1997,** *278*, 838.
[119] Armatas, G. S.; Kanatzidis, M. G., *Nature* **2006,** *,441*, 1122.
[120] Sun, D.; Riley, A. E.; Cadby, A. J.; Richman, E. K.; Korlann, S. D.; Tolbert, S. H., *Nature* **2006,** *441*, 1126.
[121] Landskron, K.; Ozin, G. A., *Science* **2004,** *306*, 1529.
[122] Meng, Y.; Gu, D.; Zhang, F. Q.; Shi, Y. F.; Yang, H. F.; Li, Z.; Yu, C. Z.; Tu, B.; Zhao, D. Y., *Angew. Chem., Int. Ed.* **2005,** *44*, 7053.
[123] Wan, Y.; Zhao, *Chemical Reviews* **2007,** *107*, 2821-2860.
[124] Tanev, P. T.; Chibwe, M.; Pinnavaia, T. J., *Nature* **1994,** *368*, 321.
[125] Huo, Q. S.; Leon, R.; Petroff, P. M.; Stucky, G. D., *Science* **1995,** *268*, 1324.
[126] Huo, Q. S.; Margolese, D. I.; Stucky, G. D., **1996,** *8*, 1147.
[127] Ying, J. Y.; Mehnert, C. P.; Wong, M. S., *Angew. Chem., Int. Ed.* **1999,** *38*, 56.
[128] Bagshaw, S. A.; Prouzet, E.; Pinnavaia, T. J., *Science* **1995,** *269*, 1242.
[129] Blin, J. L.; Leonard, A.; Su, B. L., *Chem. Mater.* **2001,** *13*, 3542.
[130] Zhao, D.; Feng, J.; Huo, Q.; Melosh, N.; Fredrikson, G.; Chmelka, B. F.; Stucky, G. D., *Science* **1998,** *279*, 548.
[131] Zhao, D.; Huo, Q.; Feng, J.; Chmelka, B. F.; Stucky, G. D., *J. Am. Chem. Soc.* **1998,** *120*, 6024.
[132] Kleitz, F.; Liu, D. N.; Anilkumar, G. M.; Park, I. S.; Solovyov, L. A.; Shmakov, A. N.; Ryoo, R., *J. Phys. Chem. B* **2003,** *107*, 14296.
[133] Kleitz, F.; Choi, S. H.; Ryoo, R., *Chem. Commun.* **2003,** 2136.
[134] Attard, G. S.; Glyde, J. C.; Goltner, C. G., *Nature* **1995,** *378*, 366-368.
[135] Feng, P.; Bu, X.; Stucky, G. D.; Pine, D. J., *Journal of the American Chemical Society* **1999,** *122*, 994-995.

[136] Göltner, C. G.; Henke, S.; Weissenberger, M. C.; Antonietti, M., *Angewandte Chemie International Edition* **1998,** *37*, 613-616.
[137] Wan, Y.; Shi, Y.; Zhao, D., *Chemical Communications* **2007,** 897-926.
[138] Blin, J. L.; Leonard, A.; Su, B. L., *Chemistry of Materials* **2001,** *13*, 3542-3553.
[139] Templin, M.; Franck, A.; DuChesne, A.; Leist, H.; Zhang, Y. M.; Ulrich, R.; Schadler, V.; Wiesner, U., *Science* **1997,** *278*, 1795.
[140] Prouzet, E.; Cot, F.; Nabias, G.; Larbot, A.; Kooyman, P.; Pinnavaia, T. J., *Chem. Mater.* **1999,** *11*, 1498.
[141] Boissière, C.; Larbot, A.; Bourgaux, C.; Prouzet, E.; Bunton, C. A., *Chem. Mater.* **2001,** *13*, 3580.
[142] Herrier, G.; Blin, J. L.; Su, B. L., *Langmuir* **2001,** *17*, 4422.
[143] Blin, J. L.; Leonard, A.; Su, B. L., *J. Phys. Chem. B,* **2001,** *105*, 6070.
[144] Jansen, J. C.; Shan, Z.; Marchese, L.; Zhou, W.; von der Puil, N.; Maschmeyer, T., *Chem. Commun.* **2001,** 713.
[145] Price, P. M.; Clark, J. H.; Macquarrie, D. J., *J. Chem. Soc.,Dalton Trans.* **2000,** 101.
[146] Ravey, J. C., in: *Prog. Colloid Polym. Sci*, 1987; Vol. 73, p 107-112.
[147] Mathis, G.; Leempoel, P.; Ravey, J. C.; Selve, C.; Delpuech, J. J., *J. Am. Chem. Soc.* **1984,** *106*, 6162-6171.
[148] Blin, J. L.; Lesieur, P.; Stébé, M. J., *Langmuir* **2004,** *20*, 491-498.
[149] Ravey, J. C.; Stébé, M. J., *Progr. Colloid. Polym. Sci.* **1987,** *73*, 127-133.
[150] Ravey, J. C.; Gherbi, A.; Stébé, M. J., *Progr. Colloid Polym. Sci.* **1988,** *76*, 234-241.
[151] Moore, R. E.; Clark, L. C. J., in: *Oxygen Carrying Colloidal Blood Substitutes, Int. Symp. Perfluorochem. Blood Substitutes, 5th* Frey, R.; Beisbarth, H.; Stosseck, K., (Eds.) W. Zuckschwerdt Verlag, Munich: Mainz, Germany, 1982; p 50.
[152] Riess, J. G., *Tetrahedron* **2002,** *58*, 4113-4131.
[153] Esquena, J.; Rodríguez, C.; Solans, C.; Kunieda, H., *Microporous and Mesoporous Materials* **2006,** *92*, 212-219.
[154] Meng, X.; Di, Y.; Zhao, L.; Jiang, D.; Li, S.; Xiao, F. S., *Chem. Mater.* **2004,** *16*, 5518-5526.
[155] Groenewolt, M.; Antonietti, M.; Polarz, S., *Langmuir* **2004,** *20*, 7811-7819.
[156] Michaux, F.; Blin, J. L.; Stébé, M. J., *J. Phys. Chem. B* **2008,** *112*, 11950-11959.
[157] Fan, J.; Yu, C.; Lei, J.; Zhang, Q.; Li, T.; Tu, B.; Zhou, W.; Zhao, D., *Journal of the American Chemical Society* **2005,** *127*, 10794-10795.
[158] Yuan, Z.-Y.; Su, B.-L., *Journal of Materials Chemistry* **2006,** *16*, 663-677.
[159] P. Yang; T. Deng; D. Zhao; P. Feng; D. Pine; B. F. Chmelka; Whitesides, G. M.; G. D. Stucky, *Science* **1998,** *282*, 2244.
[160] Sen, T.; Tiddy, G. J. T.; Casci, J. L.; Anderson, M. W., *Chem. Mater.* **2004,** *16*, 2044.
[161] B.T. Holland; C.F. Blanford; A. Stein, *Science* **1998,** *281*, 538.
[162] Sen, T.; Tiddy, G. J. T.; Casci, J. L.; Anderson, M. W., *Angew. Chem. Int. Ed.* **2003,** *42*, 4649.
[163] Imhof, A.; Pine, D. J., *Nature* **1997,** *389*, 948.
[164] D. J. Pine, *Adv. Mater.* **1998,** *10*, 697.
[165] Sen, T.; Tiddy, G. J. T.; Casci, J. L.; Anderson, M. W., *Micropor.Mesopor. Mater.* **2005,** *78*, 255.
[166] Sen, T.; Tiddy, G. J. T.; Casci, J. L.; Anderson, M. W., *Chem. Commun.* **2003,** *17*.
[167] Carn, F.; Colin, A.; Achard, M. F.; Deleuze, H.; Sellier, E.; Birot, M.; Backov, R., *J. Mater. Chem.* **2004,** *14*, 1370.
[168] Blin, J. L.; Bleta, R.; Ghanbaja, J.; Stébé, M. J., *Micropor. Mesopor. Mater.* **2006,** *94*, 74-80.
[169] Nakanishi, K., *J. Porous Mater.* **1997,** *4*, 67.

[170] Sato, Y.; Nakanishi, K.; Hirao, K.; Jinnai, H.; Shibayama, M.; Melnichenko, Y. B.; Wignall, G. D., *Colloids Surf., A* **2001,** *187*, 117.
[171] Nakanishi, K.; Sato, Y.; Ruyat, Y.; Hirao, K., *J. Sol-Gel Sci. Technol.* **2003,** *26*, 567.
[172] Nakanishi, K.; Kobayashi, Y.; Amatani, T.; Hirao, K.; Kodaira, T., *Chem. Mater.* **2004,** *16* 3652.
[173] Amatani, T.; Nakanishi, K.; Hirao, K.; Kodaira, T., *Chem. Mater.* **2005,** *17*, 2114.
[174] Bleta, R.; Blin, J. L.; Stébé, M. J., *J. Phys. Chem. B* **2006,** *110*, 23547-23556.
[175] Clark Jr, L.; Becattini, F.; Kaplan, S.; Obrock, V.; Cohen, D.; Becker, C., *Science* **1973,** *181*, 680-682.
[176] Battino, R.; Clever, H., *Chem. Rev.* **1966,** *66*, 395-463.
[177] Gollan, F.; Clark Jr, L., *Physiologist* **1966,** *9*, H292.
[178] Zimny, K.; Blin, J. L.; Stébé, M. J., *J. Phys. Chem. C* **2009,** *113*, 11285-11293.
[179] Ropers, M. H. These de doctorat, nancy, 2000.
[180] Riess, R. E., *Artificial Organs* **1984,** *8*, 44-55.
[181] Kabalnov, A. S.; Makarov, K. N.; Shchukin, E. D., *Colloids Surf.* **1992,** *62*, 101-104.
[182] Le, T. D.; Arlauskas, R. A.; Weers, J. G., *Journal of Fluorine Chemistry* **1996,** *78*, 155-163.
[183] Shinoda, K.; Ogawa, T., *Journal of Colloid and Interface Science* **1967,** *24*, 56-60.
[184] Iler, R. K., in: Section 2 General and Physical Chemistry ed.; 1955.
[185] Schnablegger, H.; Singh, Y., *A pratical guide to SAXS --Getting acquainted with the principles*. Anton Paar GmbH. 2006.
[186] Brunauer, S.; Emmett, P. H.; Teller, E., *J. Am. Chem. Soc.* **1938,** *60*, 309-319.
[187] Sing, K. S. W.; Everett, D. H.; Haul, R. A. W.; Moscou, L.; Pierotti, R. A.; Rouquerol, J.; Sienieniewsks, T., *Pure and Applied Chemistry* **1985,** *57*, 603-619.
[188] Barrett, E. P.; Joyner, L. G.; Halenda, P. P.; Inst., M.; Pittsburgh, P., *J. Am. Chem. Soc.* **1951,** *73*, 373-380.
[189] Groen, J. C.; Peffer, L. A. A.; Pérez-Ramírez, J., *Microporous and Mesoporous Materials* **2003,** *60*, 1-17.
[190] Jaroniec, C. P.; Kruk, M.; Jaroniec, M.; Sayari, A., *J. Phys. Chem. B* **1998,** *102*, 5503-5510.
[191] Gohy, J.-F.; Varshney, S. K.; Jerome, R., *Macromolecules* **2001,** *34*, 3361-3366.
[192] Evans, D. F.; Wennerstrom, H., *The Colloidal Domiain where Physics, Chemistry, Biology and Technology Meet*. VCH Pubulisher Inc. New York, 1994.
[193] Provencher, S. W., *Computer Physics Communications* **1982,** *27*, 213-227.
[194] Provencher, S. W., *Computer Physics Communications* **1982,** *27*, 229-242.
[195] Blin, J. L.; Stébé, M. J., *The Journal of Physical Chemistry B* **2004,** *108*, 11399-11405.
[196] Blin, J. L.; Stébé, M. J., *Microporous and Mesoporous Materials* **2005,** *87*, 67-76.
[197] Imhof, A.; Pine, D. J., *Chem. Eng. Technol.* **1998,** *21*, 8.
[198] Alibrahim, M.; Stébé, M. J.; Dupont, G.; Ravey, J. C., *J. Chim. Phys.* **1997,** *94*, 1614.
[199] Yuan, M.; Tang, J.; Yu, C.; Chen, Y.; Tu, B.; Zhao, D., *Chem. Lett.* **2003,** *32*, 660.
[200] Carn, F.; Colin, A.; Achard, M.-F.; Deleuze, H.; Saadi, Z.; Backov, R., *Advanced Materials* **2004,** *16*, 140-144.
[201] Carn, F.; Colin, A.; Achard, M.-F.; Deleuze, H.; Sanchez, C.; Backov, R., *Advanced Materials* **2005,** *17*, 62-66.
[202] Ottaviani, M. F.; Moscatelli, A.; Desplantier-Giscard, D.; Di Renzo, F.; Kooyman, P.; Galarneau, A., *J. Phys. Chem. B* **2004,** *108* 12123.
[203] Jana, S. K.; Nishida, R.; Shindo, K.; Kugita, T.; Namba, S., *Microporous and Mesoporous Mater.* **2004,** *68*, 133.
[204] Boissière, C.; Marines, M. A. U.; Tokumoto, M.; Larbot, A.; Prouzet, E., *Chem.*

Mater. **2003,** *15*, 509.
[205] L. Cao; T. Man; M. Kruk, *Chem. Mater.* **2009,** *21*, 1144.
[206] Nagarajan, R.; Barry, M.; Ruckenstein, E., *Langmuir* **1986,** 210.
[207] Zhang, H.; Sun, J.; Ma, D.; Weinberg, G.; Su, D. S.; Bao, X., *J. Phys. Chem. B 110 (2006) 25908.*
[208] Nagarajan, R., *Colloids Surf. B* **1999,** *16* 55.
[209] Ravey, J. C., *Microemulsions : Structure and Dynamics* CRC Press 1987; p 93.
[210] Ravey, J. C.; Buzier, M., *Surfactant in solution*. Plenum New York, 1989; Vol. 8, p 117.
[211] Du, N.; Stébé, M. J.; Bleta, R.; Blin, J. L., *Colloids and Surfaces A: Physicochemical and Engineering Aspects* **2009,** *357*, 116-127.
[212] Balinov, B.; Linse, P.; Söderman, O., *Journal of Colloid and Interface Science* **1996,** *182*, 539-548.
[213] Langenfeld, A.; Celini, N.; Stébé, M. J. in: *Proceedings of the Third World Congress on Emulsions*, Third World Congress on Emulsions, 2002; p 192.
[214] Gross, U. P., G. ; Rüdiger, S. J., *J. Fluorine Chem.* **1993,** *61*, 11.
[215] Bleta, R. system fluores pour la comception de materiaux poreux. Matrices pour la physisorption de biomolecules. Nancy University, Nancy, 2007.
[216] Brunauer, S.; Deming, L. S.; Deming, W. E.; Teller, E., *J.A.C.S.* **1940,** *62*, 1723.
[217] Dubinin, M. M., *Progress in Surface and Membrane Science* **1975,** *9*, 1-70.
[218] Zimny, K.; Blin, J. L.; Stébé, M. J., *J. Colloid Interface Sci.* **2009,** *330*, 456-462.
[219] Landry, C. C.; Tolbert, S. H.; Gallis, K. W.; Monnier, A.; Stucky, G. D.; Norby, P.; Hanson, J. C., *Chemistry of Materials* **2001,** *13*, 1600-1608.
[220] Zana, R.; Yiv, S.; Strazielle, C.; Lianos, P., *Journal of Colloid and Interface Science* **1981,** *80*, 208-223.
[221] Zana, R., *Advances in Colloid and Interface Science* **1995,** *57*, 1-64.
[222] Alexandridis, P.; Holmqvist, P.; Lindman, B., *Colloids and Surfaces A: Physicochemical and Engineering Aspects* **1997,** *129-130*, 3-21.
[223] Aramaki, K.; Olsson, U.; Yamaguchi, Y.; Kunieda, H., *Langmuir* **1999,** *15*, 6226-6232.
[224] Tomsic, M.; Bester-Rogac, M.; Jamnik, A.; Kunz, W.; Touraud, D.; Bergmann, A.; Glatter, O., *Journal of Colloid and Interface Science* **2006,** *294*, 194-211.
[225] Lin, H. P.; Cheng, Y. R.; Liu, S. B.; Mou, C. Y., *J. Mater. Chem.* **1999,** *9*, 1197-1201.
[226] Agren, P.; Linden, M.; Rosenholm, J. B.; Schwarzenbacher, R.; Kriechbaum, M.; Amenitsch, H.; Laggner, P.; Blanchard, J.; Schuth, F., *The Journal of Physical Chemistry B* **1999,** *103*, 5943-5948.
[227] Lin, H.-P.; Kao, C.-P.; Mou, C.-Y., *Microporous and Mesoporous Materials* **2001,** *48*, 135-141.
[228] Liu, S.; Cool, P.; Collart, O.; Van Der Voort, P.; Vansant, E. F.; Lebedev, O. I.; Van Tendeloo, G.; Jiang, M., *The Journal of Physical Chemistry B* **2003,** *107*, 10405-10411.
[229] Tan, B.; Rankin, S. E., *The Journal of Physical Chemistry B* **2004,** *108*, 20122-20129.
[230] Kao, H.-M.; Cheng, C.-C.; Ting, C.-C.; Hwang, L.-Y., *Journal of Materials Chemistry* **2005,** *15*, 2989-2992.
[231] Kim, T.-W.; Kleitz, F.; Paul, B.; Ryoo, R., *Journal of the American Chemical Society* **2005,** *127*, 7601-7610.
[232] Chen, S.-Y.; Cheng, S., *Chemistry of Materials* **2007,** *19*, 3041-3051.
[233] Lide, D. R., *Handbook of Chemistry and Physics*. CRC Press Boca Raton, FL, 1999-2000; Vol. 3-1.
[234] Sottmann, T.; Kluge, K.; Strey, R.; Reimer, J.; Soderman, O., *Langmuir* **2002,** *18*,

3058-3067.
[235] Ugelstad, J.; El-Aasser, M. S.; Vanderhoff, J. W., *Journal of Polymer Science: Polymer Letters Edition* **1973,** *11*, 503-513.
[236] El-Aasser, M. S.; Lack, C. D.; Choi, Y. T.; Min, T. I.; Vanderhoff, J. W.; Fowkes, F. M., *Colloids and Surfaces* **1984,** *12*, 79-97.
[237] El-Aasser, M. S.; Lack, C. D.; Vanderhoff, J. W.; Fowkes, F. M., *Colloids and Surfaces* **1988,** *29*, 103-118.
[238] Rosano, H. L.; Lan, T.; Weiss, A.; Whittam, J. H.; Gerbacia, W. E. F., *The Journal of Physical Chemistry* **1981,** *85*, 468-473.
[239] Benita, S.; Levy, M. Y., *Journal of Pharmaceutical Sciences* **1993,** *82*, 1069-1079.
[240] Esquena, J.; Solans, C., in: *Trends in Colloid and Interface Science XII*, 1998; p 235-239.
[241] Wang, L.; Li, X.; Zhang, G.; Dong, J.; Eastoe, J., *Journal of Colloid and Interface Science* **2007,** *314*, 230-235.
[242] Weiss, J.; Takhistov, P.; McClements, D. J., *Journal of Food Science* **2006,** *71*, R107-R116.
[243] Sadurní, N.; Solans, C.; Azemar, N.; García-Celma, M. J., *European Journal of Pharmaceutical Sciences* **2005,** *26*, 438-445.
[244] Sonneville-Aubrun, O.; Simonnet, J. T.; L'Alloret, F., *Advances in Colloid and Interface Science* **2004,** *108-109*, 145-149.
[245] Asua, J. M., *Progress in Polymer Science* **2002,** *27*, 1283-1346.
[246] Antonietti, M.; Landfester, K., *Progress in Polymer Science* **2002,** *27*, 689-757.
[247] Liedtke, S.; Wissing, S.; Müller, R. H.; Mäder, K., *International Journal of Pharmaceutics* **2000,** *196*, 183-185.
[248] Porras, M.; Solans, C.; González, C.; Gutiérrez, J. M., *Colloids and Surfaces A: Physicochemical and Engineering Aspects* **2008,** *324*, 181-188.
[249] Pons, R.; Carrera, I.; Caelles, J.; Rouch, J.; Panizza, P., *Advances in Colloid and Interface Science* **2003,** *106*, 129-146.
[250] Forgiarini, A.; Esquena, J.; Gonzalez, C.; Solans, C., *Langmuir* **2001,** *17*, 2076-2083.
[251] Morales, D.; Gutiérrez, J. M.; Garcia-Celma, M. J.; Solans, Y. C., *Langmuir* **2003,** *19*, 7196-7200.
[252] Mohlin, K.; Holmberg, K.; Esquena, J.; Solans, C., *Colloids and Surfaces A: Physicochemical and Engineering Aspects* **2003,** *218*, 189-200.
[253] Tadros, T.; Izquierdo, P.; Esquena, J.; Solans, C., *Advances in Colloid and Interface Science* **2004,** *108-109*, 303-318.
[254] Usón, N.; Garcia, M. J.; Solans, C., *Colloids and Surfaces A: Physicochemical and Engineering Aspects* **2004,** *250*, 415-421.
[255] Izquierdo, P.; Esquena, J.; Tadros, T. F.; Dederen, J. C.; Feng, J.; Garcia-Celma, M. J.; Azemar, N. r.; Solans, C., *Langmuir* **2004,** *20*, 6594-6598.
[256] Porras, M.; Solans, C.; González, C.; Martínez, A.; Guinart, A.; Gutiérrez, J. M., *Colloids and Surfaces A: Physicochemical and Engineering Aspects* **2004,** *249*, 115-118.
[257] Solè, I.; Maestro, A.; Pey, C. M.; González, C.; Solans, C.; Gutiérrez, J. M., *Colloids and Surfaces A: Physicochemical and Engineering Aspects* **2006,** *288*, 138-143.
[258] Pey, C. M.; Maestro, A.; Solé, I.; González, C.; Solans, C.; Gutiérrez, J. M., *Colloids and Surfaces A: Physicochemical and Engineering Aspects* **2006,** *288*, 144-150.
[259] Solè, I.; Maestro, A.; Gonzalez, C.; Solans, C.; Gutiérrez, J. M., *Langmuir* **2006,** *22*, 8326-8332.
[260] Morales, D.; Solans, C.; Gutiérrez, J. M.; Garcia-Celma, M. J.; Olsson, U., *Langmuir* **2006,** *22*, 3014-3020.

[261] Maestro, A.; Solè, I.; González, C.; Solans, C.; Gutiérrez, J. M., *Journal of Colloid and Interface Science* **2008,** *327*, 433-439.
[262] Solans, C.; Esquena, J.; Forgiarini, A. M.; Usón, N.; Morales, D.; Izquierdo, P.; Azemar, N.; Garcia-Celma, M. J., in: *Surfactant Science Series*, 2003; Vol. 109, p 525-54.
[263] Solans, C.; Izquierdo, P.; Nolla, J.; Azemar, N.; Garcia-Celma, M. J., *Current Opinion in Colloid & Interface Science* **2005,** *10*, 102-110.
[264] Wang, L.; Mutch, K. J.; Eastoe, J.; Heenan, R. K.; Dong, J., *Langmuir* **2008,** *24*, 6092-6099.
[265] Wang, L.; Tabor, R.; Eastoe, J.; Li, X.; Heenan, R. K.; Dong, J., *Physical Chemistry Chemical Physics* **2009,** *11*, 9772-9778.
[266] Date, A. A.; Nagarsenker, M. S., *International Journal of Pharmaceutics* **2007,** *329*, 166-172.
[267] Wang, L.; Dong, J.; Chen, J.; Eastoe, J.; Li, X., *Journal of Colloid and Interface Science* **2009,** *330*, 443-448.